Order Number 9303781

The physical properties of low surface brightness galaxies

McGaugh, Stacy Sutton, Ph.D.

The University of Michigan, 1992

U·M·I
300 N. Zeeb Rd.
Ann Arbor, MI 48106

THE PHYSICAL PROPERTIES OF LOW SURFACE BRIGHTNESS GALAXIES

by
Stacy Sutton McGaugh

A dissertation submitted in partial fulfillment
of the requirements for the degree of
Doctor of Philosophy
(Astronomy)
in The University of Michigan
1992

Doctoral Committee:

Associate Professor Greg Bothun, Chair
Assistant Professor Fred Adams
Associate Professor Joel Bregman
Staff Scientist Jim Schombert, NASA/IPAC

Another night of sin and perdition...

ACKNOWLEDGEMENTS

As I recall the path that has brought me here, I am both amazed and appalled by the amount of time, effort, and energy I have put into the production of this document. But this pales in comparison to the amount of tolerance and support (both moral and financial) required to bring a person to this point. It is difficult to grasp the depth and breadth of community commitment the doctoral process requires, let alone acknowledge all who contribute to its successful completion. So I apologize in advance to those who might be neglected in what follows.

First and foremost, I would like to thank my advisor, Greg Bothun. In many ways, this was a dissertation waiting to happen, and Greg was precisely the right person at the right time (if not in the right place!) to define it and get things moving. For his shared opinion of the importance of the subject of this work, and his ceaseless efforts to convey its gravity to the astronomical community, I am deeply grateful. I am also grateful to my undergraduate mentor, George Clark, for his role in inspiring and indulging my interest in things that hide beneath the sky.

Many others contributed substantially to the intellectual growth of which this is the culmination (to date, I hope!). Among them, Doug Richstone, Joel Bregman, and Will Happer deserve particular mention. Special thanks go to Jim Schombert, who found many of the galaxies which I have studied. Jim was always willing to listen to me rave, which I admit to doing on [rare] occasions. I am also grateful to Thijs van der Hulst for his interest in this subject and his role in obtaining and analyzing the VLA data. Groningen University deserves thanks for its hospitality, as do the members of the Kapteyn Lab who all spoke English and didn't complain while I used inordinate amounts of their computer resources in dealing with the VLA data. Thanks, too, to Pieter Mulder and Arpad Szomoru for getting me started in Groningen, and to Renzo Sancisi for insisting on the merits of Italian cuisine.

While my visit to Groningen proved that life as a radio astronomer is always intense, my life as an optical astronomer has been more extensive. Thanks to Bob Barr and Peter Mack for the ever improving situation at MDM Observatory, and to the Kitt Peak staff for two successful observing runs. If only you guys could do something about the weather!

To my fellow grad students I owe the greatest debt of unspecifiable nature. We were a community of scholars and comrades in arms. Sometimes we even managed to enjoy life a little. Thanks to Mark, Chris, Walt, and Sam, my closest cell mates. Much of my education in "practical astronomy" I owe to Dave, Diab, Ted, Greg, John, and Gary. I will neither confirm nor deny reports of their particular, often essential, contributions. I do not recall their involvement in the consumption of the occasional pitcher of beer, nor would I be disposed to comment on it if it did in fact happen. Patricia, Rachel, and Steve also deserve thanks for their contributions of cheerfulness, pictures, and sanity. I would also like to thank the many undergraduates whom I have had the pleasure of instructing for the paychecks and a renewed sense of wonder. Thanks particularly to those in 221/222 and GOHAM for a little perspective and a lot of amusement.

Finally, I owe an inexpressible amount to my family; immediate, extended and in-law. Without their support and encouragement, this would be neither possible nor worthwhile. Most of all, thanks to

Mom, for the fleetness of mind (or at least sharpness of tongue)
Dad, for the fire that burns (if sometimes too hot), and
Anne, for the love that sustains.

TABLE OF CONTENTS

LIST OF FIGURES

Figure

LIST OF TABLES

Table

LIST OF APPENDICES

Appendix

CHAPTER I

INTRODUCTION

Since Hubble (1936) established that spiral nebulae were stellar systems external to and comparable with our own galaxy, it has been recognized that galaxies are the fundamental constituents of the universe. As such, understanding their formation and evolution is central to astronomy as a physical science. To do this, it is obviously necessary to be aware of the full range of properties exhibited by galaxies.

The study of galaxies as physical objects is often expressed as an effort to understand the Hubble sequence. Unfortunately, the Hubble sequence is morphological rather than quantitative. The identification of the physical properties underlying it remains elusive, and those properties which can be quantitatively measured are not well correlated with morphological type (Bothun 1982). This has severely hampered the usefulness of the Hubble sequence for interpreting the physical nature of galaxies, as is illustrated by the many interpretations that have come in and out of fashion for it.

Worse, the original Hubble sequence was defined solely by prominent, nearby galaxies. Thus it is has required extensive modification and extension as additional galaxy types have been recognized. That these were initially omitted is the result of selection effects which discriminate against the unrepresented galaxies. There is good reason to believe that many types of galaxies are still excluded from galaxy catalogs. The aim here is to elucidate the physical properties of an important class of understudied galaxies: those of low surface brightness.

Motivation: The Severity of Selection Effects

Low surface brightness (LSB) galaxies are those whose surface luminosity density is substantially less than that of the "normal" high surface brightness (HSB) galaxies which define the Hubble sequence. Since galaxies are extended objects, their visibility is not determined solely by their flux as is the case for point sources. A very large but low surface brightness brightness object can have a large total flux, but remain undetected by "flux limited" surveys if the contrast against the background is low. Such galaxies do exist — Malin 1 (Bothun et al. 1987) and its cousins are examples. That Malin 1 has properties so far removed from those of "normal" galaxies (Impey & Bothun 1989) suggests that galaxies exist over a much wider range of properties than implied by the Hubble sequence.

The selection effects induced by the contrast relative to the sky background were first discussed quantitatively by Disney (1976). To illustrate the severity of these selection effects, we follow his argument here. First, the galaxies of which we are aware have surface luminosity distributions that are reasonably well described by

$$\Sigma(r) = \Sigma_0 \, e^{-(r/\alpha)^{1/\beta}}, \tag{1.1}$$

where $\beta = 1$ for disk galaxies (de Vaucoulers 1959), and $\beta = 4$ for bulges and ellipticals (de Vaucoulers 1948). Astronomical images will reach some limiting surface brightness μ_ℓ ($\propto -2.5 \log \Sigma_\ell$) which is ultimately limited by the sky brightness and detector flat field characteristics. The apparent radius r_{ap} of a galaxy on this image can be found by rewriting equation (1.1) as

$$\mu_\ell - \mu_0 = 1.086 \times \left(\frac{r_{ap}}{\alpha}\right)^{1/\beta}, \tag{1.2}$$

where μ_0 is the central surface brightness of the galaxy. Using the total luminosity from the integration of equation (1.1) to replace the scale length α leads to

$$r_{ap} \propto (\mu_\ell - \mu_0)^\beta e^{0.46\mu_0} \tag{1.3}$$

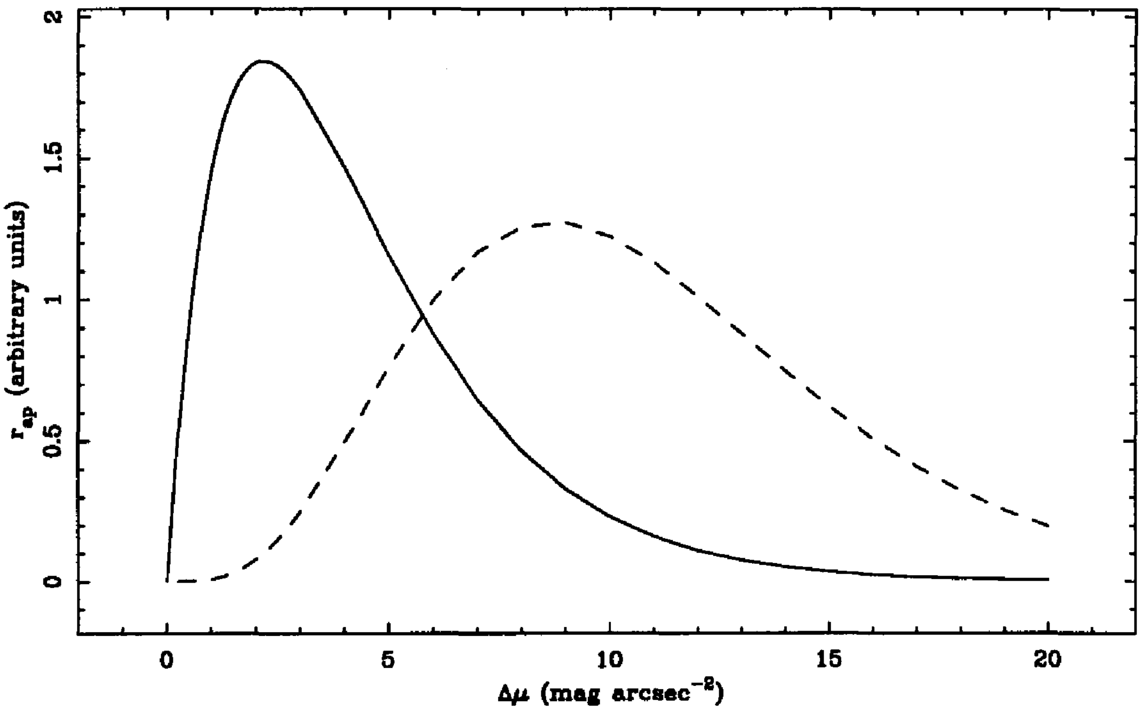

Figure 1.1 — The apparent radius r_{ap} of a galaxy as a function of the contrast $\Delta\mu = \mu_\ell - \mu_0$. The solid line is for exponential disk profiles, and the dashed line for $r^{1/4}$ elliptical profiles. In both cases, galaxies whose contrast maximizes their apparent radii will be those most readily identified.

(equation 4 of Disney 1976).

Equation (1.3) is plotted in Figure 1.1. Obviously, r_{ap} is strongly peaked around a characteristic value of the contrast for each profile type. As discussed by Disney (1976), this formulation is quite successful in explaining both the observed difference between the central surface brightnesses of elliptical and disk galaxies, and their absolute values (Fish 1964, Freeman 1970). This suggests that the observations are strongly biased towards those galaxies for which r_{ap} is maximized, i.e., those which appear largest in pictures of the sky. The selection *against* LSB galaxies is particularly severe, as the apparent radii of disks falls rapidly to zero only 2.17 magnitudes from the peak. Of course, galaxies with central surface brightnesses fainter than the detection limit will never be discovered at all!

Since there is no reason to believe that real galaxies are restricted to surface brightnesses which are readily detected, the "universal" central surface brightness of $\mu_0(B) = 21.65 \pm 0.3$ mag arcsec^{-2} (Freeman 1970) must be due to these selection effects. Given the shape of the galaxy visibility function in Figure 1.1, LSB galaxies could be quite common and remain largely unnoticed. Thus, they could be a major component of the general galaxy population, and have an important effect on the galaxy luminosity function. Since very large galaxies like Malin 1 exist, LSB galaxies can contribute to the luminosity function at bright as well as faint luminosities. However, the effect is most pronounced at the faint end, where the slope of the luminosity function is strongly affected (Impey, Bothun, & Malin 1988; Bothun, Impey, & Malin 1991).

Indeed, since galaxies are not point sources, the traditional luminosity function is rather inadequate. What one would really like to know is the space density of objects as a function of both luminosity and surface density $n(L, \Sigma_0)$, or equivalently, $n(\alpha, \mu_0)$. Because of the selection effects under consideration here, current knowledge of the luminosity function is essentially restricted to $n(L) = n(L, \Sigma_0 = \Sigma_0(r_{ap}^{max}))$. Deconvolving with confidence the true $n(L, \Sigma_0)$ distribution from the selection effects imposed by Figure 1.1 is extremely difficult.

Moreover, studies of deep plate material (Impey et al. 1988; Davies et al. 1988; Irwin et al. 1990; Bothun et al. 1991) show that galaxies fill the entire (B, μ_0) plane available within the confines of the selection function. No correlation between scale length and surface brightness or color is apparent in these samples, contrary to the case for the Hubble sequence. That LSB galaxies are observed to possess such a wide range of properties cautions against the belief that the Hubble sequence is a fair sample of the general galaxy population.

Consider the case for stellar populations. When Baade (1944) first resolved stars in the bulge of the Andromeda galaxy, he was able to introduce the concept of stellar populations with the aid of the H-R diagram for stars in our own galaxy as an interpretive tool. Even though only the brightest stars were resolved, knowledge of the H-R diagram allowed assignment of the red bulge stars to a population similar to that of globular clusters, while the bright blue stars of the disk belonged to a population similar to that of the solar neighborhood. However, the reverse is not possible — without *a priori* knowledge of the H-R diagram, one could never infer the existence of the main sequence from Baade's data. There is no equivalent of the H-R diagram for galaxies. Hence we may be looking at only the most conspicuous examples of extragalactic stellar systems, and be missing the analog of the main sequence for galaxies! This would not be the first time that our cosmological view is affected but observational limitations; the Kapteyn Universe is one modern example.

Indeed, it is fortuitous that we can observe external galaxies at all. The actual value of the night sky brightness is arbitrary. It depends on the phase of the moon, the quantity and albedo of zodiacal dust, and our location within the galaxy, among other things. (Imagine trying to observe external galaxies from within a dust lane, H II region, or dense stellar cluster.) As the artificial contributions of light pollution and debris in near Earth orbit grow, extragalactic observations may become totally impossible. Thus it is very likely that our knowledge of the galaxy population is severely limited by the sky brightness under which we happen to live.

Deeper Into the Realm of the Nebulae

In order to address this fundamental limitation imposed by the sky brightness, it is necessary to study those galaxies against which these selection effects discriminate. Naturally, obtaining such data is difficult. That LSB galaxies have not been extensively studied results not only from selection effects, but also from the technical difficulty involved in their observation. The surface brightness of the darkest terrestrial night sky is $\sim 23B$ mag arcsec^{-2}, comparable to or greater than the *peak* surface brightnesses of LSB galaxies. When the intensity of a source falls below that of the background, then the achievable signal to noise ratio suffers. This is given by

$$S/N = \frac{C_*}{\sqrt{C_* + C_{sky} + N_i^2}}, \tag{1.4}$$

where C_* is the number of counts received from the object, C_{sky} is the number of counts received from the sky over the same area, and N_i is the instrumental noise (e.g., the read noise of a charge coupled detector, or CCD). Obviously, C_* depends on the exposure time, telescope size, etc. All these things being equal, $C_* \propto \Sigma_*$. For bright objects with $\Sigma_* \gg \Sigma_{sky}$, we reach the limit

$$S/N \propto \sqrt{\Sigma_*}. \tag{1.5}$$

But when $\Sigma_* \ll \Sigma_{sky}$,

$$S/N \propto \frac{\Sigma_*}{\sqrt{\Sigma_{sky}}}. \tag{1.6}$$

This is demonstrated in Figure 1.2, which shows the achievable S/N as a function of object surface brightness. Thus the sky level presents another formidable obstacle to the study of LSB galaxies. Fortunately, improvements in detector technology (both electronic and photographic) make first steps in this direction possible without an excessive commitment of telescope time.

The Sample

The sample is composed of galaxies selected from either the UGC (Nilson 1973) or the lists of LSB galaxies of Schombert & Bothun (1988) and Schombert et al. (1992). These are diameter limited catalogs, containing galaxies with apparent diameters $\geq 1'$ (or in the case of the Schombert et al. 'V' lists, $\geq 30''$). As such, these are subject to the selection effects discussed above, regardless of the roughly two magnitudes greater depth of the material used by Schombert et al. than that which Freeman (1970) used to find the "universal" disk central surface brightness.

While obviously incomplete, these catalogs do contain a large number of galaxies with $\mu_0 \approx 23$ mag arcsec^{-2} — a value more than 4σ removed from the Freeman (1970)

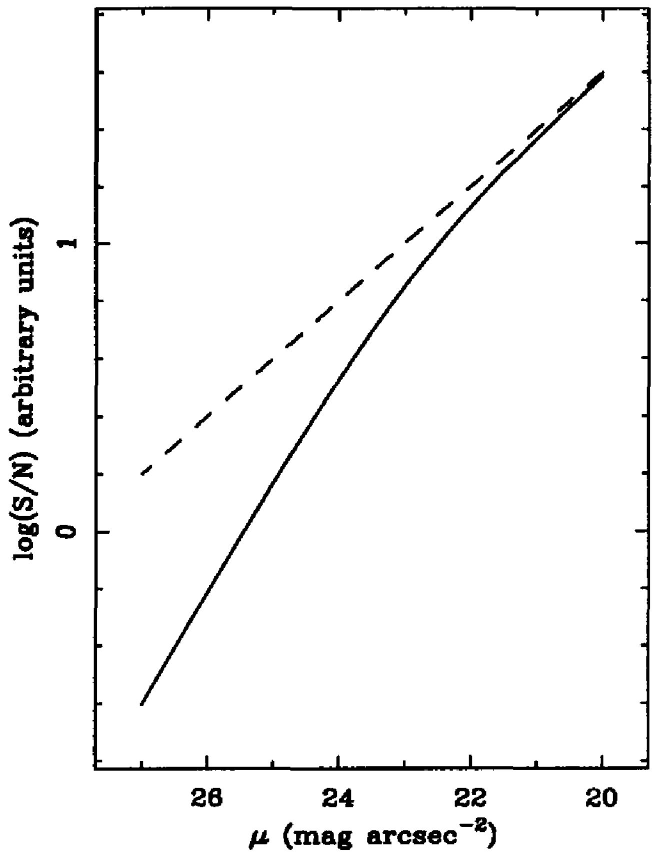

Figure 1.2 — The solid line is the obtainable S/N as a function of surface brightness for an ideal (noiseless) detector and a sky brightness of 23 mag arcsec^{-2}. When μ falls below the sky, S/N departs from the dashed line, which represents the shot noise limit for the same telescope and exposure time. Note that this only demonstrates the deficit in S/N relative to what could be expected for a bright object with the same commitment of aperture–time — instrumental limitations aside, any desired S/N could in principle be reached with a sufficient commitment of aperture–time.

result. Of these, a subset was selected for detailed study which possessed characteristics which would make them amenable to observation, such as visible H II regions. The resulting field sample is biased towards gas rich objects with some current star formation, and can in no way be considered complete or exhaustive. There are many examples of LSB galaxies which possess neither of these characteristics. Nonetheless, this is an important step in the exploration of the physical properties of galaxies not represented by the Hubble sequence.

Though we will refer to galaxies with $\mu_0 = 23$ mag arcsec^{-2} as being low surface brightness, in linear intensity this is only a factor of ~ 3.5 less than the Freeman (1970) value. Remarkable changes in galaxy properties are observed to occur with this modest drop in surface density, and much lower surface brightness ($\mu_0 > 26$ mag arcsec^{-2}) objects are known to exist (e.g., Bothun, Impey, & Malin 1991). This is the deepest study to date of the detailed physical properties of LSB galaxies (cf. Romanishin, Strom, & Strom 1983).

Organization

This dissertation is divided into several independent manuscripts, each written in the style appropriate to the current standards for astronomical journals. Each Chapter addresses a different aspect of LSB galaxies based on an independent data set. Great effort has been directed towards deriving thorough, quantitative information from technically feasible observations.

Chapter 2 makes use of sensitive modern CCDs to obtain deep broad band images of LSB galaxies. From these images the structural parameters (μ_0, α) are determined. Also, the colors derived from the multiple bandpasses give the general shape of the spectral energy distribution, which contains information about the stellar populations of which the galaxies are composed. With sufficient spectral coverage (cf. McGaugh & Bothun 1990), useful constraints can be placed on these.

Chapter 3 takes advantage of the high surface brightness emission lines from the H II regions surrounding sites of current star formation. These provide powerful probes of the physical conditions of the ionized gas in the galaxies. Using the methods described by McGaugh (1991) for the interpretation of nebular spectra, the abundances of several important chemical elements are derived and the presence of massive stars in LSB galaxies is inferred.

The gas content of LSB galaxies is addressed in Chapter 4. Just as they are optically low surface brightness, these galaxies are low in neutral hydrogen column density, despite their sometimes large gas masses. Arguments similar to those made above concerning the visibility of luminous but very extended objects apply here, so these galaxies would also be difficult to identify in H I surveys, making the interpretation of such data problematic (e.g., Weinberg et al. 1991). Furthermore, the H I surface density plays a crucial role in regulating star formation (Kennicutt 1989) and hence the rate of galaxy evolution (van der Hulst et al. 1987, Bothun et al. 1990). That these galaxies are low surface density in nature is discussed in terms of the initial conditions of galaxy formation.

Chapter 5 examines correlations (or the lack thereof) among the data sets presented in the other Chapters, especially with regard to the great range of physical properties exhibited by LSB galaxies compared to those of the Hubble sequence. However, this rich data set is beyond the scope of any one document. That this is the case should serve as a reminder that in a science like astronomy, which literally has the entire universe to explore, there is always merit to the empirical approach. Its quantitative application to the study of new objects always advances our knowledge and sheds light on old paradigms, often in surprising and unpredictable ways.

REFERENCES

Baade, W. 1944, ApJ, 100, 137

Bothun, G. D. 1982, ApJS, 50, 39

Bothun, G. D., Impey, C. D., & Malin, D. F. 1991, ApJ, 376, 404

Bothun, G. D., Impey, C. D., Malin, D. F., & Mould, J. R. 1987, AJ, 94, 23

Bothun, G. D., Schombert, J. M., Impey, C. D., & Schneider, S. E. 1990, ApJ, 360, 427

Davies, J. I., Phillipps, S., Cawson, M. G. M., Disney, M. J., & Kibblewhite, E. J. 1988, MNRAS, 232, 239

de Vaucoulers, G. 1948, Ann. d'Astrophys., 11, 247

de Vaucoulers, G. 1959, in *Handbuch der Physik, v. 53, Astrophysics IV: Stellar Systems*, ed. S. Flügge (Berlin: Springer-Verlag), 275

Disney, M. J. 1976, Nature, 263, 573

Freeman, K. C. 1970, ApJ, 160, 811

Fish, R. A. 1964, ApJ, 139, 284

Hubble, E. P. 1936, *The Realm of the Nebulae* (New Haven: Yale University Press)

Impey, C. D., & Bothun, G. D. 1989, ApJ, 341, 89

Impey, C. D., Bothun, G. D., & Malin, D. F. 1988, ApJ, 330, 634

Irwin, M. J., Davies, J. I., Disney, M. J., & Phillipps, S. 1990, MNRAS, 245, 289

Kennicutt, R. C. 1989, ApJ, 344, 685

McGaugh, S. S. 1991, ApJ, 380, 140

McGaugh, S. S., & Bothun, G. D. 1990, AJ, 100, 1073

Nilson, P. 1973, *Uppsala General Catalog of Galaxies* (Uppsala, Sweden: Societatis Scientiarum Upsaliensis) (UGC)

Romanishin, W., Strom, K. M., & Strom, S. E. 1983, ApJS, 53, 105

Schombert, J. M., & Bothun, G. D. 1988, AJ, 95, 1389

Schombert, J. M., Bothun, G. D., Schneider, S. E., & McGaugh, S. S. 1992, AJ, 103, 1107

van der Hulst, J. M., Skillman, E. D., Kennicutt, R. C., & Bothun, G. D. 1987, A&A, 177, 63

Weinberg, D. H., Szomoru, A., Guhathakurta, P., & van Gorkom, J. H. 1991, ApJ, 372, L13

CHAPTER II

STRUCTURAL CHARACTERISTICS AND STELLAR COMPOSITION OF LOW SURFACE BRIGHTNESS GALAXIES

Introduction

Low Surface Brightness (LSB) galaxies are an important but often neglected component of the general galaxy population. Severe selection effects cause them to be under-represented in galaxy catalogs, making it possible that they are a substantial or even numerically dominant population. This Chapter examines the basic structural properties of a sample of LSB galaxies, and the stellar populations of which they are composed.

That little data of this sort (e.g., Romanishin, Strom, & Strom 1983) exists for LSB galaxies is a logical consequence of their nature. With peak surface brightnesses $\mu_0 \geq 23$ mag arcsec^{-2} at or below the brightness of the night sky, they are not attractive targets for detailed study. The attainable signal to noise ratio is substantially less than that for brighter objects (Chapter 1) due to the dominance of noise from the background. Hence, even when identified in a galaxy catalog, they are unlikely to be selected for follow-up study.

The galaxies discussed here are drawn from either the UGC (Nilson 1973), or the lists of LSB galaxies compiled by Schombert & Bothun (1988) and Schombert et al. (1992). They are selected to have $\mu_0 \geq 23$ mag arcsec^{-2}, though a few turn out to have somewhat higher central surface brightnesses when measured with a linear detector. In addition, the sample selected for detailed photometric study was chosen to match that for which H II region spectroscopy was being obtained (Chapter 3). As a result, all the galaxies discussed here have H II regions. While there are many LSB galaxies which lack H II regions, a surprising number do have ongoing, sometimes substantial, star formation. For the present, it is important to be aware that this sample is not complete in any sense. Rather, it represents an attempt to examine the physical properties of some examples of a neglected class of galaxies.

Observations and Reductions

Images of 21 LSB galaxies were obtained through *UBVI* filters with the McGraw Hill 1.3 m telescope of the Michigan-Dartmouth-MIT Observatory in February 1991, November 1992, and January 1992. During the February 1991 observing session, a TI-4849 CCD (Luppino 1989) was employed as the camera. For the other runs, a Thomson CCD was used. Both of these devices gave essentially the same scale, 0.48 arcsec pixel^{-1} (Aldering 1990).

Initial reductions followed standard procedures, and were performed with IRAF. This involved bias and dark current subtraction, and flat fielding. For the Thomson CCD, the bias level for each frame was taken from the overscan region. The dark current of the Thomson CCD was fairly steady at $\sim$ 18 e^{-}hr^{-1}. Because of the many low level charge transfer traps apparent in long dark current measurements, this number was subtracted as a constant from each frame (rather than subtracting the cosmetically poor dark frame from which this number was derived). The traps were completely filled by counts from the sky in the broad band exposures. For the TI-4849, no record is kept of the overscan level, so a large number ($>$ 20) of bias frames were used to determine the zero level. Unlike the Thomson, this CCD exhibited structure in its dark current, including a large number of hot pixels and a low frequency wave pattern. These were removed by the subtraction of a dark frame which was the median of many, effectively removing cosmic rays.

Flat fields were determined from exposures of the twilight sky, or of mostly blank fields of the dark sky if time allowed. In general, the flat fields are determined to 0.1% in B, 0.2% in U and V, and 0.5% in I. A small residual gradient is present in the I, but neither CCD suffers from fringing. Typical exposure times were 3600 seconds in U, 1800 in B, and 900 in V and I. The resulting images are presented in Appendix A.

The data were calibrated with observations of standard stars from the lists of Landolt (1973, 1983). The extinction coefficients for the November 1991 observing run were found to depart noticeably from the average values for Kitt Peak, consistent with the values reported by Pilachowski et al. (1991) which resulted from the eruption of Mt. Pinatubo. These were assumed to apply to the January 1992 data as well, as bad weather prevented acquisition of enough calibration data to accurately measure the extinction coefficients. Sufficient data was obtained to determine the zero point during photometric periods; these are accurate to ~ 0.05 mag. The color solutions from the two runs using the same filters and detector are identical within the errors. Colors are accurate to ~ 0.03 mag.

Analysis and Results

Surface photometry was performed on the images following the methods described by Bothun et al. (1986). If necessary, bulge and disk components were deconvolved from the the surface brightness profile using the procedure outlined by Schombert & Bothun (1987). Most, though certainly not all, of these galaxies lack significant bulge components. If possible, an exponential profile of the form

$$\mu = \mu_0 + 1.086 \times \frac{r}{\alpha} \tag{2.1}$$

was fit to the disk component (de Vaucoulers 1959). This generally provides an adequate description of the radial distribution of the light in LSB galaxies, with structures like spiral arms being weak if present. Occasionally such features dominate the surface brightness profile, making an exponential fit impossible, but this is rare.

The radial surface brightness distributions and exponential fits are presented in Figure 2.1. The structural parameters (μ_0, α) derived from the fits are listed in Table 2.1, together with information derived from them. Column 1 contains the name of the galaxy. Those objects starting with 'F' are from the lists of Schombert & Bothun (1988) or Schombert et al. (1992), while those designated by 'U' are from the UGC. UGC 12695 has two entires, corresponding to the two acceptable fits. Column 2 gives the major axis diameter at the 25 mag arcsec^{-2} level (in arcseconds). Columns 3 and 4 give the fit parameters α and μ_0. The former is in arcseconds (accurate to $\sim 1''$), and the latter in B mag arcsec^{-2} (accurate to $\sim$ 0.1 mag) corrected for galactic extinction (Burstein & Heiles 1984). Column 5 is the scale length in kpc for the adopted distance (Column 9). The sixth and seventh columns list the apparent B magnitudes as measured within the 25 mag arcsec^{-2} isophote (Column 6) and by the integration of the exponential profile (Column 7 – see below). Column 8 is the absolute magnitude for the apparent magnitude in Column 7 and the distance in Column 9. All magnitudes have been corrected for extinction within our own galaxy, as with μ_0. The distances in Column 9 are derived from the recession velocity assuming $H_0 = 100\ \mathrm{km\,s^{-1}Mpc^{-1}}$, $D_{Virgo} = 13.7$ Mpc, and a Virgocentric infall velocity of 300 km s^{-1}. For those objects with $cz < 3000\ \mathrm{km\,s^{-1}}$, the distance was found by interpolating through Table 3 of Aaronson et al. (1982). These distances provide a basis for the comparison of absolute quantities.

It is clear from Figure 2.1 that the majority of LSB galaxies are well fit by exponential profiles. We will adopt this model as standard and discuss LSB galaxies in terms of it. All "total" quantities in Table 2.1 refer to the disk component *only*.

The total magnitude B_T is derived from the integration of equation (2.1), which

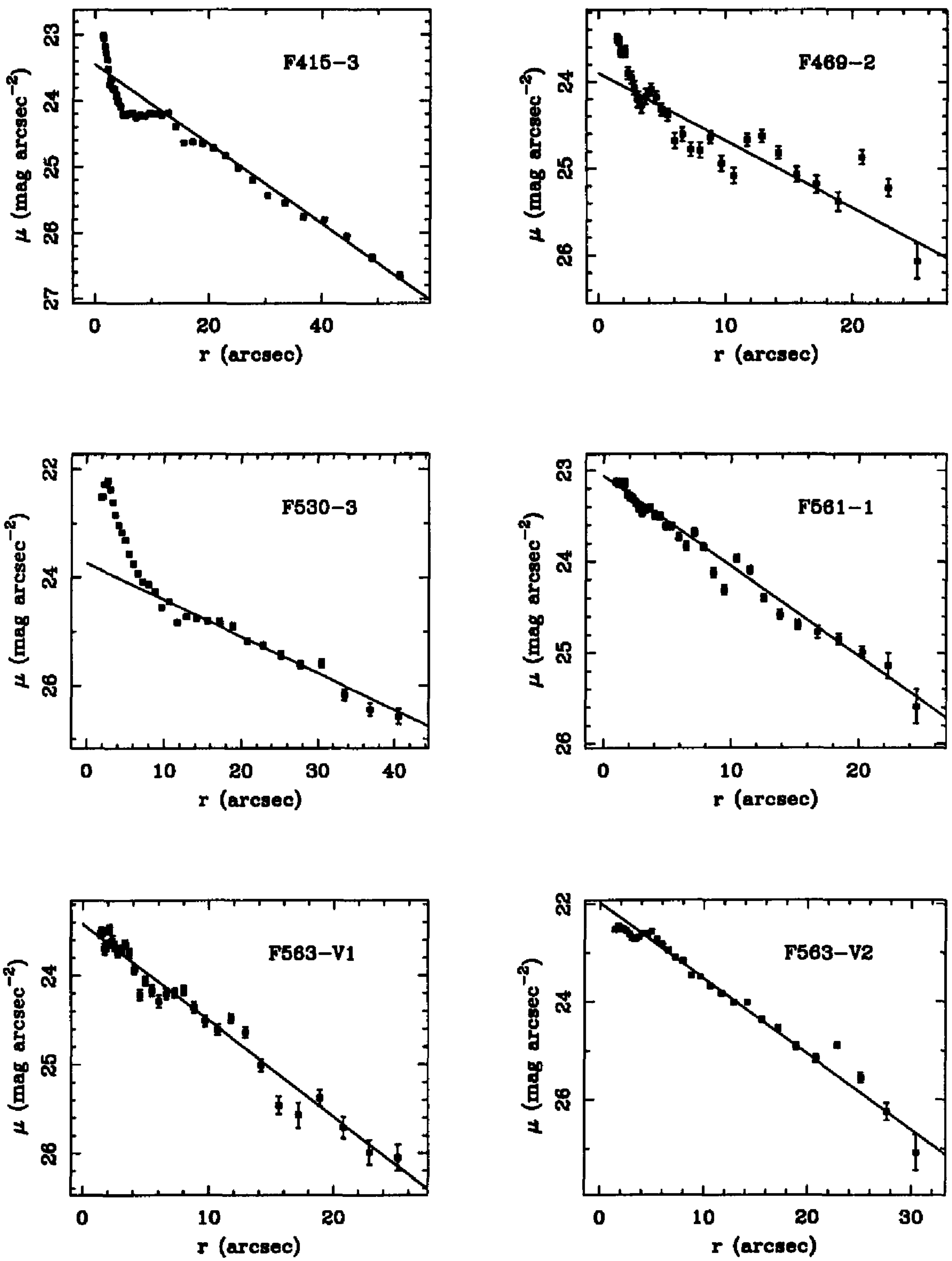

Figure 2.1 — The *B* radial surface brightness profiles of LSB galaxies (squares), together with exponential fits to the disk components (lines). The abscissa is the radius along the major axis.

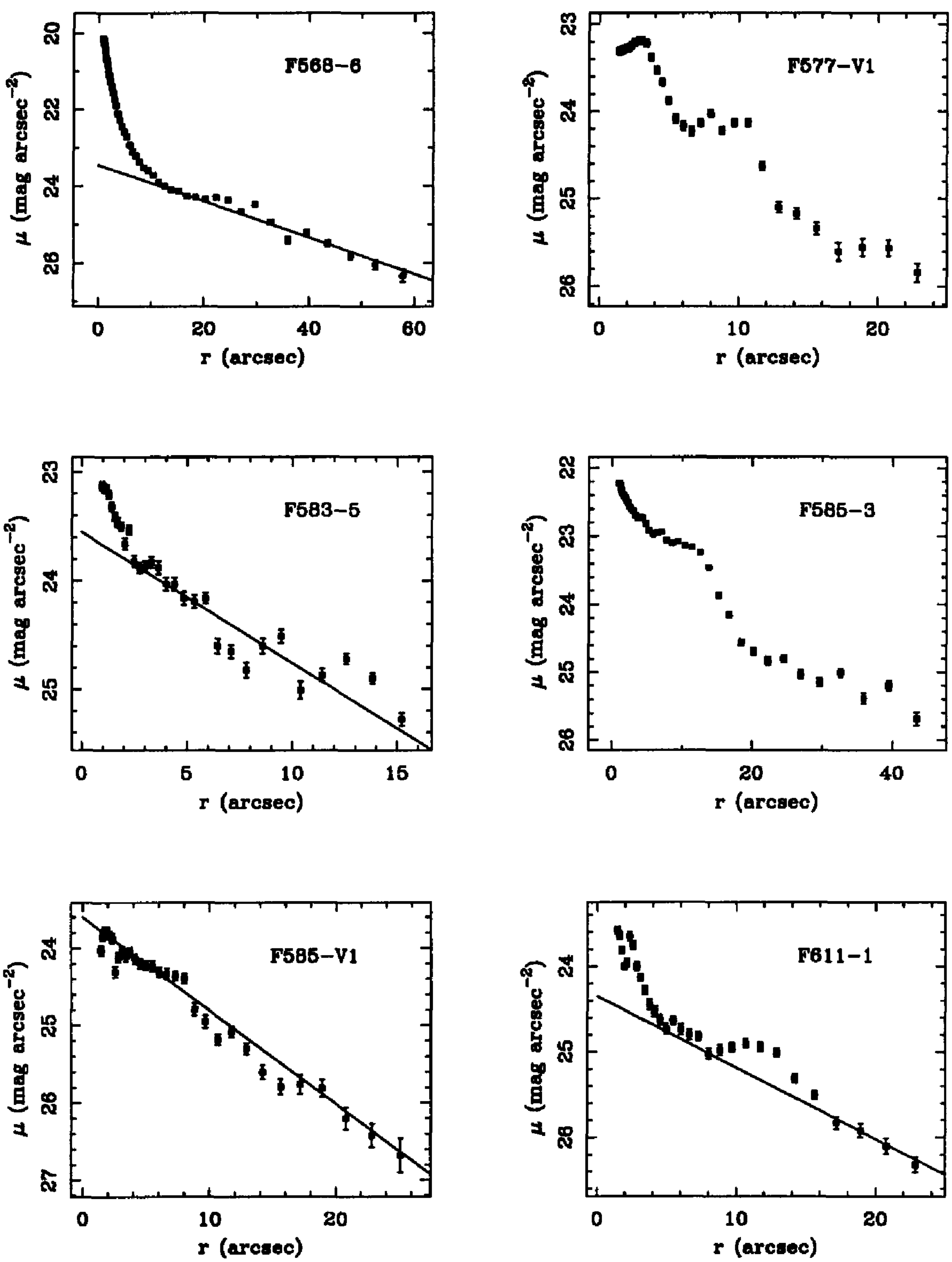

Figure 2.1 — *continued.* The profile of F568–6 is in good agreement with that reported by Bothun et al. (1990). F577–V1 and F585–3 are not well fit by exponential profiles.

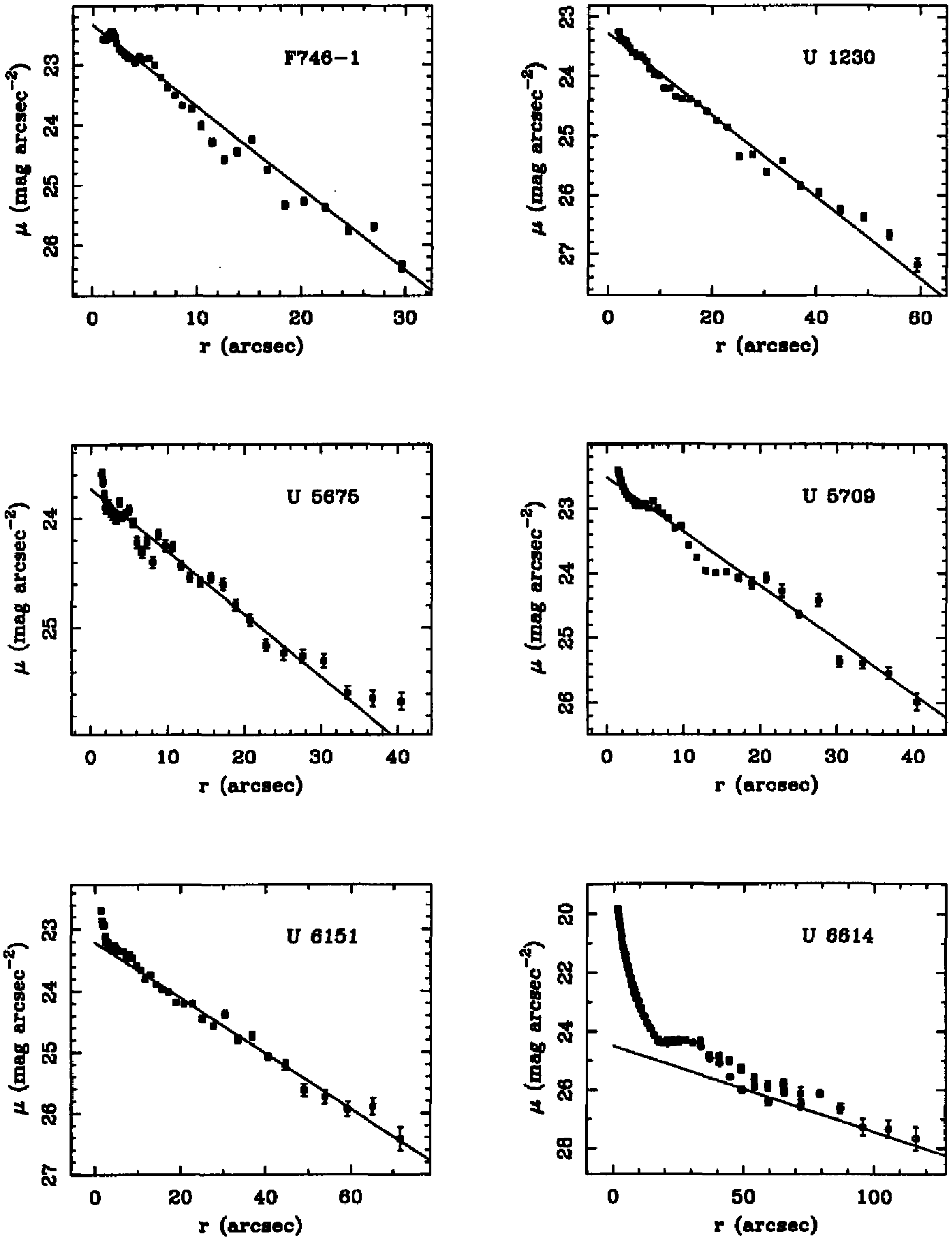

Figure 2.1 — *continued.* The surface brightness profile of UGC 6614 is in good agreement with that obtained with the OREAD (Aldering & Bothun 1991) focal reducing camera (open circles). Because of the dominance of the bulge at small radii, only points with $r > 50''$ are included in the fit to the exponential disk.

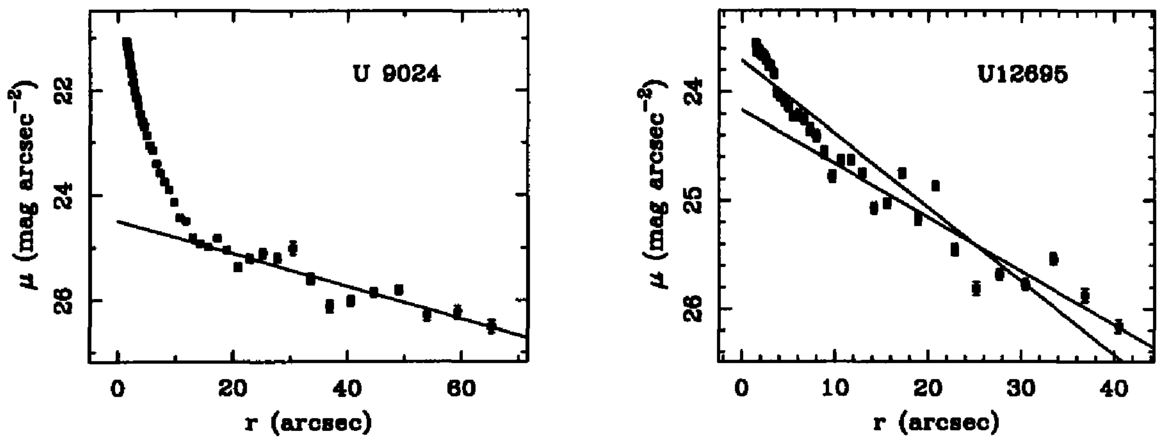

Figure 2.1 — *continued.* UGC 12695 is acceptably fit by two profiles, the one with the lower central surface brightness perhaps being consistent with the presence of a short scale length thick disk or exponential "bulge" component.

can be written in linear units as

$$\Sigma(r) = \Sigma_0 \, e^{-r/\alpha}. \tag{2.2}$$

The total luminosity of a galaxy described by such a surface luminosity distribution is simply

$$L = \int \Sigma(r) \, dA. \tag{2.3}$$

In polar coordinates, the element of integration $dA = r\,dr\,d\theta$, giving

$$L = \Sigma_0 \int_0^{2\pi} d\theta \int_0^{\infty} e^{-r/\alpha} r \, dr, \tag{2.4}$$

which can be integrated by parts to obtain

$$L = 2\pi\alpha^2 \Sigma_0. \tag{2.5}$$

While integrating the radial profile to infinity may seem inappropriate, no deviation from an exponential profile is observed in LSB galaxies for as many as three scale lengths. Integrating equation (2.4) to 3α shows that 80% of the light is contained within this radius, so the integration to infinity is not a great overestimate. Indeed, it is important to use the total magnitude obtained in this fashion for a fair comparison to HSB galaxies. Obviously, isophotal magnitudes will underestimate the luminosity

Table 2.1 — Structural Parameters

Galaxy	d_{25}	α ($''$)	μ_0	α (kpc)	B_{25}	B_T	M_T^B	D (Mpc)
F415–3	50	18	23.16	1.2	16.91	14.88	–15.86	14
F469–2	43	14	23.69	2.9	18.29	15.95	–16.77	35
F530–3	39	16	23.28	3.7	16.64	15.26	–18.15	48
F561–1	41	11	22.96	2.6	16.50	15.75	–17.65	48
F563–V1	28	10	23.37	1.9	17.75	16.37	–16.60	39
F563–V2	46	7	21.95	1.6	16.48	15.72	–17.59	46
F568–6	66	23	23.38	15.8	15.28	14.57	–21.17	141
F577–V1	25	...	...	...	18.49	...	...	81
F583–5	28	9	23.48	1.4	18.53	16.70	–15.85	33
F585–3	54	...	...	...	16.62	...	...	31
F585–V1	20	9	23.40	1.1	18.40	16.62	–15.33	25
F611–1	26	13	24.24	1.5	18.39	16.67	–15.14	23
F746–1	35	8	22.18	3.0	17.54	15.66	–18.80	78
U 1230	47	16	22.88	3.0	16.20	14.85	–18.06	38
U 5675	43	19	23.70	1.5	17.47	15.30	–15.73	16
U 5709	59	13	22.49	4.1	15.97	14.92	–19.15	65
U 6151	79	24	23.21	2.1	14.90	14.30	–16.92	18
U 6614	89	37	24.28	11.9	14.48	14.43	–19.67	67
U 9024	37	35	24.47	5.6	16.67	14.74	–17.84	33
U12695	43	16	23.56	4.6	17.95	15.53	–18.30	59
"	"	22	24.02	6.3	"	15.30	–18.53	"

of LSB galaxies relative to HSB galaxies simply because the same isophote includes a much smaller fraction of the profile of the LSB galaxy. (A galaxy with a central surface brightness lower than the chosen isophote would have no measured brightness at all!) The severity of the deficit in isophotal magnitudes for these galaxies is shown in Figure 2.2.

Table 2.2 contains the colors for those galaxies observed through all four filters. Each color has three entries. The first is the color of the nucleus as measured through a small (10$''$) aperture. The second is the luminosity weighted color, i.e., the color measured through a large isophotal aperture. This is most appropriate for comparison to data in the literature for which no decomposition of the bulge and disk components has been made. The third entry is the area weighted color, as determined from the average of the rings in the differential color profile, or from the average of a grid of

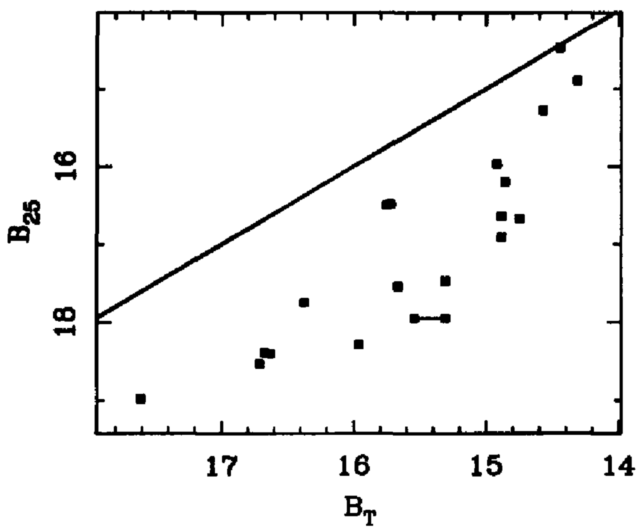

Figure 2.2 — The deficit in brightness measured by the light within the $\mu = 25$ mag arcsec^{-2} isophote and that from the integration of the exponential profile. Note that B_{25} substantially underestimates the total flux (by a factor of ~ 4 in most cases). The isophotal magnitude falls well below the line of equality despite including light from any bulge component which is *not* included in the exponential fit. The isophotal diameters d_{25} are similarly inadequate measures of the sizes of LSB disks. The points connected by a line represent the two fits for UGC 12695.

square apertures covering the galaxy ("two color mapping," Bothun 1986). Sometimes the signal in the I band was too weak for this subdivision to be successful, so only the large aperture color is given for $V - I$. The luminosity and area weighting procedures give generally similar results, since these systems have bulges which are either very weak or entirely dominant over the observed area. In galaxies which have very bright H II regions (e.g., UGC 12695), the area weighted colors will be more representative of the general disk population, while the luminosity weighted colors will be skewed towards those of the H II regions. These can have peculiar colors because of the complex, rapidly evolving population of massive stars (Campbell & Terlevich 1984, McGaugh 1991), and because of emission line contamination (Salzer et al. 1991). However, this is not generally a concern in this sample, as the H II regions usually do not produce a large fraction of the total luminosity.

Due to bad weather, some galaxies were not observed through all filters. An effort was made to observe all galaxies over as long a spectral baseline as reasonable, so

Table 2.2 — LSB Colors

Galaxy	$B-V$ *nuc*	$B-V$ *lum*	$B-V$ *area*	$U-B$ *nuc*	$U-B$ *lum*	$U-B$ *area*	$V-I$ *nuc*	$V-I$ *lum*	$V-I$ *area*
F415–3	0.37	0.46	0.52	–0.47	–0.26	–0.12	0.68	0.71	...
F469–2	0.48	0.38	0.43	–0.42	–0.33	–0.44	0.60	0.94	...
F530–3	0.67	0.67	0.64	–0.07	–0.07	0.04	0.83	0.85	...
F561–1	0.64	0.41	0.44	0.03	–0.13	–0.12	0.88	0.72	0.71
F563–V1	0.14	0.29	0.31	...	...	...	1.19	1.32	1.28
F563–V2	0.54	0.51	0.36	0.04	–0.12	0.02	1.10	1.01	1.21
F577–V1	0.44	0.35	0.37	–0.20	–0.52	–0.31	1.08	1.07	1.08
F611–1	0.34	0.39	0.44	–0.47	–0.24	–0.24	0.84	1.00	...
F746–1	0.60	0.62	0.65	–0.30	–0.35	–0.35	0.70	0.73	...
U 1230	0.62	0.45	0.42	–0.05	–0.19	–0.18	0.81	0.62	0.56
U 5709	0.83	0.47	0.48	0.13	0.03	0.04	1.34	1.31	1.35
U 6151	0.51	0.51	0.51	–0.02	–0.09	–0.07	1.08	0.90	0.89
U 6614	1.01	0.72	0.53	0.39	0.25	0.32	1.53	1.60	1.72
U12695	0.43	0.26	0.37	–0.19	–0.11	–0.17	0.82	0.95	...

Table 2.3 — $B-I$ Colors

Galaxy	$B-I$ *nuc*	$B-I$ *lum*	$B-I$ *area*
F568-6	2.77	2.36	2.26
F583-5	1.28	1.33	...
F585-3	1.32	1.44	1.44
U 5675	1.77	1.82	1.80
U 9024	1.51	1.25	1.18

at least B and I were obtained. Table 2.3 lists the $B-I$ colors of those galaxies for which photometric data were obtained only in these bands. As before, nuclear, luminosity weighted, and area weighted colors are given.

Discussion

Structure and Luminosity

LSB galaxies are well described as exponential disks. Figure 2.3 shows the histograms of the structural parameters (μ_0, α) for this sample. The typical (median) values are $\mu_0 = 23.4$ mag arcsec^{-2} and $\alpha = 2.5$ kpc. This central surface brightness is nearly 6σ from the "universal" value of $\mu_0 = 21.65 \pm 0.3$ (Freeman 1970). It is also two thirds of a magnitude fainter than the average of the Romanishin et al. (1983) sample. That such remarkably LSB disks exist but have gone largely unrecognized highlights the importance of selection effects which discriminate against stellar systems of low surface brightness (e.g., Disney 1976).

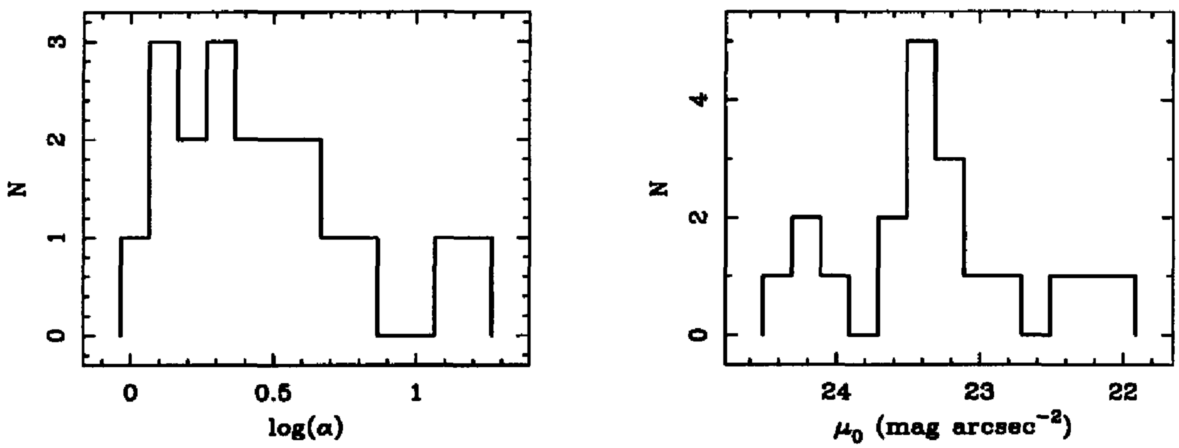

Figure 2.3 — Histograms of the structural parameters α (in kpc, left panel) and μ_0 (right panel). Note that there is no preferred value of either.

Even more remarkable than the low median surface brightnesses of these disks is that there is no preferred value of either μ_0 or α. There is a statistically insignificant peak in the μ_0 histogram due to selection effects. Objects with $\mu_0 < 23$ mag arcsec^{-2} are rare by definition of the sample, while those with $\mu_0 > 24$ mag arcsec^{-2} are obviously more difficult to identify and study in detail. Nonetheless, objects with central surface brightnesses as low as $\mu_0 \approx 24.5$ mag arcsec^{-2} are present in the sample, and objects with $\mu_0 > 26$ mag arcsec^{-2} are known to exist (e.g., Bothun, Impey, & Malin 1991).

Furthermore, the scale length distribution is very broad. Smaller objects are more common than large ones (as expected from any reasonable intrinsic distribution), but both are present. It is a common misconception that LSB galaxies are dwarf galaxies, but the median scale length of 2.5 kpc is indistinguishable from that of HSB disks (for the adopted distance scale). Thus we corroborate the result of Romanishin et al. (1983) that the sizes of LSB disks overlap those of HSB disks, and indeed Figure 2.3 shows that the range of LSB disk sizes exceeds that of HSB disks at both ends. That is, the sample contains both true dwarfs and true giants like the Malin 1 (Bothun et al. 1987) cousins F568–6 and UGC 6614 whose scale lengths exceed 10 kpc. Note that since we have adopted a short distance scale, any alteration in this only makes these objects more enormous.

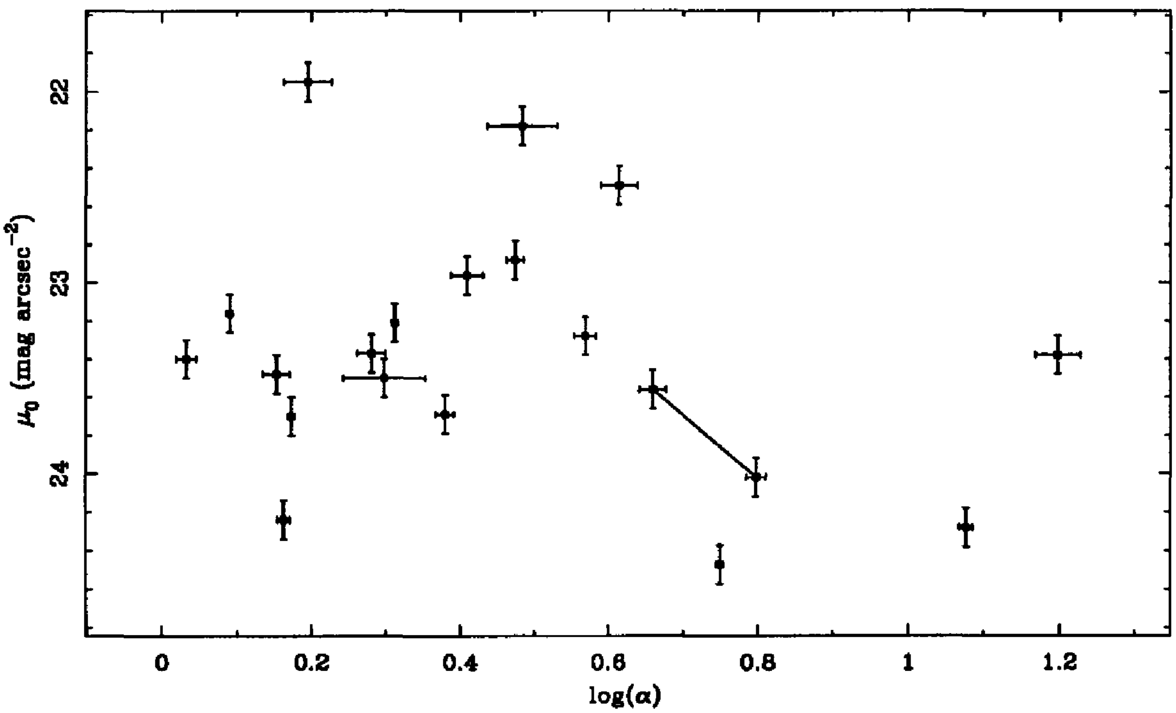

Figure 2.4 — The structural parameters (μ_0, α) plotted against one another. Objects cover a wide range in both, with no apparent correlation. The line connects the two acceptable fits for UGC 12695.

Moreover, there is no correlation between the structural parameters α and μ_0 (Figure 2.4). While the sample is too incomplete for this to be a firm conclusion (much less derive the $n(\mu_0, \alpha)$ distribution!), it is consistent with other studies (Impey, Bothun, & Malin 1988; Davies et al. 1988; Irwin et al. 1990; Bothun et al. 1991) which find that galaxies occupy *all* of observable parameter space. At the least, it is clear that disk galaxies do exist over a very large range of both scale length and central surface brightness. Selection effects resulting from the brightness of the night sky strongly limit our knowledge of the physical properties and space density of objects over much of this range.

The same situation applies for the luminosity of these disks. Despite being low in surface brightness, their integrated magnitudes can be quite bright. This is shown in Figure 2.5. The large disks have large total luminosities (and also tend to have prominent bulges, though this contribution is not included). Again, the range of both luminosity and stellar surface density greatly exceeds that exhibited by the HSB disks favored by selection effects with no preferred value and no apparent correlation. While there is a modest positive trend, we note that this is induced by the calculation of M_T from both α *and* μ_0 in equation (2.5). Though excluded by choice from this sample, there are many examples of HSB dwarf galaxies (which would occupy the upper left region of Figure 2.5), while the disk of Malin 1 would fall well below the lower right corner (Impey & Bothun 1989). Since large HSB galaxies should be quite prominent, there is (if anything) a tendency for the largest scale length disks to be low in surface density. The lack of correlations contradict the theoretical predictions of Dekel & Silk (1986), and the observed distribution in Figure 2.5 bears no resemblance to their model for the formation of LSB galaxies.

Just as there are no correlations between structural parameters, none is evident between them and color. Figure 2.6 shows this for $B - I$ and α and μ_0, but it holds true for all colors and luminosity as well. Thus the well established color–luminosity relations break down when galaxies with lower surface luminosity densities are examined (though we note that the two very large objects have similar colors). While this break down is remarkable (and is another indication of the extent to which selection effects can affect our appraisal of galaxies as physical objects), an even more

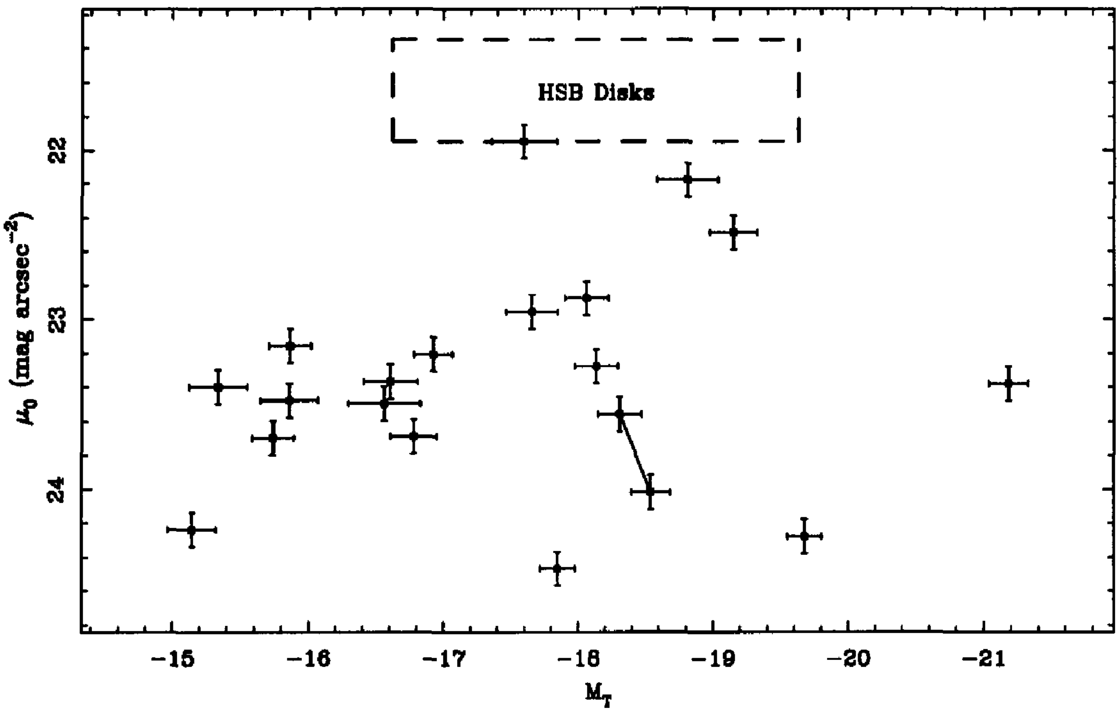

Figure 2.5 — The central surface brightness plotted against the absolute magnitude of the disk component. Again, no correlation is apparent, and LSB galaxies cover an enormous range in both. For comparison, the area occupied by disk galaxies within 1σ of the Freeman (1970) value $\mu_0 = 21.65 \pm 0.3$ mag arcsec^{-2} and with a generous range of scale lengths $1 \le \alpha \le 4$ kpc is enclosed by dashed lines. As in previous figures, the solid line connects the two plausible values for UGC 12695.

remarkable aspect of Figure 2.6 is that LSB galaxies are very blue (a typical, actively star forming HSB disk has $B - I > 1.8$, but very few LSB disks are this "red"). It is difficult to understand the stellar composition of LSB galaxies which lead to these very blue colors.

Stellar Content

The observed blue colors of LSB galaxies immediately rules out the most obvious possibility for their star formation history. That is, these are *not* HSB disks which have simply faded after the cessation of star formation. If this were the case, the galaxies would become progressively more red as their stellar populations evolve. For a normal stellar mass spectrum (i.e., the IMF), $B - V$ will redden by 0.25 mag for every 1 mag of fading in μ_B. That there is no such trend of color with surface

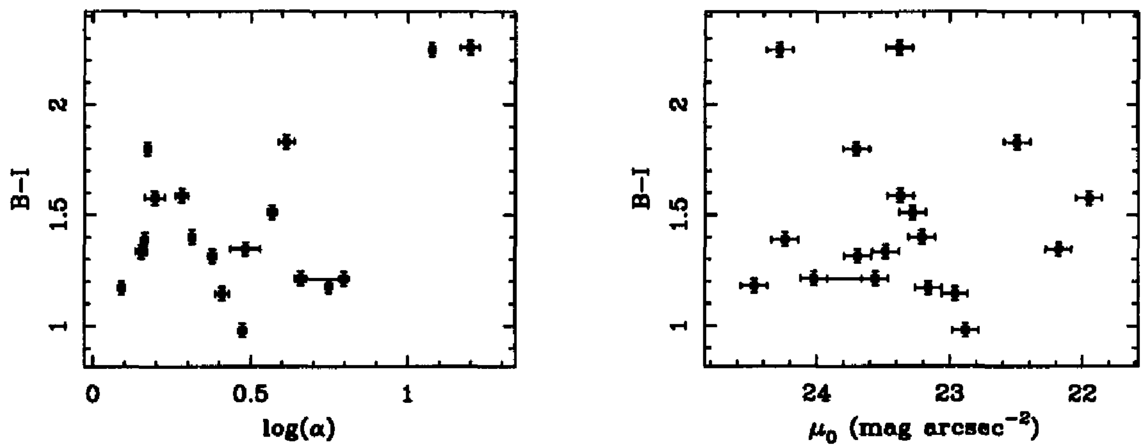

Figure 2.6 — $B-I$ vs. α and μ_0. No correlation exists between this (or any other) color and any structural parameter. Note also that the majority of LSB galaxies are quite blue, with $B-I<1.8$, a typical value for actively star forming HSB disks.

brightness in Figure 2.6 completely rules out this possibility.

Another simple star formation history which approximately matches the observed properties of LSB galaxies is one with a low, constant star formation rate (SFR). A disk galaxy with scale length $\alpha = 2.5$ kpc and $SFR = 0.1\,L_{\odot}\mathrm{yr}^{-1}$ will, after 10^{10}yr, have a luminosity $L_B = 10^9 L_{\odot}$ and central surface brightness $\mu_0 = 23.5$, numbers which are not unreasonable for this sample. The median colors for galaxies in Table 2.2 are $B-V=0.44$, $U-B=-0.12$, and $V-I=0.95$. This $B-V$ and $U-B$ are not far different from that predicted by the constant star formation rate model of Larson & Tinsley (1978).

However, the real situation cannot be this simple. While the time averaged SFR may be $\sim 0.1\,L_{\odot}\mathrm{yr}^{-1}$, it does not necessarily follow that there has been a constant rate of conversion of *mass* into stars. Worse, the models of Larson & Tinsley (1978) are solar metallicity, while these LSB galaxies are substantially subsolar ($Z < 30\%\ Z_{\odot}$, Chapter 3). Thus they would almost certainly *not* correctly predict $V-I$, and the crude agreement with the other colors must be coincidental. In comparison, the HSB galaxies to which these models were meant to apply have knots of star formation over the entirety of their disks (certainly not the case for LSB galaxies!), and have typical colors of $B - V = 0.46$, $U - B = -0.23$, and $V - I = 1.4$.

Other models have been constructed since the work of Larson & Tinsley (1978), but tend also to be of solar metallicity. Those of Buzzoni (1989) and Olofsson (1989) do address low metallicity systems, but Buzzoni (1989) presents only single generation populations, while Olofsson (1989) is concerned with the rapidly evolving star burst populations of blue compact galaxies. The models of Buzzoni (1989) do imply that $V - I$ should be a reasonable metallicity indicator, but this is likely to be complicated when a spread of ages is present.

Though there is a lack of appropriate models, we can make an empirical comparison. Low metallicity globular clusters have integrated colors which are roughly $B - V \approx 0.65$, $U - B \approx 0.1$, and $V - I \approx 0.95$ (Reed 1985). This is a good match to $V - I$ for LSB galaxies, but is too red in the other colors. This suggests the possibility that LSB galaxies possess an old population similar to that of the metal poor globular clusters which dominates $V - I$, but that $B - V$ and $U - B$ have contributions from more recent, perhaps sporadic, star formation.

Again, however, this is likely to be overly simplistic. Since the disks of LSB galaxies are not dominated by star formation in a fashion similar to HSB disks, it seems wrong to simply ascribe their $U - B$ and $B - V$ colors to star formation, and their $V - I$ colors to low metallicity. Moreover, as with the structural parameters, it is not fair to consider the median colors to be typical. Though mostly all blue, LSB galaxies do cover a wide range in color, and there are no correlations among the colors (Figure 2.7). There is a slight tendency for objects which are most blue in $B - V$ to also be blue in $U - B$, but if anything, those galaxies tend to be relatively red in $V - I$. On the whole, these must be considered scatter diagrams, indicating a broad range of mean stellar ages and metallicities. This is inconsistent with any single, simple scenario adequately describing the entire sample. Rather, it indicates a rich variety of star formation histories.

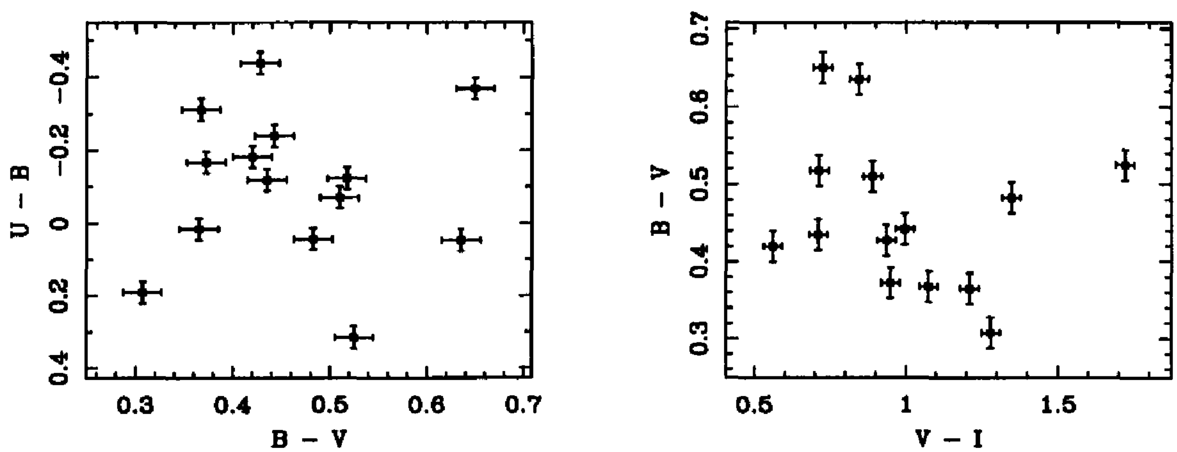

Figure 2.7 — $U-B$ vs. $B-V$ (left panel) and $B-V$ vs. $V-I$ (right panel). The area weighted colors are used when available; luminosity weighted colors are used when not. Though mostly blue, LSB disks do cover a wide range of color. As with the structural parameters, no correlations are evident. The centroid of the $(U-B, B-V)$ colors is near the color of the latest Hubble types, and the scatter fills the entire range between the outer envelopes of extreme star formation histories of the models of Larson & Tinsley (1978).

Indeed, it is difficult to be more precise than this with only broad band colors. For the composite, unresolved populations in galaxies, the interpretations of the colors can be ambiguous. Colors are sensitive to both the mean age and the shape of the age distribution, with blue colors generally indicating young ages. Also, low metallicity can cause blue colors as well, through changes in both line blanketing and the positions of the main sequence (Maeder 1990) and giant branch (Bothun, Romanishin, Strom, & Strom 1984). Nonetheless, $B-V$ should be more sensitive to mean age, while $V-I$ will be sensitive to both the position of the giant branch (metallicity) and its degree of development (age). $U-B$ will be sensitive to both metallicity and the presence of hot, very young stars. Fortunately, we are not restricted to the broad band colors, and know that the metallicity in the gas, and presumably in the stars, is low (Chapter 3). Given the colors of metal poor globular clusters, it seems unlikely that low metallicity alone is sufficient to explain the blue colors of LSB galaxies.

While an old, metal poor population is likely to exist in most of these galaxies, the complex star formation histories do seem to be weighted towards young populations.

That $U - B < 0$ in most cases immediately implies that substantial star formation has occurred in the last 10^8yr (Larson & Tinsley 1978), consistent with the presence of H II regions (which live $\sim 10^7$yr). The median colors are remarkably blue for composite stellar populations, and *some* LSB galaxies are *extremely* blue. It follows that these may have a very young mean age, as was recently argued to be the case for the H I cloud in Virgo (Salzer et al. 1991), a typical LSB galaxy by the standards of this sample.

Another possibility is that the IMF is somehow different in these galaxies (Schombert et al. 1990). This is *not* inferred from the H II region observations (Chapter 3), but neither is it ruled out. The time flattening IMF model of Arimoto & Tarrab (1990) approximately matches the median LSB colors, but not the very blue ones. It is in principle possible to match nearly any observation if sufficient violence is done to the IMF (von Hippel & Bothun 1990), so we prefer to seek other possibilities first. The model which best fits the very blue LSB galaxies is that of Katz (1992). This is for disks early in their evolution (corresponding to HSB spirals at redshifts of ~ 1 to 2), so the hypothesis of a young mean age is favored.

Individual Cases

In what follows, we discuss some interesting individual cases. These are the more extreme objects, and the individual interpretations do not necessarily apply to the whole sample. It should be kept in mind that the sample does contain objects with old populations, though some of the following galaxies may not.

F415–3

F415–3 is a small ($\alpha = 1.2$ kpc), amorphous galaxy with a bright H II region near the center and very low surface brightness plumes (Figure 2.A.1). It has $(B-V)_A = 0.52$, which is blue but not excessively so. However, $(V-I)_L = 0.71$, which is remarkable – this is approximately a quarter magnitude more blue than the most extreme stellar systems known (e.g., metal poor globular clusters). F415–3 is metal poor, but not as metal poor as the most extreme globular clusters (Chapter 3). Nor is $V-I$ dominated by current regions of star formation, which are not prominent in these filters. Hence this extreme $V-I$ seems to indicate a feebly developed giant branch, a situation which could occur if star formation has commenced only recently (within the last several Gyr) so that only a limited range of ages are contributing stars to the giant branch (i.e., the giant to dwarf ratio is lower than in "normal," constant SFR disks in which many generations are contributing to the giant branch). This is consistent with the morphology, which aside from the blue star forming knots, is similar in all filters, as expected if all the light is being produced by a young population which is not segregated dynamically.

F561–1

F561–1 is a normal sized ($\alpha = 2.6$ kpc) galaxy with a one arm spiral pattern (Figure 2.A.5) and purely exponential profile (Figure 2.1). It is also very blue in $V-I$ for its $B-V$, with $(B-V)_A = 0.44, (V-I)_A = 0.71$. This again suggests a deficiency of giants, and a relatively young age. Unlike F415–3, there is a small but clear color gradient ($(B-V)_{nuc} = 0.64$, $(V-I)_{nuc} = 0.88$), suggesting that star formation has propagated slowly outwards since its ignition, or that it has been more severely inhibited in the outer regions.

F563–V1

This is an amorphous, extremely metal poor galaxy (Chapter 3). The light distribution is identical in each filter (Figure 2.A.6), suggesting that it is produced by a homogeneous population. It is very blue in $B-V$, with $(B-V)_A = 0.31$, but relatively red in $U-B$ (≈ 0.1), consistent with a single burst $\approx 2 \times 10^8$yr ago. $V-I$ is also relatively red in this case, with $(V-I)_A = 1.28$. This is expected for ages less than one Gyr, as the AGB rather than RGB dominates at these young ages (Renzini

& Buzzoni 1986). Moreover, the low metallicity of this galaxy can be produced in a very short time by a single burst (Kunth & Sargent 1986).

F577–V1

This galaxy is not well fit by an exponential profile (Figure 2.1). It has a blue central bar and an outer ring dominated by star forming knots (Figure 2.A.11). The area weighted colors are all quite blue, with $(U-B)_A = -0.31$, $(B-V)_A = 0.37$, and $(V-I)_A = 1.08$. While the central bar may have a mean age as high as 5 Gyr, the rest of the galaxy is likely to be less than a Gyr old, with the star forming knots of course being very young ($< 10^7$yr or so).

UGC 1230

Like F561–1, UGC 1230 has a modest color gradient (Figure 2.A.16) in a purely exponential disk (Figure 2.1). It is extraordinarily blue for a stellar system, with $(V-I)_A = 0.56$. As such it the best example of a galaxy with a young, underdeveloped giant branch. It is also quite metal poor (Chapter 3), indicating that there has been little total star formation over its lifetime, limiting the mass of any ancient population which has faded to undetectablity unless it had a peculiar IMF or efficiently ejected metals (unlikely given the large ($\alpha = 3$ kpc) disk.)

UGC 12695

UGC 12695 has a chaotic morphology with many prominent regions of star formation (Figure 2.A.17). These appear to have evolved on the expected short time scales (a few $\times 10^7$yr) over a substantial portion of the galaxy. Aside from these star forming knots, the light distribution is similar in each filter, and the total colors are quite blue: $(U-B)_A = -0.17$, $(B-V)_A = 0.37$, and $(V-I)_L = 0.95$. Star formation seems to have ignited and propagated across the disk of this galaxy only recently, probably within the last few $\times 10^8$yr judging from the color, morphology and low metallicity (Chapter 3).

UGC 9024

UGC 9024 is another extremely blue galaxy with an underdeveloped giant branch and low mean age. The large ($\alpha = 5.6$ kpc), very low surface brightness disk ($\mu_0 = 24.47$) has $(B-I)_A = 1.18$, which means that $V-I$ is very blue unless $B-V$ is *extremely* blue ($B-V < 0.2$). Even the bulge component is relatively blue, with $(B-I)_{nuc} = 1.51$ — a typical bulge has $B-I \approx 2.3$.

These are some of the more extreme examples of a family of galaxies which is typically quite blue in all colors. While a weakly populated giant branch and young mean age are the most plausible interpretation for this, other interpretations are plausible. In particular, it is difficult to rule out the presence of an old, faded population, though its mass is constrained by the need to prevent an overpopulation of giants and the overproduction of metals. Note that such a population is likely to exist in the less extreme objects which were not discussed individually. Also, it is conceivable that a peculiar IMF is responsible for the blue colors, though this would not really alter the argument in favor of youth insofar as the most obvious alteration to the IMF would be one biased towards massive, blue stars, which are short lived.

In galaxies with amorphous or fairly regular structure (many galaxies exhibit well organized spiral structure despite their low surface densities), star formation must be spread in time at least enough for the star formation knots to diffuse into the smooth distribution. This will occur on epicyclic time scales, and should not pose a problem in most cases. Indeed, the young object UGC 12695 seems to be dominated by knots which have not completely diffused. However, F563–V1 shows little structure despite apparent youth. It is possible that star formation in these low surface densitiy environments occurs in an intrinsically diffuse way, and the stars are born spread apart. This may follow from the nonlinearity of the star formation law near a critical gas density (Kennicutt 1989), and the lack of molecular gas in some of these galaxies (Schombert et al. 1990): star formation may proceed in a fundamentally different manner than in HSB galaxies, without the presence of giant molecular clouds.

That LSB galaxies are observed to be low in gas surface density (Chapter 4) supports the notion that the H I surface density controls the evolutionary rate of disk galaxies (van der Hulst et al. 1987). That these galaxies appear to be young confirms that low surface density disks can remain quiescent for as long as a Hubble time (Bothun et al. 1990). It further suggests that the dissipative formation of these very extended, tenuous disks must have proceeded gradually without violent star formation or disruption by neighboring systems.

If this is the case, and these objects are relatively young, then where are the true protogalaxies which have not yet begun to form stars? Unless we live at a favored cosmological time, it follows that these should exist. That they have so far gone undetected by H I surveys (e.g., Weinberg et al. 1991) may be a natural consequence of the requirement that the gas be low surface density in order to postpone star formation, thus making them subject to the same sort of selection effects which act against optically low surface brightness objects.

Conclusions

We have presented broad band observations of a sample of low surface brightness galaxies. We find that these objects are well fit by the standard exponential disk model, and that often their surface brightness profiles are purely exponential. These galaxies have no preferred value of either scale length or central surface brightness. The median scale length (2.5 kpc) is indistinguishable from that of "normal" high surface brightness disks (i.e., these are *not* dwarf galaxies), despite the median central surface brightness (23.4 mag arcsec^{-2}) being nearly 6σ below the canonical Freeman (1970) value.

Furthermore, there are no correlations between the structural parameters μ_0 and

α, and these LSB galaxies cover a much larger region in the (μ_0, M_T) plane than do HSB disks. This extends to both high and low luminosity, since both small and very large scale length objects exist. Also, there are no correlations between color and luminosity or structure as is found in samples restricted to HSB galaxies. That LSB galaxies cover such a wide range in these parameters indicates that there are many evolutionary paths which do not lead to the Hubble sequence. It also makes it clear that the selection effects imposed by the arbitrary level of the night sky brightness severely impairs our knowledge of the intrinsic $n(\mu_0, \alpha)$ distribution.

LSB galaxies are observed to be very blue, with median colors $B-V = 0.44$, $U-B = -0.12$, and $V-I = 0.95$. The spread in colors is large, generally indicating complex star formation histories. *Some* LSB galaxies are *extremely* blue. These are most plausibly interpreted as being young objects with sparsely populated giant branches. We caution, however, that it is difficult to be confident of this interpretation. While other obvious possibilities (e.g., a variable IMF) are less satisfactory, these very blue colors may, like the structural parameters, just be another indication of the extent of our ignorance about stellar systems.

APPENDIX II.A
UBVI IMAGES

This Appendix contains broad band images of the low surface brightness galaxies discussed in the text. These images form the data set discussed in Chapter 2. All images were obtained with the McGraw Hill 1.3 m telescope at the Michigan–Dartmouth–MIT Observatory. A Thomson CCD was used as a camera in most cases, though in some a TI–4849 CCD was employed. The Thomson CCD has superior flattening and cosmetic properties, but a substantially lower quantum efficiency. It also suffers from a deferred charge problem, wherein charge depositied in the CCD substrate by bright stars continues to bleed in subsequent exposures. The images are all scaled in the same fashion, with a fixed contrast relative to the sky. The contrast is high enough that the imperfections in the I–band flat field are visible. This high contrast also means that even modestly low surface brightness features will appear saturated.

The galaxies depicted here were, among other things, selected by the presence of H II regions which could be studied spectroscopically (Chapter 3). Thus star forming knots are visible in the U filter. Otherwise, they represent a broad spectrum of morphologies, some having clearly defined spiral structure and distinct bulge components, others being chaotic or amorphous blobs. They also cover the full gamut in size, ranging from true dwarfs to giants (e.g., Malin 2). What they share in common are disk surface brightnesses many standard deviations below the "universal" value of Freeman (1970).

In all images, North is up and East is to the left. Unless otherwise noted, each image is 2.4′ on a side. At the scale these CCDs give on the MDM 1.3 m telescope (0.48 arcsec pixel^{-1}), this corresponds to 300 pixels.

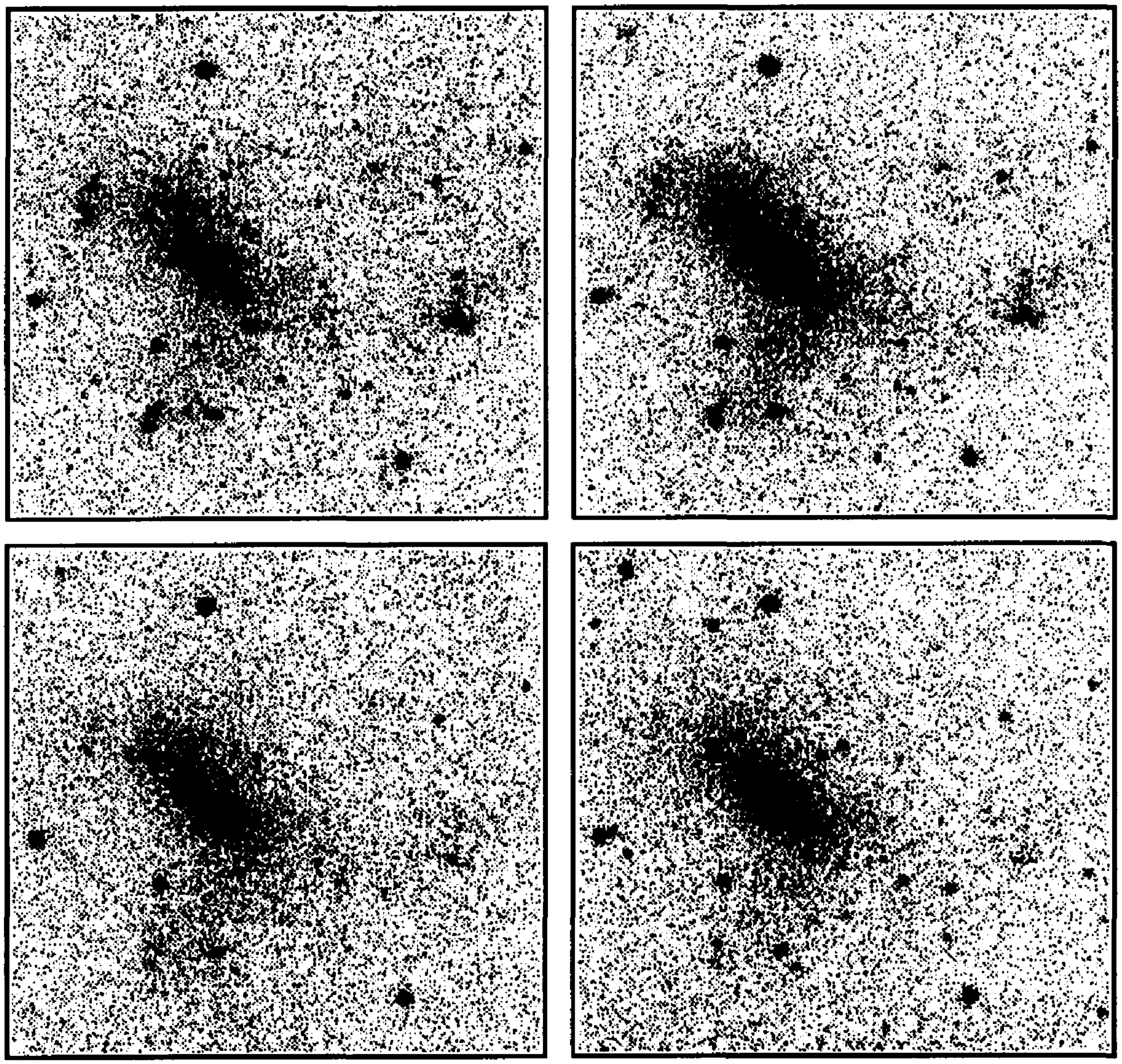

Figure 2.A.1— **F415–3.** Each panel corresponds to a different filter — **a)** upper left: *U* **b)** upper right: *B* c) lower left: *V* d) lower right: *I*. The strong knot near the center is an H II region. This galaxy has amorphous, very low surface brightness plumes extending away from the ends of the major axis of the main body. The western plume has several knots which are prominent in the blue filters.

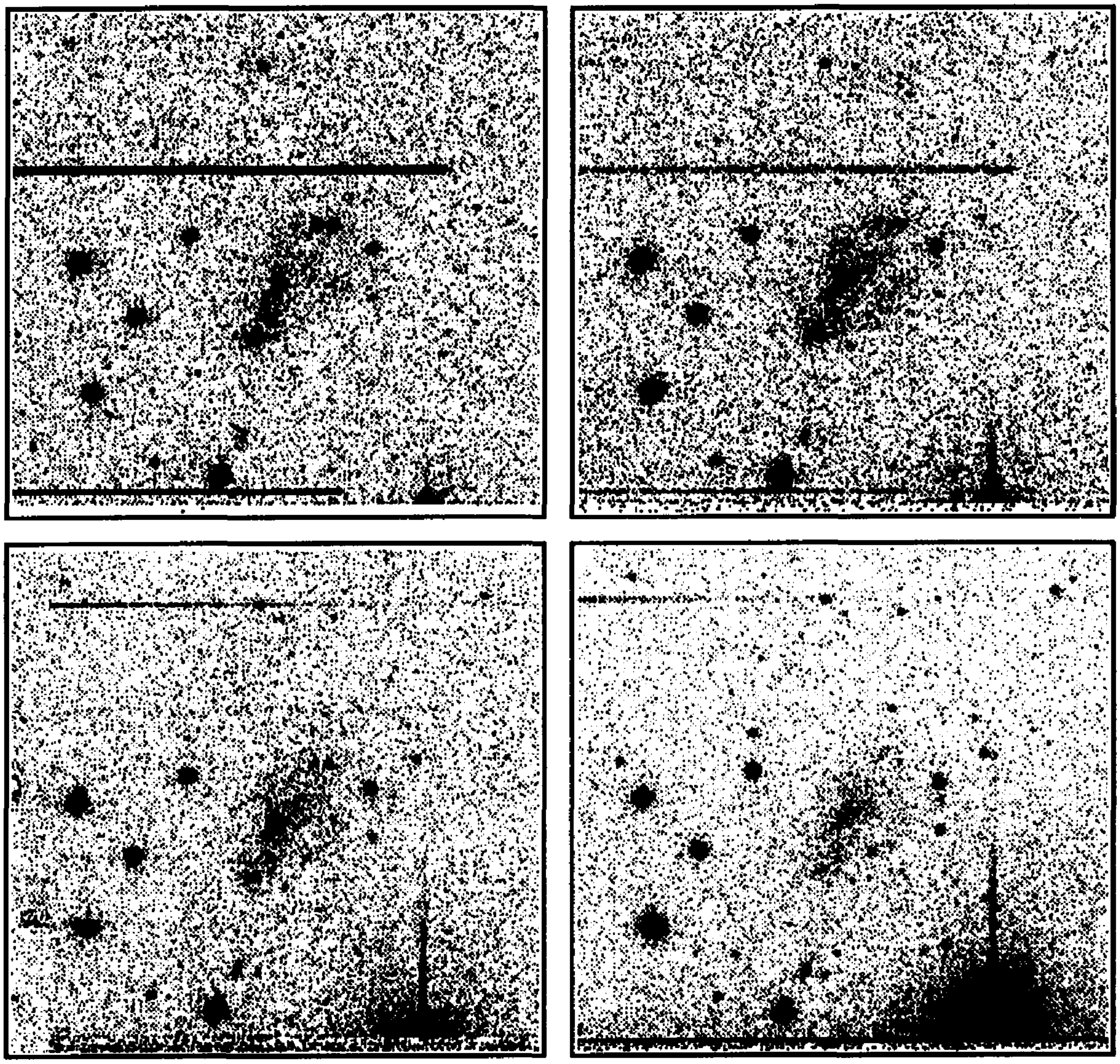

Figure 2.A.2— F469–2. a) U b) B c) V d) I. The linear streaks result from deferred charge from bright stars in previous exposures. All of the brighter knots in this galaxy are H II regions.

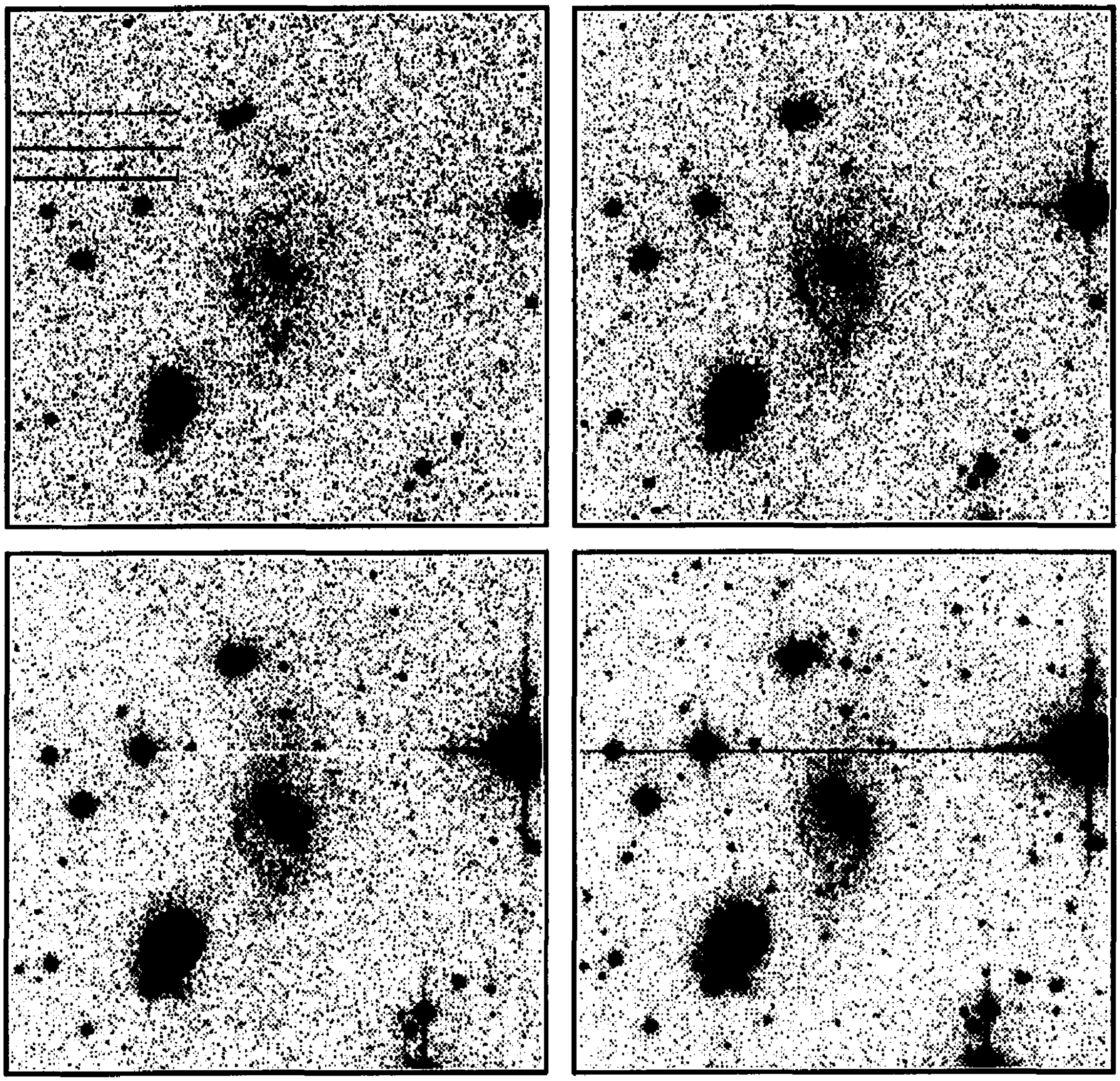

Figure 2.A.3— F530–3. a) U b) B c) V d) I. The linear streaks in the U image are from deferred charge. A weak spiral pattern is visible, with some star forming knots in the lower arm. The H II region immediately southwest of the bulge remains prominent in the red filters.

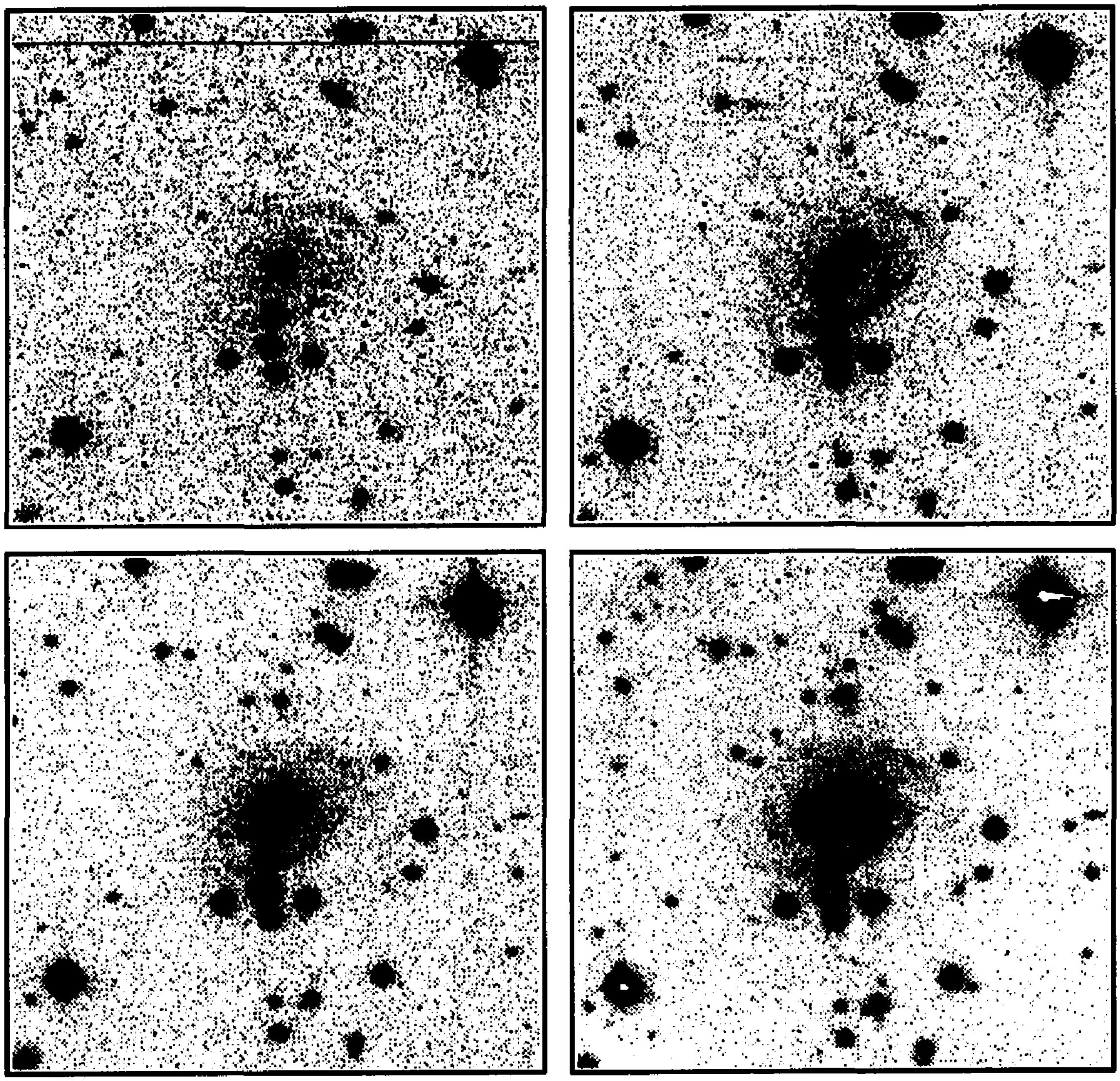

Figure 2.A.4— F558–1. a) *U* b) *B* c) *V* d) *I*. This galaxy has clear spiral structure, but with only a few star forming regions in the southern arm (near the group of five stars).

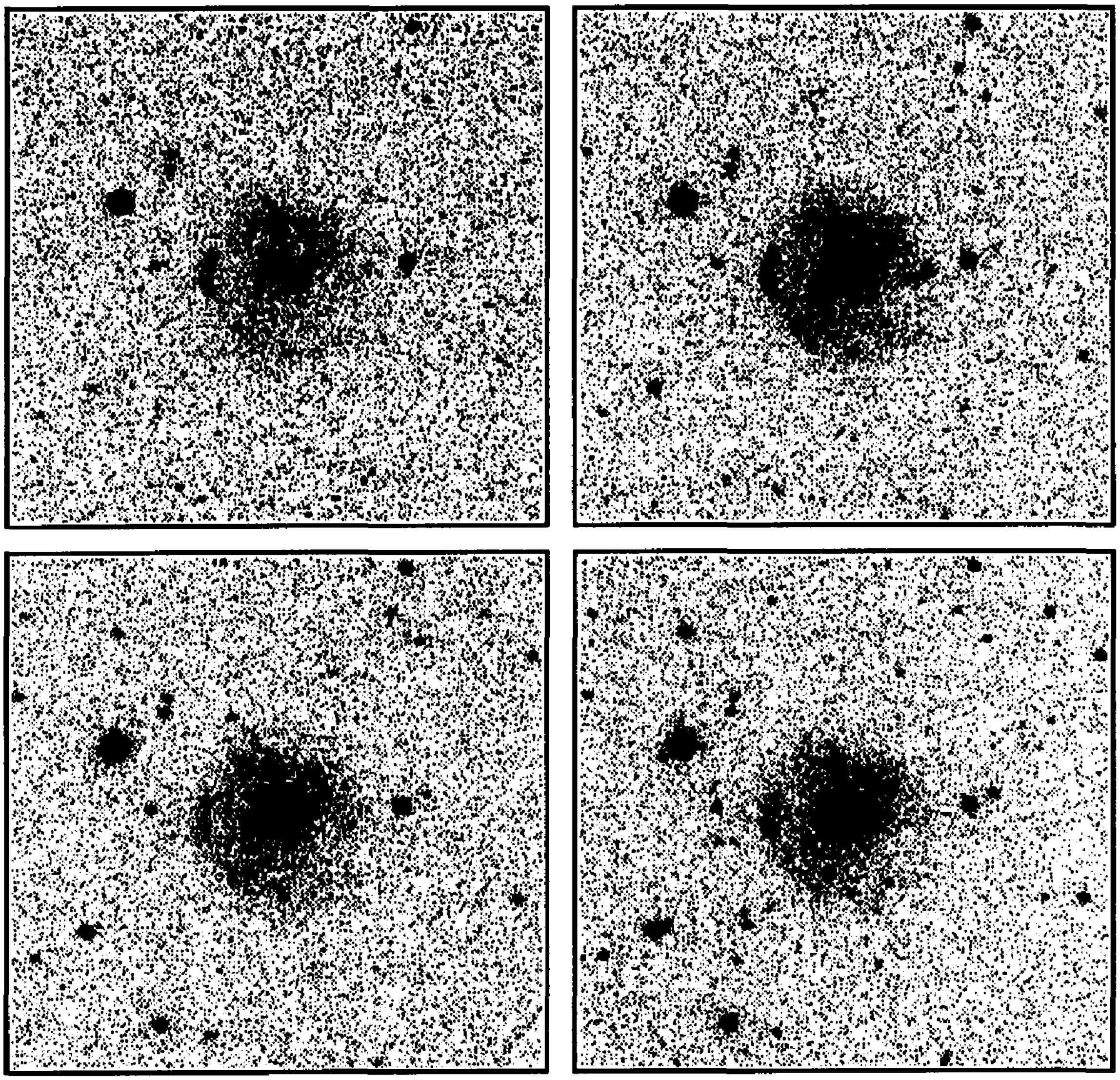

Figure 2.A.5— F561–1. a) U b) B c) V d) I. This galaxy has a strong, one arm spiral pattern.

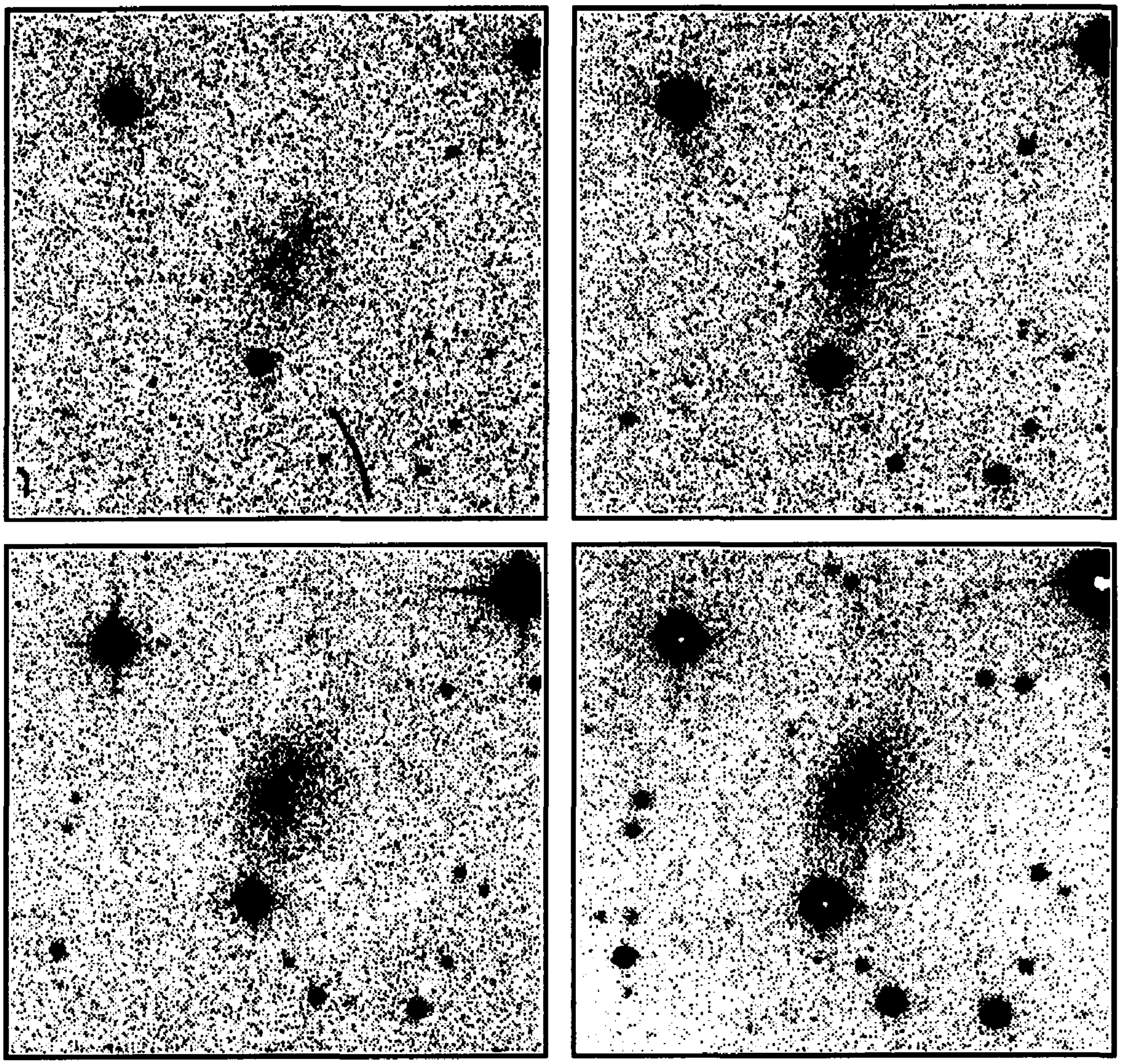

Figure 2.A.6— **F563–V1. a)** *U* **b)** *B* **c)** *V* **d)** *I*. **The light from this galaxy has the same distribution in every filter. This, together with the low metallicity (Chapter 3) and very blue color, suggests that this may be a young object.**

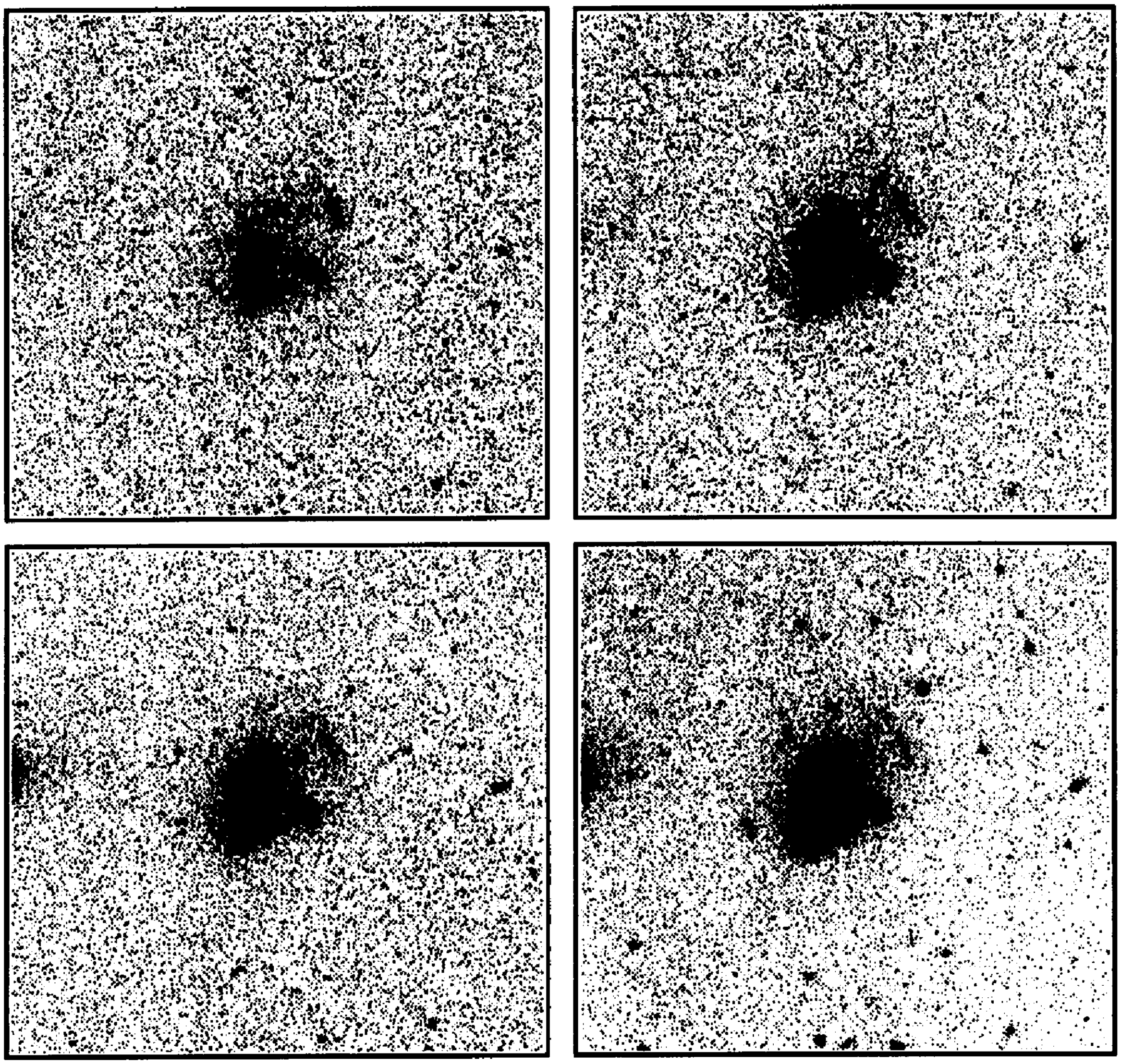

Figure 2.A.7— **F563–V2. a)** U **b)** B **c)** V **d)** I**. This galaxy has two H II regions west of the relatively HSB central bar, and a blue, LSB plume to the northwest.**

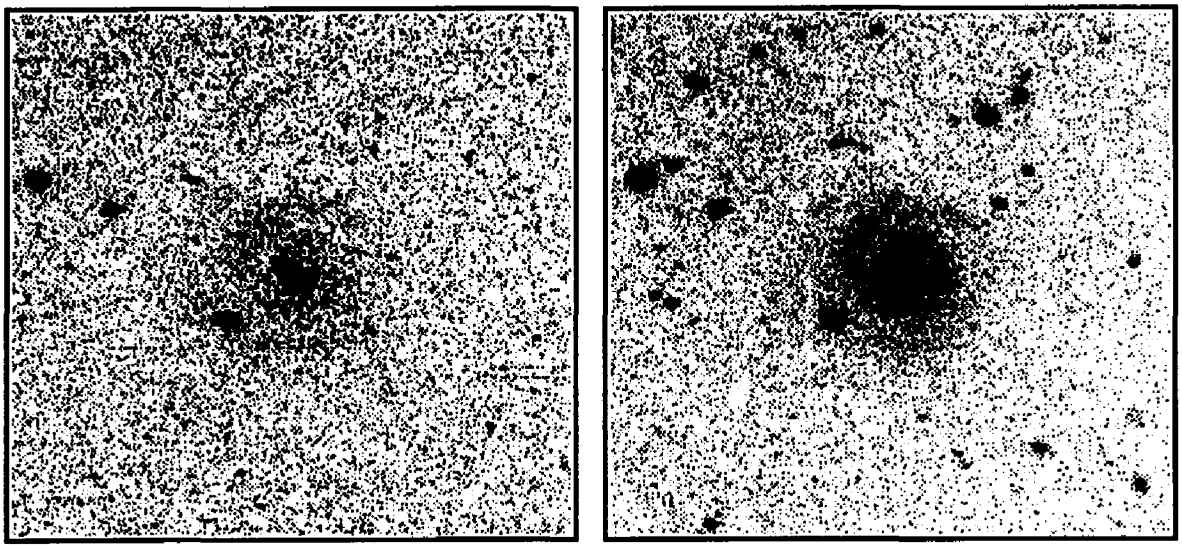

Figure 2.A.8— F568–1. Only a) *B* and b) *I* pass bands were observed. Some spiral structure is visible in the LSB disk.

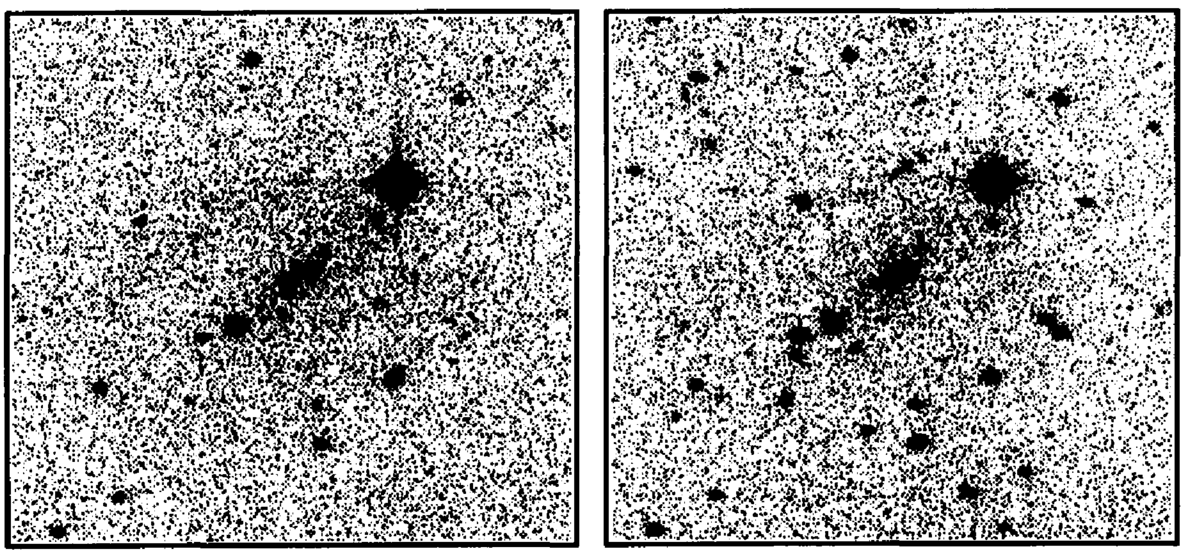

Figure 2.A.9— F583–5. a) *B* b) *I*. This galaxy has a central H II region embedded in a very LSB disk.

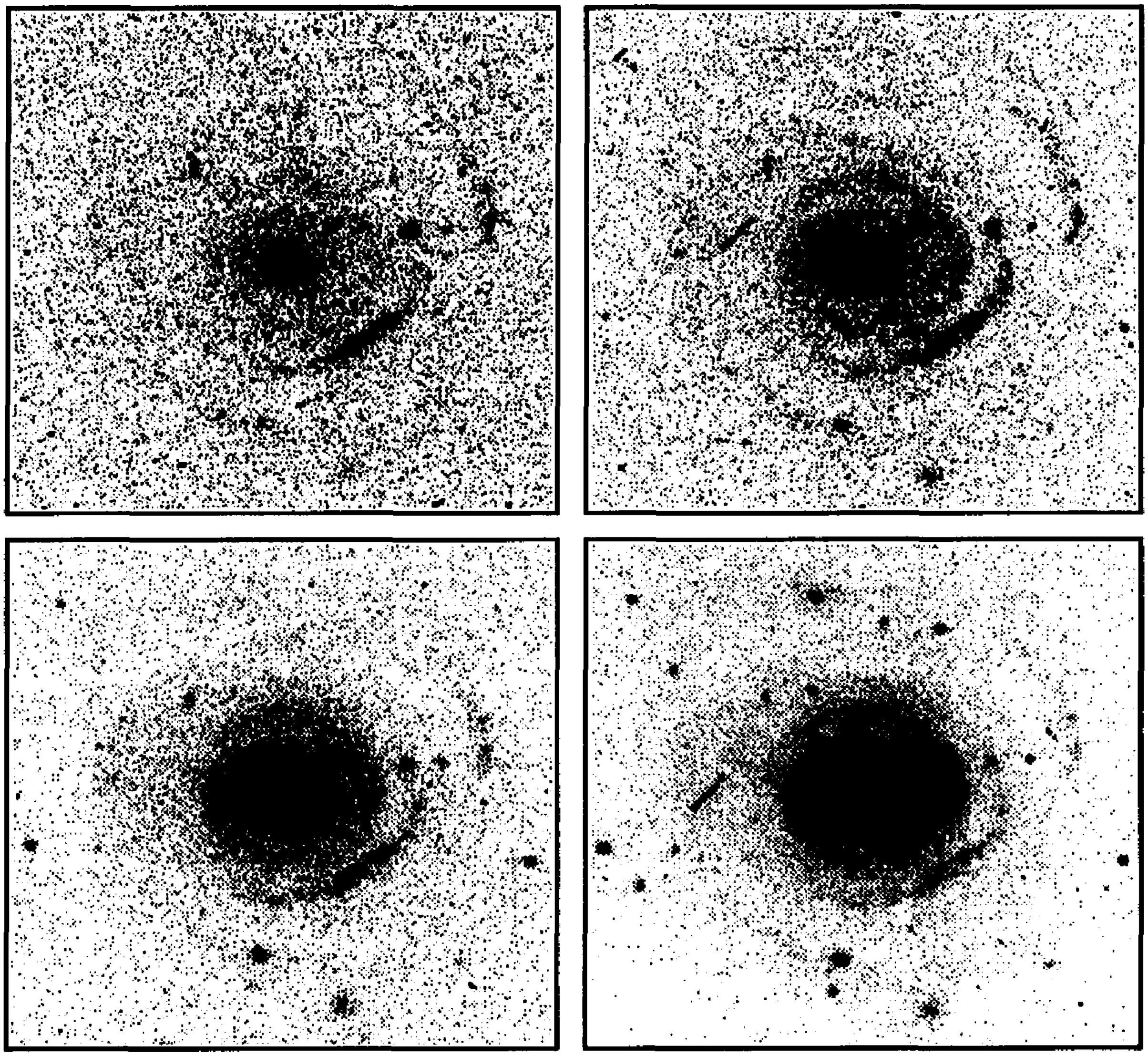

Figure 2.A.10— **F568–6 (Malin 2). a)** *U* **b)** *B* **c)** *V* **d)** *I*. **This giant galaxy has a number of luminous H II regions, predominantly in the western arm. Spiral structure is traceable to very large (> 44*kpc*) radii. There is also a peculiar jet-like structure, which may be a background (or foreground!) galaxy.**

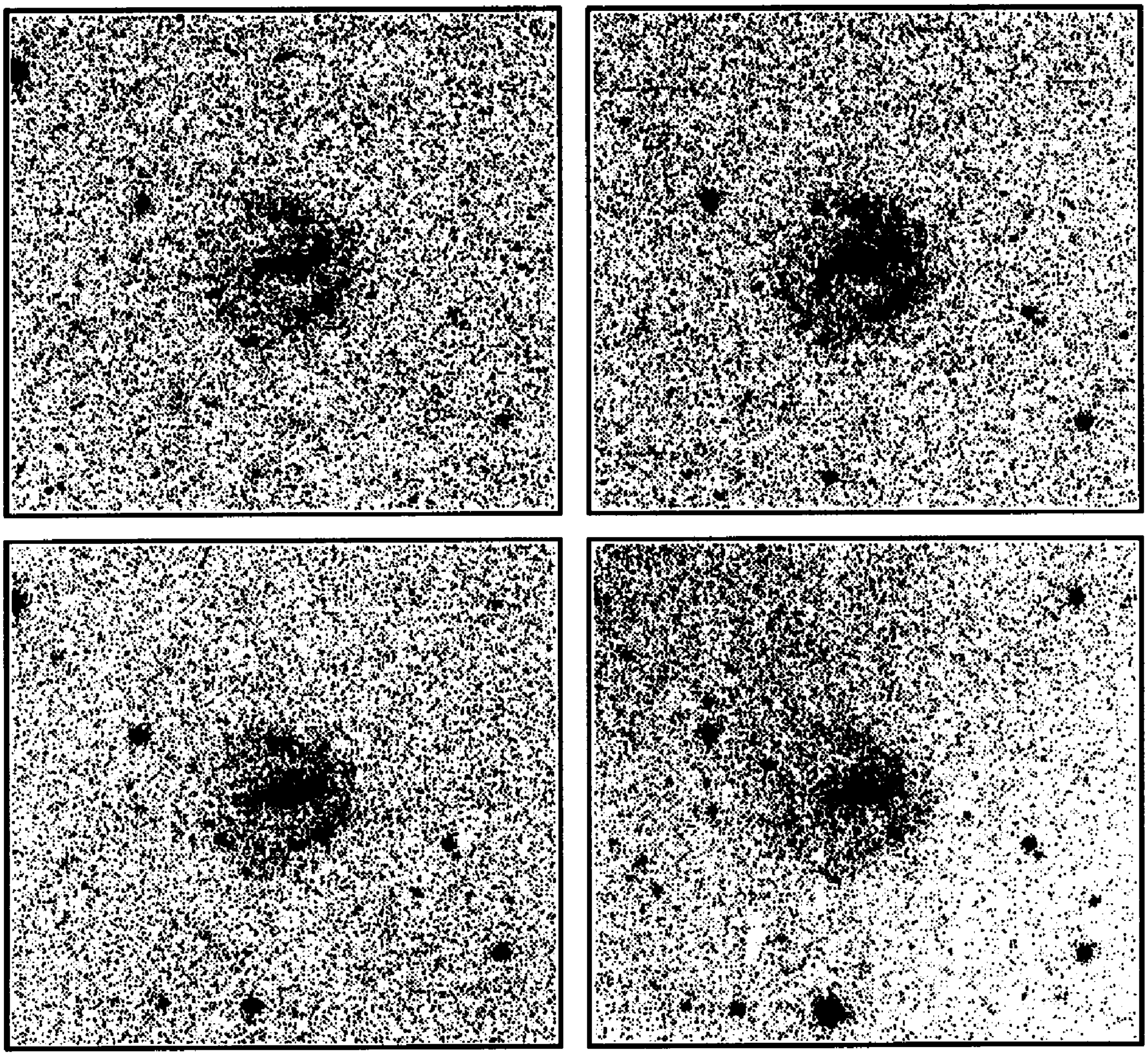

Figure 2.A.11— F577–V1. a) U b) B c) V d) I. This galaxy has a bar plus a ring structure.

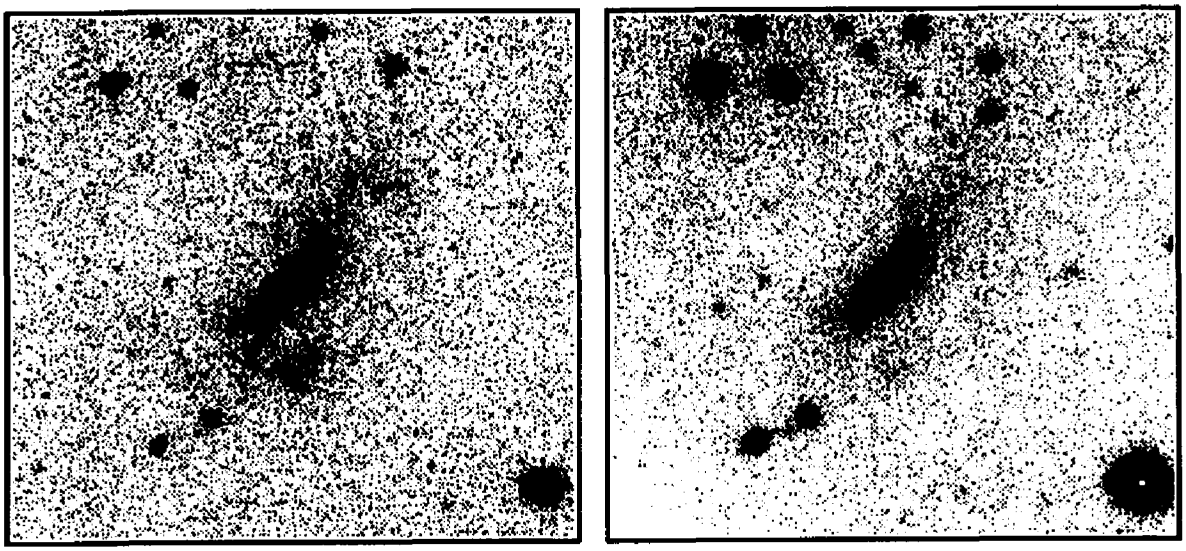

Figure 2.A.12— F585–3. a) *B* b) *I*. There are many star forming regions embedded in the amorphous central region.

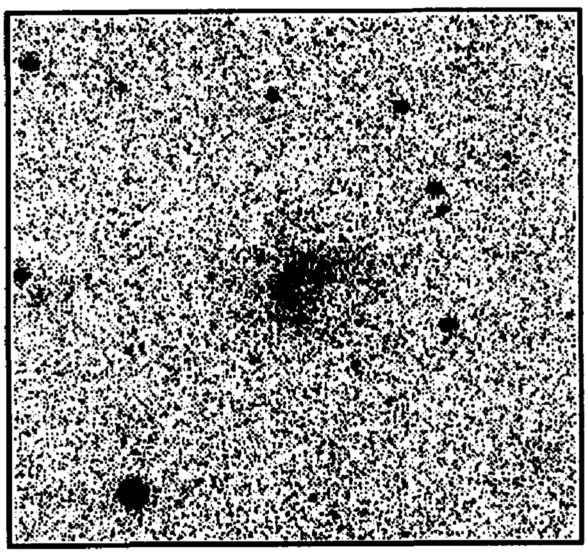

Figure 2.A.13— F585–V1. a) *B*. This amorphous galaxy does have weak knots of star formation.

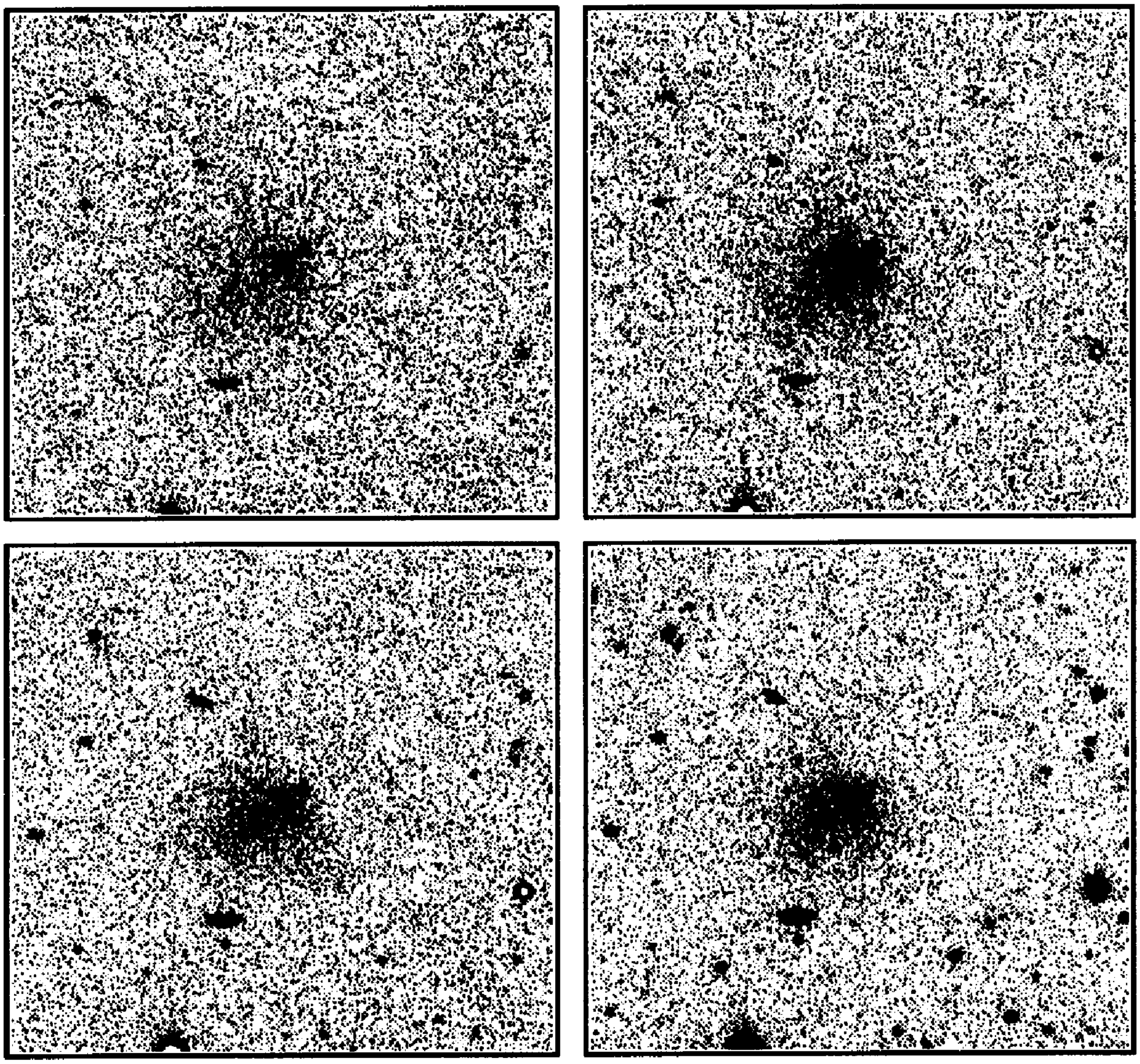

Figure 2.A.14— F611–1. a) *U* b) *B* c) *V* d) *I*. The knots in the northwest of this galaxy are H II regions. Aside from these, the light is distributed similarly in all filters, suggesting a homogeneous stellar population.

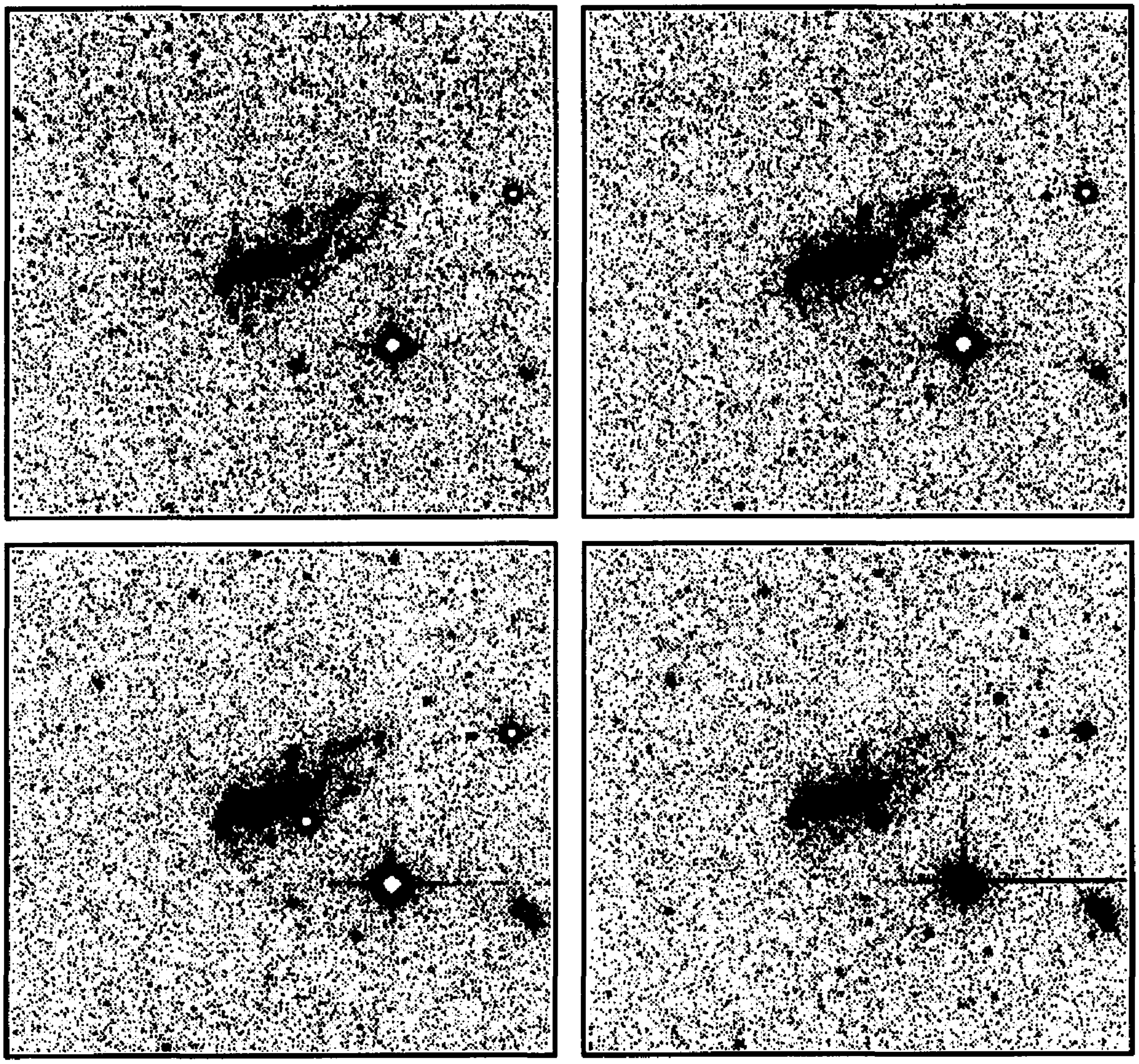

Figure 2.A.15— F746–1. a) *U* b) *B* c) *V* d) *I*. This irregular galaxy has many star forming clumps, and an odd loop to the northwest.

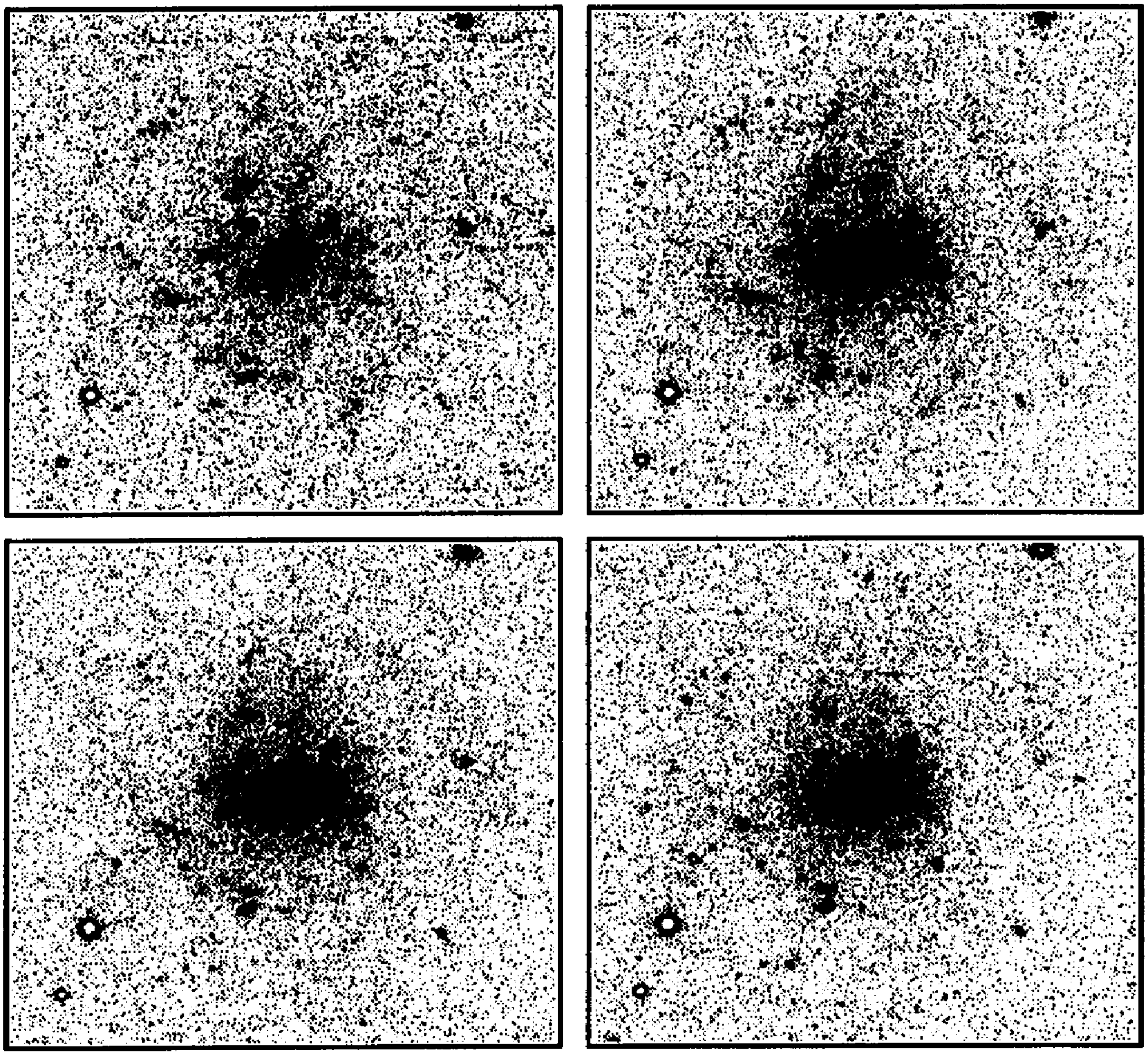

Figure 2.A.16— UGC 1230. a) U b) B c) V d) I. A loose spiral pattern radiating out from the central concentration is apparent in this galaxy. The arms are not well traced by the H II regions, which occur at sporadic intervals along them. The pair of knots to the south which are prominent in the I-band are also H II regions. That nebular emission is present in these red clusters indicates that star formation has continued in the vicinity long enough for the the first stars formed in the current episode of star formation to evolve to the red supergiant phase.

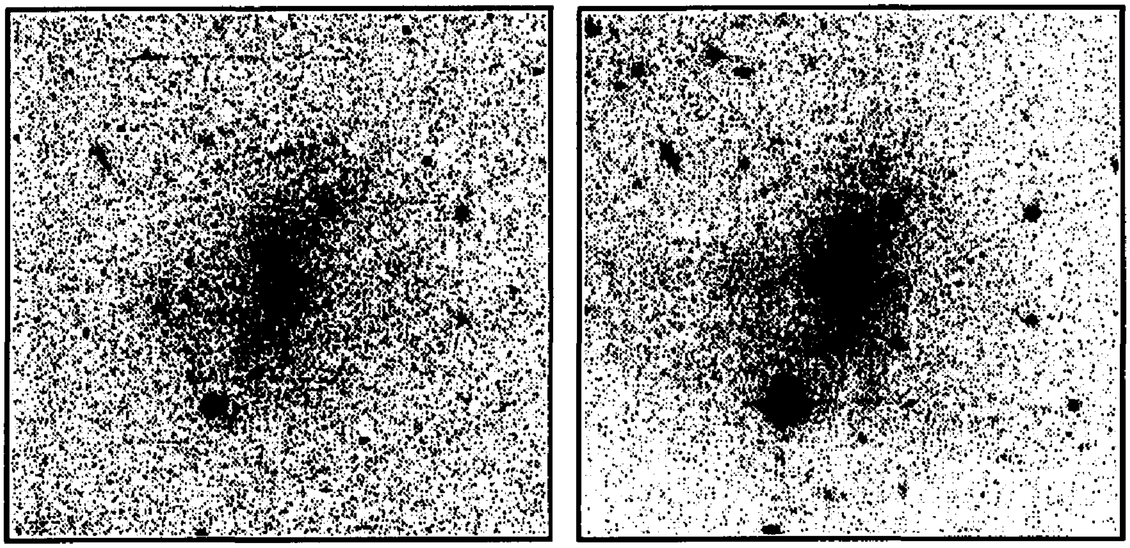

Figure 2.A.17— UGC 5675. a) B b) I. The B-band light from this galaxy is more diffuse and has a different position angle than that in the I-band.

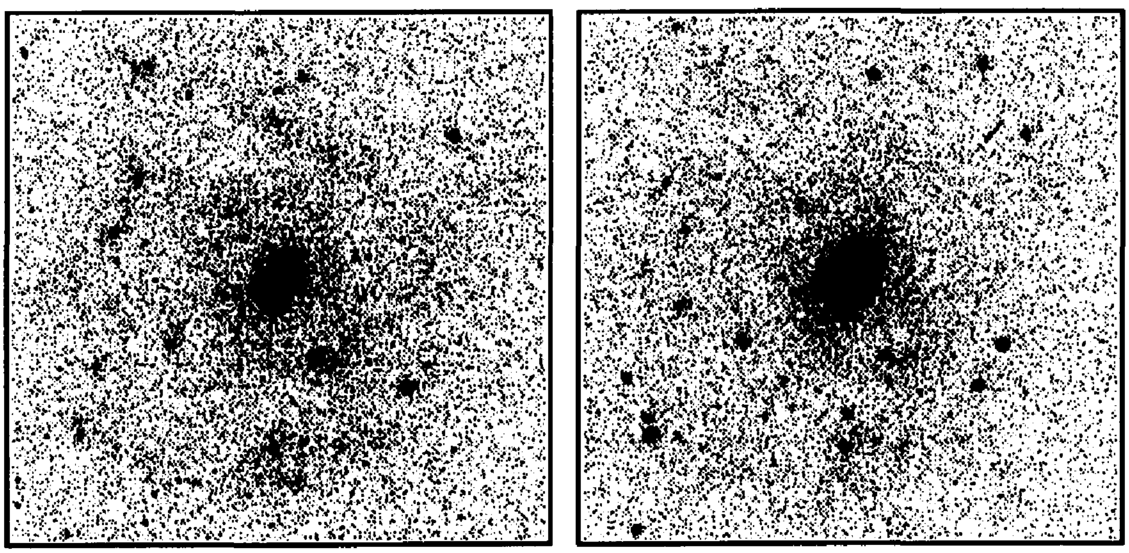

Figure 2.A.18— UGC 9024. a) B b) I. This galaxy has a very blue, very LSB disk which nevertheless has a well organized spiral pattern. Knots of star formation are widely dispersed.

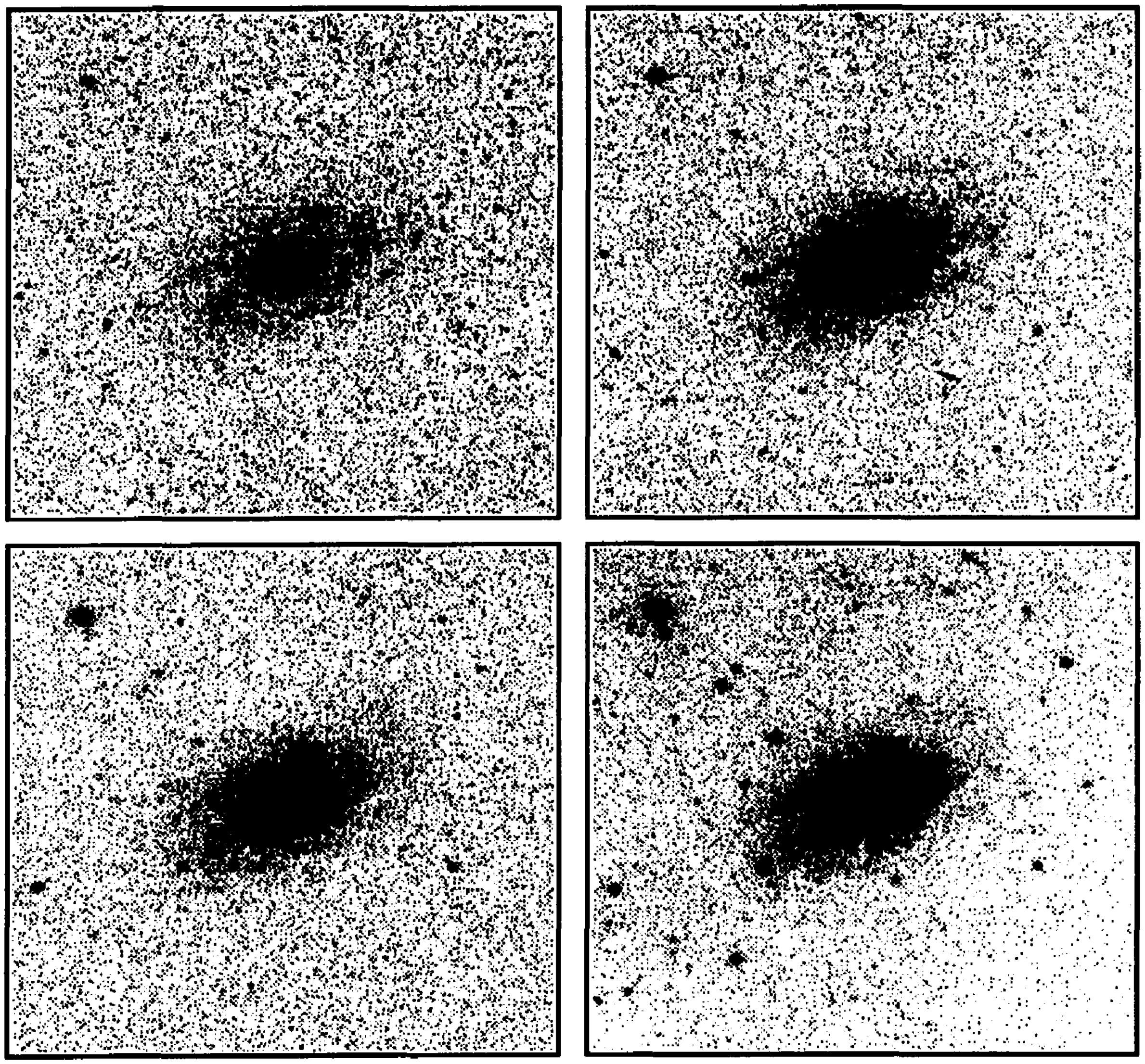

Figure 2.A.19— UGC 5709. a) U b) B c) V d) I. This is a relatively high surface brightness galaxy, and shows how greatly the morphological appearance of "normal" galaxies can change over the large wavelength change from U to I, unlike many of the LSB galaxies presented here.

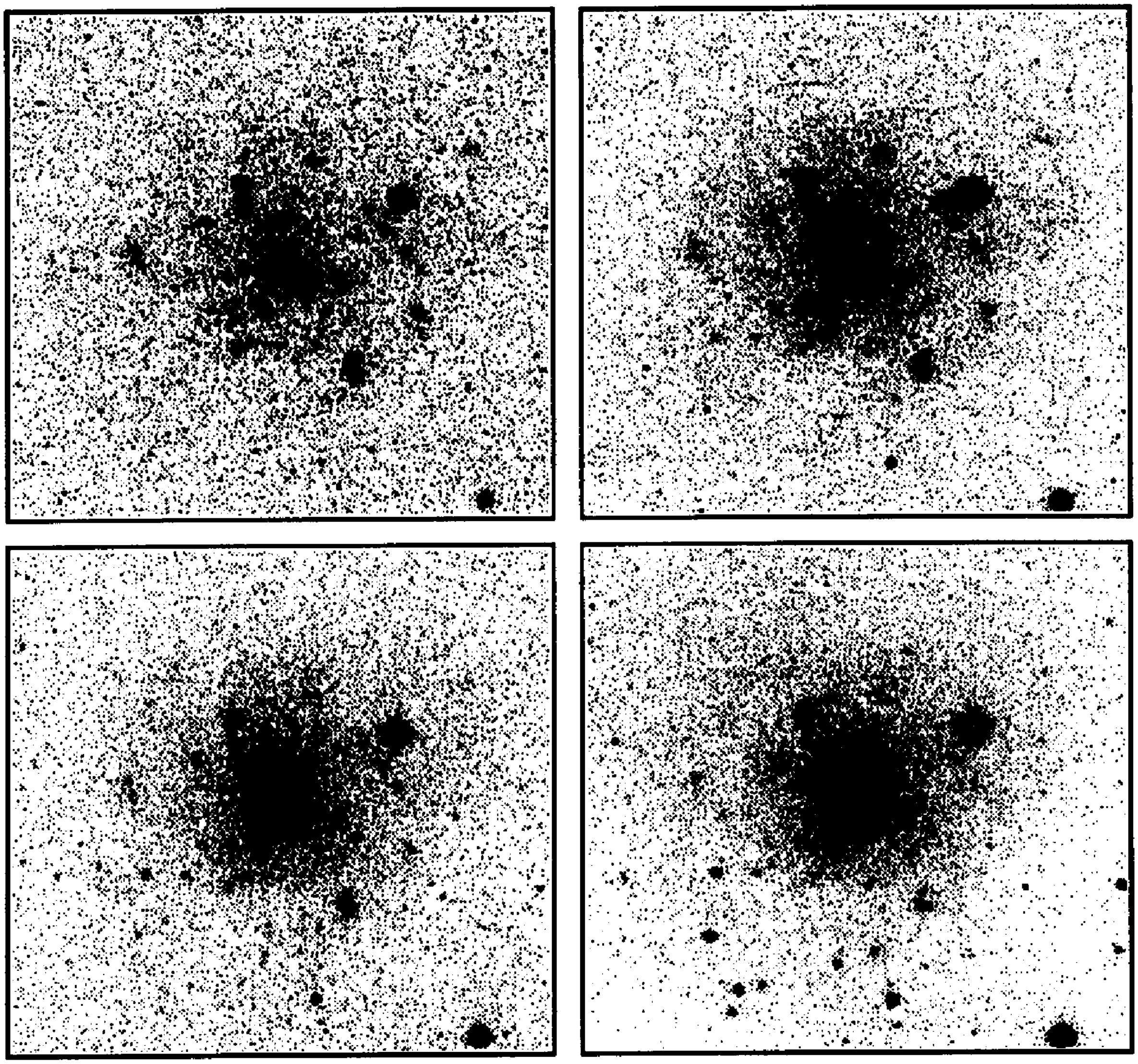

Figure 2.A.20— UGC 6151. a) *U* b) *B* c) *V* d) *I*. Despite its low surface brightness, this galaxy has a number of prominent star forming knots, and perhaps a faint spiral structure.

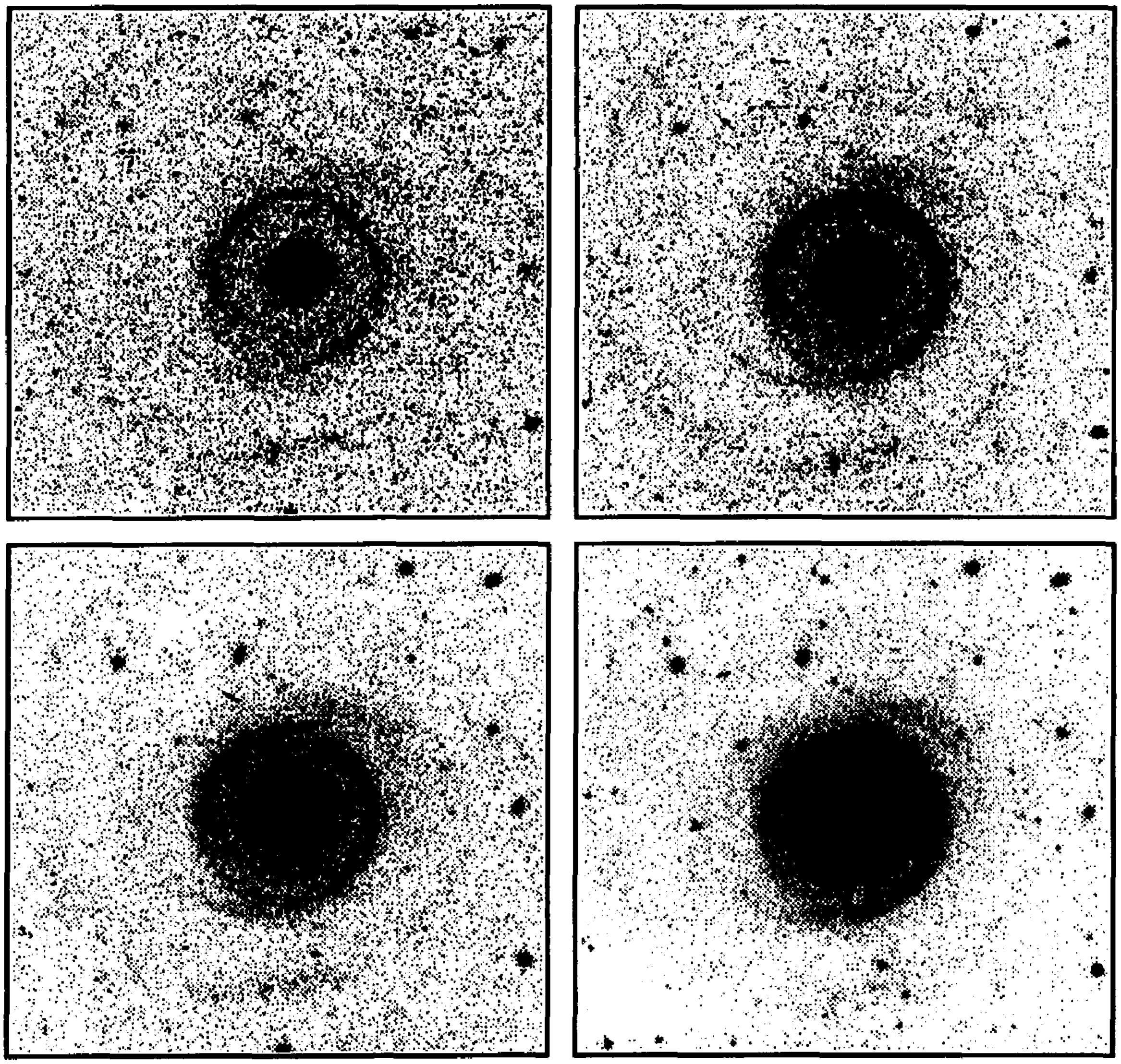

Figure 2.A.21— UGC 6614. a) U b) B c) V d) I. Note that in this case, each image is 3.1 arcminutes on a side. UGC 6614 is a very large galaxy, and its disk (and spiral pattern) extends well beyond the edge of the frame. This makes it difficult to reliably estimate the scale length and central disk surface brightness. However, it is very low surface brightness ($\mu_B(0) > 24 mag\ arcsec^{-2}$), and this galaxy could easily be classified as an elliptical on shallow plate material. Even the apparently prominent ring has $\mu_B \approx 24.1$. There are some knots of star formation in the ring, which has a mean $(U - B) = 0.18 \pm 0.03$. Despite the very extended, diffuse nature of this disk, there is a clear, smooth, well organized spiral pattern.

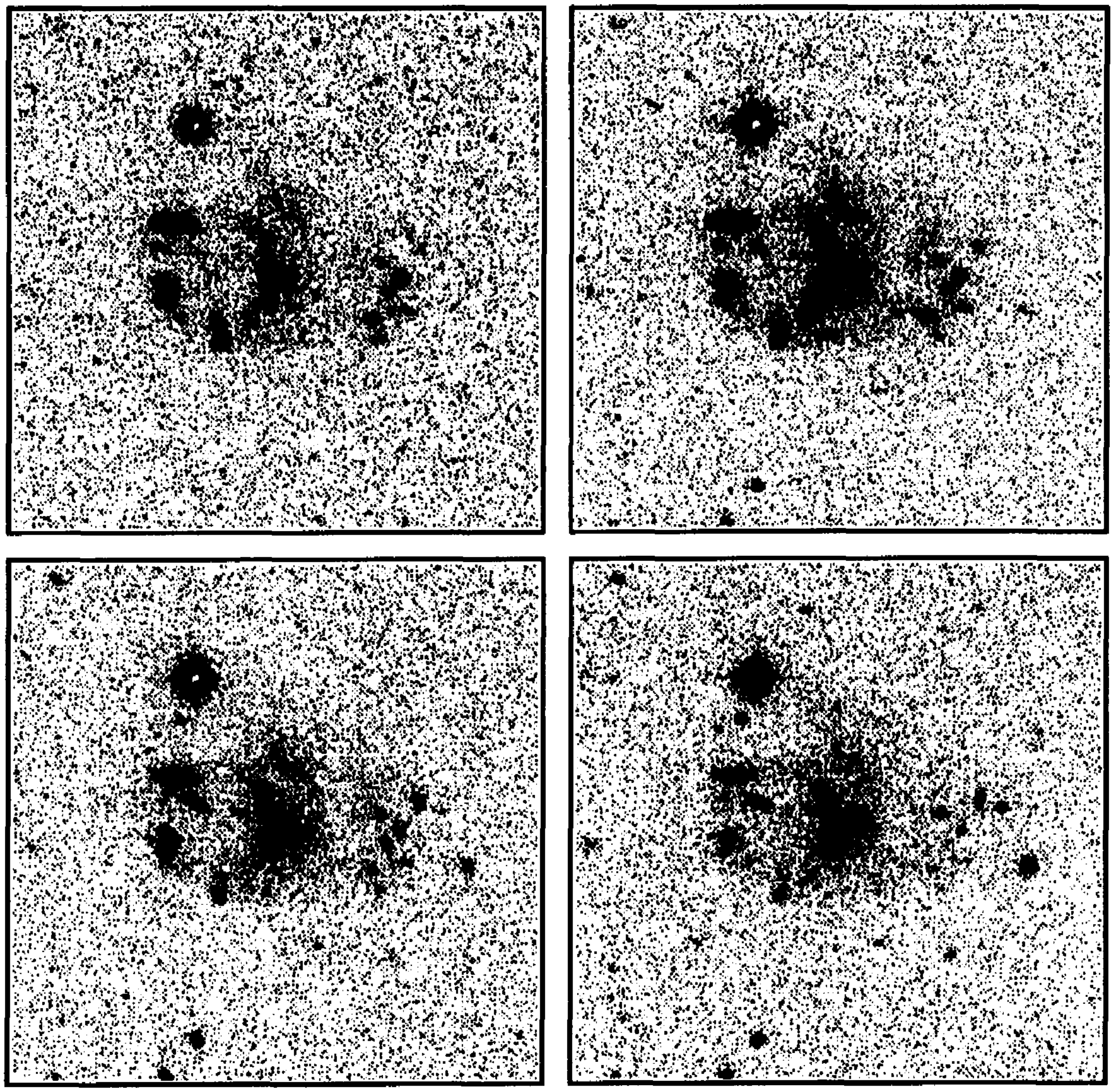

Figure 2.A.22— UGC 12695. a) U b) B c) V d) I. This galaxy has an odd structure, with spokes rather than arms projecting out from the center. These features are present in all filters, indicating a fairly homogeneous stellar population. There are a number of bright H II regions around the edges of the galaxy. In those to the west, a clear trend of color is present in the sense that the southern clusters are bluer than the northern ones, perhaps indicating the propagation of star formation in this direction. The proximity of a very red and blue cluster in the east may indicate a similar situation. Since these star clusters evolve on short (a few $\times 10^7$ yr) time scales, and contribute a substantial fraction of the total light even at I, the light from this galaxy may be dominated by young stars.

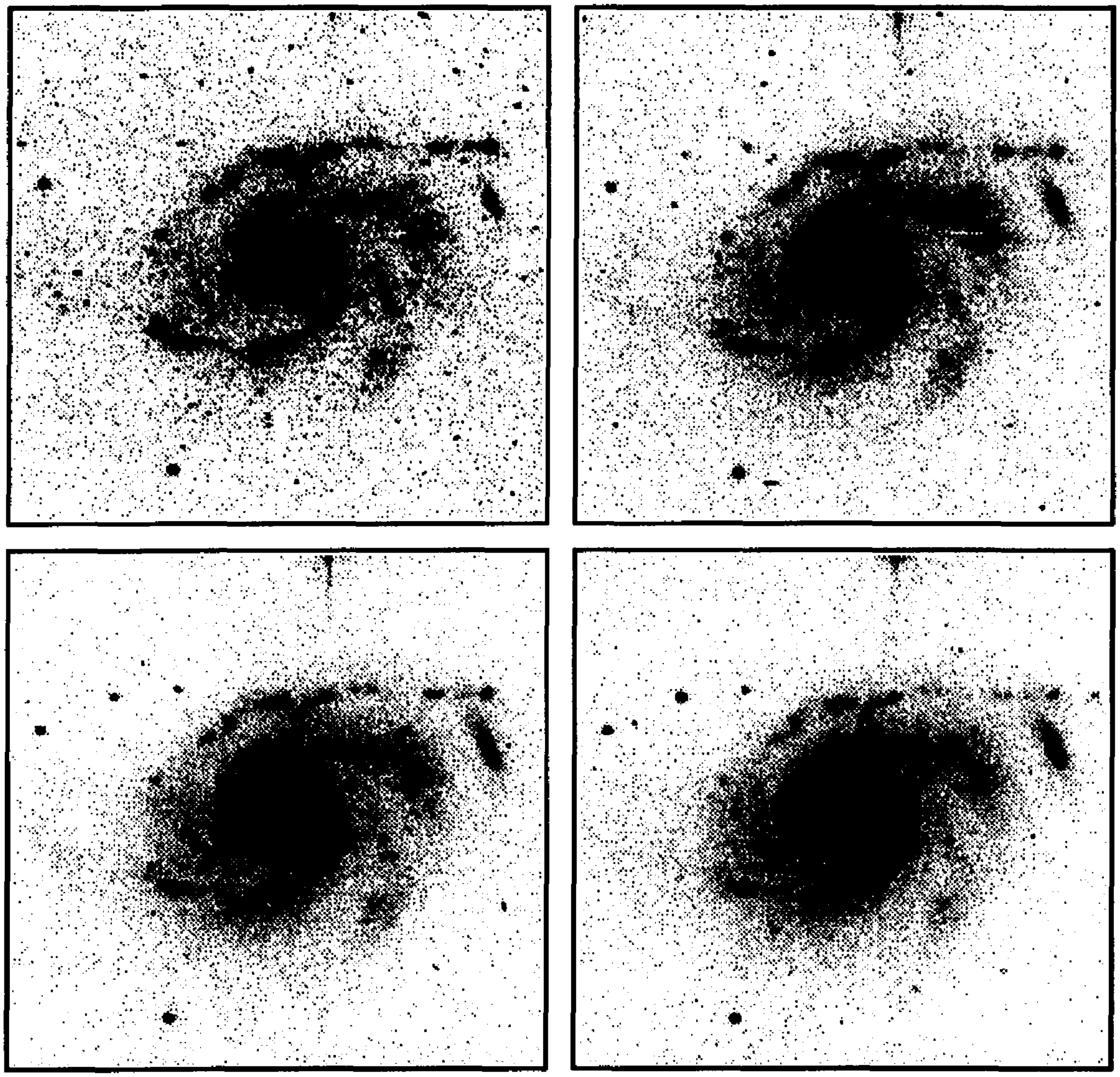

Figure 2.A.23— NGC 7757. a) *U* b) *B* c) *V* d) *I*. This is an HSB Sc spiral included for comparison. Note the prominent appearance of this galaxy, which is displayed with the same contrast as the preceding LSB galaxies. The exposure time, and hence the S/N in the sky, is actually *less* than in the other images. If displayed in such a way as to make the sky value (rather than the contrast relative to the sky) appear similar, most detail would be lost to saturation. The disk of this galaxy is consumed by star formation as traced by the many knots of young stars prominent in the *U* image. Despite the much higher star formation rate per unit area, this galaxy is not as blue as most of the LSB galaxies discussed here.

REFERENCES

Aaronson, M., Huchra, J., Mould, J. R, Tully, R.B, Fisher, J. R., van Woerden, H., Goss, W. M., Chamaraux, P., Mebold, U., Siegman, B., Berriman, G., & Persson, S. E. 1982, ApJS, 50, 241

Aldering, G. S. 1990, Ph.D. thesis, University of Michigan

Aldering, G. S., & Bothun, G. D. 1991, PASP, 103, 1296

Arimoto, N., & Tarrab, I. 1990, A&A, 228, 6

Bothun, G. D. 1986, AJ, 91, 507

Bothun, G. D., Beers, T. C., Mould, J. R., & Huchra, J. P. 1986, ApJ, 308, 510

Bothun, G. D., Impey, C. D., & Malin, D. F. 1991, ApJ, 376, 404

Bothun, G. D., Impey, C. D., Malin, D. F., & Mould, J. R. 1987, AJ, 94, 23

Bothun,G. D., Romanishin, W., Strom, K. M., & Strom, S. E 1984, AJ 89, 1300

Bothun, G. D., Schombert, J. M., Impey, C. D., & Schneider, S. E. 1990, ApJ, 360, 427

Burstein, D., & Heiles, C. 1984, ApJS, 54, 33

Buzzoni, A. 1989, ApJS, 71, 817

Campbell, A. W., & Terlevich, R. 1984, MNRAS, 211, 15

Davies, J. I., Phillipps, S., Cawson, M. G. M., Disney, M. J., & Kibblewhite, E. J. 1988, MNRAS, 232, 239 de Vaucoulers, G. 1959, in *Handbuch der Physik, v. 53, Astrophysics IV: Stellar Systems*, ed. S. Flügge (Berlin: Springer-Verlag), 275

Disney, M. J. 1976, Nature, 263, 573

Freeman, K. C. 1970, ApJ, 160, 811

Impey, C. D., & Bothun, G. D. 1989, ApJ, 341, 89

Impey, C. D., Bothun, G. D., & Malin, D. F. 1988, ApJ, 330, 634

Irwin, M. J., Davies, J. I., Disney, M. J., & Phillipps, S. 1990, MNRAS, 245, 289

Katz, N. 1992, ApJ, 391, 502

Kennicutt, R. C. 1989, ApJ, 344, 685

Kunth, D., & Sargent, W. L. W. 1986, ApJ, 300, 496

Landolt, A. U. 1973, AJ, 78, 959

Landolt, A. U. 1983, AJ, 88, 439

Larson, R. B., & Tinsley, B. M. 1978, ApJ, 219, 46

Luppino, G. A. 1989, PASP, 101, 931

Maeder, A. 1990, A&AS, 84, 139

McGaugh, S. S. 1991, ApJ, 380, 140

Nilson, P. 1973, *Uppsala General Catalog of Galaxies* (Uppsala, Sweden: Societatis Scientiarum Upsaliensis) (UGC)

Olofsson, K. 1989, A&AS, 80, 317

Pilachowski, C., Landolt, A., Massey, P., & Montani, J. 1991, *NOAO Newsletter*, 28, 26

Reed, B. C. 1985, PASP, 97, 120

Renzini, A., & Buzzoni, A. 1986, in *Spectral Evolution of Galaxies*, ed. C. Chiosi & A. Renzini (Reidel: Dordrecht), 195

Romanishin, W., Strom, K. M., & Strom, S. E. 1983, ApJS, 53, 105

Salzer, J. J., Alighieri, S. D. S., Matteucci, F., Giovanelli, R., & Haynes, M. P. 1991, AJ, 101, 1258

Schombert, J. M., & Bothun, G. D. 1987, AJ, 93, 60

Schombert, J. M., & Bothun, G. D. 1988, AJ, 95, 1389

Schombert, J. M., Bothun, G. D., Impey, C. D., & Mundy, L. G. 1990, AJ, 100, 1523

Schombert, J. M., Bothun, G. D., Schneider, S. E., & McGaugh, S. S. 1992, AJ, 103, 1107

van der Hulst, J. M., Skillman, E. D., Kennicutt, R. C., & Bothun, G. D. 1987, A&A, 177, 63

von Hippel, T., & Bothun, G. 1990, AJ, 100, 403

Weinberg, D. H., Szomoru, A., Guhathakurta, P., & van Gorkom, J. H. 1991, ApJ, 372, L13

CHAPTER III

CHEMICAL ABUNDANCES IN LOW SURFACE BRIGHTNESS GALAXIES: IMPLICATIONS FOR EVOLUTION AND COSMOLOGY

Introduction

Low Surface Brightness (LSB) galaxies are an important but often neglected part of the galaxy content of the universe. Their importance stems both from the selection effects which cause them to be under-represented in galaxy catalogs, and from what they can tell us about the physical processes of galaxy evolution. Here, emphasis is placed on the latter, as probed by the gas phase chemical abundances in LSB galaxies.

That LSB galaxies have been neglected is not surprising considering the technical difficulties imposed by their nature. With *peak* surface brightnesses $\mu_0 \geq 23B$ mag arcsec^{-2}, spectral observations of their stellar continua are virtually impossible because the sky background always dominates the signal. This problem is circumvented here by concentrating on the regions within LSB galaxies for which it is possible to attain reasonable quality data.

To this end, spectra of a sample of H II regions in LSB galaxies have been obtained. The H II regions provide powerful probes of the physical conditions in the galaxies in which they reside. The strong emission lines are more readily observable than the weak continuum, and line ratio diagnostics contain information about the chemical abundances in the gas and the stars which ionize it. These H II regions are almost always giant H II regions ionized by clusters of stars rather than individual stars.

The H II regions were identified from narrow band Hα images (see Appendix B) of a sample selected from either the lists of LSB galaxies of Schombert & Bothun (1988) and Schombert et al. (1992), or from the UGC (Nilson 1973). All of these galaxies have central surface brightnesses well below the canonical Freeman (1970) value of $\mu_0 = 21.65$ mag arcsec^{-2}, and most below $\mu_0 = 23$ mag arcsec^{-2} (Chapter 2). It should be noted that while these are all disk systems of low surface brightness, they are *not* all dwarf galaxies. While some dwarfs are included, so are some giants (e.g., Malin 2). The typical size for this sample is indistinguishable from that of typical high surface brightness disks (Chapter 2). There is no linear size criterion in the sample selection, only surface brightness. Another *de facto* selection effect in a study of this kind is the presence of H II regions. While these are more common than might be expected in galaxies selected for low surface brightness, the sample can in no way be considered complete. It nevertheless provides the opportunity to study the physical properties an interesting class of objects.

Observations and Reductions

Optical spectra of 73 H II regions in 22 LSB galaxies were obtained over the course of several observing seasons from September 1989 through February 1992. In September 1990 and March 1991 blue spectra covering the 3600 – 5400 Å range were acquired with the Kitt Peak 2.1 m telescope and Gold Camera Spectrograph using a TI 800 x 800 CCD as the detector. Red spectra covering 5700 – 7000 Å were obtained with the Hiltner 2.4 m telescope, Mk III spectrograph, and TI-4849 CCD (Luppino 1989), as were long baseline 4500 – 7300 Å spectra. Most of the data reported here were obtained in October 1991 and February 1992; data acquired prior to 1991 were of limited usefulness because of problems with the mirror surface.

Since LSB galaxies and their H II regions are impossible to see with the finder cameras of these telescopes, the slit was positioned by offsetting from nearby stars. The offsets were measured from the Hα images used to identify the target H II regions. Slit angles were chosen to maximize the number of H II regions which could be observed simultaneously. To minimize the impact of differential atmospheric refraction and the uncertainty in the offset procedure, a wide (3.4″) slit was used. This resulted in a resolution of $\sim$ 11 Å for the blue spectra, $\sim$ 8 Å for the red spectra, and $\sim$ 15 Å for the long baseline spectra. These latter overlap the red and blue spectra and were used to place them on the same relative flux scale. The linking spectra also provide a consistency check. Except in the few cases where the offset procedure obviously failed, the line *ratios* agree to within the errors expected from counting statistics and the read noise of the CCD detectors. Because the spectra were not always obtained under photometric conditions, the *fluxes* of individual lines observed multiple times were not always the same. Fortunately, this study requires only line ratios, and is unaffected by uncertainties in the absolute zero point of the flux scale.

Data reduction was accomplished primarily in IRAF. This began with subtraction of the bias level and dark current. The frames were flattened in the spectral direction with lamp flats, and the slit illumination was made uniform with twilight sky flats. Emission line lamps provided spectral calibration, and standard star observations were used to flux calibrate the object frames. This latter step also corrected for the spectral shape of the instrumental response. Apertures containing individual H II regions were then extracted and stored as one dimensional spectra. Line fluxes were extracted from these by using the FIGARO package to fit gaussians to the nebular emission lines.

The resulting data are presented in Tables 3.1 and 3.2. Table 3.1 contains information about the Balmer emission lines and information derived from them. Column 1 contains the galaxy name. Galaxies beginning with 'F' are from the lists of Schombert & Bothun (1988) and Schombert et al. (1992), and are designated by sky survey field number. Galaxies beginning with 'U' are from the UGC. Column 2 contains the H II region specification. Column 3 contains the observed Hβ flux in units of 10^{-18}erg cm^{-2}s^{-1}. Because conditions were not always photometric, these numbers may not always be within the formal errors listed in Column 4. Columns 5, 6, and 7 contain the observed equivalent width in Å of the Balmer lines Hγ, Hβ, and Hα, respectively. Being a measure of the line relative to the surrounding continuum, these are not subject to uncertainties in the zero point caused by nonphotometric conditions. Indeed, the greatest uncertainty here is in the placement of the low continuum level. The error in the equivalent widths is ~ 3 Å. Column 8 contains the reddening coefficient c, related to the more familiar $E(B-V)$ by $E(B-V) = 0.78c$. The error in c is listed in Column 9.

The reddening coefficient is determined from the interstellar extinction curve of Savage & Mathis (1979) with the observed Balmer decrements by assuming Case B ratios for a $T_e = 10,000K$ nebula in the low density limit. This is an adequate assumption, as the ratios of the [S II] lines generally indicate the low density limit, and never $N_e > 10^3$cm^{-3}, and the Balmer decrement is not very sensitive to either density or electron temperature. In a few cases of zero reddening and hot nebulae, modestly negative reddenings are derived. These are set to zero in the subsequent analysis. Only two Balmer lines are necessary for the derivation of c; where three have been observed an attempt was made to simultaneously derive the absorption equivalent widths in the the underlying stellar continuum. No absorption lines were detected to a limit of $W_\lambda \approx 3$ Å.

Table 3.2 contains the observed fluxes of the important nebular lines relative to Hβ. Column 1 contains the galaxy name and Column 2 the H II region. Column 3 contains the linear intensity ratio [O II]/Hβ, Column 4 [Ne III]/Hβ, Column 5 Hγ/Hβ, Column 6 [O III] λ4959/Hβ, Column 7 [O III] λ5007/Hβ, Column 8 Hα/Hβ, Column 9 [N II]/Hβ, Column 10 [S II] λ6717/Hβ, and Column 11 [S II] λ6731/Hβ.

Table 3.1 — Balmer Line Data

Galaxy	H II	$F(H\beta)$	$\sigma_{H\beta}$	$W_\lambda(H\gamma)$	$W_\lambda(H\beta)$	$W_\lambda(H\alpha)$	c	σ_c
F415–3	A1	2964	94	16	35	113	0.397	0.047
F469–2	A1	1368	74	34	50	350	0.187	0.078
F469–2	A2	414	58	8	15	152	0.462	0.254
F469–2	A3	2123	84	21	39	259	0.133	0.053
F469–2	A4	515	60	18	32	152	0.580	0.214
F530–3	A1	1727	79	33	97	466	0.405	0.070
F530–3	A2	509	60	5	26	134	0.103	0.183
F558–1	A1	575	61	...	5	17	1.482	0.230
F558–1	A2	323	56	...	5	...	...	...
F561–1	A1	164	53	...	5	28	−0.007	0.521
F561–1	A2	52	51	...	...	13	0.305	1.850
F561–1	A3	9250	67	...	22	49	0.486	0.123
F563–V1	A1	2760	56	...	13	49	0.151	0.337
F563–V1	A2	3060	56	...	8	11	0.151	0.304
F563–V2	A1	2940	56	5	12	32	0.153	0.317
F563–V2	A2	3990	58	2	10	48	0.996	0.299
F563–V2	A3	1693	78	9	32	131	0.923	0.084
F568–1	A1	219	54	...	...	...	...	...
F568–1	A2	225	55	...	14	...	...	...
F568–6	S1A1	683	63	...	8	97	1.200	0.189
F568–6	S1A2	744	64	...	11	109	0.863	0.164
F568–6	S3A1	62	51	...	...	12	0.472	1.650
F568–6	S3A2	1030	69	5	19	171	0.582	0.115
F568–6	S3A3	116	52	...	8	118	1.230	1.020
F577–V1	A1	213	54	...	25	155	0.656	0.510
F577–V1	A2	128	53	...	7	41	1.460	0.960
F577–V1	A3	1157	71	11	28	164	0.455	0.100
F577–V1	A4	720	65	...	...	...	0.445	0.500
F577–V1	A5	908	67	8	31	130	0.435	0.123
F583–1	A2	166	53	...	10	39	0.275	0.581
F583–1	A3	1502	76	14	47	125	−0.004	0.066
F583–5	A1	753	64	5	13	...	0.041	0.610
F583–5	A2	802	65	...	43	...	...	...
F585–3	S1A1	880	66	...	9	152	...	...
F585–3	S1A2	1413	74	...	8	48	...	...
F585–3	S1A3	368	57	...	8	76	...	...
F585–3	S2A1	94	52	...	19	...	...	...
F585–3	S2A2	487	60	...	30	...	...	...
F585–3	S2A3	817	65	...	6	...	...	...
F585–3	S2A4	692	63	...	21	...	...	...
F611–1	A1	1391	74	20	46	303	0.358	0.083
F611–1	A2	788	65	...	53	982	0.181	0.126
F746–1	A1	2864	93	18	53	120	0.298	0.046
F746–1	A2	1524	76	3	12	47	0.715	0.086
F746–1	A3	433	59	...	25	...	...	...
U 1230	A1	392	58	5	45	264	0.214	0.246
U 1230	A2	1045	69	14	28	174	0.195	0.099
U 1230	A3	2218	85	21	51	249	0.180	0.053
U 1230	A4	242	55	8	11	58	0.764	0.461
U 1230	A5	527	60	17	33	101	0.144	0.180
U 5675	A1	263	55	...	9	...	...	...
U 5675	A2	28	51	...	2	...	...	...
U 5675	A3	466	59	...	17	...	...	...
U 5709	A1	493	60	...	2	34	...	...
U 5709	A2	99	52	...	...	57	1.580	1.250
U 5709	A3	1212	72	...	19	47	0.310	0.091
U 6151	S1A1	3073	96	16	47	148	0.163	0.041
U 6151	S1A2	2742	92	13	33	182	0.690	0.055
U 6151	S3A1	4460	59	...	10	...	−0.003	0.197
U 6151	S3A2	1839	80	...	...	424	−0.004	0.055
U 6614	A1	298	56	...	7	...	...	...
U 6614	A2	258	55	...	9	...	...	...
U 6614	A3	244	55	...	9	...	...	...
U 9024	S1A1	1238	72	23	61	...	0.638	0.513
U 9024	S1A2	857	66	...	29	...	...	...
U 9024	S1A3	266	55	...	20	...	...	...
U 9024	S2A1	1369	74	...	54	...	...	...
U12695	S1A1	999	68	27	8	346	0.141	0.100
U12695	S1A2	3411	99	11	44	265	0.178	0.038
U12695	S1A3	1118	70	25	74	338	−0.095	0.080
U12695	S2A1	3611	102	38	91	85	0.542	0.044
U12695	S2A2	3730	103	19	61	173	0.147	0.035
U12695	S2A3	1667	78	16	51	...	0.234	0.317

Table 3.2 — Line Ratios

Galaxy	H II	[O II] λ3727	[Ne III] λ3869	Hγ λ4861	[O III] λ4959	[O III] λ5007	Hα λ6563	[N II] λ6583	[S II] λ6717	[S II] λ6731
F415–3	A1	2.370	0.453	0.507	1.033	3.625	4.039	0.153	0.272	0.217
F469–2	A1	2.063	0.266	0.683	0.812	2.367	3.377	0.143	0.216	0.176
F469–2	A2	2.330	0.604	0.639	1.264	3.879	4.269	0.107	0.257	0.406
F469–2	A3	1.303	0.381	0.597	1.790	5.812	3.225	0.078	0.157	0.144
F469–2	A4	1.683	0.200	...	0.736	1.243	4.724	...	...	...
F530–3	A1	1.205	0.389	0.401	1.392	3.888	4.067	0.198	0.441	0.279
F530–3	A2	...	...	0.236	1.682	3.655	3.145	0.158	0.199	0.044
F558–1	A1	4.971	0.764	...	0.584	1.290	3.271	0.496	...	...
F558–1	A2	5.322	...	...	...	0.304	...	...	...	...
F561–1	A1	2.715	...	...	0.667	2.441	2.941	0.223	0.430	0.601
F561–1	A2	...	...	...	2.812	5.388	3.737	...	...	...
F561–1	A3	3.133	...	0.513	0.795	2.375	4.357	0.199	0.664	0.531
F563–V1	A1	2.713	...	...	1.849	4.423	3.275	0.073	...	...
F563–V1	A2	0.868	...	...	0.570	1.701	3.275	0.033	0.238	0.310
F563–V2	A1	1.469	0.366	0.490	0.494	1.200	3.281	0.237	0.966	0.635
F563–V2	A2	3.083	...	0.279	0.926	3.047	6.734	0.673	1.212	1.025
F563–V2	A3	2.515	0.386	0.391	1.059	3.037	6.328	0.280	...	0.733
F568–1	A1	1.483	...	...	0.568	1.693	...	...	...	...
F568–1	A2	3.033	...	...	0.805	2.400	...	...	...	...
F568–6	S1A1	3.224	...	...	0.344	1.027	8.015	...	...	...
F568–6	S1A2	2.014	...	...	0.279	0.833	6.014	...	...	...
F568–6	S3A1	8.426	...	...	...	...	4.308	2.139	1.397	0.409
F568–6	S3A2	2.818	0.191	0.301	0.274	0.818	4.731	1.286	0.821	0.150
F568–6	S3A3	5.717	...	...	0.472	1.409	8.270	2.546	1.090	1.316
F577–V1	A1	3.900	...	...	0.860	2.564	5.038	...	...	...
F577–V1	A2	4.693	...	...	1.723	5.137	10.052	0.668	2.553	3.307
F577–V1	A3	4.322	0.210	0.472	1.001	2.998	4.247	0.340	0.685	0.468
F577–V1	A4	1.479	...	...	0.178	0.524	4.195	0.247	0.573	0.288
F577–V1	A5	3.966	0.319	0.347	1.451	4.210	4.174	0.377	...	...
F583–1	A2	4.158	...	...	0.896	2.670	3.640	...	...	...
F583–1	A3	1.356	0.526	0.308	1.726	5.145	2.870	...	...	...
F583–5	A1	2.739	0.311	0.461	1.094	3.261	...	...	...	...
F583–5	A2	0.703	...	...	1.102	3.284	...	...	...	...
F585–3	S1A1	3.483	0.364	...	1.341	3.997	3.009	0.072	...	...
F585–3	S1A2	3.038	0.489	...	1.387	4.133	1.050	0.123	0.140	0.119
F585–3	S1A3	...	...	...	0.845	3.262	3.009	0.416	0.391	0.566
F585–3	S2A1	4.274	...	...	0.756	2.515	...	...	...	...
F585–3	S2A2	2.754	...	...	1.074	3.432	...	...	...	...
F585–3	S2A3	3.823	0.717	...	1.190	4.157	...	...	...	...
F585–3	S2A4	2.289	...	...	1.186	3.430	...	...	...	...
F611–1	A1	1.541	...	0.464	1.143	3.456	3.910	0.247	0.361	0.172
F611–1	A2	1.098	0.428	...	0.763	2.682	3.360	0.112	0.174	0.120
F746–1	A1	3.368	0.793	0.385	1.300	4.064	3.715	0.112	...	...
F746–1	A2	5.975	1.445	0.317	1.082	3.235	5.301	0.617	0.967	0.872
F746–1	A3	3.876	1.115	...	1.156	3.035	...	...	...	...
U 1230	A1	2.139	...	0.155	0.884	2.067	3.455	0.132	0.457	0.308
U 1230	A2	2.640	...	0.578	0.866	2.751	3.402	0.280	0.423	0.277
U 1230	A3	2.011	...	0.461	0.941	2.515	3.358	0.260	0.337	0.281
U 1230	A4	2.975	...	0.787	1.604	3.926	5.527	0.171	0.374	0.489
U 1230	A5	1.177	...	0.502	1.699	4.883	3.256	0.266	0.314	0.289
U 5675	A1	5.704	...	...	0.599	1.787	...	...	...	...
U 5675	A2	6.034	...	...	4.045	12.056	...	...	...	...
U 5675	A3	3.320	...	...	0.751	2.869	...	...	...	...
U 5709	A1	4.030	...	...	0.527	1.573	2.893	0.732	...	...
U 5709	A2	7.108	...	...	1.831	5.459	11.082	3.504	...	...
U 5709	A3	2.351	...	...	0.606	1.807	3.752	0.932	...	...
U 6151	S1A1	3.762	0.335	0.429	0.975	2.962	3.310	0.284	0.567	0.360
U 6151	S1A2	4.160	0.421	0.466	1.057	3.094	5.188	0.187	0.944	0.552
U 6151	S3A1	11.449	...	...	0.354	1.055	2.869	0.116	0.503	0.345
U 6151	S3A2	2.922	...	...	0.258	0.770	2.870	0.152	0.401	0.202
U 6614	A1	1.628	...	...	0.059	0.176	...	...	...	...
U 6614	A2	1.824	...	...	0.207	0.618	...	...	...	...
U 6614	A3	1.173	...	...	0.065	0.195	...	...	...	...
U 9024	S1A1	2.438	0.683	0.386	1.597	4.759	...	...	...	...
U 9024	S1A2	3.270	...	...	0.758	2.259	...	...	...	...
U 9024	S1A3	2.691	...	...	0.452	1.347	...	...	...	...
U 9024	S2A1	3.004	...	...	1.060	3.161	...	...	...	...
U12695	S1A1	1.141	0.557	0.454	1.319	3.986	3.249	0.007	0.194	0.009
U12695	S1A2	2.016	0.438	0.357	1.375	3.917	3.351	0.078	0.239	0.085
U12695	S1A3	1.775	0.468	0.413	1.584	4.338	2.653	0.034	0.107	0.038
U12695	S2A1	0.730	0.444	0.447	1.786	5.398	4.573	...	...	...
U12695	S2A2	1.909	0.316	0.430	1.158	3.274	3.266	0.098	0.485	0.144
U12695	S2a3	1.903	0.260	0.435	1.524	4.402	...	...	...	...

The flux measurements are shot noise limited for all but the weakest lines, so their uncertainties are proportional to $\sigma_{H\beta}$ (Column 4 of Table 3.1). The uncertainty is rather larger for the weak lines near the detection limit of a few $\times 10^{-17}$ ergs cm^{-2}s^{-1}, the exact limit depending on the particular observing run.

Method

Figure 3.1 shows an example H II region spectrum with the important nebular lines identified. Note that this is not a typical spectrum; it is one of the better obtained and is chosen for illustration of the relevant lines. Most H II regions in this sample are too faint for any but the strongest lines to be measured with confidence. In particular, while the [O III] λ4363 line is frequently visible, it is generally not observed with sufficiently high signal to noise for a reliable electron temperature to be determined. This makes it impossible to derive abundance information from the nebular spectra using standard methods (Osterbrock 1989). To overcome this difficulty, an extensive theoretical investigation of the behavior of the strong nebular lines was undertaken (McGaugh 1991). This resulted in a new calibration of the empirical abundance indicating line ratio $R_{23} \equiv$ ([O II] λ3727 + [O III] $\lambda\lambda$4959, 5007)/Hβ first discussed by Pagel et al. (1979). This calibration rivals the accuracy of the standard method when an electron sensitive line ratio is available, but has the advantage of relying only on the strongest nebular lines.

Oxygen Abundances from the Strong Line Method

Figure 3.2 shows the reddening corrected data for LSB H II regions plotted on the model grid of McGaugh (1991). The oxygen abundance and volume averaged nebular ionization parameter <U> (essentially the ratio of ionizing photon density to particle density) can be extracted from this plot. While R_{23} alone is sufficient for determining the oxygen abundance on the upper branch (i.e., the solid lines of constant abundance in Figure 3.2 are nearly vertical), this is not the case on the

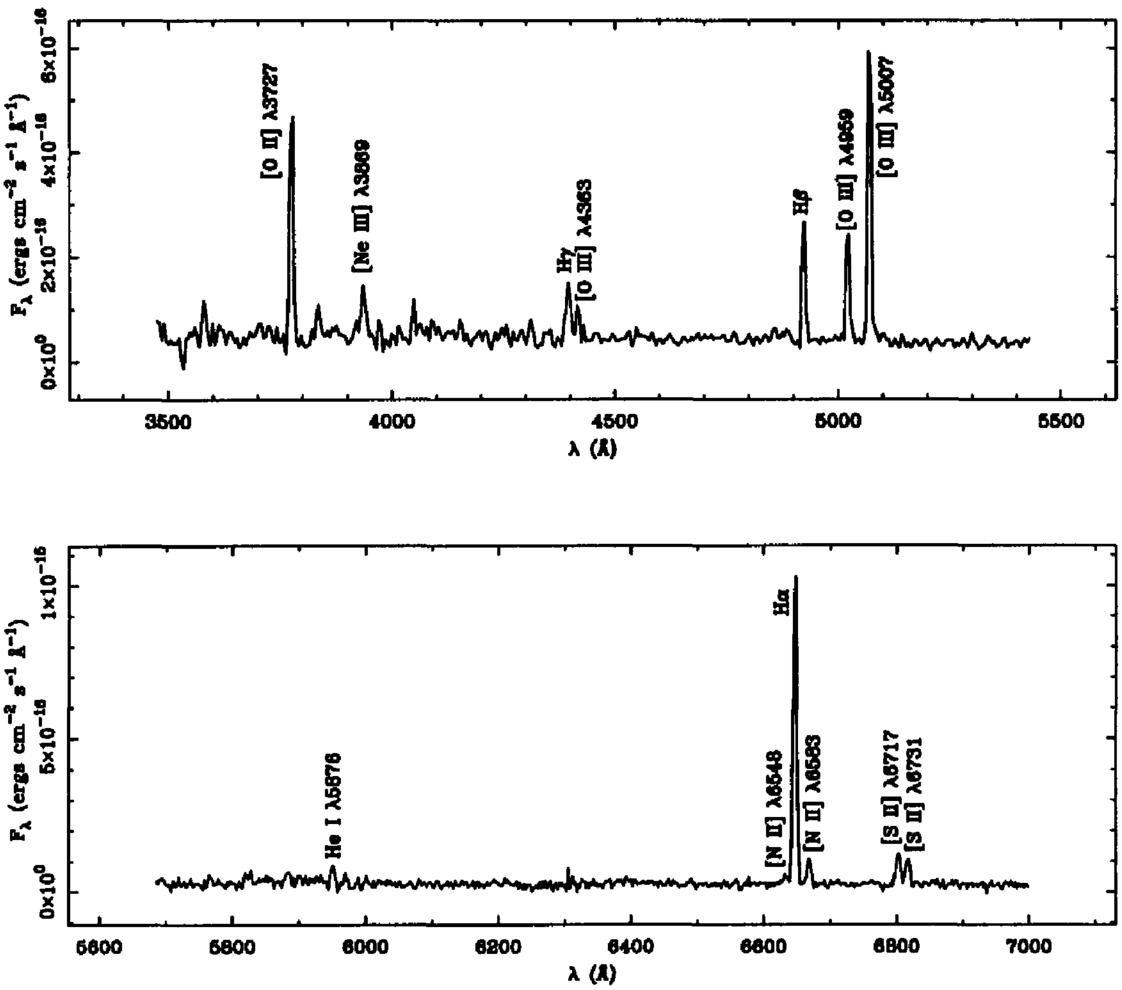

Figure 3.1 — Spectrum of a bright H II region in UGC 1230 with important nebular emission lines labeled.

lower branch. Here R_{23} depends on <U> as well as on abundance, and so these must be determined simultaneously. This is accomplished by plotting the ionization sensitive line ratio $O_{32} \equiv$ ([O III] $\lambda\lambda$4959, 5007)/([O II] λ3727) as the ordinate of Figure 3.2. While both O_{32} and R_{23} depend on both <U> and oxygen abundance on the lower branch, together they contain sufficient information to determine both, and have the further advantage of involving the same strong lines observable in the same wavelength region.

In general, the strong lines are measured with sufficient accuracy that the uncertainty in the calibration dominates, though in some instances the data are the limiting factor. The actual uncertainty in the calibration varies with abundance. On the upper branch (the solid-lined surface of Figure 3.2), R_{23} is accurate to ~ 0.1 dex in log(O/H) (which is the separation between the grid lines!). The uncertainty in <U> on the upper branch is ~ 0.15 dex. The uncertainty in both grows larger above solar abundance as opacity effects become significant in important cooling lines and the models become sensitive to assumed abundance ratios. Fortunately, virtually all LSB galaxies are on the lower branch (the dashed surface of Figure 3.2), as will be shown. Here these uncertainties are unimportant, as the observed oxygen lines and collisional Lyα dominate the nebular cooling. The lower branch calibration is accurate to ~ 0.05 dex in oxygen abundance and ~ 0.1 dex in ionization parameter. For a complete discussion of the uncertainties in the calibration and a comparison to abundances determined with a direct measurement of the electron temperature, see McGaugh (1991).

One weakness of this method is that it is *not* a good indicator of the oxygen abundance in the turnover region (around $\log(O/H) \approx -3.6$, roughly 30% of solar). This results from the bunching of lines of constant abundance near the fold of the model grid in Figure 3.2. It occurs because the lines used by R_{23} and O_{32} totally dominate the nebular physics in this region of parameter space, and hence are sensitive to all variables. This means that for objects near the fold, one can only determine that the abundance is within ~ 0.2 dex of $\log(O/H) = -3.6$. Many H II regions inhabit this region of the R_{23} - O_{32} diagram, which causes a somewhat artificial crowding of values at $\log(O/H) = -3.6$. This point should be kept in mind when interpreting abundances determined in this fashion.

An important result follows directly from casual inspection of Figure 3.2. Many points fall to the right of the fold, outside the range occupied by the model grid. This grid is for H II regions ionized by stellar clusters with a mass spectrum (initial mass function, or IMF) truncated at $M_u = 60M_\odot$. A grid for $M_u = 100M_\odot$ would

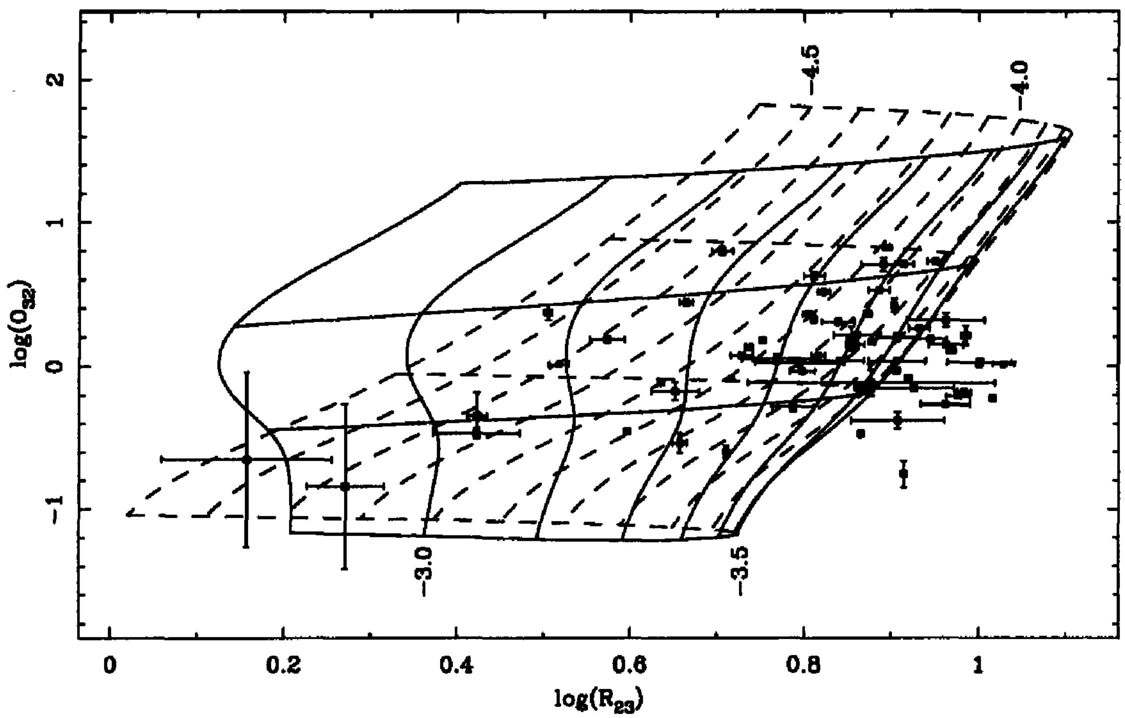

Figure 3.2 — LSB H II region data (solid squares) plotted against the model grid of McGaugh (1991). Solid lines refer to the upper branch (log(O/H) > −3.6) of the R_{23} calibration, while dashed lines refer to the lower branch. Vertical lines of constant abundance are labeled by log(O/H). Horizontal lines of constant ionization parameter range from log<U> = −4 at the bottom to log<U> = −1 at the top. This grid is for a set of H II regions ionized by a cluster IMF with $M_u = 60 M_{\odot}$. A larger M_u would shift the grid to the right slightly, while a smaller M_u would shift it to the left.

be displaced slightly to the right, bringing the ridge line of the fold into agreement (within the errors) with almost all the data. This is a strong indication that high mass stars *are* present in low surface brightness galaxies, a result corroborated by the often large ionizing luminosities implied by the Hβ fluxes in Table 3.1. Thus the properties of these galaxies cannot be the result of an IMF lacking in massive stars (Romanishin, Strom, & Strom 1983, Schombert et al. 1990) unless the IMF is strongly time or space variable.

Of course, that there is a fold in the grid results in an ambiguity – while R_{23} and O_{32} specify O/H and <U> with good precision on both branches, they do not specify which branch is appropriate! That is, the surfaces represented by solid and dashed lines in Figure 3.2 overlap, so that the values of (O/H, <U>) corresponding to any observed (R_{23}, O_{32}) are twofold degenerate, so that two very different H II regions might have identical (R_{23}, O_{32})! While <U> is not too sensitive to this ambiguity (since the lines of constant log<U> do not diverge much), oxygen abundance is. Indeed, the ambiguity can be terribly severe, as it grows as R_{23} decreases: the leftmost point in Figure 3.2 can have either $\log(O/H) = -4.56$ or $\log(O/H) = -2.88$, different by a factor of almost 50! This has caused serious problems in the past (cf. Skillman, Kennicutt, & Hodge 1989).

Fortunately, the easily observable line [N II] λ6583 can resolve the degeneracy. It is strong at high abundance, and quite weak at low abundance. Skillman (1989) suggested using it in the form of the empirical abundance indicator [O III]/[N II] of Alloin et al. (1979). This line ratio varies monotonically with abundance, but is also sensitive to <U>. A superior ratio for this purpose is [N II]/[O II]. This also varies monotonically with oxygen abundance, but is much less sensitive to <U>, and is observed to form a very narrow sequence over a large range of metallicity (McCall, Rybski, & Shields 1985 – see Figure 3.3). The use of [N II]/[O II] in this fashion is also supported by the data of Webster et al. (1983), as well as by the models of McGaugh (1991). Indeed, because it is monotonic and relatively insensitive to other nebular parameters, [N II]/[O II] would be superior to R_{23} as an abundance indicator *if* the N/O ratio were known *a priori.* This is not the case, as N/O varies in a complicated fashion with O/H (see below). Nevertheless, it is adequate to clearly distinguish between the upper and lower branches. In Figure 3.3, the division between upper and lower branches (the fold in Figure 3.2) occurs around $\log([N II]/[O II]) \approx -1$. H II regions in HSB spirals all have [N II]/[O II] equal to or larger than this value (i.e., are on the upper branch; see the data of McCall et al. 1985). In contrast, the majority of LSB H II regions have [N II]/[O II] weaker than this, indicating that they are on the lower, dashed surface of Figure 3.2. That the narrow sequence defined by the McCall et al. data disperses as $\log([N II]/[O II])$ decreases past -1 is expected from the fact that the abscissa R_{23} is sensitive to <U> on the lower branch, and also results from the variation of the N/O abundance ratio in LSB galaxies (see below).

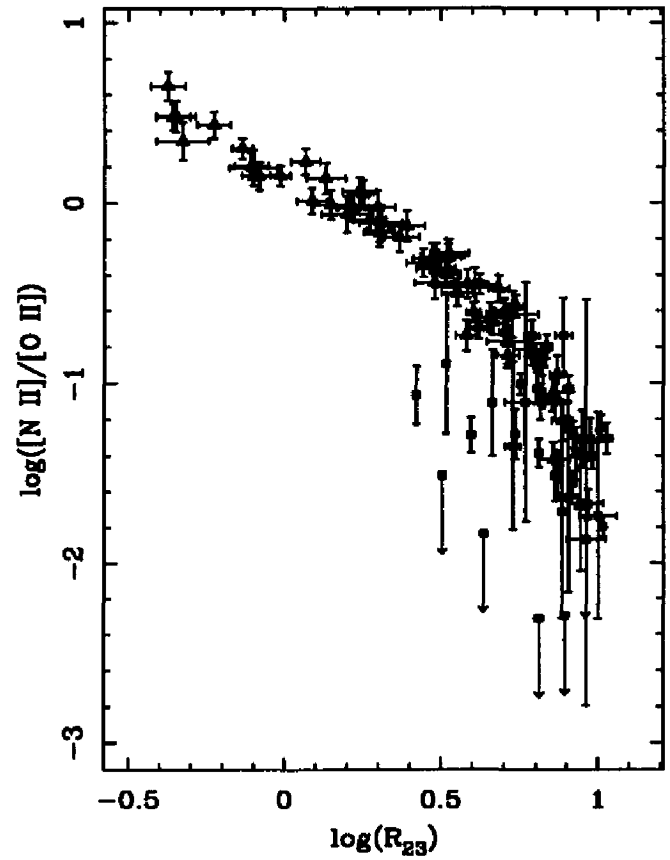

Figure 3.3 — [N II] λ6583/[O II] λ3727 plotted against the abundance indicating line ratio R_{23}. The open triangles are data for HSB spirals taken from McCall et al. (1985). Solid squares are data for LSB galaxies. The LSB data picks up where the HSB galaxy data trail off, indicating that the majority of LSB galaxies are on the lower branch of the R_{23} relation. This transition through the R_{23} turnover region occurs around log([N II]/[O II]) ≈ −1, below which the scatter is expected to increase due to the sensitivity of R_{23} to <U> on the lower branch.

Abundances of Other Elements

Once the key parameters (O/H, <U>) of the H II region are determined in this fashion, it becomes possible to measure the abundances of other elements with emission lines present in the observed spectra. In the observed spectral region, lines of nitrogen, neon, and sulfur are frequently strong enough to be measured (see Figure 3.1). Helium is occasionally present as well, but the determination of helium abundances, while very interesting, is a complicated problem requiring much higher signal to noise in the weak helium lines than is available in this data set (Davidson & Kinman 1985). Hence this discussion will be limited to N, Ne, and S.

Each of these elements are represented in the optical by lines from a single ionization state. In standard practice where the electron temperature is known and the abundance of each ionic state of oxygen (O^0/H, O^+/H, O^{++}/H) can be determined directly, the abundance of elements represented by a single ionization state can be measured by assuming that they arise in the same zone as the equivalent ionization state of oxygen, i.e.,

$$\frac{\mathrm{X}}{\mathrm{H}} = \frac{\mathrm{O}}{\mathrm{O}^+} \times \frac{\mathrm{X}^+}{\mathrm{H}^+} \tag{3.1}$$

(cf. Torres-Peimbert, Peimbert, & Fierro). The factor O/O^+ is known as the ionization correction factor (ICF).

Here, $\mathrm{X}^+/\mathrm{H}^+$ cannot be determined from the line strengths, as there is no direct measure of the electron temperature. It is possible, however, to rewrite equation (3.1) as

$$\frac{\mathrm{X}}{\mathrm{O}} \propto \frac{[\mathrm{X\ II}]}{[\mathrm{O\ II}]}, \tag{3.2}$$

where the observed line strength [X II] replaces the ionic abundance that would be calculated from it. The proportionality can be converted into an equality by defining the moral, if not literal, equivalent of the ICF:

$$\frac{\mathrm{X}}{\mathrm{O}} = I_X \frac{[\mathrm{X\ II}]}{[\mathrm{O\ II}]}. \tag{3.3}$$

I_X (or in practice, its logarithm) can be determined by interpolation through the H II region models. In principle, I_X will depend on all nebular parameters (O/H, <U>, and the shape of the ionizing spectrum, $T_*(M_u)$). In practice, it is not sensitive to T_* as long as $M_u > 30 M_\odot$, a condition which is satisfied for all the H II regions in this sample. Hence the determination of I_X is simply a matter of interpolating through the models to find the offset between logarithmic abundance and line strength

$$\log I_X = \log\frac{\mathrm{X}}{\mathrm{O}} - \log\frac{[\mathrm{X\ II}]}{[\mathrm{O\ II}]} \tag{3.4}$$

for the particular (O/H, <U>) already determined from (R_{23}, O_{32}).

This method is obviously tied to the oxygen abundance and ionization parameter measured from the R_{23}-O_{32} diagram, as well as to the abundances relative to oxygen X/O assumed in the models for the various X. To test how variations in X/O might affect the determination of I_X, a series of models were run wherein the abundances of the elements in question were varied by large (Δ(X/O) = 1 dex) amounts. In all cases, the variation in I_X due directly to the increase was small, $\Delta log I_X \leq 0.03$ dex. That is, the lines in question are almost exactly proportional to the abundance of X/O, at least at low O/H. The indirect effect on the nebular cooling, and hence on the strength of the oxygen lines and the abundance derived therefrom, was slightly more important: $\Delta log I_X \leq 0.05$ dex. Including the effects of the uncertainties in O/H and <U> on I_X, a conservative estimate of the error in the derived abundances is 0.1 dex. Indeed, this method should be *more* accurate than the traditional ICF method, as there is no assumption about the zone in which the lines originate – the complete ionization structure is computed for each element. Moreover, the models are a more sophisticated way of doing the same calculations used by standard techniques. The difference is that one must guess at the inputs (i.e., the abundances) in order to calculate the line ratios rather than using the observed line ratios to compute the abundances. The derived abundances are less sensitive to the other assumed inputs that go into the models (e.g., $T_*(M_u)$) than they are to the assumptions made by the standard method (e.g., isothermality – see discussion in McGaugh 1991).

That theoretically this method *should* work is comforting, but another, more robust test is to apply it to published data with the abundances X/O determined by standard methods. To this end, data of comparable O/H were collected from the literature. These are taken from Kinman & Davidson (1981), Kunth & Sargent

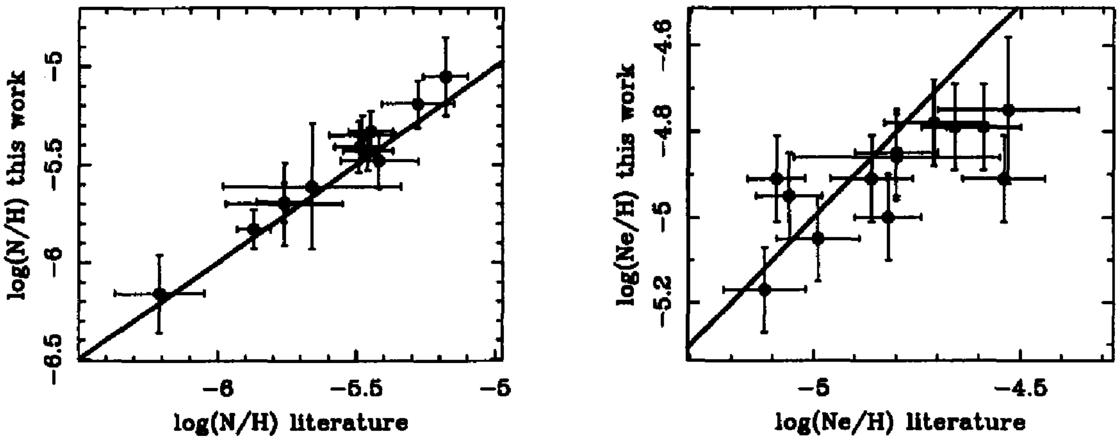

Figure 3.4 — The abundances of nitrogen and neon determined by the methods described here compared to published values. The lines have slope unity. The methods are in excellent agreement, despite a small zero point offset

(1983), and Pagel et al. (1991). Where samples overlap, the more recent value is taken. The galaxies in these samples are predominantly the high surface brightness blue compact galaxies (BCGs) typically found in objective prism surveys.

The results of this exercise are displayed in Figure 3.4. The two methods give nearly identical results for both nitrogen and neon. There appears to be a small zero point offset, but it is within the errors. A similar comparison for sulfur is not possible because of the lack of reported abundances, probably due to the desirability of including [S III] in the abundance determination via the standard method. Because of uncertainties in the atomic data (particularly the photoionization cross section), the sulfur lines are difficult to model (see discussion in Skillman 1989). Hence it is possible that there is some zero point offset to the S/H values reported here. Such an offset would not affect the conclusions, however, as the distribution of relative abundances is more important in this case than their absolute values (see below). Even with this caveat, it is clear that the methods employed here are very good for the task at hand.

Results

The results of the analysis are presented in Table 3.3. Column 1 contains the galaxy name, and Column 2 the H II region. The derived oxygen abundance is in Column 3, and the uncertainty in Column 4. All entries are logarithmic, with abundances by number relative to hydrogen. The ionization parameter and its uncertainty are in Columns 5 and 6. The abundances of nitrogen, neon, and sulfur are reported in Columns 7, 9, and 11, with their respective uncertainties in Columns 8, 10, and 12.

Because of bad weather, not all galaxies that were observed in the blue (where the R_{23} lines are) were also observed in the red (where the [N II] line is). If no other indicator (such as the presence of [O III] λ4363) of the appropriate branch is available, then the abundances determined from (R_{23}, O_{32}) remain ambiguous. Table 3.4 contains the possible oxygen abundances for those galaxies for which this is the case. Column 1 is the galaxy name, and Column 2 the H II region. The oxygen abundance and ionization parameter for the case of the lower branch are reported in Columns 3 and 5. Columns 7 and 9 contain this information for the upper branch case. Associated uncertainties are reported in Columns 4, 6, 8, and 10. Following the results for the galaxies for which the ambiguity is resolved, most of these objects are probably on the lower branch. An exception may be UGC 6614, which is more similar morphologically to F568–6 (Malin 2) than to the rest of the objects in the sample. If this is an indicator, then UGC 6614 may belong on the upper branch with F568–6 (see below). The choice of branch makes an enormous difference in UGC 6614: it is either the most metal poor or most metal rich object in the sample. The ambiguity in this important case needs to be resolved by further observation.

Table 3.3 — LSB Abundances

Galaxy	H II	O/H	σ_O	<U>	σ_U	N/H	σ_N	Ne/H	σ_{Ne}	S/H	σ_S
F415–3	A1	-3.88	0.05	-2.65	0.10	-5.52	0.10	-4.98	0.10	-5.46	0.10
F469–2	A1	-4.14	0.05	-2.73	0.10	-5.57	0.10	-4.98	0.10	-5.56	0.12
F469–2	A2	-3.81	0.07	-2.61	0.10	-5.66	0.31	-4.39	0.15	-5.31	0.16
F469–2	A3	-3.91	0.05	-2.07	0.10	-5.43	0.10	-4.86	0.10	-5.21	0.11
F469–2	A4	-4.20	0.05	-3.02	0.10	-5.83	1.50	-4.93	0.25	...	...
F530–3	A1	-4.12	0.05	-2.31	0.10	-5.29	0.10	-4.87	0.10	-5.16	0.10
F558–1	A1	-3.60	0.20	-3.27	0.20	-5.89	0.25	...	...	...	...
F561–1	A1	-4.07	0.09	-2.81	0.10	-5.32	0.23	...	...	-5.09	0.14
F561–1	A3	-3.74	0.11	-3.01	0.20	-5.51	0.10	...	...	-5.23	0.10
F563–V1	A1	-3.65	0.21	-2.41	0.20	-5.55	0.87	...	...	...	...
F563–V1	A2	-4.54	0.05	-2.54	0.10	-6.05	1.50	...	...	-5.38	0.28
F563–V2	A1	-4.40	0.05	-2.93	0.10	-5.44	0.10	-4.89	0.22	-5.07	0.10
F563–V2	A2	-3.60	0.20	-3.01	0.20	-5.21	0.25	...	...	-5.22	0.25
F563–V2	A3	-3.60	0.20	-2.91	0.20	-5.45	0.25	-4.24	0.25	-5.20	0.25
F568–6	S1A1	-3.60	0.20	-3.51	0.20	...	...	...	...	...	...
F568–6	S1A2	-3.22	0.10	-3.24	0.15	...	...	...	...	...	...
F568–6	S3A2	-3.39	0.10	-3.35	0.15	-4.53	0.15	-4.61	0.16	-5.28	0.15
F568–6	S3A3	-3.60	0.20	-3.39	0.20	-5.09	0.62	...	...	-5.76	0.40
F577–V1	A1	-3.60	0.20	-3.08	0.20	-5.35	0.45	...	...	...	...
F577–V1	A2	-3.60	0.20	-2.79	0.20	-5.68	0.28	...	...	-5.24	0.25
F577–V1	A3	-3.60	0.20	-2.99	0.20	-5.30	0.25	-4.66	0.25	-5.29	0.25
F577–V1	A4	-4.33	0.07	-3.42	0.10	-5.60	0.24	...	...	-5.67	0.21
F577–V1	A5	-3.60	0.20	-2.82	0.20	-5.19	0.25	-4.57	0.25	...	...
F583–1	A2	-3.60	0.20	-2.97	0.20	...	...	...	...	...	...
F583–1	A3	-4.00	0.05	-2.09	0.10	...	...	-4.82	0.10	...	...
F585–3	S1A1	-3.60	0.20	-2.52	0.20	-5.54	0.25	-4.53	0.25	...	...
F585–3	S1A2	-3.62	0.20	-2.47	0.20	-5.27	0.25	-4.42	0.25	-5.39	0.28
F585–3	S2A1	-3.66	0.39	-2.95	0.20	...	...	...	...	...	...
F585–3	S2A3	-3.60	0.20	-2.60	0.20	...	...	-4.26	0.25	...	...
F611–1	A1	-4.11	0.05	-2.47	0.10	-5.28	0.10	...	...	-5.36	0.10
F611–1	A2	-4.34	0.05	-2.43	0.10	-5.56	0.16	-4.95	0.10	-5.57	0.29
F746–1	A1	-3.60	0.20	-2.59	0.20	-5.54	0.25	-4.12	0.25	...	...
F746–1	A2	-3.60	0.20	-2.59	0.20	-5.32	0.25	-3.88	0.25	-5.31	0.25
F746–1	A3	-3.65	0.20	-2.77	0.20	...	...	-4.06	0.25	...	...
U 1230	A1	-4.13	0.05	-2.79	0.10	-5.63	0.25	...	...	-5.31	0.12
U 1230	A2	-3.98	0.05	-2.77	0.10	-5.26	0.10	...	...	-5.85	0.10
U 1230	A3	-4.13	0.05	-2.68	0.10	-5.29	0.10	...	...	-5.33	0.10
U 1230	A4	-3.60	0.20	-2.76	0.20	-5.62	0.29	...	...	-5.40	0.25
U 1230	A5	-3.38	0.10	-1.89	0.15	-4.42	0.20	...	...	-4.47	0.17
U 5675	A1	-3.60	0.20	-3.14	0.20	...	...	...	...	...	...
U 5675	A2	-3.65	0.55	-2.34	0.20	...	...	...	...	...	...
U 5709	A1	-3.36	0.10	-3.04	0.15	-4.52	0.15	...	...	...	...
U 5709	A2	-3.60	0.20	-3.74	0.20	-5.31	0.25	...	...	...	...
U 5709	A3	-3.25	0.10	-2.83	0.15	-4.31	0.15	...	...	...	...
U 6151	S1A1	-3.60	0.20	-2.84	0.20	-5.11	0.71	-4.48	0.25	-5.09	0.39
U 6151	S1A2	-3.60	0.20	-3.02	0.20	-5.70	0.35	-4.32	0.27	-5.32	0.26
U 6151	S3A1	-3.60	0.20	-3.74	0.20	-5.96	0.32	...	...	-5.85	0.32
U 6151	S3A2	-4.10	0.05	-3.38	0.10	-5.60	0.10	...	...	-5.58	0.10
U 9024	S2A1	-3.60	0.20	-2.53	0.20	...	...	-4.15	0.25	...	...
U12695	S1A1	-4.18	0.05	-2.20	0.10	-6.52	2.00	-4.84	0.10	...	...
U12695	S1A2	-3.98	0.05	-2.46	0.10	-5.66	0.10	-4.76	0.10	-5.47	0.10
U12695	S1A3	-4.01	0.05	-2.28	0.10	-5.81	0.53	-4.86	0.10	-5.60	0.65
U12695	S2A1	-4.08	0.05	-2.00	0.10	-6.14	1.50	-4.83	0.10	...	...
U12695	S2A2	-4.09	0.05	-2.51	0.10	-5.62	0.10	-4.96	0.10	-5.23	0.10
U12695	S2A3	-3.92	0.05	-2.38	0.10	...	...	-4.95	0.15	...	...

Table 3.4 — Ambiguous Abundance Determinations

		Lower Branch				Upper Branch			
Galaxy	H II	O/H	σ_O	<U>	σ_U	O/H	σ_O	<U>	σ_U
F568–1	A1	-4.38	0.05	-2.75	0.10	-3.13	0.10	-2.37	0.15
F568–1	A2	-4.00	0.09	-2.85	0.10	-3.33	0.10	-2.64	0.15
F583–5	A1	-3.95	0.05	-2.65	0.10	-3.40	0.10	-2.47	0.15
F583–5	A2	-4.39	0.05	-2.07	0.10	-3.18	0.10	-1.70	0.15
F585–3	S2A2	-3.94	0.07	-2.61	0.10	-3.41	0.10	-2.46	0.15
F585–3	S2A4	-4.03	0.05	-2.52	0.10	-3.36	0.10	-2.33	0.15
U 5675	A3	-3.91	0.08	-2.87	0.10	-3.40	0.10	-2.69	0.15
U 5675	A3	-3.91	0.08	-2.87	0.10	-3.40	0.10	-2.69	0.15
U 6614	A1	-4.37	0.07	-3.83	0.58	-2.94	0.10	-3.55	0.58
U 6614	A2	-4.38	0.05	-3.30	0.16	-3.03	0.10	-2.97	0.20
U 6614	A3	-4.56	0.12	-3.62	0.62	-2.88	0.10	-3.27	0.72
U 9024	S1A2	-3.97	0.05	-2.91	0.10	-3.34	0.10	-2.77	0.15
U 9024	S1A3	-4.15	0.05	-3.06	0.10	-3.19	0.10	-2.83	0.15
U 9024	S2A1	-3.92	0.05	-2.67	0.10	-3.41	0.10	-2.52	0.15

Discussion

Global Evolution

A fundamental measure of the extent of evolution that a galaxy has undergone is the degree to which it has converted the primordial gas from which it formed into stars and, through them, to metals. The latter is traditionally quantified as the metallicity Z, or mass fraction in elements heavier than hydrogen and helium. However, only within the solar system is this quantity actually measured. In studies of stars, what is usually quoted is [Fe/H], the abundance of iron relative to the solar level. The conversion to Z depends on the relative abundance of all other elements to iron, usually *assumed* to be solar. This turns out to be a very bad assumption for low metallicity stars in our own galaxy, where iron contributes a much smaller relative fraction to Z than does oxygen (cf. Abia & Rebolo 1989). This situation is complicated by the extreme variations that can occur in the iron to oxygen ratio depending on the star formation history of a galaxy (Gilmore & Wyse 1991). In other galaxies, the matter is further complicated in that studies of stellar metallicities are usually based on yet another element, usually magnesium (e.g., Thomsen & Baum 1987), while studies of the gas phase metallicity as probed by H II regions (such as this one) report the oxygen abundance. These differences, together with the fact that galactic absorption line strengths reflect the luminosity weighted average metallicity of a composite stellar population, while H II region abundances probe the local gas phase abundance, makes intercomparison of the results from these various methods problematic.

Of the possible approaches, the data presented here are probably best suited to the purpose at hand. The current gas phase abundance should represent the highest metallicity reached by contributions from all generations of stars. Oxygen is the most abundant of the metals, and provides the plurality of mass therein. As such, it is the best tracer of the metallicity Z. Also, it is produced in quantity exclusively by massive ($M > 10M_{\odot}$) stars. Thus it originates in a well defined population and is returned to the interstellar medium (ISM) on short timescales. In contrast, iron is contributed by several sources on a variety of timescales (Wheeler, Sneden, & Truran 1989).

Figure 3.5 shows the histogram of abundances for LSB galaxies for which the branch assignment is certain, and for the compilation of McGaugh (1991). The latter is dominated by BCGs, and so peaks at low (10 – 15% of solar) metallicity. Both samples are plagued by severe selection effects, which makes the interpretation of Figure 3.5 difficult. As argued by McGaugh (1991), the low peak of the BCG data may be induced partially by the requirement that λ4363 be detected in order for an abundance determination to be made; this results in a bias towards high electron temperatures, which in turn means low abundance (of coolants). There is no such abundance selection effect in the LSB sample, but this is by no means complete, so the distribution cannot be interpreted quantitatively. In particular, the prominent peak at $\log(O/H) = -3.6$ results in part from the uncertainty in the R_{23} method

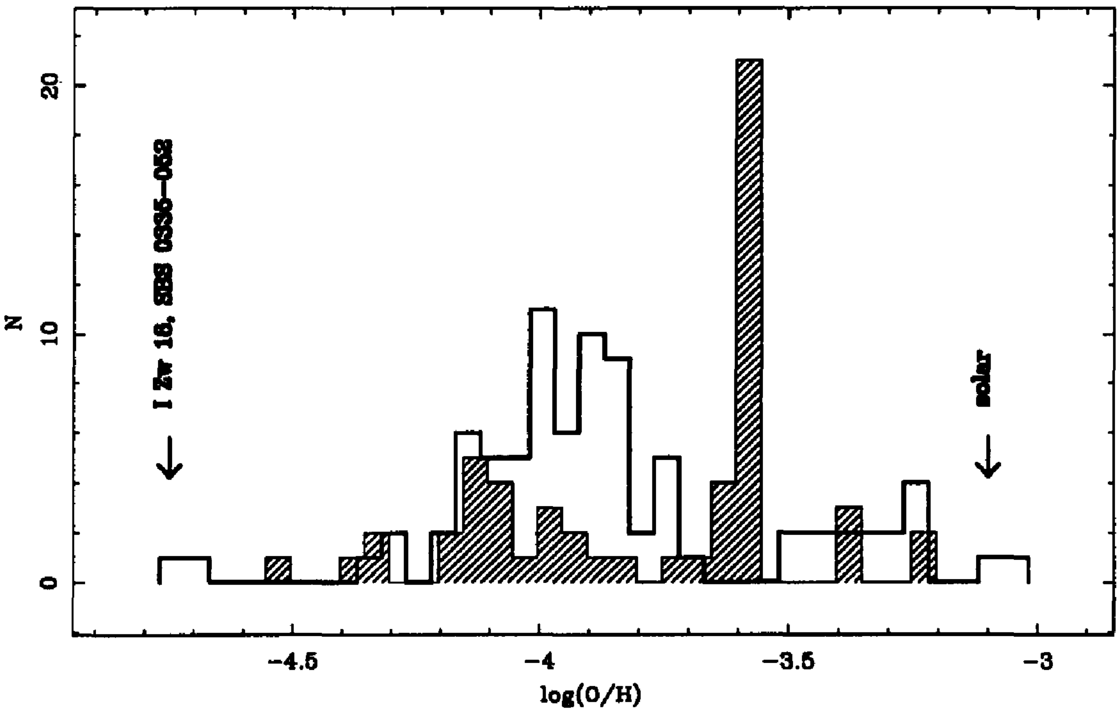

Figure 3.5 — Histogram of oxygen abundances for LSB galaxies (hatched histogram) and for the compilation of McGaugh (1991) (open histogram). The latter is dominated by BCGs. For reference, solar abundance and the abundance of the most metal poor galaxies known, I Zw 18 and SBS 0335 − 052, are marked with arrows. LSB galaxies are generally metal poor, with $Z \lesssim 30\% Z_{\odot}$. The strong peak at log(O/H) = −3.6 is *partly* an artefact of the method employed to determine the oxygen abundance.

at this abundance. There really are a fair number of H II regions *centered* around log(O/H) = −3.6, but the larger errors at this abundance cause the appearance of an artificially sharp spike.

In spite of these difficulties, several points can be made. First, LSB systems cover a wide range in metallicity, over an order of magnitude in O/H, with no obviously preferred value or well defined mean. Thus, these galaxies represent a broad spectrum of enrichment timescales. This is not surprising given the diversity of size and morphology represented in this sample, and suggests that many evolutionary histories are possible which lead to galaxies which are not represented by the Hubble sequence.

Second, the LSB galaxies with the lowest metallicities are as low as any known extragalactic objects with the exception of I Zw 18 and SBS 0335 − 052 (Izotov et al. 1990). This is indeed extremely metal poor. Kunth & Sargent (1986) showed that an abundance of $\log(O/H) \approx -4.3$ can be reached in a very short time (a few million years) as the result of production in the first stars to explode as supernovae. They suggest that this may be the reason that objects more metal poor than this are extremely rare: as soon as star formation commences, even primordial gas will be enriched to this level very rapidly. Thus it is possible that objects with $\log(O/H) \leq -4.3$ are undergoing their first episode of star formation. Indeed, based on abundance and color, Salzer et al. (1991) conclude that the stars producing the bulk of light of the optical component of the H I cloud in Virgo are extremely young. This object is a typical low surface brightness galaxy by the standards of this sample. Regardless of the age of the stellar population, it is clear that these galaxies are underevolved relative to their HSB counterparts, and that selecting for low surface brightness is as effective as other means of discovering low metallicity objects (cf. Skillman et al. 1988).

That these galaxies are relatively unevolved is the third, and most important, point. Virtually all LSB galaxies have substantially subsolar abundances. The only galaxies containing H II regions with $\log(O/H) > -3.6$ are UGC 5709, F568-6, and UGC 1230. The latter has four low abundance H II regions and one high abundance one with an anomalously large [N II]/[O II] for its R_{23} (see Figure 3.3). This may indicate that this nebula is gas bounded, which would invalidate the abundance determined for it by the methods employed here. UGC 5709 is relatively high surface brightness ($\mu_0 = 22.49$ mag arcsec^{-2}, Chapter 2), brighter than the other galaxies by about half a magnitude. F568-6 is also known as Malin 2, the second example of an extremely large, low surface brightness disk (Bothun et al. 1990), and as such may be fundamentally different from the other galaxies in this sample. Excluding these few objects leaves only those with $\log(O/H) \leq -3.6$. This low degree of chemical evolution confirms the inference of Bothun et al. (1990) that LSB disks evolve slowly, and can remain quiescent for a Hubble time.

Local Conditions

The H II regions also provide powerful probes of the local conditions where star formation is occurring. This is of considerable interest in the more pristine systems, which may be as close to the first epoch of star formation as is observable. The mode of star formation in LSB galaxies is in some way different from that in other low abundance systems (e.g., BCGs) which result in very high surface brightnesses. In particular, the strict limits placed on molecular emission from LSB galaxies (Schombert et al. 1990) and their low H I column densities (Chapter 4) imply that the formation of molecular clouds may be impaired, and thus may not be the sites of star formation as is usually presumed to be the case. Another important constituent of molecular stellar cocoons is substantial quantities of dust to shield the molecules from the interstellar radiation field, and provide sites for the formation of molecular hydrogen. The reddening towards H II regions, usually high in HSB disks (Kennicutt 1983), provides an indication of the available dust content.

Dust and Molecular Gas

A histogram of the dust content as measured by the reddening $E(B-V)$ along the line of sight to the H II regions as determined by the Balmer decrements and corrected for reddening due to our own galaxy (Burstein & Heiles 1984) is presented Figure 3.6. Also shown is the data for Sc galaxies of McCall et al. (1985). Again, selection effects make the quantitative interpretation of the distribution in this histogram problematic. In particular, the McCall et al. (1985) sample might exclude heavily obscured objects. Taken at face value, though, the two distributions look similar, with perhaps a slight tendency for LSB galaxies to contain less dust. Nevertheless, there appears to be dust in at least some LSB galaxies which could potentially be associated with molecular material.

The lack of CO detections by Schombert et al. (1990) could result from the breakdown of the CO/H_2 conversion at low metallicity (Maloney & Black 1988). If the conversion factor scales simply as the abundance, and C/H approximately follows O/H, then the paucity of C and O can marginally explain the nondetections. That is, if

$$\frac{L(CO)}{M(H_2)} \propto \frac{\mathrm{C}}{\mathrm{H}} \times \frac{\mathrm{O}}{\mathrm{H}} \propto \left(\frac{\mathrm{O}}{\mathrm{H}}\right)^2, \tag{3.5}$$

then the mean upper limit $M(H_2)/M(HI) \leq 0.1$ of Schombert et al. (1990) can be satisfied *if* $(\mathrm{O/H}) \leq 0.33(\mathrm{O/H})_\odot$ (a condition which is satisfied by almost all LSB galaxies), ***and if*** $M(H_2) \leq M(HI)$ (usually $M(H_2) \geq M(HI)$ in HSB disks). But there are stricter limits placed on individual galaxies, and it seems unlikely that the CO/H_2 conversion follows the simple behavior suggested by equation (3.5). Indeed, Sage et al. (1991) find no correlation between $L(CO)/M(HI)$ and metallicity, in which case the large H I masses of LSB galaxies should lead to easily detectable molecular gas if the latter is present in "normal" relative quantities.

Given these caveats concerning the interpretation of the CO line (see also Adler, Allen, & Lo 1991), it seems that either LSB galaxies are devoid of molecular gas, or possess modest amounts likely to be distributed in a cloud mass spectrum different from HSB galaxies as a result of the low H I column densities. Any impairment of molecular cloud formation could in turn impair star formation, and lead to the current, relatively unevolved state of LSB galaxies. This supports the notion (van der Hulst et al. 1987, Bothun et al. 1990) that the surface density of H I is the fundamental physical quantity which controls the rate of disk evolution. Also, it should be noted that if LSB galaxies are indeed devoid of molecular gas, then the observed star formation is proceeding without the benefit of molecular clouds in sites fundamentally different from those observed in our own galaxy.

Not only can star formation proceed without apparent molecular clouds, it also seems able to proceed before dust is produced. Figure 3.7 shows the reddening to-

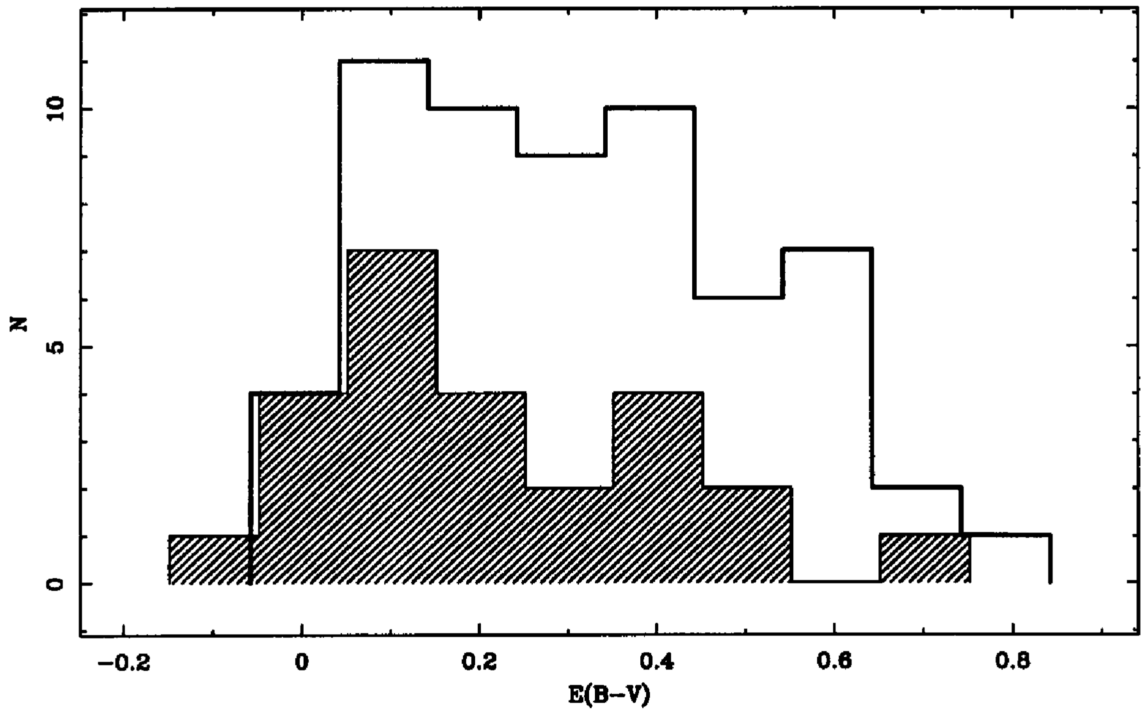

Figure 3.6 — A histogram of the reddenings determined from the Balmer decrements and corrected for the galactic contribution. The hatched histogram is for LSB galaxies, while the open histogram is taken from the data of McCall et al. (1985). Only well determined values ($\sigma_{E(B-V)} \leq 0.1$, i.e., the bin size) are included. Inclusion of the entirety of both data sets does not much affect the shape of the distribution.

wards H II regions in this sample as a function of abundance. While there is no tight correlation, a trend of dust content increasing with metallicity is apparent (see also Campbell, Terlevich, & Melnick 1986). That there is a positive trend indicates that dust, like the heavy elements of which it is composed, is a stellar product which exists only in trace amounts in the least evolved systems. Indeed, that there are so many systems with low reddening immediately suggests that the low surface brightness of these galaxies is *not* induced by large internal extinction. This is corroborated by the lack of IRAS detections of LSB galaxies (Schombert & Bothun 1988), which further suggests that they do not contain large amounts of gray dust. It also means that the IRAS database is incomplete in LSB galaxies as are optical catalogs.

The large scatter in Figure 3.7 probably indicates that the stellar population responsible for dust production is not closely related to that responsible for oxygen production. This is not surprising, since the latter is made by hot, massive stars, while the former is probably made in the atmospheres of very cool stars. Thus the scatter is a natural result of fluctuations between the relative numbers of these stars as they evolve through the HR diagram. That is, one expects the dust to oxygen ratio to be very sensitive to the details of the star formation history, at least in systems with low abundance or irregular star formation rates, where no steady state has been reached between these quantities.

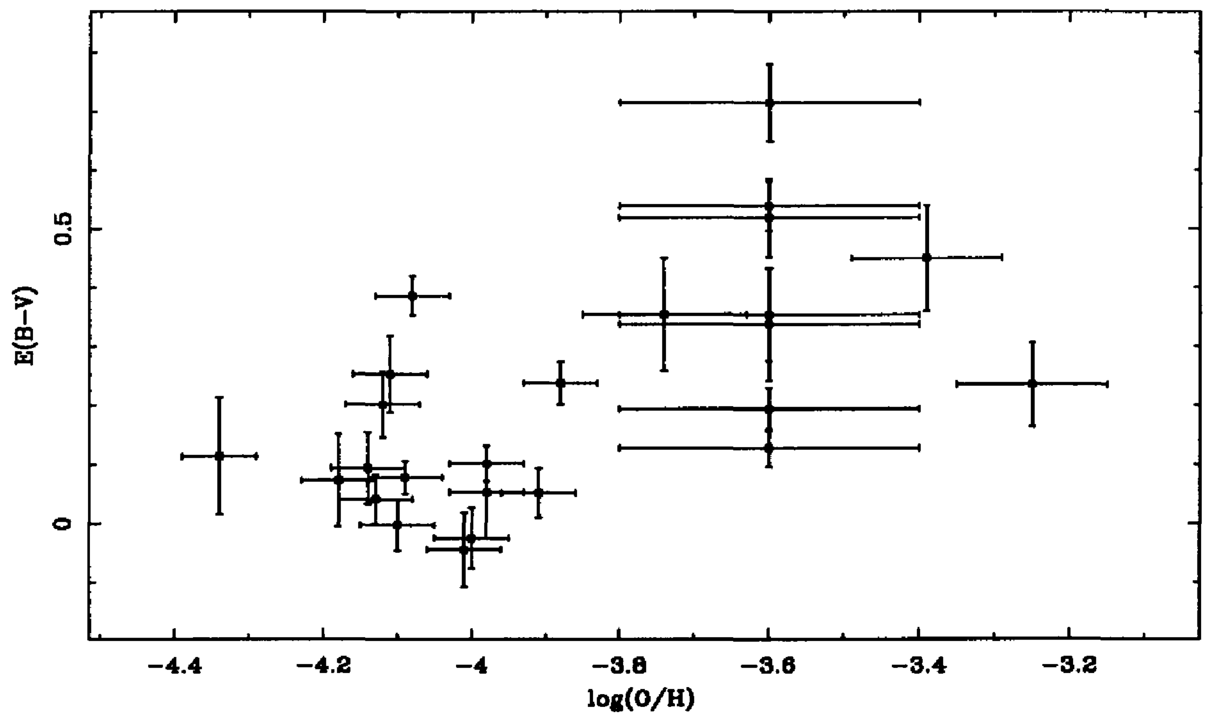

Figure 3.7 — The reddening towards LSB H II regions, corrected for galactic contribution, is plotted against the oxygen abundance. Only well determined ($\sigma_{E(B-V)} \leq 0.1$) values are included. The stacking at log(O/H) = −3.6 is an artefact of the R_{23} method.

Ionization

Another indicator of the local conditions under which star formation is proceeding is provided by the ionization parameter. From equation (6) of McGaugh (1991), it follows that

$$<U> \propto Q^{1/3} N_H^{1/3} \epsilon^{2/3}. \tag{3.6}$$

That is, <U> depends on the ionizing luminosity of the star cluster Q, the gas density N_H, and the gas filling factor ϵ. Bright, compact nebulae are characterized by high <U>, while dim or diffuse nebulae have low values of <U>.

The existence of a correlation between the ionization parameter and the oxygen abundance in the H II regions of HSB galaxies is apparently well established (Dopita & Evans 1985, Campbell 1988, Diaz et al. 1991). The existence of such a relation would imply either that low metallicity stars clusters produce more ionizing luminosity than high metallicity ones, or that the resulting H II regions are preferentially more diffuse at high metallicity, or both. The first possibility could result if the mass spectrum of clusters is a function of metallicity, or if at high metallicity larger amounts of dust are present and absorb a larger fraction of the ionizing luminosity. The second possibility, that high metallicity H II regions are more diffuse could result from metallicity dependent wind strengths or radiation pressure.

However, no such correlation exists for LSB galaxies (Figure 3.8). This suggests that the correlation observed in HSB galaxies is a selection effect, as argued by McGaugh (1991) on theoretical grounds. It is possible that an envelope of decreasing <U> with increasing O/H is present in Figure 3.8 if the one point at high (O/H, <U>) is ignored. This point is due to the H II region in UGC 1230 suspected of being gas bounded, in which case it should be ignored. If this envelope is real, then one would expect an apparent correlation to be induced by observing only the highest surface brightness H II regions, which would be those with the highest <U> at a given metallicity. However, it is clear from Figure 3.8 that many values of <U> exist at any given O/H. This is expected from simple evolutionary considerations: as an H II region ages, the stars providing the ionizing luminosity will die, and perhaps disperse the gas through the actions of stellar winds and supernovae. Both of these will reduce <U>. The stars will also enrich the H II region in oxygen, but this will hardly be perceptible except at low abundance. This will result in an evolutionary track of decreasing <U> at nearly constant O/H. Hence one expects an unbiased sample to contain many <U>, not just those along the envelope. This predicts that studies to faint levels within HSB galaxies would find that lower surface brightness H II regions fill in the area below the envelope; i.e., they would have a distribution similar to that in Figure 3.8.

If evolution is the cause of the distribution in Figure 3.8, then the existence of an envelope suggests that star clusters which become the ionizing sources for extragalactic H II regions form with the same typical mass and density that will result in the <U> value along the envelope for the appropriate metallicity. However, it is also possible that the clusters form over a wider variety of conditions rather than evolving to the various observed <U>. If this is the case, then an envelope would represent some limiting factor to the star formation process rather than being a universal result thereof. That many low <U> H II regions are found in LSB systems suggests that star formation may be proceeding in a more diffuse environment in these diffuse galaxies.

Note that the widespread distribution in (O/H, <U>) is an inevitable consequence of that in (R_{23}, O_{32}) (Figure 3.2). That the physical properties of H II regions cover such a range with no apparent preference reinforces the importance of selection effects in astronomy. In this case, selection effects have led to the impression that low abundance H II regions are automatically high excitation, but here are many examples of low abundance H II regions for which this is not the case.

The Abundances of Nitrogen, Neon, and Sulfur

Just as the low oxygen abundances indicate that LSB galaxies are relatively unevolved, the abundances of other elements may hold clues to their star formation histories and IMFs. Variations in these can leave different signatures for different

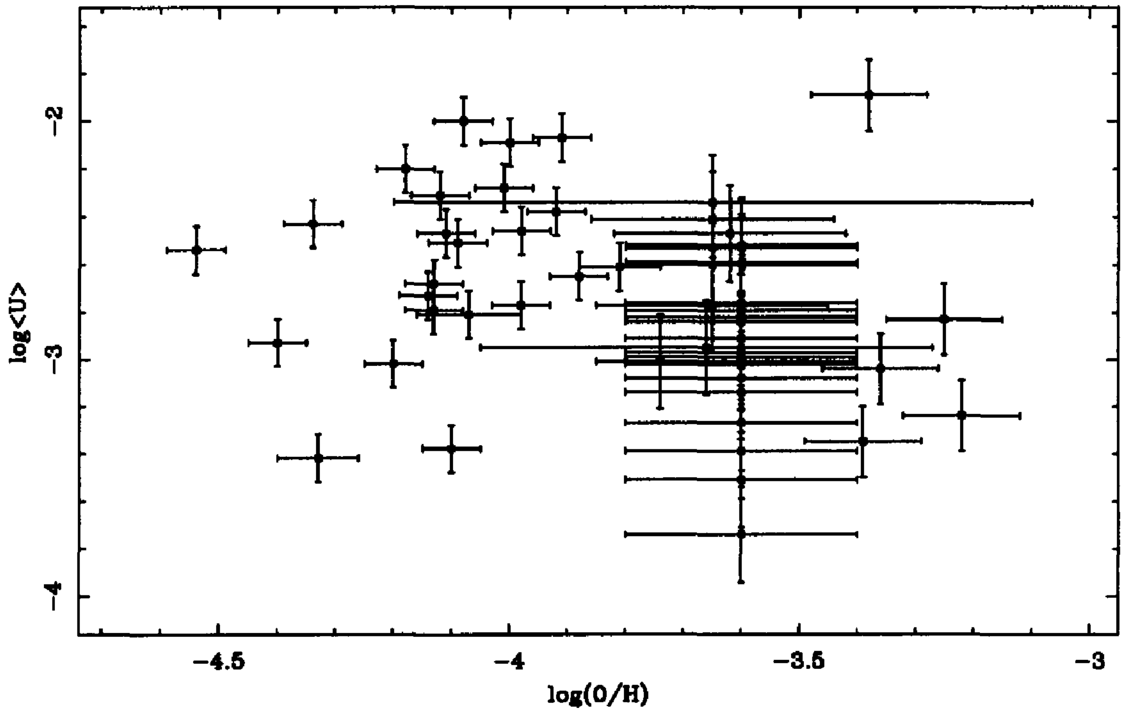

Figure 3.8 — Nebular ionization parameters and oxygen abundances. One can think of this as the result of the transformation of Figure 3.2 from (R_{23}, O_{32}) to (O/H, <U>) coordinates. As in Figure 3.2, no correlation is evident. The stacking of points at log(O/H) = −3.6 is an artefact of the R_{23} method induced by the rapid change in the manifold of Figure 3.2 near this value of the abundance.

scenarios (see Wheeler et al. 1989). At the least, comparison to different samples of similar oxygen abundance should make apparent similarities or differences in these.

Nitrogen

The abundance of nitrogen in LSB galaxies is compared to that in a sample of other low abundance galaxies in Figure 3.9. This sample, as above, is drawn from Kinman & Davidson (1981), Kunth & Sargent (1983), and Pagel et al. (1991). These are predominantly high surface brightness BCGs.

The most striking feature of Figure 3.9 is the difference in the trend followed by each sample. The LSB galaxies follow a line of zero slope below log(O/H) $\lesssim -3.6$, while the HSB objects follow a line of unity slope. That is, N/H is approximately constant in LSB galaxies, while it tracks O/H in HSB galaxies (i.e., N/O is constant).

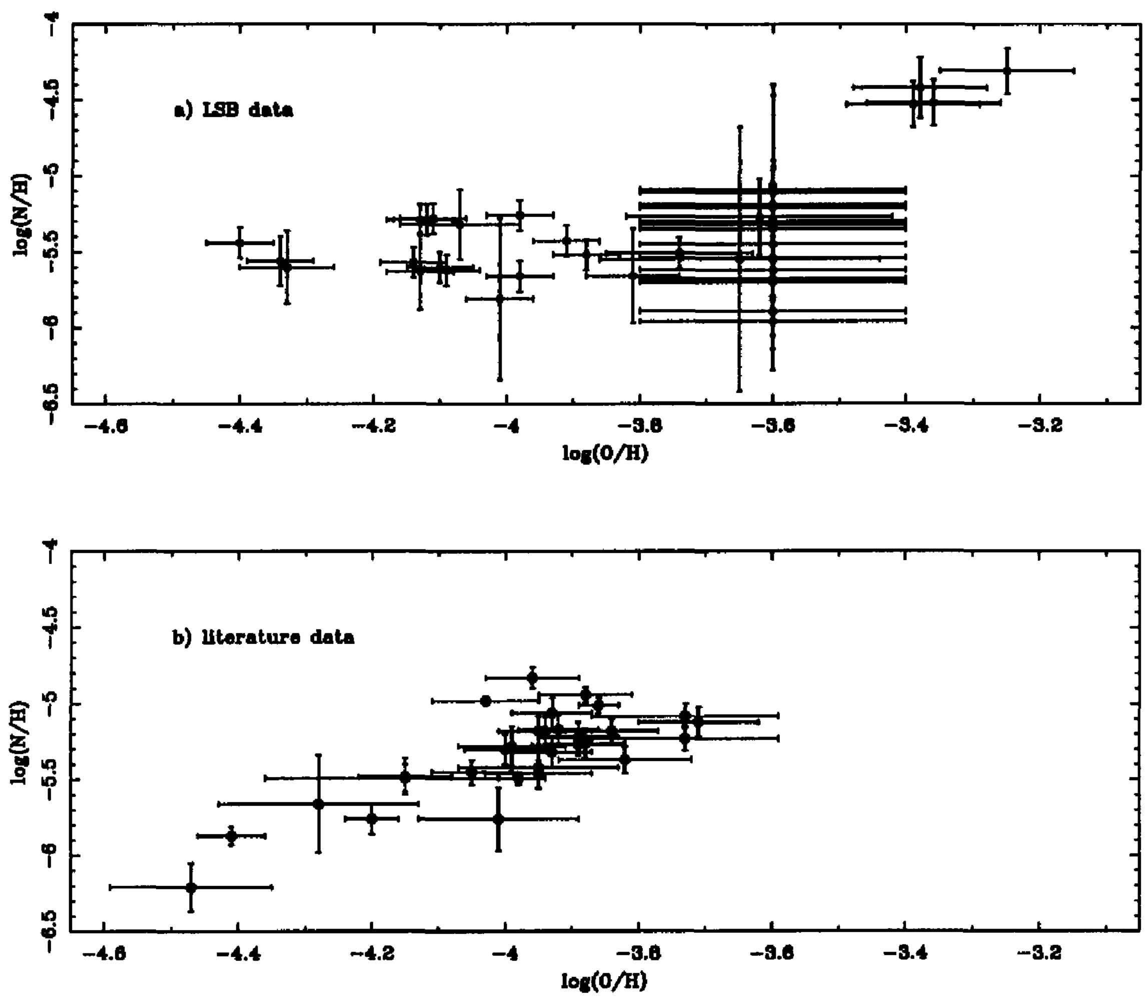

Figure 3.9 — The abundance of nitrogen by number relative to hydrogen plotted against the oxygen abundance. a) LSB galaxies. b) A comparison sample of HSB galaxies drawn from the literature, plotted on the same scale. Note the very different behavior with decreasing oxygen abundance. The stacking of values at log(O/H) = −3.6 is an artefact of the R_{23} method.

This difference is not an artefact of the method, since the method employed here reproduces the results for HSB BCGs (see above). What, then, could cause this difference?

To address this question, it is useful to review what is known about the nucleosynthesis of nitrogen. Nitrogen is an end product of the CNO cycle, and as such is produced mainly as a secondary element in intermediate ($2M_{\odot} \leq M \leq 8M_{\odot}$) mass stars (Matteucci 1986). That is, its abundance depends on the abundance of seed species, so that the expectation is that N/O should increase in proportion to O/H, a line of slope *two* in Figure 3.9. At high abundance, this is nearly the case, so that the high abundance LSB data is approximately "normal." It has been suggested that the change to slope one seen in BCGs is evidence of a primary (i.e., one which requires no seed) source of nitrogen production (Matteucci 1986). While this is possible, it gives no hint of how to produce a slope of zero where N/H remains constant as O/H increases by nearly an order of magnitude. Indeed, even models with many adjustable parameters have difficulty in reproducing the trend in the BCG data (Matteucci & Tosi 1985), and certainly never result in anything like what is seen in Figure 3.9a.

Neon

The situation for neon is even more perplexing. In Figure 3.10, neon is seen to behave in the same way as nitrogen. The low abundance ($\log(O/H) < -3.8$) LSB data cluster around a constant neon abundance with with small scatter, while the HSB galaxies follow a trend with unity slope. This latter is what is expected, as neon is produced as a primary element in approximately the same sites as oxygen (massive stars). While the models are uncertain (cf. Wheeler et al. 1989), the sum over a fixed IMF should result in a fixed Ne/O ratio (so that Ne/H increases in lock step with O/H) regardless of star formation history (since both are produced on the same short time scale). While a difference in the IMF could conceivably cause the observed difference, this is hard to reconcile with the observation that the IMF of LSB galaxy H II regions is not obviously distinguished from that in BCGs (see above).

Sulfur

The situation is similar for sulfur (Figure 3.11). Regardless of possible zero point shifts discussed previously, the abundance of sulfur is scattered around an approximately constant value as the oxygen abundance increases. Like neon, sulfur should be produced as a primary element in massive stars (cf. Wheeler et al. 1989), and S/O

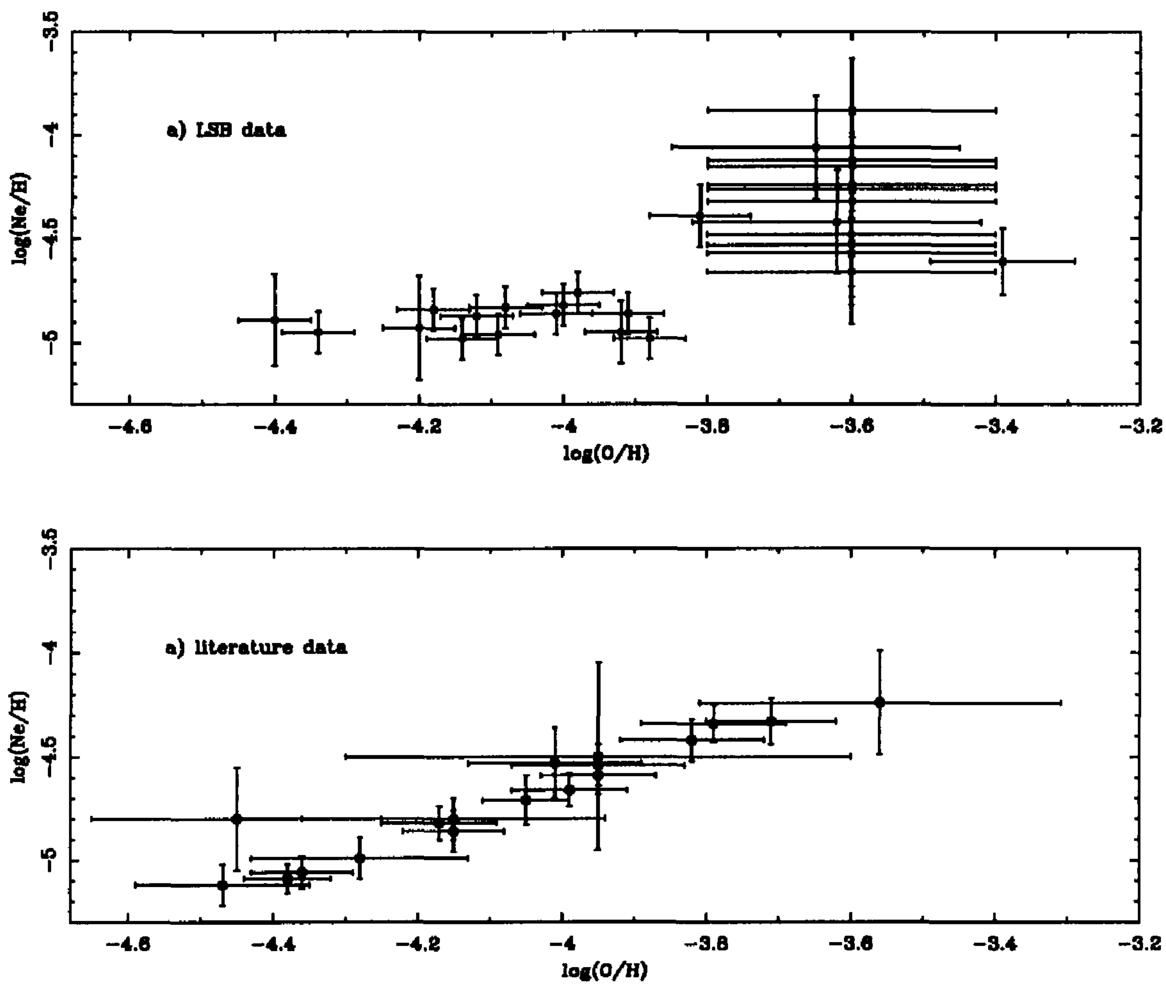

Figure 3.10 — The abundance of neon by number relative to hydrogen plotted against the oxygen abundance. a) LSB galaxies. b) A comparison sample of HSB galaxies drawn from the literature, plotted on the same scale. Note the very different behavior with decreasing oxygen abundance. The stacking of values at log(O/H) = −3.6 is an artefact of the R_{23} method.

should be fixed for a fixed IMF. As with the other observed elements, this is clearly not the case in LSB galaxies. It is also observed not to be the case in HSB spirals (Diaz et al. 1991 and references therein), though the slope at these high abundances is different. Regardless of the cause of the behavior at high metallicity, it is difficult to understand how LSB galaxies maintain constant levels of both secondary (nitrogen) and primary (neon and sulfur) elements while oxygen increases.

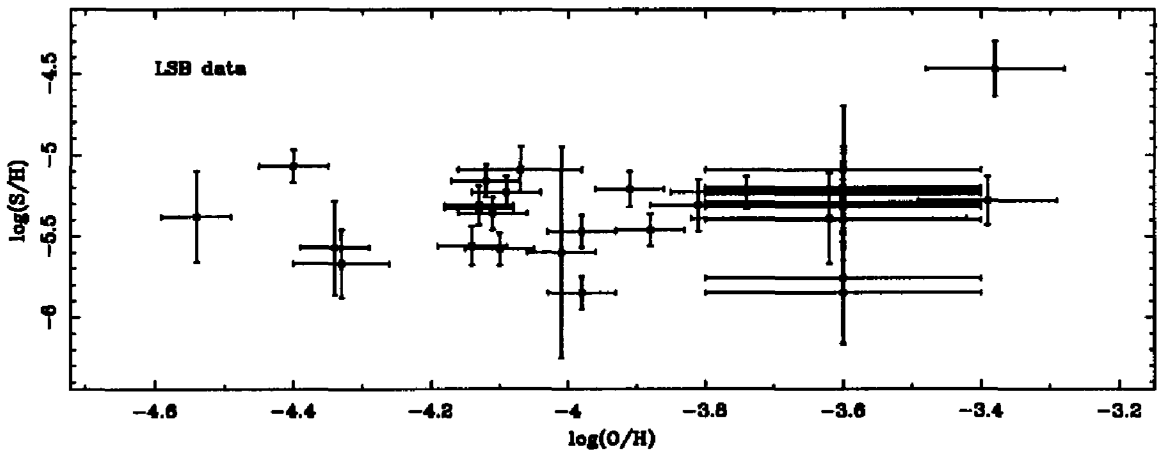

Figure 3.11 — The abundance of sulfur by number relative to hydrogen plotted against the oxygen abundance for LSB galaxies. A comparable sample is not available in the literature. The stacking of values at log(O/H) = −3.6 is an artefact of the R_{23} method.

Possibilities

One possibility is that oxygen is preferentially lost through the action of supernova driven winds. The large gas mass fractions of many of these galaxies (Chapter 4) indicate that substantial gas loss has not occurred, so this seems unlikely. Moreover, a detailed study of one LSB galaxy (Puche et al. 1992) shows that bubbles can expand relatively farther than in HSB galaxies without breaking out of the disk. While gas loss may be important in some cases, it is rather *ad hoc* to invoke it to explain the observed abundance ratios. In particular, it is unclear how preferential oxygen ejection could result in a constant level of neon and sulfur (presumably made in the same stars which eject oxygen) while the oxygen remaining in the galaxy *increases*. This mechanism must then change behavior around $\log(O/H) \approx -3.8$ to allow neon to increase as well. Hence it seems best not to invoke preferential oxygen ejection to explain the observed abundances. It should, however, be noted that if oxygen *is* lost preferentially in great quantity, then the previous conclusions about the unevolved state of LSB galaxies must be reevaluated. That the abundances of the other elements are comparably (if not explicably) low suggests that this is not likely.

The IMF and Star Formation History

The differences in the observed abundance trends between LSB and HSB galaxies are most likely the result of some combination of variation in the IMF and star formation history in these galaxies. That the star formation history in LSB galaxies should be different from HSB galaxies is hardly surprising. But it is not clear that a quantitatively satisfactory scenario can be found.

One possibility is that star formation in LSB galaxies is bimodal. That is, massive stars responsible for the production of oxygen are formed in events separate from those which form intermediate mass stars which produce nitrogen. In this way, the production of oxygen could be suppressed by preventing the high mass stars from forming, until the present observed H II regions if necessary. Even ignoring neon and sulfur, however, this scenario fails. It should result in gradually increasing N/H while O/H remains fixed, opposite of what is observed!

The polarity of the bimodality could be reversed, inhibiting intermediate mass star formation while massive stars are formed quasi-continuously. This would reproduce the oxygen abundances acceptably, but would not get the nitrogen right. If the massive star mode produced some primary nitrogen, its abundance would increase in lock step with oxygen. If instead nitrogen production is left to a generation of intermediate mass stars, N/H should increase gradually (though not in a way correlated with O/H) because of the long ($\approx 10^9$ year) timescales on which these stars evolve. Perhaps Figure 3.9 can be explained if all contributors to the nitrogen abundance have died by the present epoch, and have already contributed all the nitrogen that will be made. Then if all LSB galaxies shared some mechanism which made the same relative numbers of intermediate mass stars at some early epoch, a fixed N/H would be reached and remain unaltered. However, not only is such a mechanism *ad hoc*, it does nothing to address the situation for neon and sulfur, and requires that no intermediate mass stars be present and contributing nitrogen to the ISM at the epoch of observation. It would be very difficult to match the observed surface brightnesses and colors of these galaxies (Chapter 2) with only massive stars!

Variations in the star formation history can lead to very different abundance ratios between elements produced on different timescales (cf. Wheeler et al. 1989). Gilmore & Wyse (1991) showed that a galaxy which forms stars in a few discrete bursts will have a very different Fe/O ratio than one in which the star formation rate remains roughly constant. This occurs because iron is produced in significant quantities in sites and on timescales different from those of oxygen production. Hence a burst will rapidly increase the oxygen abundance, which will then remain constant as iron is more gradually produced. Since nitrogen is analogous to iron in its difference from oxygen with respect to nucleosynthetic sites and timescales, a similar scenario might occur in LSB galaxies. But a discrete burst scenario predicts that the oxygen abundance will remain fixed as the nitrogen abundance increases, again the opposite of what is observed. Since a continuous, roughly constant level of star formation also fails to produce abundances like those observed, perhaps the star formation rate in LSB galaxies has been gradually *increasing* with time. This is consistent with the observed blue colors (Chapter 2), but again it is unclear that such a star formation history would lead to the observed abundances, and no models address this situation.

Another possibility is that differences in the IMF are responsible. This could conceivably explain all elemental abundances, for while neon and sulfur are, like oxygen, produced in massive stars, they are not produced in the same ratios by individual stars of different masses. Thus variations in the IMF could lead to different abundance ratios when the yield is integrated over the entire mass range. While no difference in the IMF is inferred from the H II region spectra, these are only sensitive to the presence of massive stars, and not to the IMF slope. So while massive stars are clearly present in LSB H II regions, the precise shape of the IMF is not constrained. However, it seems that a simple alteration of the IMF slope would change the Ne/O and S/O ratio, but not maintain a constant Ne/H and S/H while O/H increases. A more extreme variation might succeed in doing this, but seems likely to require the complete suppression of particular mass ranges. Taking sufficient liberty with the IMF *might* produce an acceptable fit to the data, but seems physically implausible.

Cosmological Implications

If causes intrinsic to the galaxies do not provide a sufficient explanation, perhaps external mechanisms are at work. The simplest case would be the infall of primordial gas, which would dilute the observed abundances by arbitrary amounts. This immediately fails for the same recurring reason, that the abundances of nitrogen, neon, and sulfur fail to change as the oxygen abundance does, as they must for the case of the infall of pristine (H an He only) gas.

Another possibility is the infall of non-primordial gas, or the formation of the galaxies from a pre-enriched intergalactic medium. In either case, the constant levels of nitrogen, neon, and sulfur would just be representative of the levels of these elements in that gas, while oxygen can be produced to any level by the galaxy, with the galactic contribution eventually dominating at high abundance (hence the upturn for $\log(O/H) > -3.8$). However, it is clear from the previous discussion that these abundances cannot be produced in stars with a quasi-normal IMF, thus ruling out the infall of gas polluted by other galaxies *unless* there is a mechanism for stripping the oxygen out of the gas. (This would be the opposite of the more likely preferential loss of oxygen in galactic winds!)

Empirically, formation from pre-enriched gas provides the best fit to the LSB data, regardless of the source of enrichment. Consider Figure 3.9. If a slope of two indicates secondary production of an element, and a slope of one a primary mode, then a zero slope is most naturally explained by the presence of pre-existing material. This would naturally maintain a constant level until overwhelmed by stellar production.

The putative explosions suggested to be responsible for the observed large scale structure in the universe (Ostriker & Cowie 1981) are one possible site for the production of the observed elements. The mechanism is uncertain, which makes it possible to speculate about what abundance ratios might be produced. Whatever the mechanism, it is not unreasonable that some nucleosynthesis be associated with events of this magnitude, if they occurred. If this were the case, there might well be detectable abundance differences between objects in voids and walls.

It could also be that the observed floors to the abundances of nitrogen, neon, and sulfur are primordial. Elements this heavy are not produced in the standard primordial nucleosynthesis model. However, it is possible to make some heavy elements if there are inhomogeneities in the baryon distribution during primordial nucleosynthesis (Applegate, Hogan, & Scherrer 1988) as a result of a first order QCD phase transition (Witten 1984). Indeed, Applegate et al. (1988) *predict* a detectable amount of nitrogen production in neutron rich regions.

The level of nitrogen reported here is at least two orders of magnitude greater than the models of Applegate et al. (1988) predict. The level of neon is seven orders of magnitudes too high. However, the models are not robust (Terasawa & Sato 1990); the reaction chains are incomplete and there are many uncertainties. What is important is a physical mechanism by which heavy ($A \geq 12$) nuclei can be reached. This is provided in the neutron rich regions by the constructive $^{11}B(n,\gamma)^{12}B(\beta)^{12}C$ reaction competing with the destructive $^{11}B(p,2\alpha)^{4}He$ reaction which dominates the proton rich regions and prevents heavy elements from being synthesized in the standard model. Once $A \geq 12$ is reached, virtually any level of heavy elements can be generated depending on the neutron concentrations, diffusion times, etc. That neon is so abundant may be the signature of a resonant reaction along a neutron rich chain which ultimately leads to neon, in analogy with the triple alpha reaction.

While a pre-existing component (regardless of its source) provides the best empirical fit to the LSB data in Figures 3.9 – 3.11, it is marginally in conflict with the data for HSB BCGs. There seems to be no interruption in their trend towards lower abundances at the point where the floor to the LSB data occurs. However, only a few points actually lie below the floor, and they may be consistent with a floor within the errors. Interestingly, the two most metal poor galaxies known (I Zw 18 and SBS 0335 – 052, which fall off the scale of Figures 3.9 – 3.11), follow *neither* trend, having abundances intermediate to those which would be obtained by extrapolating the trends observed in the other galaxies (Izotov et al. 1990; Kennicutt, private communication). If HSB galaxies do lack a floor, this difference between LSB and HSB abundance ratios could be a signature of environmental influences. That is, if LSB and HSB galaxies form in segregated environments, they might well start with different abundances. However, the size of inhomogeneities at the epoch of nucleosynthesis is far too small to cause observable differences on galactic scales.

Intrinsic or Extrinsic?

It is very difficult to explain the basic observation that there is a floor to the abundance of nitrogen, neon, and sulfur in LSB galaxies. Since there is a striking difference between LSB and HSB galaxies, the most likely explanation is one intrinsic to the galaxies, such as differences in the star formation history or IMF. However, it seems difficult to devise a scenario in which stellar nucleosynthesis would result in a constant level of these elements while oxygen changes by an order of magnitude. On the other hand, an extrinsic source of production of these elements provides an empirically natural explanation of the observed trend. But this has difficulty explaining the striking difference between the HSB and LSB samples. If an extrinsic source is responsible, it has significant implications for the standard cosmological model.

Conclusions

The methods described by McGaugh (1991) have been applied to a sample of low surface brightness galaxies, yielding accurate abundances and important clues to the star formation histories of these enigmatic objects. LSB galaxy H II regions are observed to contain massive ($M > 60M_{\odot}$) stars, so no variation in the IMF is inferred, though the exact shape of the IMF is not constrained. The correlation between the nebular ionization parameter and metallicity observed in high surface brightness galaxies is *not* seen in this sample. It may be present as an envelope of limiting maximum ionization at a given metallicity, which suggests that either the H II regions in this sample are more evolved on average than those selected for observation in high surface brightness galaxies, or that the ionizing star clusters in LSB galaxies form over a wider range of conditions than do clusters in HSB galaxies.

LSB galaxies are low metallicity, slowly evolving systems. The low degree of chemical enrichment confirms the inference of Bothun et al. (1990) that LSB disks evolve slowly, and can remain quiescent for a Hubble time. This may result from their low H I column densities and lack of molecular gas. Indeed, the low H I column densities may inhibit the formation of molecular clouds, and be the physical attribute which determines the rate of galaxy evolution.

A floor to the abundances of nitrogen, neon, and sulfur has been discovered in these LSB galaxies. This could result from either processes intrinsic to these galaxies, such as an unusual IMF or star formation history, or an extrinsic process, such as formation from pre-enriched material. Neither possibility provides a completely satisfactory explanation. The intrinsic scenario is preferred because of the distinct difference between the abundance ratios in these LSB galaxies and a sample of HSB galaxies of similar metallicity. However, it is difficult to reproduce the observed LSB abundances with stellar processes, and the extrinsic scenario provides a better empirical explanation. If the extrinsic scenario is correct, it has major implications for the standard model of primordial nucleosynthesis.

The abundance ratios of LSB galaxies suggest that many paths of galaxy evolution are possible which have not been considered. That LSB galaxies can remain relatively unevolved to the present epoch implies that selection effects may mask the true range of galaxy properties. Recovery of the entire spectrum of galaxy properties is essential to a comprehensive understanding of galaxy formation and evolution.

APPENDIX III.A
ANALYTIC ABUNDANCE FORMULAE

The H II region model grid of McGaugh (1991) depicted in Figure 3.2 can be approximated by fitting a multivariate function to the grid points. This provides powerful analytical formulae for transforming from observed (R_{23}, O_{32}) coordinates to (O/H, $<U>$). While this method is somewhat less accurate than direct interpolation through the grid (since the fit to the surface of Figure 3.2 is not perfect), it is a much more convenient way of deriving the desired information directly from the observations, especially for large data sets.

In principle, a complete fit to the model grid of McGaugh (1991) would require four variables: R_{23}, O_{32}, [N II]/[O II] to distinguish between upper and lower branch surfaces, and a parameter sensitive to the shape of the ionizing radiation field $T_*(M_u)$. The radiation softness parameter η' (Vilchez & Pagel 1988), involving the near-IR [S III] lines, might provide some measure of this, but it is also sensitive to $<U>$. Since the position of the grid in Figure 3.2 is not very sensitive to $T_*(M_u)$, we will suppress this dimension and fit only the $M_u = 60 M_\odot$ grid. This is adequate as long as the H II region is ionized by a cluster rather than a single star, which is generally the case for observable extragalactic H II regions. The uncertainty induced by the suppression of $T_*(M_u)$ is included in the estimation of the accuracy of the fit.

Empirically, it was found to be very difficult to find a functional form which could reasonably fit the sharp turnover of the manifold as well as both branches. In addition, the precise value of [N II]/[O II] depends on the abundance of N/O, which has been shown to vary in a complicated manner. Hence we choose to suppress this dimension as well, and fit separate functions to the upper and lower branch surfaces. [N II]/[O II] can still be used to determine which branch is appropriate, as any value of log([N II]/[O II]) > −0.9 indicates the the upper branch, while log([N II]/[O II]) < −1.1 indicates the lower branch. Nebulae with log([N II]/[O II]) ≈ −1 are in the turnover region where the R_{23} method is not particularly useful anyway.

This leaves a function of two variables for both O/H and <U>. For convenience, we define

$$Z \equiv \log(\mathrm{O/H}) \tag{3.A.1}$$

$$U \equiv \log\langle\mathrm{U}\rangle \tag{3.A.2}$$

$$x \equiv \log(\mathrm{R}_{23}) \tag{3.A.3}$$

$$y \equiv \log(\mathrm{O}_{32}). \tag{3.A.4}$$

Using MATHEMATICA, the following functions were fit to the model grid. On the lower branch,

$$Z_\ell(x,y) = -4.93 + 4.25x - 0.26y - 3.35\,sin(x) - 0.12\,sin(y) \tag{3.A.5}$$

$$U_\ell(x,y) = -2.95 + 0.17x^2 + 1.02y, \tag{3.A.6}$$

while on the upper branch,

$$Z_u(x,y) = -2.65 - 0.91x + 0.12y\,sin(x) \tag{3.A.7}$$

$$U_u(x,y) = -2.39 - 0.35x + 1.29y - 0.15xy. \tag{3.A.8}$$

These functional forms were determined by trial and error, seeking a reasonable fit with relatively few terms. It is a fortunate coincidence that x and y have reasonable values as arguments of trigonometric functions when taken to be in radians.

Note that on the upper branch, $Z_u(x,y)$ depends only weakly on y. This is simply a result of R_{23} being a single parameter sequence in oxygen abundance on the upper branch. Since this is not the case on the lower branch, single variable fits (e.g., Edmunds & Pagel 1984, Skillman 1989) are inadequate there.

These fits are restricted in their validity to the following regimes:

$$-4.6 < Z_\ell(x,y) < -3.8 \tag{3.A.9}$$

$$-3.4 < Z_u(x,y) < -2.9 \tag{3.A.10}$$

$$-4 < U(x,y) < -1 \tag{3.A.11}$$

(this range is valid for $U(x,y)$ on both branches). The accuracy of these formulae worsen near the edges of the grid, but in general the lower branch fits are good to 0.1 dex, and the upper branch fits to 0.15 dex. As discussed by McGaugh (1991), the uncertainty in both $Z_u(x,y)$ and $U_u(x,y)$ increases at supersolar abundances, with $U_u(x,y)$ likely to return values which are systematically too low. Despite the systematic uncertainties in this regime, these formulae provide powerful, direct tools for the interpretation of nebular spectra over a wide range of parameter space.

APPENDIX III.B
Hα IMAGES

The Hα images used to identify the H II regions discussed in the text are displayed here, with descriptions of the slit placements. In addition to the galaxies for which H II region spectroscopy was obtained, some other LSB galaxies with positive detections of Hα emission are also presented. Together, these give some indication of the sporadic nature of star formation in LSB galaxies. Typically, each galaxy possesses few bright H II regions, in stark contrast with the situation for late type HSB disks (see Figure 3.B.29).

Indeed, it is rather surprising how many LSB galaxies have H II regions at all, given their nature. Of sixty LSB galaxies imaged in Hα with the McGraw Hill 1.3 m telescope, twenty were readily detected in Hα. Since the priority was to find H II regions amenable to spectroscopy, there was a selection in favor of those objects which showed some indication of star formation on POSS-II prints. However, this was not always a good indicator, as many apparently smooth galaxies do turn out to have knots of star formation. Though the selection effects prevent quantitative statements about the frequency of H II regions in LSB galaxies, one in three seems to be a high detection rate for objects which were preselected to be of low surface brightness.

The imaging performed at MDM observatory used the Kitt Peak Hα filter set and a Thomson CCD, yielding the same pixel scale as for the images in Appendix 2.A (0.48 arcsec pixel^{-1}). Additional Hα imaging was done with the KPNO 2.1 m and a TI 800×800 CCD, binned 2×2 to give a scale of 0.38arcsec pixel^{-1} (Bothun & Impey, private communication). The cosmetic properties of the TI CCD are somewhat worse than those of the Thomson; images obtained with the 2.1 m telescope are denoted (TI) in the caption. This is an important distinction, as these images reach a much deeper limiting flux, since both the aperture and the exposure times were larger.

Each image is 2.4′ on a side, with North up and East to the left. In general, both the narrow, on-band Hα image and the continuum subtracted Hα image are shown. The continuum was subtracted by using a scaled broad (usually R) band image. This has the advantage of speed (since reasonable S/N in the continuum can be obtained much more rapidly with a broad band filter than with a narrow, off-band filter), but has some residual Hα present. Also, the scaling implied by stellar fluxes is sometimes different from the level which optimally subtracts the galaxy due to the different shapes of the spectral energy distributions. To find the optimal level for each galaxy, the broad band images were divided by the on-band images, and the scaling taken from surface photometry of areas which avoided H II regions.

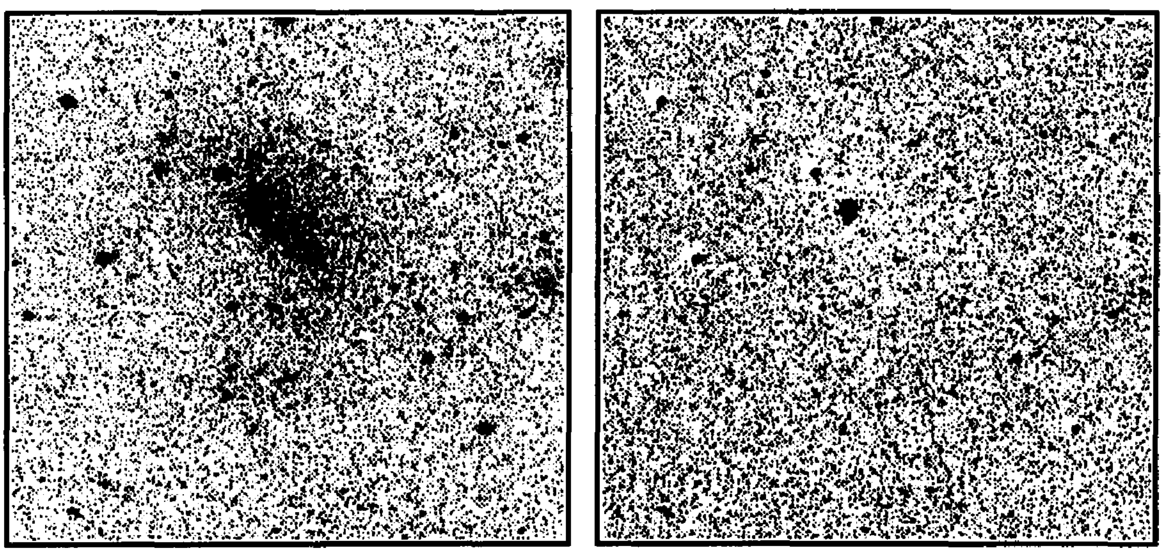

Figure 3.B.1— **F415–3. a) Left panel: Hα image. b) Right panel: Continuum subtracted Hα image. This galaxy possesses a single, prominent H II complex near its center.**

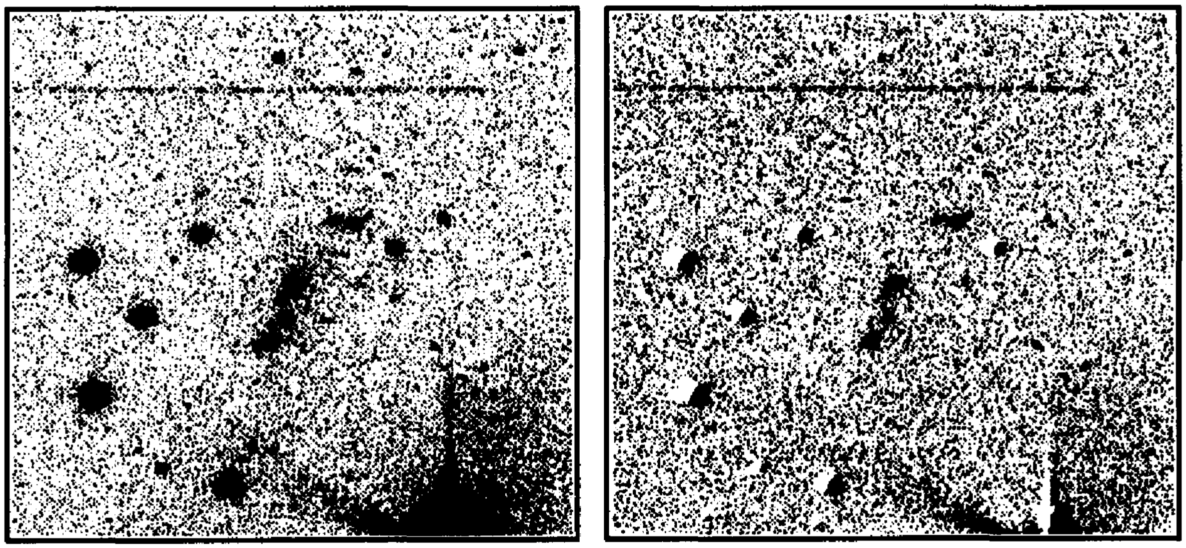

Figure 3.B.2— F469–2. a) Hα image. b) Continuum subtracted Hα image. This galaxy has a number of nearly aligned H II regions. A1 is the bright, southernmost H II region, and the labeling proceeds northwards to A4 at the north, somewhat removed from the other three.

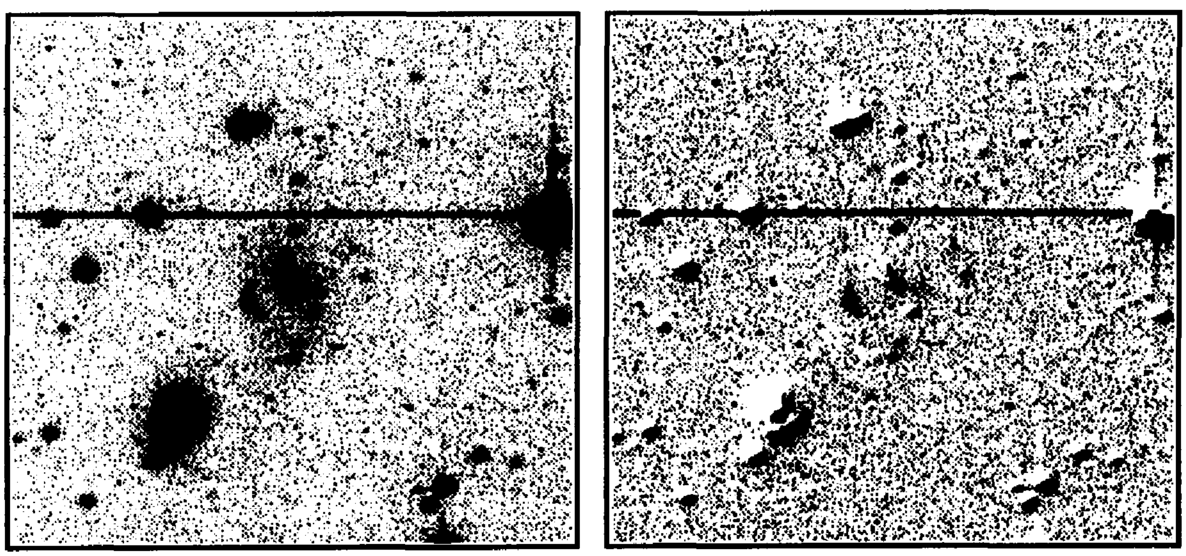

Figure 3.B.3— F530–3. a) Hα image. b) Continuum subtracted Hα image. The H II region A1 is the bright object on the eastern side of the disk, with A2 being the fainter object to the south.

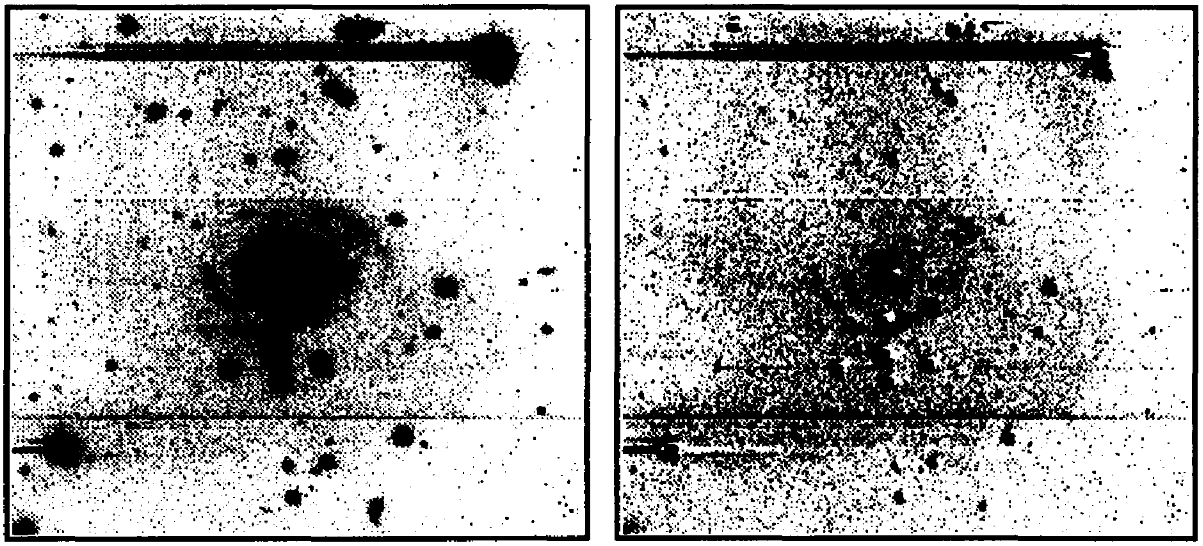

Figure 3.B.4— F558–1 (TI). a) Hα image. b) Continuum subtracted Hα image. The bright H II regions of F558–1 are confined to the southern arm which lies along the line of sight towards the group of five stars. A1 is the object adjacent to the northernmost of these stars, and A2 is the next H II region along the arm, to the southwest of the nucleus.

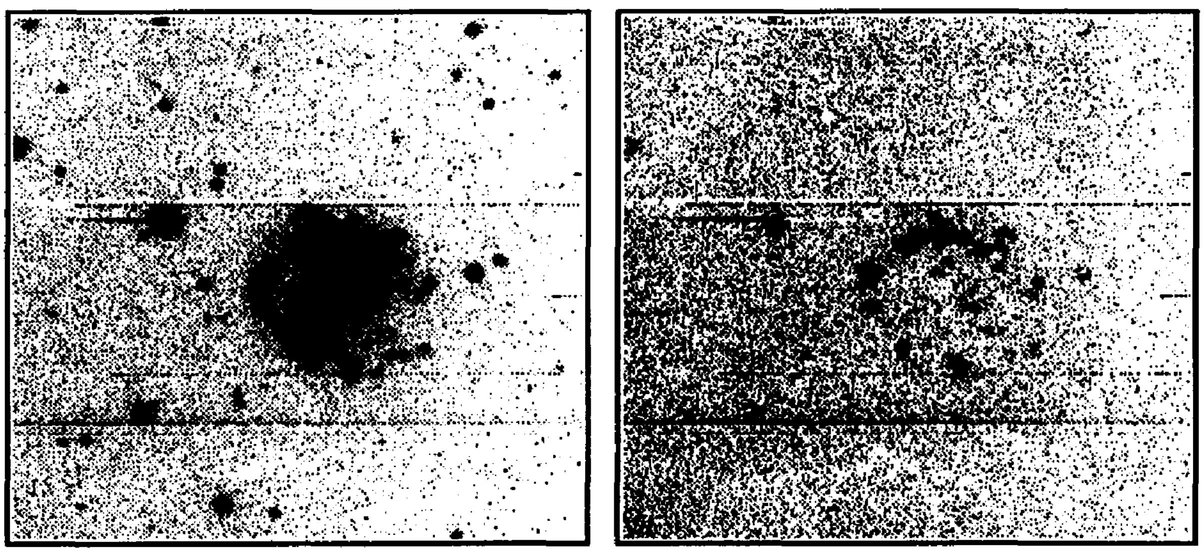

Figure 3.B.5— F561–1 (TI). a) Hα image. b) Continuum subtracted Hα image. The single armed spiral pattern of this galaxy is very well traced by Hα (b). Rings of star formation similar to this are not uncommon in LSB galaxies, and are predicted to occur by the star formation density threshold in Chapter 4. The H II region A1 is the bright, easternmost object, A3 is the northernmost H II region, and A2 is the H II region between these two.

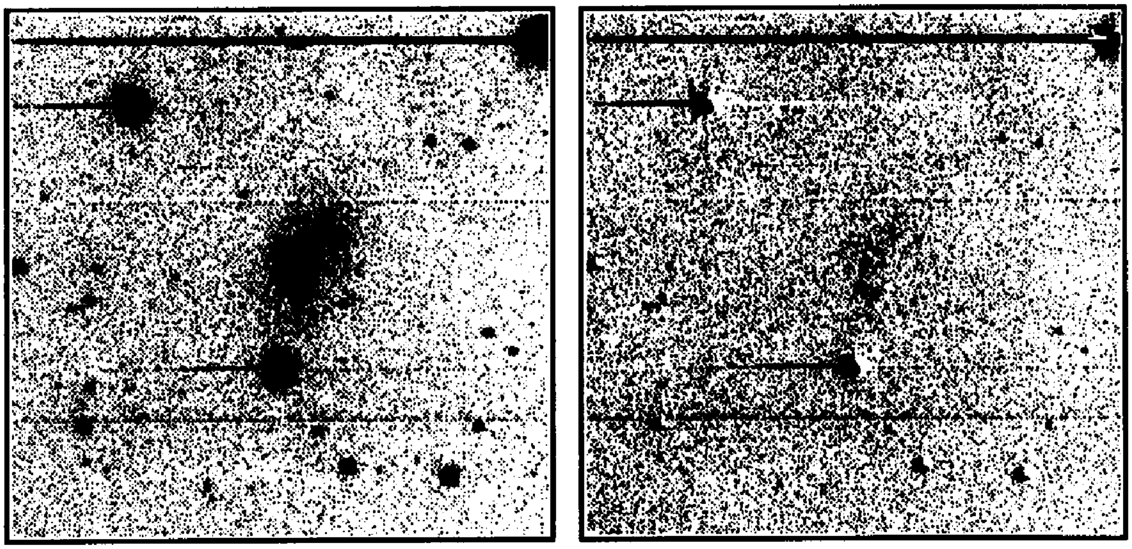

Figure 3.B.6— F563–V1 (TI). a) Hα image. b) Continuum subtracted Hα image. There are a few sites of star formation in this otherwise amorphous galaxy. A1 is the more eastern of the pair of H II regions in the south, and A2 is the H II region near the nucleus.

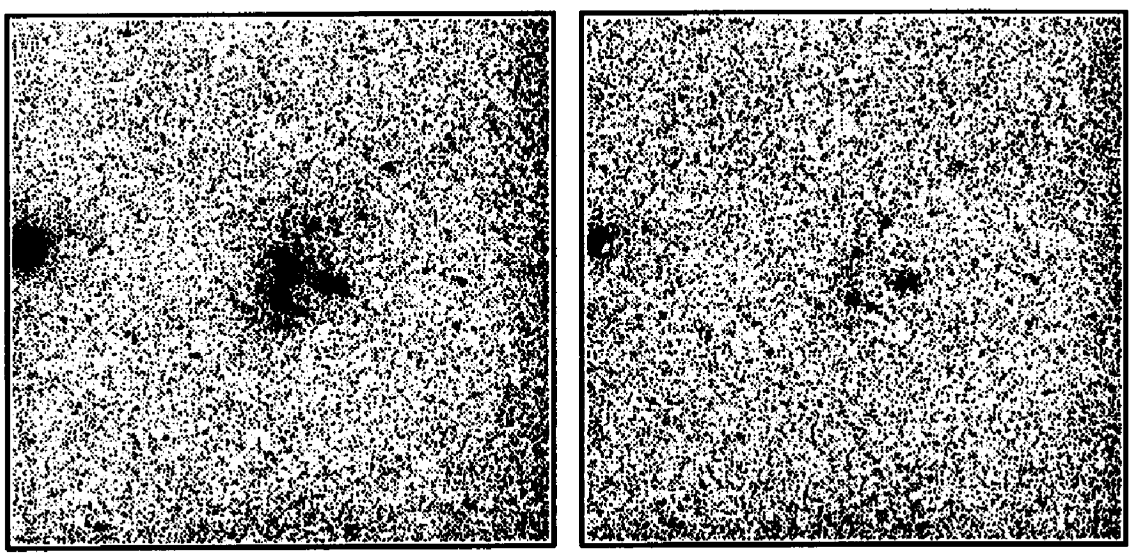

Figure 3.B.7— F563–V2. a) Hα image. b) Continuum subtracted Hα image. A1 is the H II region in the bar, and A3 is the western H II region.

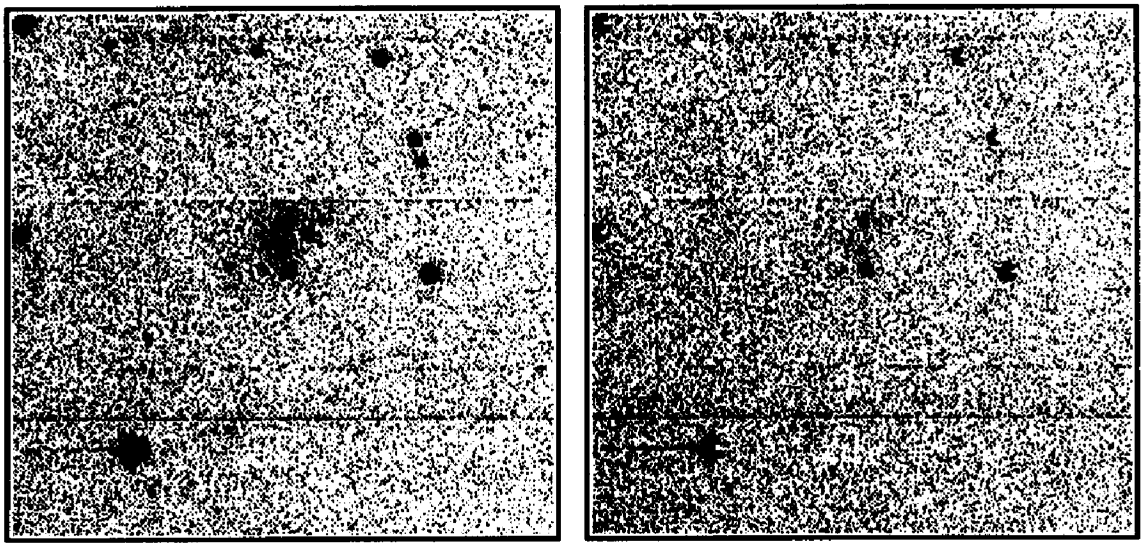

Figure 3.B.8— F565–V1 (TI). a) Hα image. b) Continuum subtracted Hα image. There are at least two H II regions in this featureless LSB galaxy.

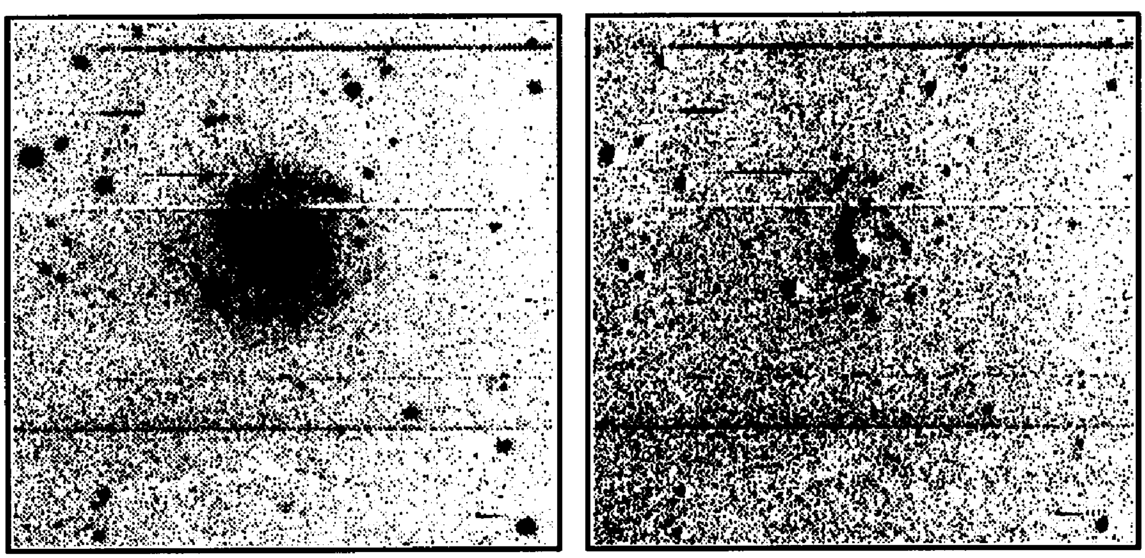

Figure 3.B.9— F568–1 (TI). a) Hα image. b) Continuum subtracted Hα image. A1 is south and a little west of the nucleus, A2 is just west of it.

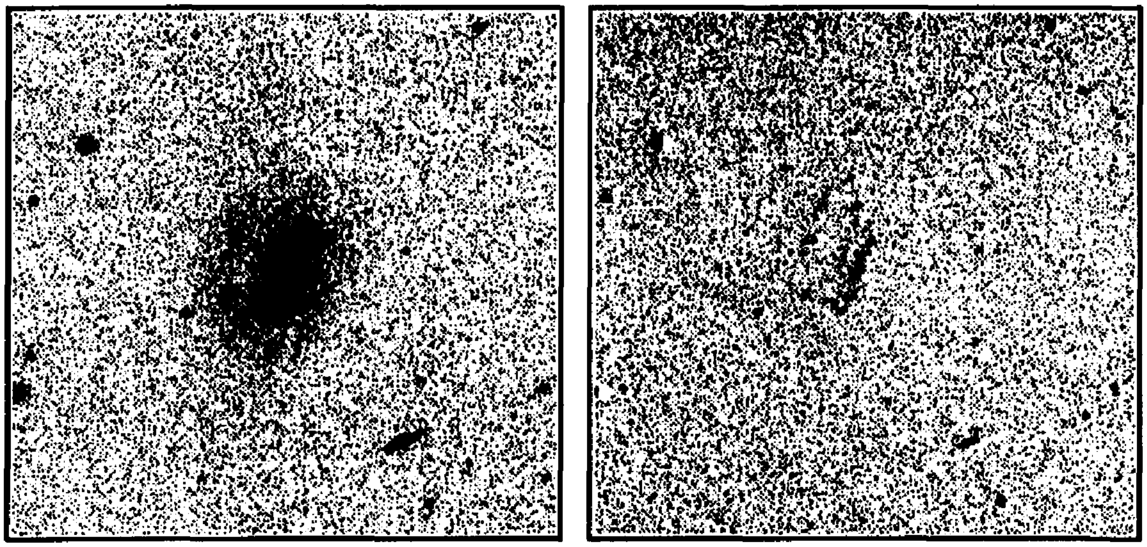

Figure 3.B.10— F568–3. a) *V* image. b) Continuum subtracted Hα image.

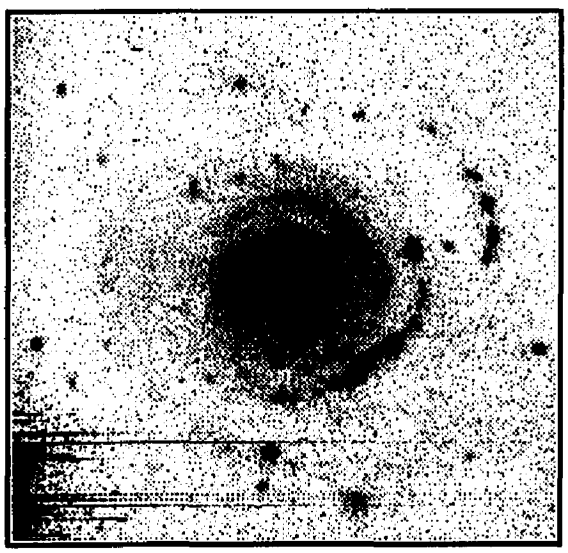

Figure 3.B.11— F568–6 (TI). Hα image. Most of the current sites of star formation are in the western arm fragments of this giant galaxy. Slit position one covered the southwest arm, with S1A1 being the more southern and S1A2 the more northern of the bright pair of H II regions there. Slit position three runs approximately east-west through the elongated object near the center (S3A1) and the bright H II region to the west (S3A2). S3A3 is in the outer western arm.

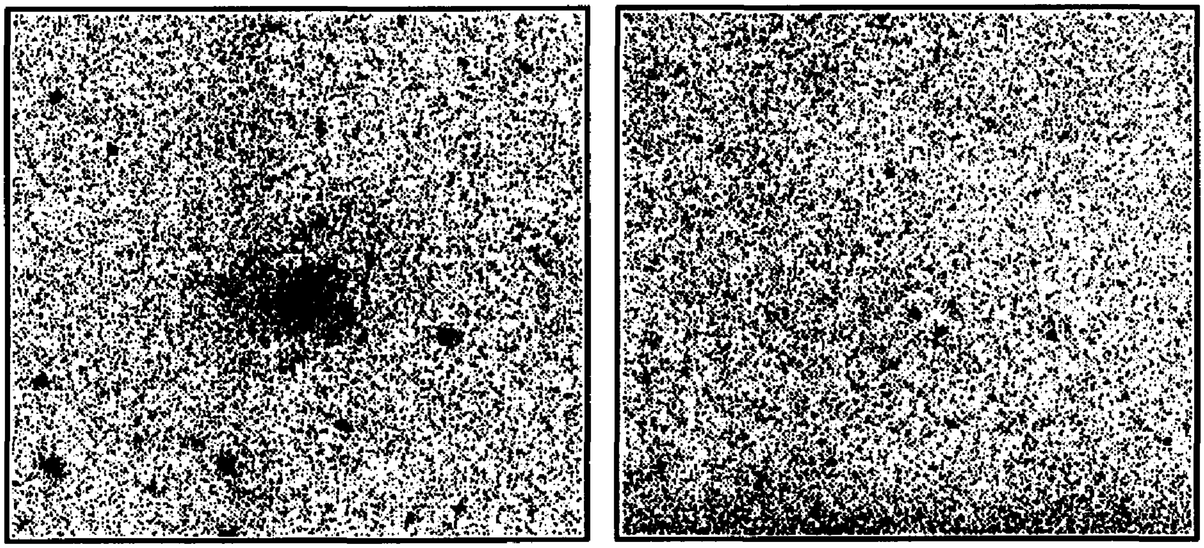

Figure 3.B.12— F571–5. a) *V* image. b) Continuum subtracted Hα image. There are a few weak H II regions in this galaxy, mostly to the southwest of the center.

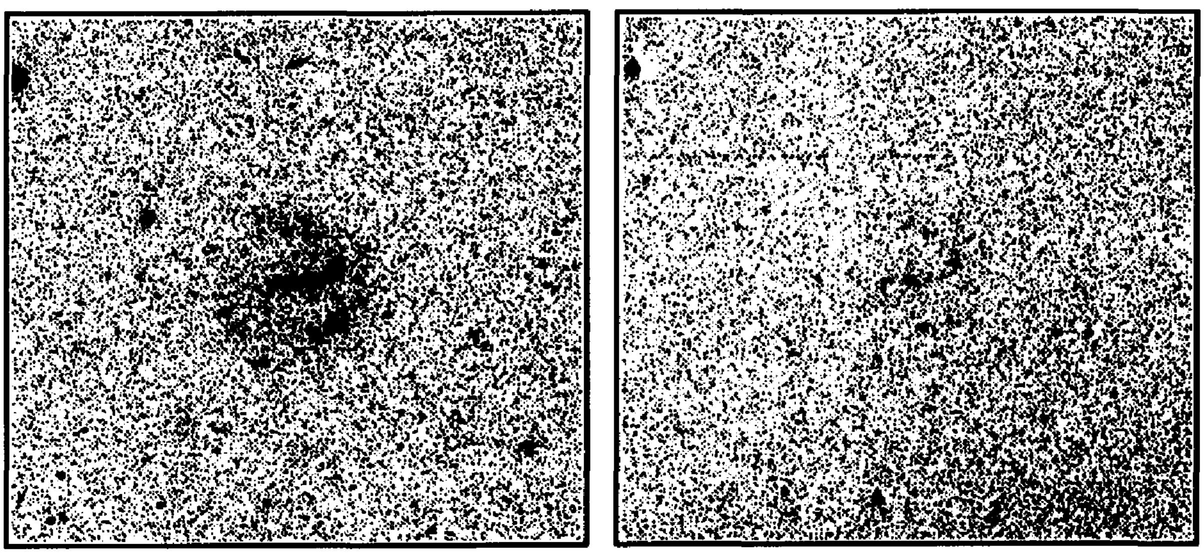

Figure 3.B.13— F577–V1. a) *U* image. b) Continuum subtracted Hα image. Here a *U*-band image is displayed rather than the short Hα exposure. F577–V1 is dominated by H II regions, both in the central bar and in the outer ring, with there being little other light (see Figure 2.1). The H II regions A1 through A5 lie predominantly along the bar, ordered form west to east. Only the brighter A3 and A5 are apparent in (b).

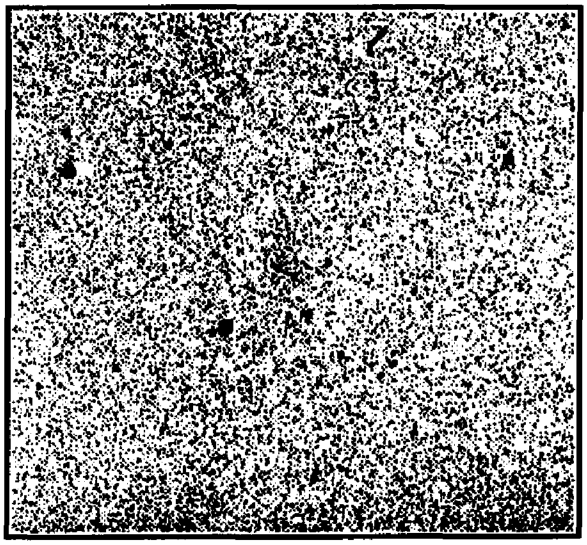

Figure 3.B.14— F583–1. Continuum subtracted Hα image. Only the brightest H II region (A3) is discernible in this image; the others lie to the southeast below the nearby star.

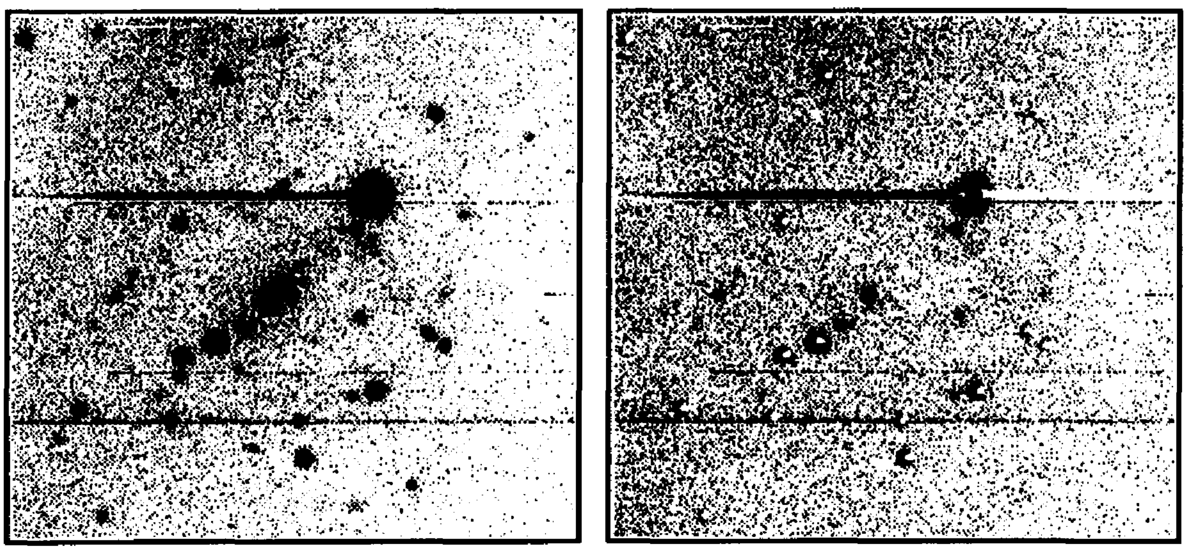

Figure 3.B.15— F583–5 (TI). a) Hα image. b) Continuum subtracted Hα image. A1 is the H II region near the center of the galaxy, and A2 is the object near the bright star to the northwest.

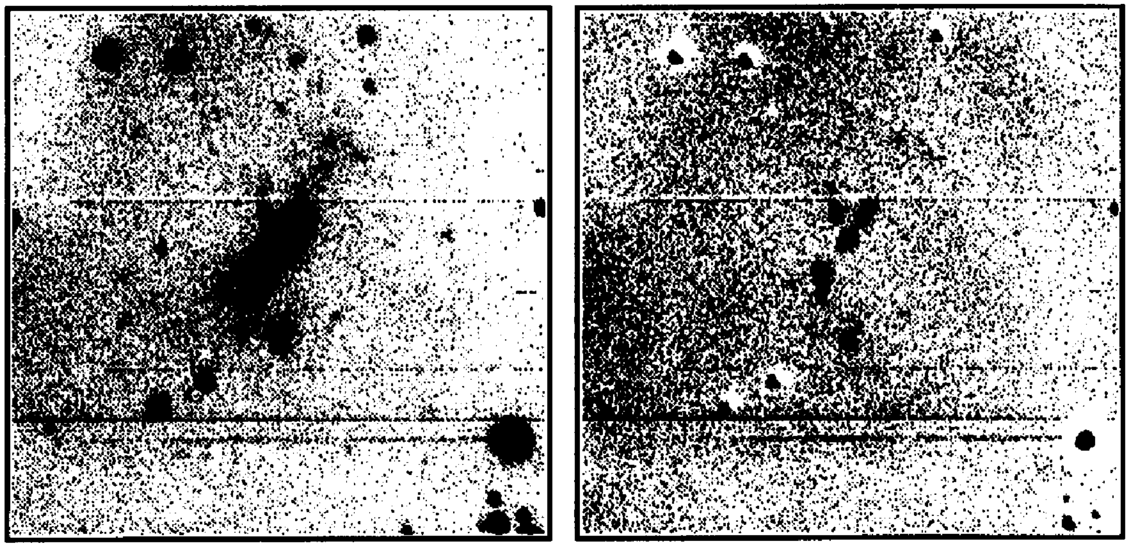

Figure 3.B.16— F585-3 (TI). a) Hα image. b) Continuum subtracted Hα image. Slit position one runs along the major axis, with S1A1 being in the south. The second slit position is in the obvious place, starting with S2A1 in the north.

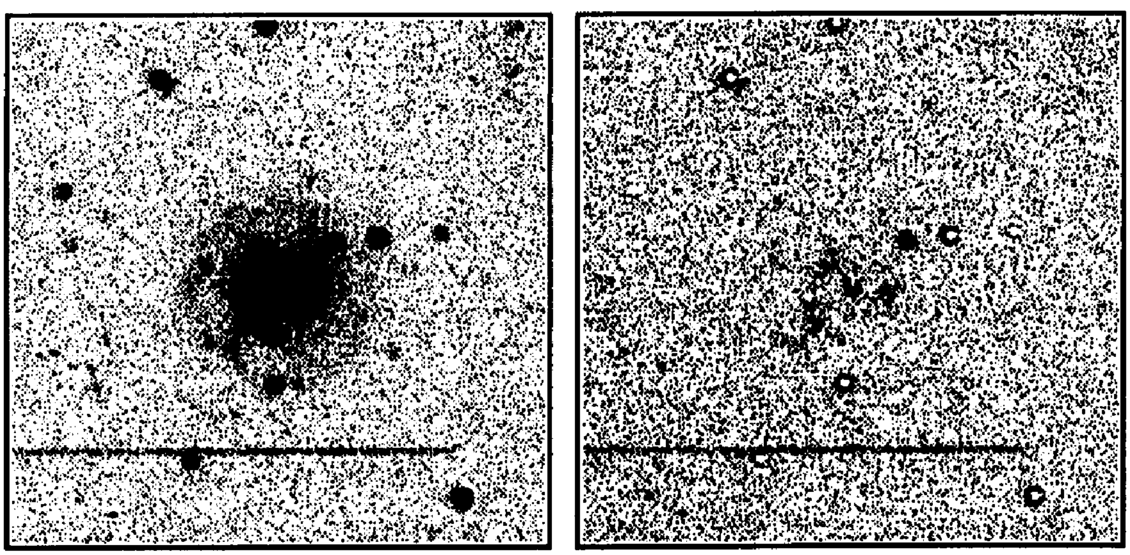

Figure 3.B.17— F602-1. a) Hα image. b) Continuum subtracted Hα image. Despite the well developed spiral structure, there is only one prominent H II region in this galaxy, and it does not lie in an arm.

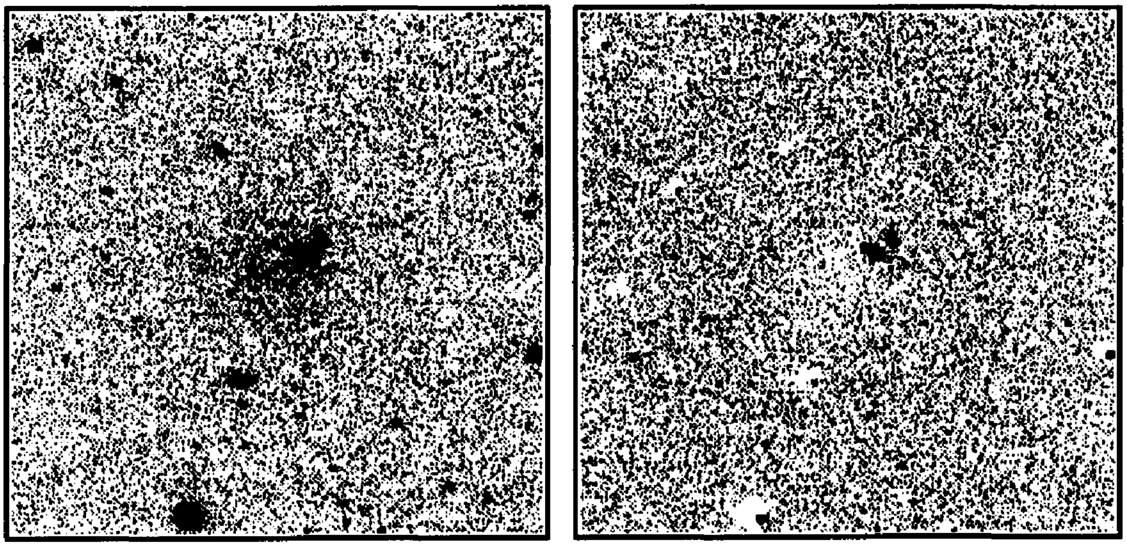

Figure 3.B.18— F611-1. a) Hα image. b) Continuum subtracted Hα image. There are two H II regions in this small, amorphous galaxy. A1 is the brighter one closer to the center of the galaxy, and A2 is the one to the northwest.

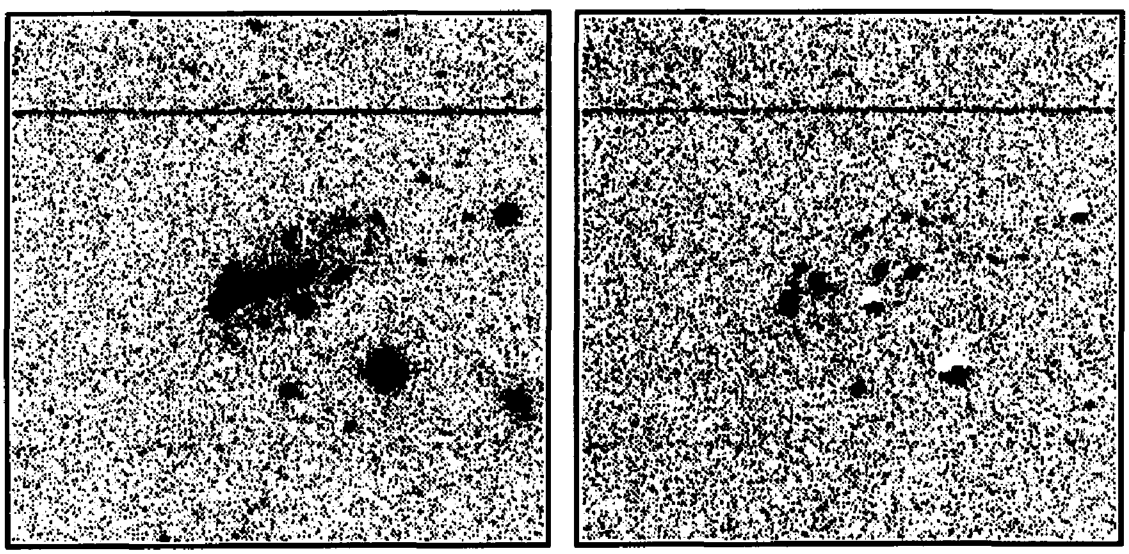

Figure 3.B.19— F746-1. a) Hα image. b) Continuum subtracted Hα image. This peculiar galaxy has a number of star forming knots, including several fainter ones in the northwest loop structure. A1 is the bright H II region to the southeast, and A2 is the next bright one nearby. A3 occurs along this line, being the easternmost of the H II regions in the loop.

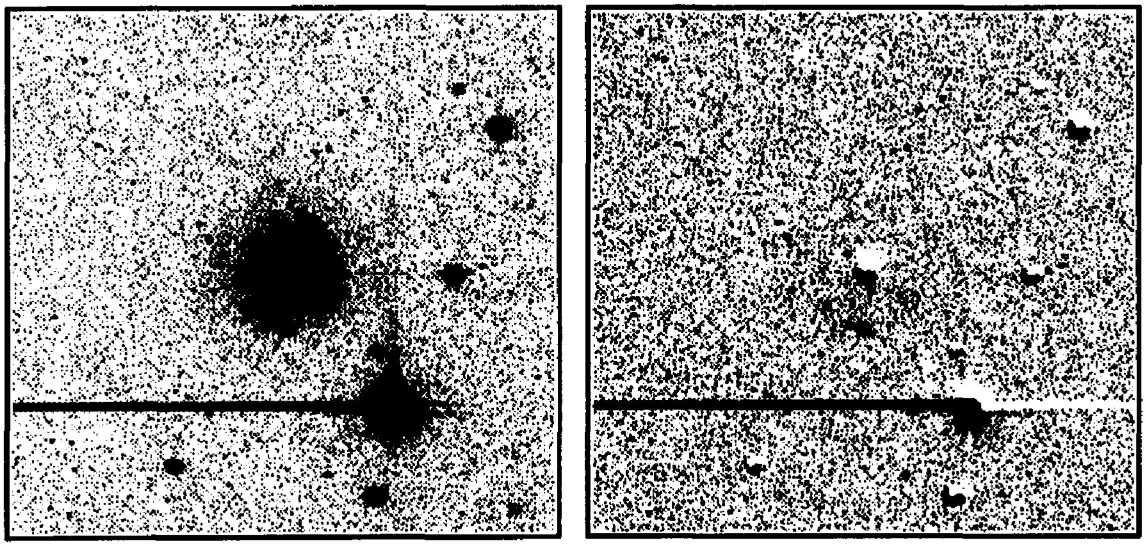

Figure 3.B.20— F746-2. a) Hα image. b) Continuum subtracted Hα image. There is a single prominent H II region to the south of the nucleus imbedded in the otherwise smooth disk of this galaxy.

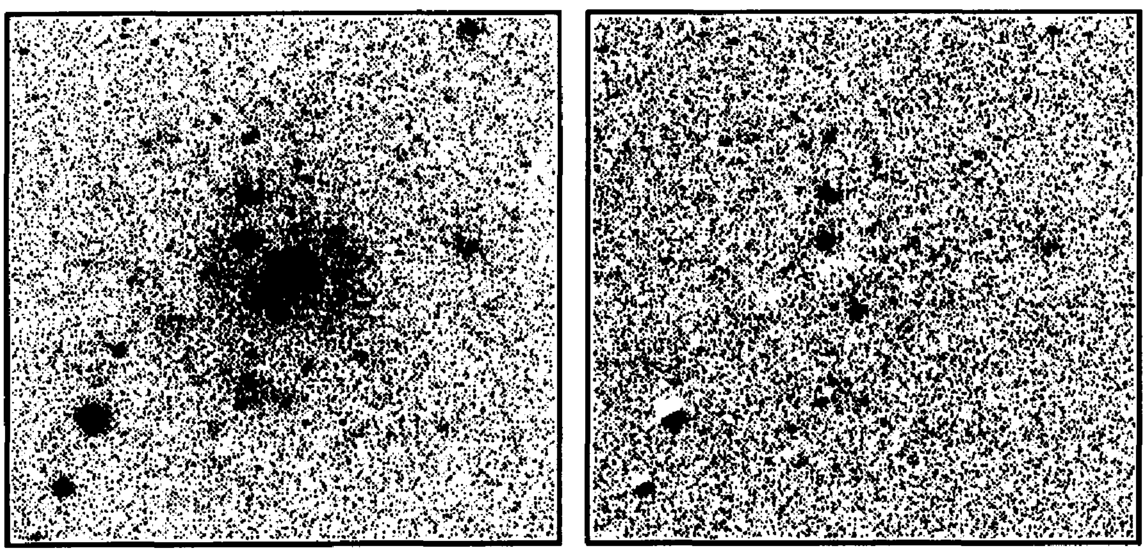

Figure 3.B.21— UGC 1230. a) Hα image. b) Continuum subtracted Hα image. UGC 1230 has a number of H II regions vaguely associated with its weak spiral structure. The H II regions for which spectra are reported lie in a north-south line, with A1 being the faint, northernmost object, A2 and A3 being the brighter H II regions on the northeast side of the galaxy, and A4 and A5 being the pair of objects in the south.

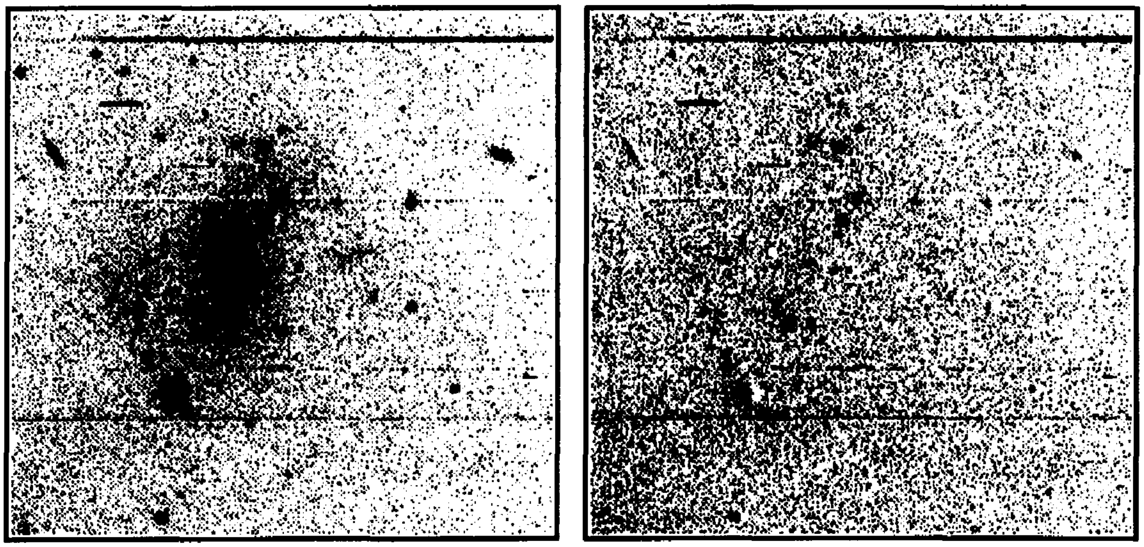

Figure 3.B.22— UGC 5675 (TI). a) Hα image. b) Continuum subtracted Hα image. A1 is the H II region on the southeast side of the galaxy, and A2 and A3 are on the northwest side adjacent to one another. A2 is much fainter than A3, and appears as a small point in (b).

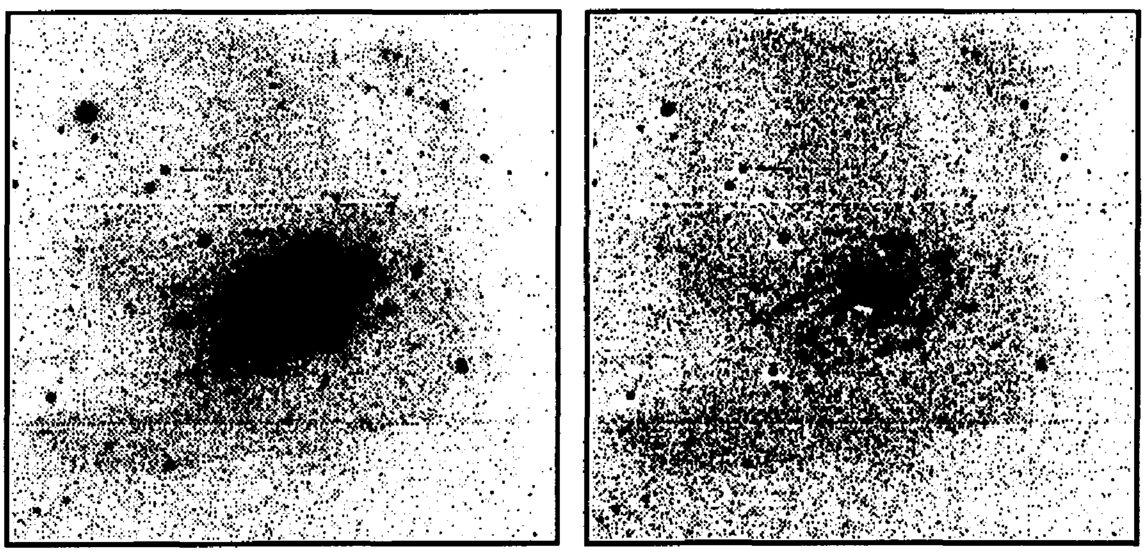

Figure 3.B.23— UGC 5709 (TI). a) Hα image. b) Continuum subtracted Hα image. There are many H II regions in this relatively HSB galaxy. The slit passed at an angle through the northeast side of the galaxy, so that A1 is near the nucleus on that side, and A3 is the H II complex to the north.

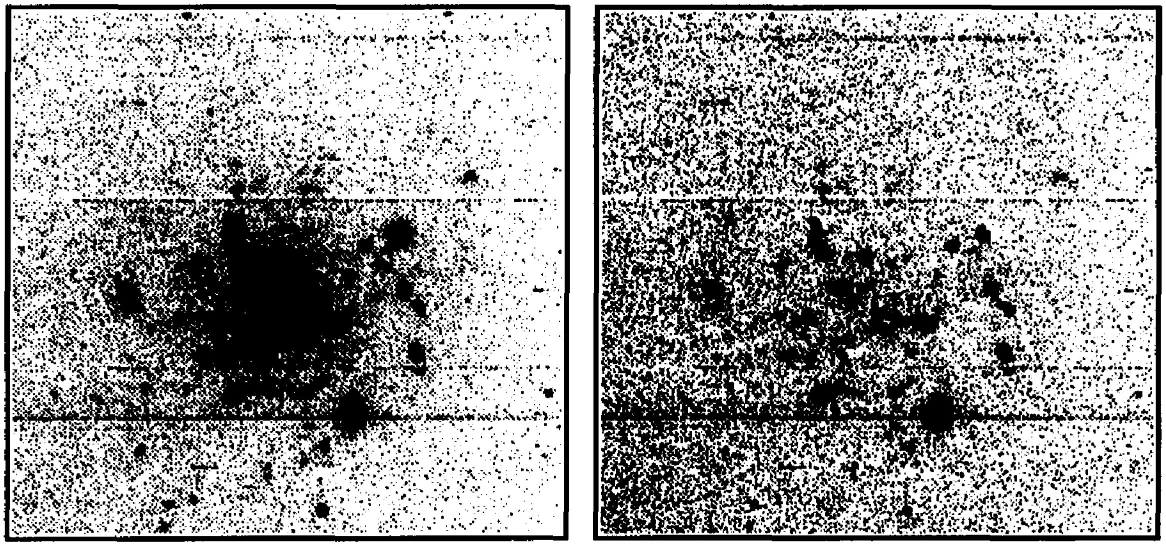

Figure 3.B.24— UGC 6151 (TI). a) Hα image. b) Continuum subtracted Hα image. There are many H II regions scattered about the face of this galaxy, contributing to its chaotic appearance. Slits were placed in approximately north-south orientations. S1A1 is the bright H II region slightly west and south of the center of the galaxy, and S1A2 is the bright object south of that. S3A1 is on the west side of the galaxy, south of the star. S3A2 is south of that.

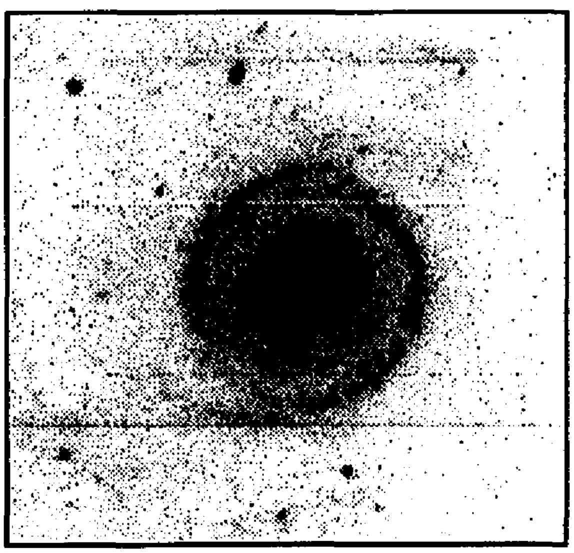

Figure 3.B.25— UGC 6614 (TI). Hα image. Like F561–1, UGC 6614 is another galaxy with a ring of star formation at a particular radius. In this case, the slit was placed along the northeastern edge of the ring. A1 is to the northeast of the nucleus, and A3 almost due north.

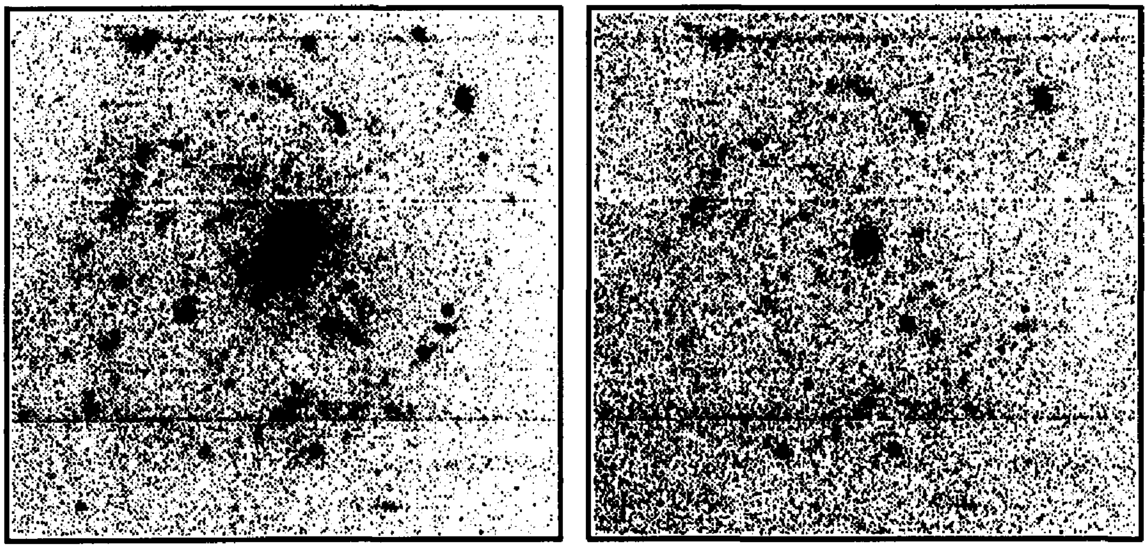

Figure 3.B.26— UGC 9024 (TI). a) Hα image. b) Continuum subtracted Hα image. S1A1 is the bright H II region on the eastern edge of the galaxy, a little north of the nucleus. S1A2 is closer to the center of the galaxy, to the south and west. S1A3 is a fainter H II region just to the southwest of that. S2A1 is the bright H II region near the northwest corner of the image.

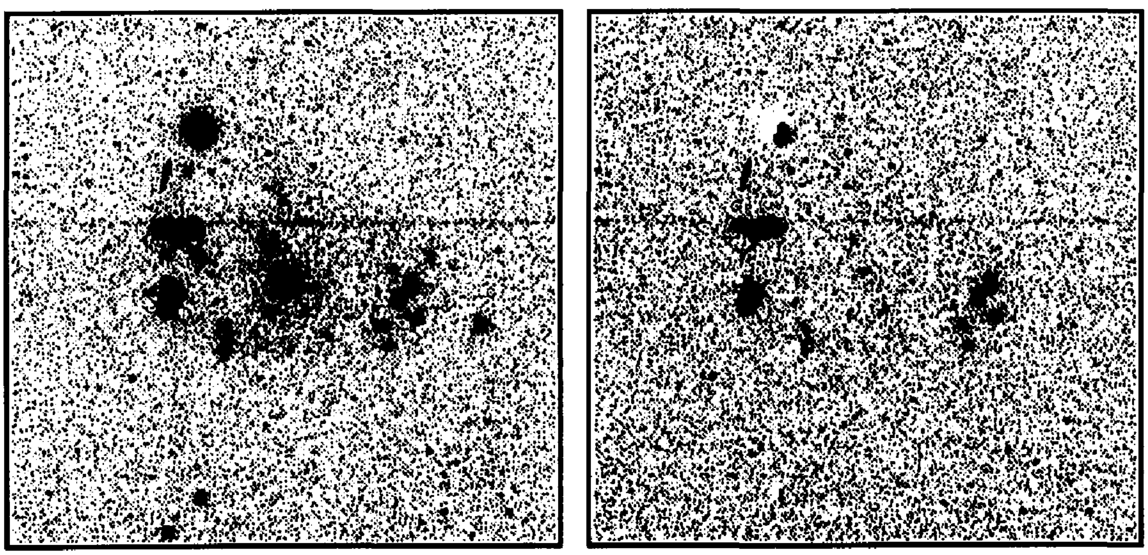

Figure 3.B.27— UGC 12695. a) Hα image. b) Continuum subtracted Hα image. There are a number of luminous H II complexes on both the eastern and western sides of this galaxy. Slit one runs east-west through the northern H II regions on the east side, and slit two approximately north-south through the southern ones. Labeling begins at the east and south, respectively.

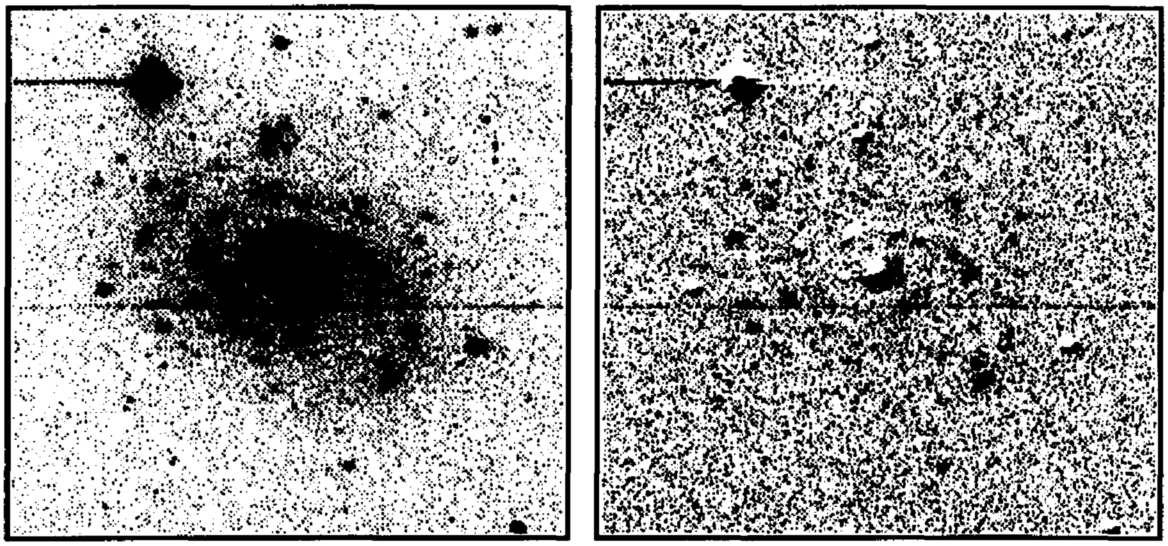

Figure 3.B.28— UGC 12845. a) Hα image. b) Continuum subtracted Hα image. This is a good example of a galaxy with a low surface brightness disk with a well developed spiral pattern and few prominent H II regions.

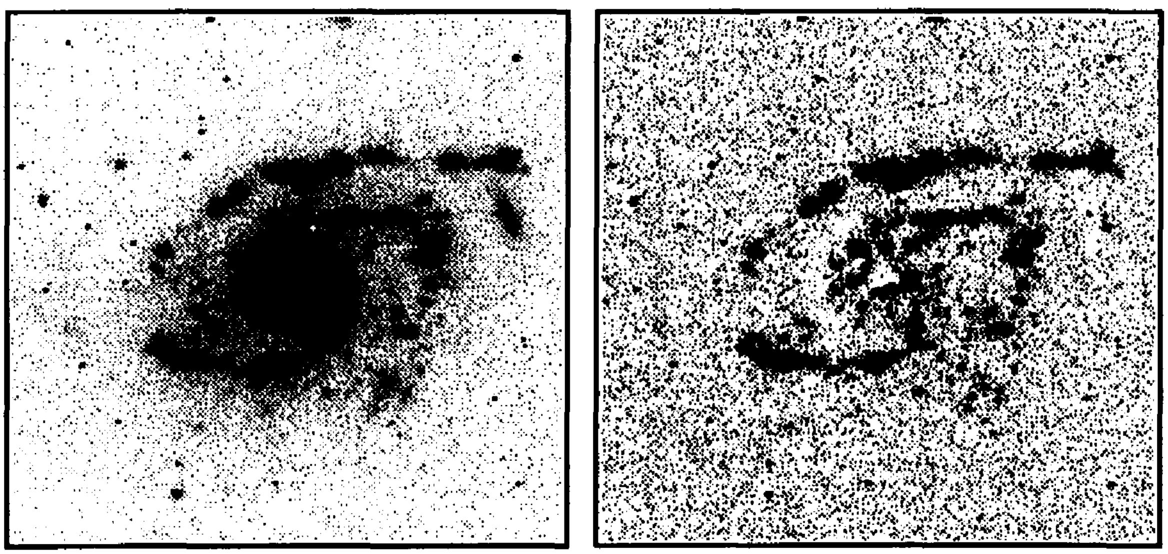

Figure 3.B.29— NGC 7757. a) Hα image. b) Continuum subtracted Hα image. This HSB Sc galaxy is included for comparison. Though also a late type galaxy, it has very different star formation characteristics than the LSB galaxies discussed here. Prominent H II regions trace nearly the entire lengths of the spiral arms, which is never the case in LSB galaxies. Many more H II regions are present as well, implying a much higher current star formation rate per unit area.

REFERENCES

Abia, C., & Rebolo, R. 1989, ApJ, 347, 186

Adler, D. S., Allen, R. J., & Lo, K. Y. 1991, ApJ, 382, 475

Alloin, D., Collin-Souffrin, S., Joly, M., & Vigroux, L. 1979, A&A, 78, 200

Applegate, J. H., Hogan, C. J., & Scherrer, R. J. 1988, ApJ, 329, 572

Bothun, G. D., Schombert, J. M., Impey, C. D., & Schneider, S. E. 1990, ApJ, 360, 427

Burstein, D., & Heiles, C. 1984, ApJS, 54, 33

Campbell, A. 1988, ApJ, 335, 644

Campbell, A., Terlevich, R., & Melnick, J. 1986, MNRAS, 223, 811

Davidson, K., & Kinman, T. D. 1985, ApJS, 58, 321

Diaz, A. I., Terlevich, E., Vilchez, J.M., Pagel, B. E. J., & Edmunds, M. G. 1991, MNRAS, 253, 245

Dopita, M. A., & Evans, I. N. 1986, ApJ, 307, 431

Edmunds, M. G., & Pagel, B. E. J. 1984, MNRAS, 211, 507

Gilmore, G., & Wyse, R. F. G. 1991, ApJ, 367, L55

Freeman, K. C. 1970, ApJ, 160, 811

Izotov, Yu. I., Lipovetskii, V. A., Guseva, N. G., Kniazev, A., Yu., & Stepanian, J. A. 1990, Nature, 343, 238

Kennicutt, R. C. 1983, ApJ, 272, 54

Kinman, T. D., & Davidson, K. 1981, ApJ, 243, 127

Kunth, D., & Sargent, W. L. W. 1983, ApJ, 273, 81

Kunth, D., & Sargent, W. L. W. 1986, ApJ, 300, 496

Luppino, G. A. 1989, PASP, 101, 931

Maloney, P., & Black, J. H. 1988, ApJ, 325, 389

Matteucci, F. 1986, PASP, 98, 973

Matteucci, F., & Tosi, M. 1985, MNRAS, 217, 391

McCall, L. M., Rybski, P. M., & Shields, G. A. 1985, ApJS, 57, 1

McGaugh, S. S. 1991, ApJ, 380, 140

Nilson, P. 1973, *Uppsala General Catalog of Galaxies* (Uppsala, Sweden: Societatis Scientiarum Upsaliensis) (UGC)

Osterbrock, D. E. 1989, *Astrophysics of Gaseous Nebulae and Active Galactic Nuclei* (Mill Valley: University Science Books)

Ostriker, J. P., & Cowie, L. L. 1981, ApJ, 243, L127

Pagel, B. E. J., Edmunds, M. G., Blackwell, D. E., Chun, M. S., & Smith, G. 1979, MNRAS, 193, 219

Pagel, B. E. J., Simonson, E. A., Terlevich, R. J., & Edmunds, M. G. 1991, preprint

Puche, D., Westphal, D., Brinks, E., & Roy, J.-R. 1992, AJ, 103, 1841

Romanishin, W., Strom, K. M., & Strom, S. E. 1983, ApJS, 53, 105

Sage, L. J., Salzer, J. J., Loose, H.-H., & Henkel, C. 1991, BAAS, 23, 1401

Salzer, J. J., Alighieri, S. D. S., Matteucci, F., Giovanelli, R., and Haynes, M. P. 1991, AJ, 101, 1258

Savage, B. D., & Mathis, J. S. 1979, ARA&A, 17, 73

Schombert, J. M., & Bothun, G. D. 1988, AJ, 95, 1389

Schombert, J. M., Bothun, G. D., Impey, C. D., & Mundy, L. G. 1990, AJ, 100, 1523

Schombert, J. M., Bothun, G. D., Schneider, S. E., & McGaugh, S. S. 1992, AJ, 103, 1107

Skillman, E. D. 1989, ApJ, 347, 883

Skillman, E. D., Kennicutt, R. C., & Hodge, P. W. 1989, ApJ, 347, 875

Skillman, E. D., Melnick, J., Terlevich, R., & Moles, M. 1988, A&A, 196, 31

Terasawa, N., & Sato, K. 1990, ApJ, 362, L47

Thomsen, B., & Baum, W. A. 1987, ApJ, 315, 460

Torres-Peimbert, S., Peimbert, M., & Fierro, J. 1989, ApJ, 345, 186

van der Hulst, J. M., Skillman, E. D., Kennicutt, R. C., & Bothun, G. D. 1987, A&A, 177, 63

Vilchez, J. M., & Pagel, B. E. J. 1988, MNRAS, 231, 257

Webster, B. L., Longmore, A. J., Hawarden, T. G., & Mebold, U. 1983, MNRAS, 205, 643

Wheeler, J. C., Sneden, C., & Truran, J.W. 1989, ARA&A, 27, 279

Witten, E. 1984, Phys. Rev. D, 30, 272

CHAPTER IV

GAS CONTENT OF LOW SURFACE BRIGHTNESS GALAXIES: GALAXY FORMATION AND EVOLUTION

Introduction

Low Surface Brightness (LSB) galaxies are an important but rarely studied galaxy type. Severe selection effects discourage detailed study, but such information can shed much light on the evolutionary processes which lead to the physical properties of galaxies not represented by the Hubble sequence of spirals. A comprehensive awareness of these processes is very important if we are to understand the formation and evolution of all galaxies, and the large scale structures which they trace.

With peak surface brightnesses ($\mu_0 \geq 23$ mag arcsec^{-2}) at or below the level of the sky background, it is difficult to identify and study LSB galaxies optically. This is not necessarily the case at radio wavelengths. If the low optical surface brightness is a consequence of a low degree of evolution, then LSB galaxies will not have converted a large fraction of their gas into stars. This should be detectable in the 21 cm line of hydrogen if the gas is atomic, or in a CO transition if the gas is molecular. LSB galaxies are *not* readily detected in the latter (Schombert et al. 1990, Knezek 1992), and we will restrict this discussion to what can be gleaned from the hydrogen line.

The sample galaxies are drawn from either the UGC (Nilson 1973), or the lists of LSB galaxies of Schombert & Bothun (1988) and Schombert et al. (1992). The primary selection criterion is that they be low in surface brightness. The median central surface brightness is $\mu_0 = 23.4$ mag arcsec^{-2} (Chapter 2), nearly 6σ below the "universal" value (Freeman 1970). Other than this, these galaxies exhibit a wide range of size, star formation rates, and other properties. The sample is not complete in any sense, but it does represent a large number of interesting objects which illustrate the importance of LSB galaxies to our understanding of galaxy formation and evolution.

Single Dish Results

Single dish data employed in the analysis here are taken from Schombert et al. (1992). These consists of the flux density and velocity width of the 21 cm line as observed with the Aricebo 305 m telescope. Radii, inclinations, and other optical properties are derived from the data presented in Chapter 2. In order that these quantities be available, the sample is limited to that described in the preceding chapters.

These data are used to derive the dynamical and H I masses, as well as inclinations and B luminosities. The results are presented in Table 4.1. The first column contains the the galaxy name. Objects beginning with 'F' are those identified in the list of Schombert et al. (1992); those beginning with 'U' are from the UGC. The entries for columns 2 – 7 are logarithmic. Column 2 contains the B luminosity of the disk component (in $L_\odot$), Column 4 the mass of hydrogen gas (in $M_\odot$), and Column 6 the dynamical mass (also in $M_\odot$). Columns 3, 5, and 7 contain the formal uncertainties in these quantities. Column 8 contains the inclination (in degrees) with the uncertainty in Column 9. Column 10 contains the adopted distance determined in the same fashion as in Chapter 2. This is a short distance scale, with $H_0 = 100$ km s^{-1}Mpc^{-1}.

The H I masses are determined directly from the observed fluxes. The dynamical masses are determined in from the 20% H I line widths corrected for inclination and the radius at four optical scale lengths ($4 \times \alpha$ from Table 2.1). While it is traditional to use the radius at $\mu = 26.5$ mag arcsec^{-2} for this purpose, isophotal radii substan-

Table 4.1 — Global Properties

Galaxy	L_B	σ_{L_B}	M_{HI}	$\sigma_{M_{HI}}$	M_{dyn}	$\sigma_{M_{dyn}}$	i	σ_i	D (Mpc)
F415–3	8.54	0.06	8.77	0.05	9.31	0.05	59	3	14
F469–2	8.90	0.07	8.88	0.05	9.82	0.05	70	6	35
F530–3	9.59	0.06	9.18	0.08	10.51	0.06	54	5	48
F561–1	9.26	0.08	8.81	0.10	...	...	24	10	48
F563–V1	8.83	0.08	8.47	0.17	9.58	0.05	54	3	39
F563–V2	9.23	0.10	9.12	0.08	10.00	0.05	39	2	46
F568–1	...	...	9.28	0.10	...	...	20	15	68
F568–6	10.66	0.06	10.22	0.11	12.03	0.07	36	3	141
F577–V1	...	...	9.34	0.09	...	...	50	12	81
F611–1	8.25	0.07	8.28	0.06	8.86	0.08	47	5	23
F746–1	9.72	0.09	9.58	0.08	10.24	0.05	68	4	78
U 1230	9.42	0.07	9.52	0.05	10.20	0.12	36	5	38
U 5675	8.49	0.06	8.55	0.05	9.36	0.05	56	4	16
U 5709	9.85	0.07	9.57	0.14	10.65	0.05	69	4	65
U 6151	8.96	0.06	8.75	0.05	9.32	0.15	30	5	18
U 6614	10.06	0.05	10.00	0.05	11.66	0.19	33	7	67
U 9024	9.33	0.05	9.35	0.05	10.45	0.16	42	8	33
U12695	9.57	0.11	9.62	0.08	9.98	0.21	54	15	59

tially underestimate the size of LSB galaxies (Chapter 2). This would lead to an underestimate the dynamical mass, so we instead choose to use $r = 4\alpha$. This choice is somewhat arbitrary, but so is an isophotal radius, and we make it to include nearly all of the light (at least 90%; see equation 2.4).

The importance of this choice is illustrated in Figure 4.1, which shows the deficit which results from calculating the dynamical mass with an isophotal radius. Using $r(\mu = 26.5 \text{ mag arcsec}^{-2})$ underestimates the mass within the optical extent of the galaxy by as much as a factor of two. That substantial amounts of mass are present at large (many scale lengths) radii is confirmed by the fact that for several of these galaxies, the gas mass *exceeds* the dynamical mass computed with the isophotal radius.

The median mass of LSB galaxies in this sample is $10^{10}\,M_\odot$. The mass of these systems covers a wide range, from $7 \times 10^8\,M_\odot$ (F611–1) to $10^{12}\,M_\odot$ (F568–6). Thus, LSB galaxies are not necessarily dwarfs, despite their low surface density. In general,

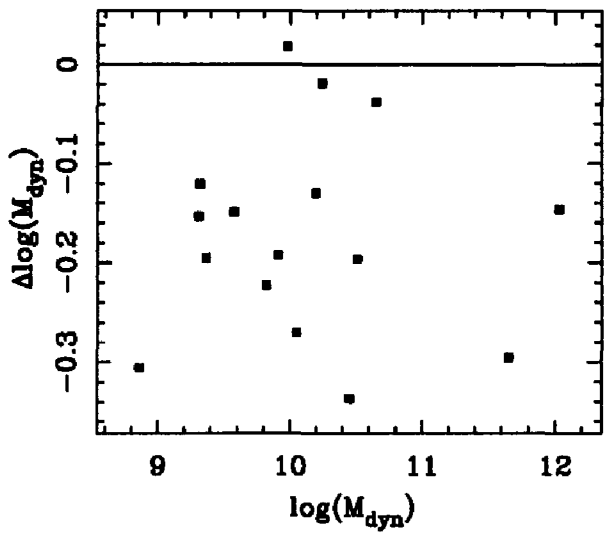

Figure 4.1 — The deficit in dynamical mass computed with isophotal radii relative to that computed at four scale lengths ($\Delta \log M_{dyn} = \log\{M_{dyn}[r(\mu = 26.5\,\mathrm{mag\,arcsec^{-2}})]/M_{dyn}(r = 4\alpha)\}$) plotted against the adopted (4α) mass (in $M_{\odot}$). Only the relatively HSB galaxy F563–V2 exceeds the line of unity, and the slightly higher isophotal mass is adopted for this object.

objects exist which exceed the large mass range of this sample at both ends. There are many examples of low mass LSB systems, and Malin 1 is even larger than F568–6 (Impey & Bothun 1989). In over three decades of mass, we still have not covered the full spectrum of possible masses of LSB galaxies.

This is emphasized by Figure 4.2, in which the mass of atomic hydrogen and the dynamical mass are plotted against the structural parameters (μ_0, α) derived in Chapter 2. Mass scales naturally with size as indicated by the scale length. The mass of atomic hydrogen increases roughly with a slope of two, indicating that it is proportional to the area of the disk, as expected. The scatter is real, and results both from differences in gas mass fraction and the fact that the exponential scale length of the stellar disk is not a good descriptor of the radial distribution of the gas disk (see below). The dynamical mass follows a trend with approximately slope three, as expected for a spherical distribution of mass (i.e., mass $\propto$ volume), consistent with the presence of a dark matter halo.

That neither mass is correlated with the central surface brightness corroborates the results of Chapter 2. That is, galaxies exist over a wide range of both size and surface density. LSB galaxies are not simply the faded remnants of HSB disks which have exhausted the fuel for star formation. If this were the case, the gas mass would decrease or show some cut off with surface brightness.

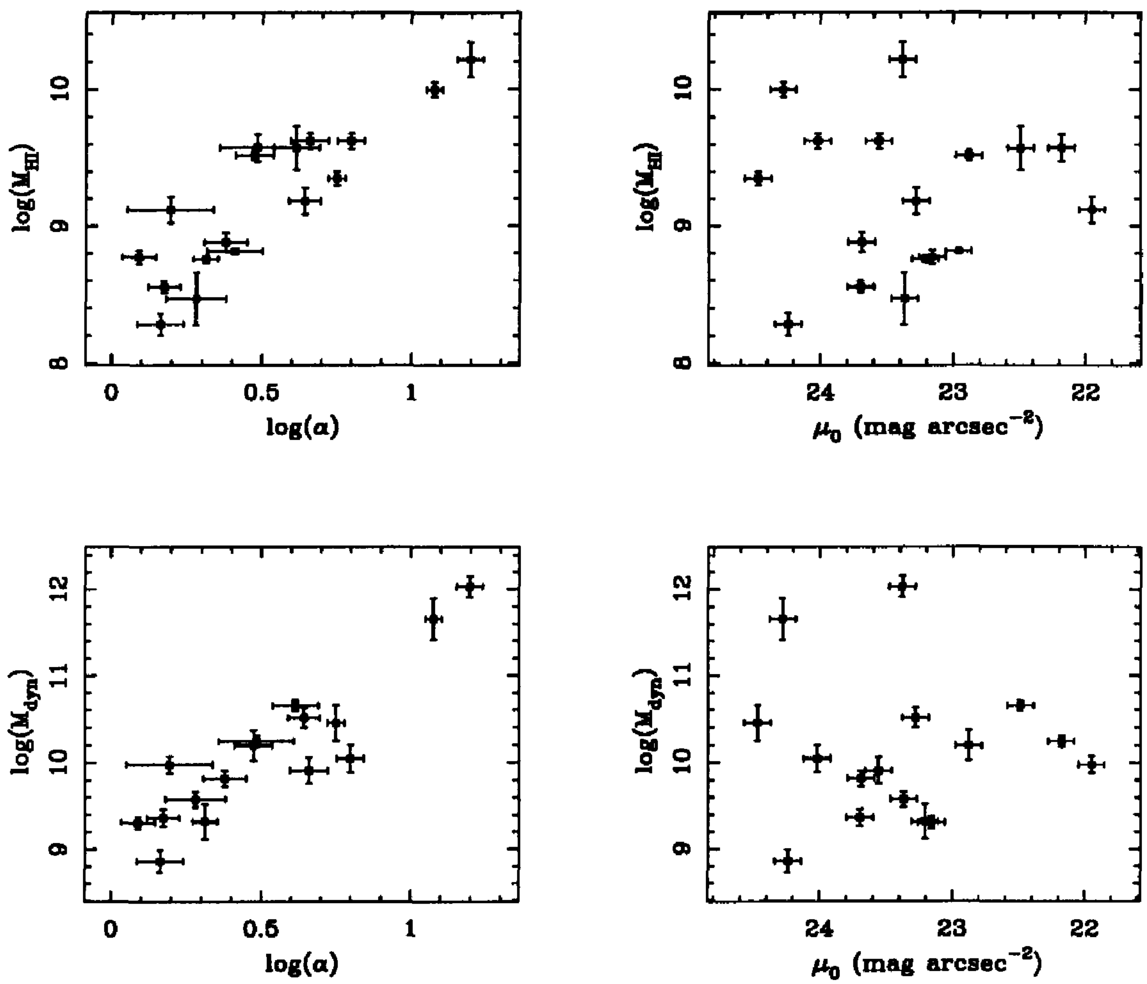

Figure 4.2 — Atomic hydrogen mass (top) and dynamical mass (bottom) (both in $M_\odot$) vs. the structural parameters α (left, in kpc), and μ_0 (right). Mass increases with size in a natural fashion. However, it is not correlated with central surface brightness. Surface density is not a good indicator of total mass, and LSB systems can be very large.

The ratios of the global properties listed in Table 4.1 are listed in Table 4.2. Column 1 lists the galaxy name. Column 2 gives the ratio of hydrogen mass to blue luminosity. Column 3 is the dynamical mass to light ratio, and Column 4 is the

Table 4.2 — Mass Ratios

Galaxy	$\frac{M_{HI}}{L_B}$	$\frac{M_{dyn}}{L_B}$	$\frac{M_{HI}}{M_{dyn}}$
F415–3	1.71	5.9	0.29
F469–2	0.94	8.2	0.11
F530–3	0.39	8.2	0.05
F563–V1	0.43	5.5	0.08
F563–V2	0.77	5.6	0.14
F568–6	0.36	23.3	0.02
F611–1	1.07	4.1	0.26
F746–1	0.72	3.3	0.22
U 1230	1.27	6.0	0.21
U 5675	1.16	7.5	0.15
U 5709	0.53	6.3	0.08
U 6151	0.62	2.3	0.27
U 6614	0.86	39.2	0.02
U 9024	1.04	13.2	0.08
U12695	1.16	2.6	0.45
HSB Sc	0.37	10	<0.1

fraction of the total mass in the form of atomic hydrogen. Columns 2 and 3 are in solar ($M_{\odot}/L_{\odot}$) units, while Column 4 is dimensionless. To the extent to which morphology is meaningful, the majority of these objects are late type disk galaxies. For comparison, the nominal values for a "normal," HSB Sc galaxy are included.

The median values of these ratios for this sample of LSB galaxies are roughly $M_{HI}/L_B \sim 0.9$, $M_{dyn}/L_B \sim 6$, and $M_{HI}/M_{dyn} \sim 0.15$. The incompleteness of the sample makes it difficult to use these numbers to make general statements about LSB systems. Indeed, it is clear that there are many classes of LSB galaxies, and the sample as a whole represents a wide variety of evolutionary paths. Some galaxies have relatively "normal" ratios in Table 4.2, while others are very different. Interestingly, it is the giant galaxies UGC 9024 (α = 5.6 kpc), UGC 6614 (α = 11.9 kpc), and F568-6 (α = 15.8 kpc) which are most "normal" in this regard. A number of other galaxies are distinctly different from the nominal values. Half of the sample has ratios differing from the nominal values by a factor of two or more in the sense that M_{HI}/L_B and M_{HI}/M_{dyn} are large while M_{dyn}/L_B is low.

When the gas mass fraction is small, as is the case for HSB disk galaxies, these ratios accurately reflect the mass fractions of the various components. However, this is not the case for many LSB galaxies. Nonetheless, limits can be placed on the mass to light ratio of the stellar population (Υ) and the gas mass fraction (η) in a simple way.

The total mass is

$$M_* + M_{gas} + M_{dark} = M_{tot}. \tag{4.1}$$

The mass in stars is $M_* = \Upsilon L_B$. The mass in gas is $M_{gas} = (M_{HI} + M_{H_2})/X$, where X is the mass fraction of hydrogen and HI and H_2 refer to the atomic and molecular components respectively (the mass of ionized gas is negligible). We will refer to M_{dark} as the mass in nonbaryonic dark matter (if present), with stellar remnants or brown dwarfs being considered part of the stellar population. The dynamical mass gives the total mass within the radius to which it applies. Hence

$$\Upsilon L_B + \frac{M_{HI} + M_{H_2}}{X} + M_{dark} = M_{dyn}. \tag{4.2}$$

Giving the maximum credit to the stars (i.e., assuming no dark matter) leads directly to an upper limit on the mass to light ratio of the stellar population:

$$\Upsilon \leq \frac{M_{dyn} - (M_{HI} + M_{H_2})/X}{L_B}. \tag{4.3}$$

(Equation 4.3 becomes an equality if no exotic dark matter exists.) Neglecting the molecular gas and setting $X = 0.75$ as appropriate for the low metallicities of these systems (Chapter 3) simplifies equation (4.3) to

$$\Upsilon \leq \frac{M_{dyn} - \frac{4}{3} M_{HI}}{L_B}. \tag{4.4}$$

The mass to light ratios calculated from equation (4.4) are listed in Table 4.3. If either molecular gas or dark matter is present in quantity, the limit on the value of Υ would be forced lower.

Table 4.3 — Limits on Υ and η

Galaxy	Υ ($\frac{M_\odot}{L_\odot}$) (upper limit)	η (lower limit)
F415–3	3.6	0.27
F469–2	7.0	0.16
F530–3	7.8	0.14
F563–V1	5.0	0.20
F563–V2	4.9	0.21
F568–6	23.0	0.05
F611–1	2.6	0.34
F746–1	2.3	0.36
U 1230	4.3	0.24
U 5675	5.9	0.19
U 5709	5.6	0.19
U 6151	1.5	0.47
U 6614	38.6	0.03
U 9024	11.8	0.10
U12695	1.1	0.56

Once an upper limit on stellar mass to light ratio has been determined, a lower limit can be placed on the baryonic gas mass fraction η.

$$\eta = \frac{M_{gas}}{M_{gas} + M_*}, \tag{4.5}$$

which we will approximate as

$$\eta \geq \frac{\frac{4}{3}M_{HI}}{\frac{4}{3}M_{HI} + \Upsilon L_B}, \tag{4.6}$$

again ignoring molecular gas. This is also listed in Table 4.3. Naturally, any molecular gas will raise the value of η. Also, note that since M_{HI} and $L_B \propto D^2$ while $M_{dyn} \propto D$, any adjustment to the adopted short distance scale will make the limits in Table 4.3 even more restrictive.

The median values listed in Table 4.3 are $\Upsilon \sim 5$ and $\eta \sim 0.2$. However, as with other properties, the median values cannot be considered typical. LSB galaxies exhibit an enormous range in both mass to light ratio and gas mass fraction, with $1 < \Upsilon < 40$ and $0.03 < \eta < 0.6$. This large range indicates a broad spectrum of evolutionary histories.

The giant galaxies have approximately "normal" gas mass fractions, with Υ being somewhat large. F568–6 and UGC 6614 have colors which are not unusual for HSB disks (Chapter 2), and the range of metallicities in the disk of F568–6 is also similar to that in HSB disks (Chapter 3). This implies that the evolutionary histories of the giant LSB disks might be crudely similar to that of HSB disk galaxies, with roughly constant star formation rates. However, the situation must be more complicated than this in order for these galaxies to match the HSB characteristics and simultaneously be low in surface brightness. A cessation of star formation could explain the low surface brightnesses and high mass to light ratios, but violates the basic observation that star formation is ongoing in these galaxies. An initial mass function (IMF) biased towards low mass stars might explain these properties without violating the constraints provided by the other observations. This seems inadequate though, as UGC 9024 is quite blue despite having other characteristics in common with the giants (large size, high mass to light ratio, and low gas mass fraction). Even size is an inadequate indicator of Υ and η, as UGC 12695 is as large as UGC 9024 but has the smallest mass to light ratio and largest gas mass fraction in Table 4.3. Hence there are many types of galaxies within the seemingly narrow restriction to large size and low surface brightness. These galaxies must represent a wide range of evolutionary histories with considerable variation from galaxy to galaxy in star formation history and perhaps in IMF as well.

Similarly interesting are those objects with low mass to light ratios and large gas mass fractions. Eight (over half) of the galaxies in Table 4.3 have $\Upsilon \leq 5$ and $\eta > 1/5$, and four have $\Upsilon < 3$ and $\eta > 1/3$. These are quite different from the nominal values of $\Upsilon \sim 10$ and $\eta < 1/10$, despite the overlap in size with HSB disks. HSB galaxies have consumed the majority of their gas supply, and are near to exhausting it completely (Kennicutt 1983). In contrast, the large gas mass fractions of many LSB galaxies indicate that they are relatively unevolved (in the sense that they have converted little of their gas into stars), and may continue to from stars long after currently high surface brightness galaxies have burned out.

Given that a substantial fraction of the mass can be in the form of gas, it is interesting that the mass to light ratios are low. $\Upsilon \sim 5$ is a reasonable value for the mass to light ratio of the stellar population of actively star forming HSB galaxies with old populations (Silva 1991). Thus the mass to light ratios of LSB galaxies with large gas mass fractions are roughly consistent with a simple star formation history consisting of a continuous, constant star formation rate. However, LSB galaxies are not active star forming galaxies in this sense, and their star formation histories are generally complex (Chapter 2). Moreover, the dynamical mass to light ratios of "normal" galaxies exceeds that of their stellar population, implying the presence of large amounts of dark matter. For LSB galaxies to have a star formation history with a quasi-continuous star formation rate would require that very little dark matter be present or that the IMF be skewed in favor of high mass stars (opposite to the case discussed above for giant LSB galaxies) in order to satisfy the mass to light ratios of the gas rich LSB galaxies. Dark matter is likely to be present in LSB galaxies, as implied by Figure 4.2 and flat rotation curves (van der Hulst, McGaugh, & Bothun 1993). The presence of substantial quantities of dark matter within the optical (four scale length) radius would cause the mass to light ratio of the stellar population to be even lower than what is listed in Table 4.3. This would mean a stellar population with a relatively young mean age (consistent with the colors reported in Chapter 2), even if the IMF is weighted towards high mass stars (as these have short lifetimes). Alternatively, the dark matter halo could be rather diffuse so that it contributes little mass within the optical radius. Most likely, a combination of a diffuse dark matter halo and a population weighted towards young stars is responsible for the small Υs in the gas rich LSB galaxies.

Aperture Synthesis Results

While the single dish data provide interesting limits on global properties, they contain no information about how the gas is distributed. This can be addressed with the technique of interferometric aperture synthesis. Data presented here were obtained with the VLA radio telescope for a slightly different sample than that above (though it too is drawn form the Schombert et al. (1988, 1992) lists of LSB galaxies), and there is some overlap.

The detailed treatment of this data will be discussed elsewhere (van der Hulst et al. 1993). In brief, the *uv* databases were edited to remove interference and bad baselines. These were then transformed into data cubes with the AIPS routine HORUS. The data were calibrated with observations of standard VLA calibrators, and the background was removed from the data cubes by subtracting the average of channels lacking signal from the galaxies. Deconvolution of sidelobes with CLEAN was found to be unnecessary. Velocity and surface density maps were extracted from the full resolution data cubes using cubes smoothed in both spatial and velocity dimensions to determine the threshold for inclusion of individual pixels in the final maps. The total fluxes measured from the VLA surface density maps are consistent (within the errors) with the Aricebo fluxes.

Here, we examine only the surface density maps. When possible, the methods of optical surface photometry (Bothun et al. 1986) are employed to determine the radial surface density distribution as in Chapter 2. This provides a basis for the comparison of the optical and H I radii, and can be compared to the surface density profiles of HSB galaxies (e.g., Warmels 1988).

In general, the distribution of H I is quite clumpy (see Appendix A). Sometimes central holes are present, but not always. The resolution (beam size $\approx 13''$) is too coarse to reveal any spiral structure, if present. The radial profiles are shown in Figure 4.3. Because of the clumpiness, no attempt has been made to correct the profiles for edge brightening, as is sometimes done under the assumption of a homogeneous, optically thin disk. Since the inclinations are generally modest, this is not an important correction for these galaxies. Moreover, the analogous correction cannot be made for the optical profiles without detailed knowledge of the dust distribution, so for comparison purposes it is best to treat both sets of data in the same manner.

The radial surface density profiles tend not to be smooth, and are not well fit by a simple analytic function as is the case for the stellar distribution (Chapter 2). Rather than falling off exponentially with radius, the surface density of the gas tends to drop off in a linear fashion, sometimes with a change in slope at a particular radius. It would facilitate comparison of the two components (via the structural parameters of central surface density and scale length) if the gas were distributed in an exponential disk as are the stars, but this is not the case.

Nevertheless, we can compare isophotal radii for those galaxies with both optical and H I profiles. This is done in Table 4.4, which contains the optical radii at $\mu = 25$ and 26.5 mag arcsec^{-2}, and the H I radius at $\Sigma_{HI} = 1\ M_{\odot}\mathrm{pc}^{-2}$ (all in arcseconds). These values are taken for consistency with the work of Wevers (1984) and Warmels (1986). These references provide the "normal" values of the ratio of H I to optical radii listed in Table 4.4. Note that since the metallicity of LSB galaxies is generally lower than that of HSB galaxies, the 1 $M_{\odot}\mathrm{pc}^{-2}$ H I isophote actually refers to a slightly lower *gas* surface density in LSB disks (since the mass fraction of H I is higher there).

While there are few galaxies which have both optical and H I profiles, it is clear that LSB galaxies have H I disks which are larger relative to their stellar disks than do HSB galaxies. This is partially a result of using isophotal radii, which tends to underestimate the size of the optical disk (Chapter 2). Perhaps a better technique would be to measure the radii at a point where both optical and H I profiles have dropped to some nominal fraction of their peak intensity (e.g., 5%), or the radii which contain half the light and mass. We will not do this here because there are no comparison

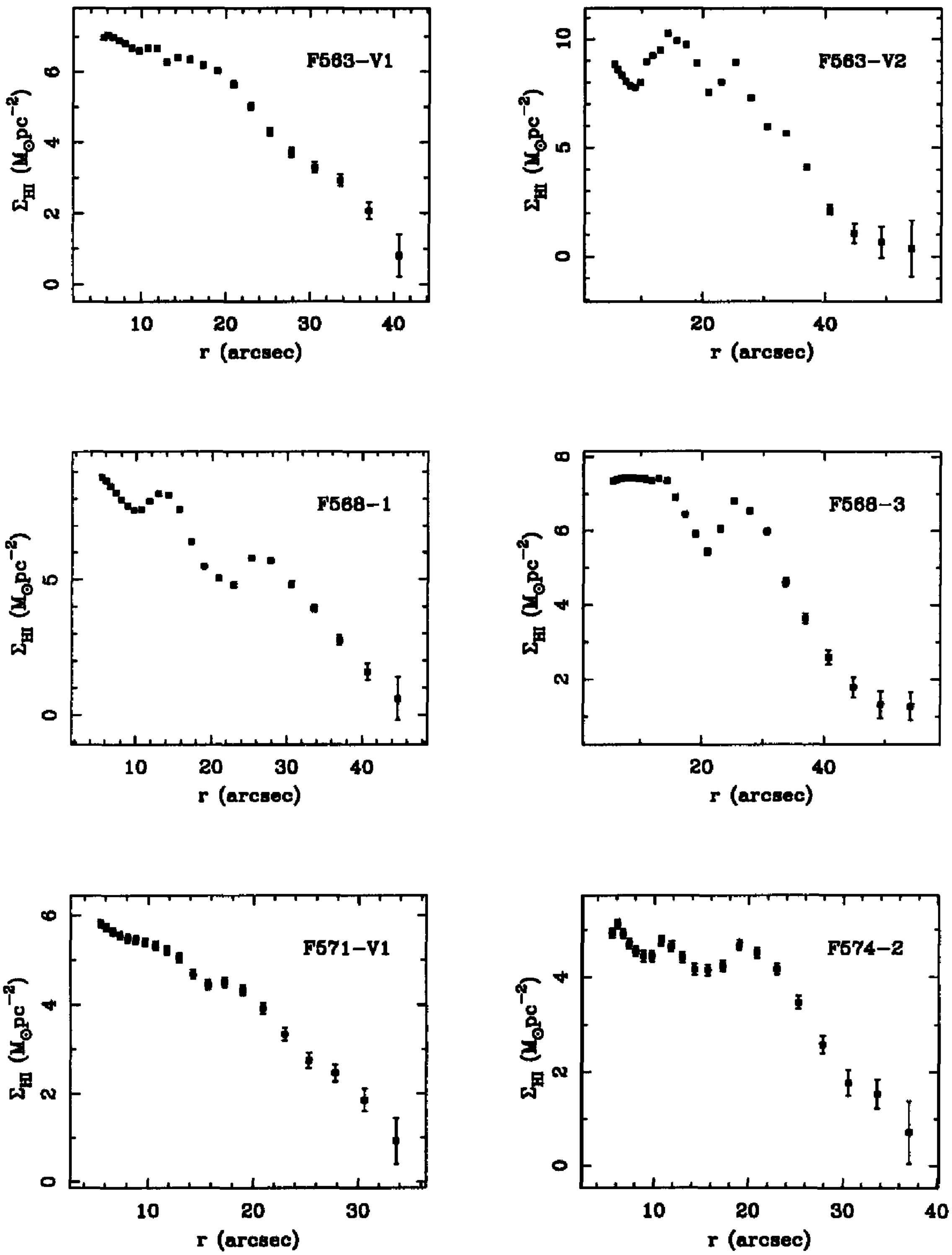

Figure 4.3 — The radial surface density distribution of atomic hydrogen gas. The profiles are often rough, and when smooth tend to decline in a linear rather than exponential fashion. Note also that the peak surface densities are low, in all but one case less than 8 $M_\odot \mathrm{pc}^{-2}$.

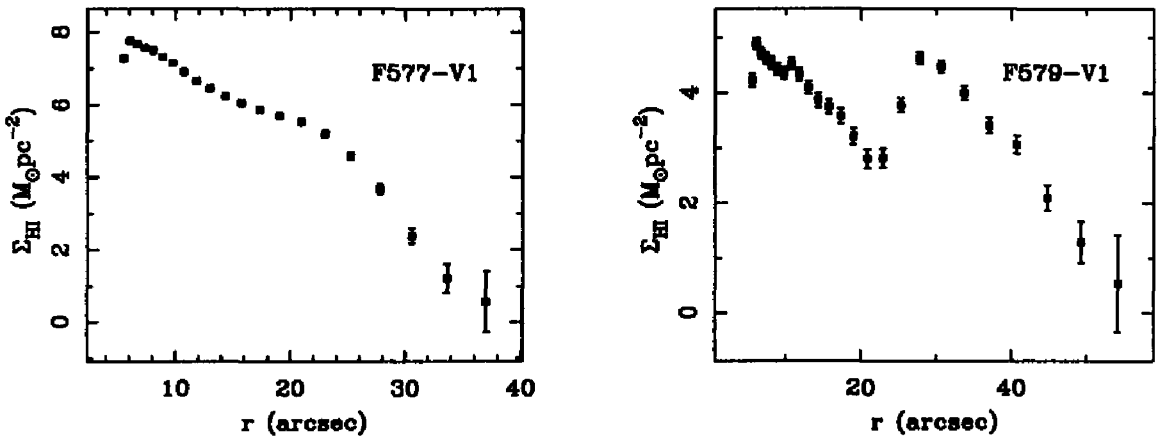

Figure 4.3 — *continued.* Because of the clumpiness of the H I maps and the presence of central holes in some galaxies, these profiles are not always centered on the same spot as the optical profiles (e.g., F577–V1).

data which follow these conventions, and our own data are limited. Nonetheless, the H I radius is also an isophotal one, so that it will be similarly underestimated if the H I is, like the optical component, low surface brightness. This is indeed the case, so the H I disks of LSB galaxies are in fact more extended than those of their HSB brethren.

Table 4.4 — Optical and H I radii

Galaxy	r_{25}	$r_{26.5}$	r_{HI}	$\frac{r_{HI}}{r_{25}}$	$\frac{r_{HI}}{r_{26.5}}$
F563–V1	14.1	28.4	40	2.84	1.41
F563–V2	23.2	29.2	45	1.94	1.54
F577–V1	12.5	24.5	35	2.80	1.43
Normal	...	...	...	1.61	1.18

Though HSB galaxies display a considerable range in H I surface density, they generally peak above 8 $M_{\odot}\text{pc}^{-2}$ (Warmels 1988). This is higher than in most LSB galaxies, for which Σ_{HI} is usually $< 8\ M_{\odot}\text{pc}^{-2}$. So, just as these galaxies are low in optical surface brightness, they are low in H I surface density.

Discussion

Star Formation and Galaxy Evolution

LSB galaxies are observed to have undergone a relatively small degree of evolution, as indicated by their large gas mass fractions and low metallicities (Chapter 3) as well as by their feeble stellar components. It follows naturally from the Schmidt (1959) star formation law that galaxies with low gas densities will have low star formation rates (SFRs) and hence evolve slowly. The Schmidt law can be parameterized as

$$SFR \propto \Sigma_{gas}^{N}. \tag{4.7}$$

Obviously, this will lead to the slow evolution of low surface density disks as long as $N > 0$. This is certainly the case; Kennicutt (1989) finds $N = 1.3 \pm 0.3$ for the range of densities exhibited by HSB disks.

However, this alone is not adequate to explain the low degree of evolution of LSB galaxies. While they are low surface density in both gas and stars, LSB galaxies are not *as* LSB in H I as they are optically. Despite the difference in hydrogen mass fraction and the much larger amounts of molecular gas generally present in HSB galaxies, the gas surface density of LSB galaxies is usually within a factor of two of that in HSB galaxies. In contrast, there is a factor of five difference between the canonical Freeman (1970) value ($\mu_0 = 21.65$ mag arcsec^{-2}) and the median central surface brightness of this sample of LSB galaxies ($\mu_0 = 23.4$ mag arcsec^{-2}). This corresponds to a factor of five difference in the star formation rate per unit area averaged over the life of the galaxy. Taking the maximum value for the difference between LSB and HSB gas surface densities (i.e., 2),

$$\frac{SFR_{HSB}}{SFR_{LSB}} = \left(\frac{\Sigma_{HSB}}{\Sigma_{LSB}}\right)^{N} \rightarrow 5 = 2^{N} \tag{4.8}$$

requires a value of $N \approx 2.3$, much larger than observed. In most cases the ratio of gas surface densities is less than two, and if the stellar population in LSB galaxies is younger on average than that in HSB galaxies, as seems likely, then the difference in SFR is greater than a factor of five. Either of these would cause the derived index N to be even larger. Thus a simple Schmidt law fails to describe the star formation and evolutionary rates of LSB galaxies.

Star Formation Threshold

Kennicutt (1989) has discussed a modification of the simple Schmidt law which includes a critical density threshold below which star formation is strongly suppressed. This modified star formation law successfully describes many quantitative aspects of star formation in disk galaxies. Physically, the threshold is based on the criterion for gravitational instability in a rotating disk (Toomre 1964). Under the simplifying assumption of a flat rotation curve, the expression for the critical density can be written (equation 6 of Kennicutt 1989):

$$\Sigma_c \, (M_{\odot}\mathrm{pc}^{-2}) = 0.59\,\xi \left(\frac{\varsigma}{6\ \mathrm{km\,s^{-1}}}\right) \frac{v_r\ (\mathrm{km\,s^{-1}})}{r\ (\mathrm{kpc})}, \tag{4.9}$$

where Σ_c is the critical density, ξ is a dimensionless stability parameter of order unity, ς is the velocity dispersion of the gas, and v_r is the rotation velocity of the galaxy. When the gas density exceeds this critical density, the normal Schmidt law applies. Below this threshold, the star formation law becomes highly nonlinear, and star formation is largely suppressed.

Application to LSB galaxies has obvious relevance because of their low surface densities. We do this here under the assumption that the rotation curves are flat at the level indicated by the velocity widths of the 21 cm Aricebo observations and the inclinations in Table 4.1. This assumption obviously fails in the inner regions of the galaxies, but the VLA data cubes confirm that it is adequate over most of the disk area. While the VLA data show that the rotation curves are flat, the signal is too weak to offer much improvement over the velocities determined from the Aricebo line widths. Also, there is marginal evidence that the inclinations of the optical and gas disks do not always coincide, and that occasionally warps are present. While these increase the uncertainties in the current argument, they are not present at a level which alters it. The VLA cubes contain no useful information about the velocity dispersion of the gas, so for lack of information to the contrary we adopt the values Kennicutt (1989) gives for the stability parameter and the velocity dispersion ($\xi = 0.67$ and $\varsigma = 6\ \mathrm{km\,s^{-1}}$). These values must be approximately correct, and this velocity dispersion is consistent with that found by Puche et al. (1992) for one LSB galaxy.

Figure 4.4 shows the radial dependence of the critical density relative to the actual gas surface density for those galaxies with sufficient data for the critical density calculation. The H I surface densities have been corrected to gas surface densities assuming a mass fraction of hydrogen $X = 0.75$ and no molecular gas (as before). Molecular gas is not likely to be abundant in LSB galaxies (Chapter 3), nor is it well correlated with star formation in HSB galaxies (Kennicutt 1989). There is some uncertainty in the positions of the lines of critical density due to the factors discussed above, but the the results are not seriously affected.

LSB galaxies are near but below the threshold for star formation over most of their area. Since many of these galaxies are selected by the presence of H II regions which can be studied spectroscopically (Chapter 3), it is not surprising that there are places where the gas density exceeds the critical density. Indeed, the H II regions coincide with these spots, and are located at the radii indicated by Figure 4.4. The simple gravitational instability criterion for this threshold density for star formation not only predicts successfully the radii at which star formation should occur, but also adequately predicts the two dimensional positions of the sites of star formation, at least on $\sim$ kiloparsec scales (see Appendix). That this is the case lends strong support to both the existence of a density threshold for star formation and to the physical cause proposed for it (i.e., gravitational instability in a thin rotating disk, Toomre

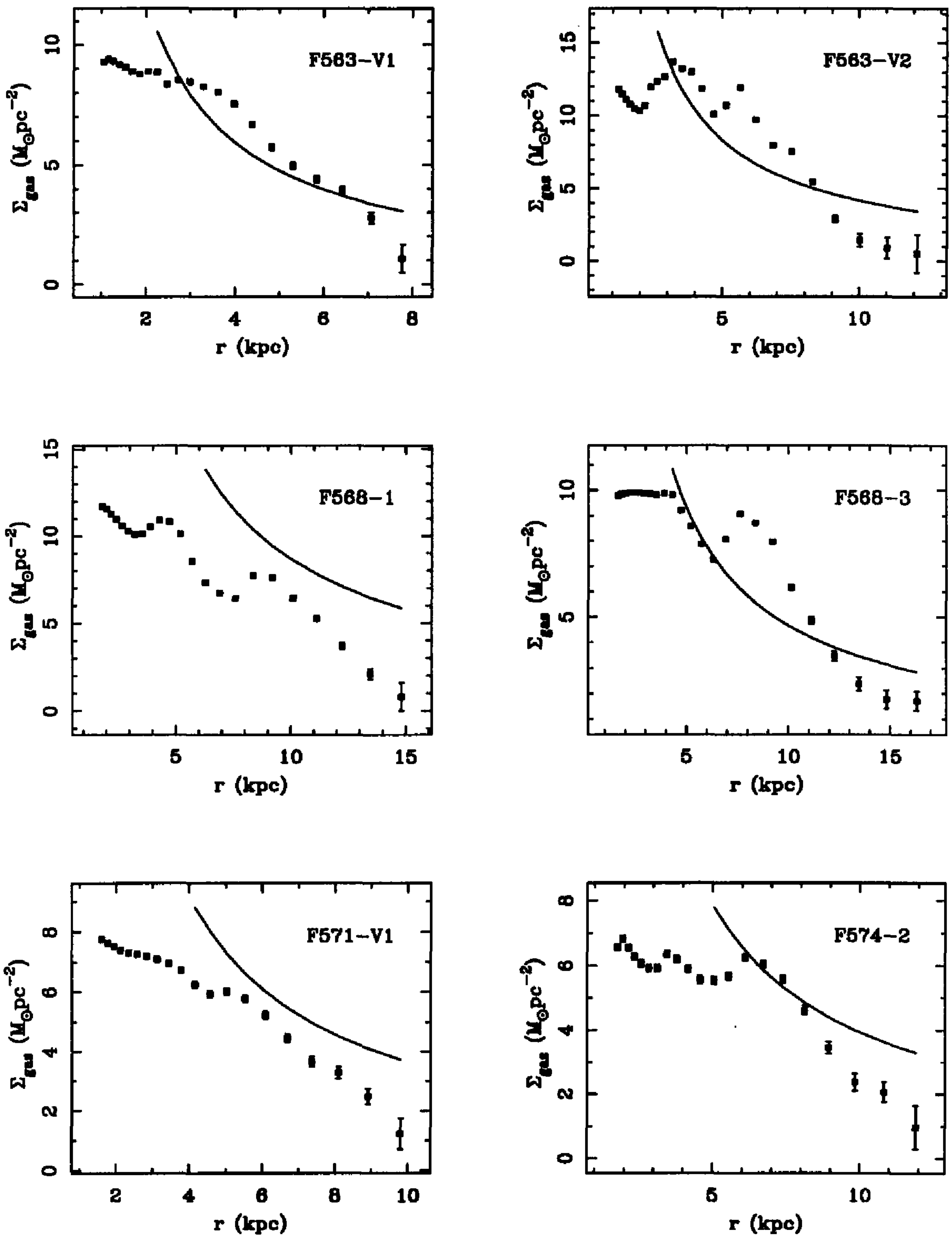

Figure 4.4 — The critical density threshold for star formation (lines) plotted with the observed gas surface density (points). These galaxies are generally below the critical density, except for small regions. The radii at which the threshold is exceeded coincides with the actual radii where star formation is occurring.

1964, Quirk 1972, Kennicutt 1989). If some other physical effect caused there to be a similar threshold, it would be a surprising coincidence that the lines of critical density calculated with the gravitational instability criterion fall anywhere near the observed gas densities in Figure 4.4.

Examination of the critical density images in Figures 4.A.4 through 4.A.8 makes it clear that only isolated regions exceed the star formation threshold. The vast majority of the area of LSB disks are safely below the critical density. This immediately suggests itself as the cause of the low degree of evolution of LSB galaxies. That is, the majority of their gas disks are stable against star formation at any given time, so star formation occurs only sporadically, and evolution proceeds gradually.

This confirms the suggestion by van der Hulst et al. (1987) that star formation depends on local conditions rather than global properties (such as gas mass), and that the evolutionary rate of a galaxy is driven by the H I surface density (Bothun et al. 1990). The low gas surface densities may also explain the feeble appearance of spiral arms in LSB galaxies (when present), as the SFR should not be large even when the threshold is exceeded and the normal Schmidt law applies. In HSB disks, the critical density can be sufficiently high that modest excesses lead to high star formation rates, and thus to high contrast spiral arms (Kennicutt 1989). Hence, the existence of a threshold density appears to be more relevant to the appearance and evolutionary characteristics of a galaxy than is the precise form of the Schmidt law.

The low, subcritical gas surface densities in LSB galaxies are the physical cause for their low degree of evolution. If galaxies which are well below the threshold exist, then we would never detect them, as they would never form stars and remain extremely LSB at both optical and radio wavelengths. There is no reason to believe that this could not occur, and this situation is observed to arise in the outer parts of giant galaxies like Malin 1 and Malin 2 (F568–6), where the rotation velocities (and hence the critical densities) are large and the surface densities are low. That these large galaxies could go undetected for so long, and have only been noticed because of their prominent central bulges, suggests that such "invisible" galaxies could well exist.

Galaxy Formation

If the slow rate of evolution of LSB galaxies stems from their low surface densities, what causes these densities to be low? Presumably, it is related to the initial conditions of formation. Indeed, not only is the baryonic component of LSB galaxies diffuse, but so is any dark matter halo, as implied by the low mass to light ratios. Such diffuse galaxies will form naturally from weak density perturbations which are ineffective at concentrating matter to the same degree observed in HSB galaxies.

LSB Galaxies as Modest Initial Fluctuations

A common, simple model for the formation of galaxies is the gravitational collapse of homogeneous, spherical overdensities ("top hats") which arise from some random field of fluctuations. These can be treated as locally closed Robertson-Walker universes, the expansion and contraction of which are described by the equation of a cycloid (e.g., Weinberg 1972):

$$Ht = \frac{1}{2}\,\Omega\,(\Omega-1)^{-3/2}\,(\theta - sin\theta), \tag{4.10}$$

where $H = \dot{R}/R$ is the expansion rate, t is time, Ω is the density parameter, and θ is the development angle defined for convenience by

$$1 - cos\theta = 2\left(\frac{\Omega-1}{\Omega}\right)\frac{R(t)}{R_0}. \tag{4.11}$$

The overdensities reach their maximum size when $\theta = \pi$, after which they collapse.

Traditionally, the degree of the fluctuation is expressed in terms of the perturbation $\delta\rho/\rho$, where $\rho_p = \delta\rho + \rho$, ρ_p being the density within the top hat and ρ the average density of the universe in which the fluctuation is imbedded. The density parameter can then be written as

$$\Omega \to \Omega_p = \frac{\rho_p}{\rho} = \frac{\delta\rho + \rho}{\rho} = \frac{\delta\rho}{\rho} + 1. \tag{4.12}$$

Together with the preceeding equations, this gives the time to reach maximum expansion,

$$t_m = \frac{\pi}{2H}\Big[(\frac{\delta\rho}{\rho})^{-1/2} + (\frac{\delta\rho}{\rho})^{-3/2}\Big], \tag{4.13}$$

and the expansion factor,

$$\frac{R_m}{R_i} = 1 + (\frac{\delta\rho}{\rho})^{-1}. \tag{4.14}$$

These are plotted in Figure 4.5.

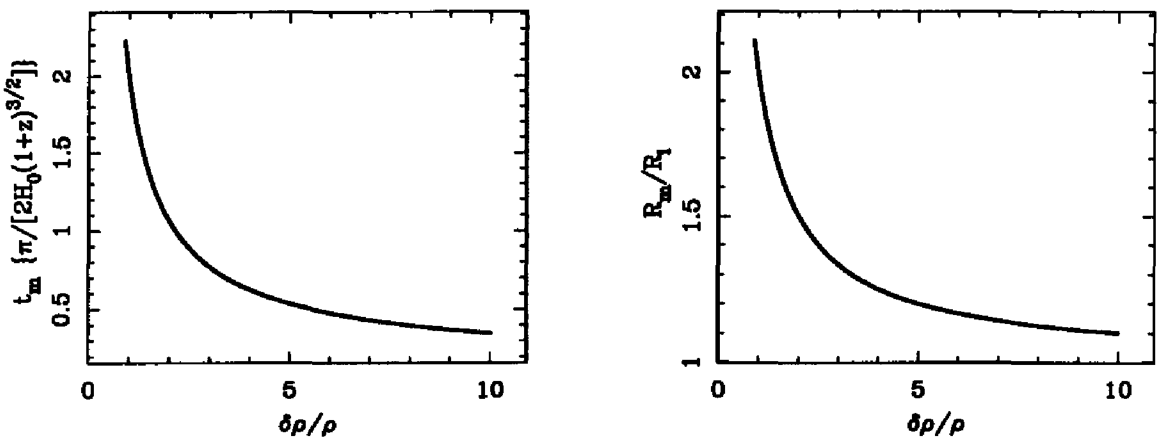

Figure 4.5 — The time for a top hat perturbation to reach maximum expansion (left) and the expansion factor at that point (right) as a function of the perturbation size $\delta\rho/\rho$. Small perturbations take longer to reach the turn around point, and become relatively more extended. The physical time for this to occur depends on the magnitude of the expansion which must be overcome, and hence the redshift at which the perturbations are free to grow.

Clearly, the larger the perturbation, the more rapidly it reaches its maximum extent, and the more rapidly it collapses. Formally, collapse to a point would occur when the development angle reaches $\theta = 2\pi$, so $t_c = 2\,t_m$. Of course, galaxies do not collapse to singularities, and the actual formation time takes rather longer. If violent relaxation occurs, the protogalaxy will become virialized on a time scale

$$t_{vir} \sim (G\rho_p)^{-1/2} \propto \left(\frac{\delta\rho}{\rho} + 1\right)^{-1/2}, \tag{4.15}$$

which for a homogeneous sphere is about twice as long as implied by t_c. That is, starting from the point of maximum expansion, $t_{vir} \sim 2t_m$. The ratio t_{vir}/t_m is a weak function of $\delta\rho/\rho$ for large perturbations, but becomes singular as $\delta\rho/\rho \to 0$. This is simply a restatement of the classic result that small, linear perturbations cannot grow fast enough to overcome the general expansion, as expected since $\delta\rho/\rho = 0$ corresponds to a region which does not deviate from a pure Hubble flow.

It may be fair to state that a galaxy has formed when its dissipationless dark matter component has virialized. However, the formation of the dissipational baryonic component can take substantially longer (Katz & Gunn 1991). Indeed, disk formation may not occur at a well defined instant. For our current purposes, it is adequate to realize that galaxies arising from small perturbations will take longer to form than large ones.

More importantly, a small perturbation will expand to relatively greater size than a large perturbation. At a particular mass, this will result in a softer potential, and a larger final size. Stated simply, low density galaxies result naturally from small density perturbations. Thus we can identify the diffuse LSB galaxies with formation from modest initial density fluctuations, and HSB galaxies with larger perturbations.

Implications

The identification of LSB galaxies with small density fluctuations is hardly surprising (e.g., Dekel & Silk 1986). However, it has a number of striking implications for our understanding of galaxy populations and cosmology. To elucidate these, we will adopt the density fluctuation spectrum of the standard cold dark matter (CDM) cosmology (Blumenthal et al. 1984). This choice is not important for most of the points which follow, but it does provide a familiar, quantitative framework for the discussion.

A galaxy of any given mass can arise from a range of fluctuations. A $\sim 10^{10} M_{\odot}$ galaxy (the median mass of this sample of LSB galaxies), can result from a modest perturbation of $\delta\rho/\rho = 2$ or a strong perturbation of $\delta\rho/\rho = 10$. For the CDM fluctuation spectrum, these correspond approximately to 0.5σ and 2.5σ perturbations, respectively (the exact degree of the fluctuation depending slightly on the choice of Ω_0 and H_0). Irrespective of the adopted cosmology or fluctuation spectrum, small fluctuations will be more common than large ones. How much more common depends on the shape of the probability distribution (i.e., $P(\delta\rho/\rho)$ at a given mass), which can evolve to a nongaussian form even from initially gaussian conditions (Bernardeau 1992). Even so, these simple considerations predict that LSB galaxies should be more common than HSB galaxies at *all* masses.

This could well be the case, given the severe selection effects against LSB objects (Chapter 1). If so, current galaxy catalogs give a very incomplete picture of the galaxy population, and we are largely unaware of the numerically dominant component thereof. However, it is possible for fluctuation spectra which are relatively flat over the mass range of interest (like that of CDM) to complicate this situation, as small fluctuations which collapse at late times can become incorporated into larger structures as hierarchical structure formation proceeds. To the limited depth which has been probed, the number density of galaxies does not appear to increase strongly as surface brightness decreases (Schombert & Bothun 1988). This indicates that both the fluctuation spectrum and the probability distribution are relatively flat.

Note that the same scenario applies to the giant ($\alpha > 10$ kpc, $\sim 10^{12} M_{\odot}$) galaxies like F568–6. Such objects could form from $\sim 1\sigma$ fluctuations at this mass scale, and do not need to be large fluctuations in voids as suggested by Hoffman, Silk, & Wyse (1992). However, their survival as individual objects may depend on the environment. That is, they must have time to collapse without fragmenting or being incorporated into larger structures. That giant LSB galaxies appear to avoid high density regions (Knezek 1992) suggests that this is indeed the case. If so, these galaxies provide powerful probes of the effect of environment on the galaxy formation process.

That the smooth, gradual collapse of LSB galaxies proceeds best undisturbed suggests a connection to the morphology-density relation (Oemler 1974, Dressler 1980). If the ultimate morphological type is largely determined by the amount of small scale structure within the initial perturbation, such that clumpy protogalaxies tend to become ellipticals and smooth ones disk galaxies (Katz 1992), then the occurrence of large disk galaxies in regions of low density implies that the source of the small scale structure may be perturbations from nearby protogalaxies. Thus, objects in low density environments collapse smoothly to from late type disk galaxies, while those in high density environments interact enough to preferentially cause early type systems. This is consistent with the otherwise puzzling result that LSB galaxies follow the morphology-density relation, but also trace the same very large scale structures as HSB galaxies (Schombert et al. 1992). In this case, the morphology-density relation arises from causes different than the scale association of CDM, and does not require the CDM fluctuation spectrum in order to occur.

This removes one of the major attractions of the CDM model. An additional, serious difficulty posed for CDM is the observed lack of biasing. That is, LSB galaxies arise naturally from weak density perturbations, so their very existence means that there is no lower limit to the fluctuations which are able to form galaxies, except that they be large enough to collapse at all, as discussed above. Being the results of such common, modest fluctuations, LSB galaxies should be good tracers of the underlying mass, and be distributed more uniformly than HSB galaxies. That this is not the case requires a mechanism for the formation of large scale structure other than biased galaxy formation with purely cold dark matter. This mechanism must be efficient at directing baryonic matter to the observed structures, within which galaxy formation can proceed normally.

The traditional association of LSB galaxies with dwarfs leads to other difficulties for the standard CDM model. Within this framework, LSB galaxies are viewed as being the result of gas loss from dwarfs stemming from supernovae driven winds during an early epoch of star formation (Dekel & Silk 1986). However, the LSB galaxies in this sample are *not* dwarfs, despite having arisen from weak density fluctuations. They certainly do not owe their LSB nature to extensive gas loss, as these are generally gas rich systems. Indeed, the smallest galaxy in the sample (F611–1) has an enormous amount of gas ($\eta > 0.34$). Not only are the gas mass fractions large, but the distribution in the (μ, M) plane bears no resemblance to the predictions of the model of Dekel & Silk (1986). Moreover, these galaxies do not fall into either category suggested by Dekel & Silk (1986), nor do they follow the radius-metallicity-luminosity relations which their model predicts (their observed relations are based on preliminary data and probably arise as a result of selection effects). While gas loss may well play a significant role in the evolution of low mass galaxies, it is not a panacea for explaining LSB stellar systems.

Though the evolution of individual LSB galaxies can be quite complicated, a coherent picture has emerged for their relation to HSB galaxies. This is depicted schematically in Figure 4.6. In order to assign a degree to the fluctuation $\delta\rho/\rho$ at a particular mass scale, we have adopted the CDM fluctuation spectrum and assumed that the observed ratio of surface densities corresponds to the ratio of the initial overdensities. While the latter depends on the details of the dissipational formation of the disk, it should be approximately correct, and does not really matter to the schematic picture. Similarly, the assumption of the CDM fluctuation spectrum is made only to quantify the picture, which holds regardless of the actual form of the fluctuation spectrum.

The general picture is that since LSB galaxies arise from modest (low σ) density perturbations, they will be more common than HSB galaxies of the same mass, and take longer to form. Once formed, LSB galaxies will evolve more gradually because of their low surface densities. When observed at the current epoch, they will appear

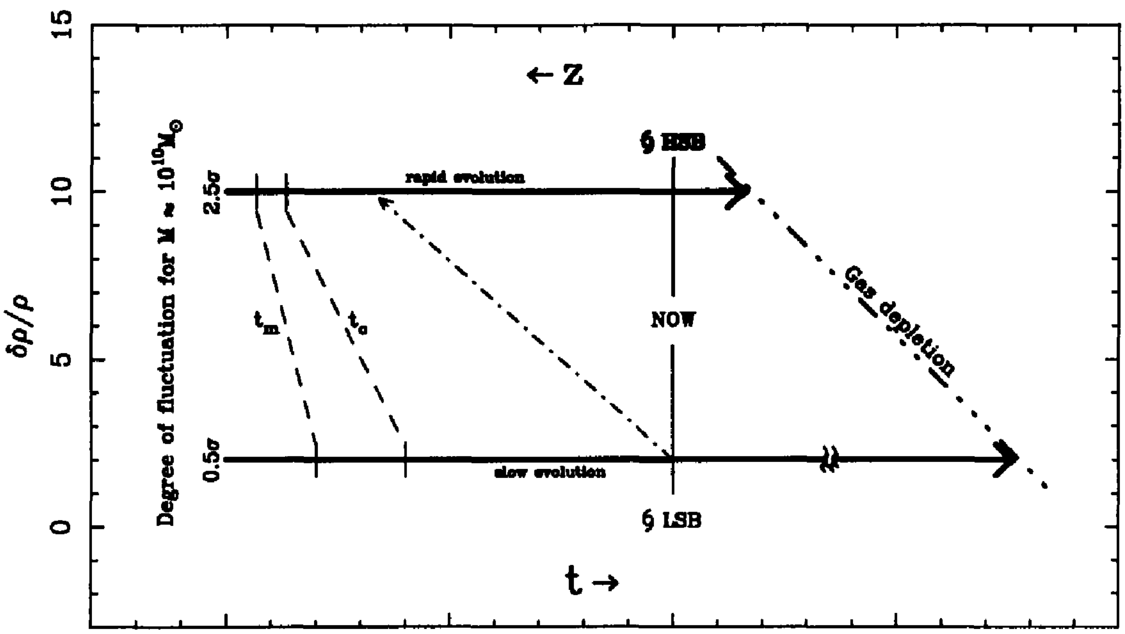

Figure 4.6 — Simple scheme showing the relative evolutionary paths of HSB and LSB galaxies. Cosmic time increases along the abscissa, and the overdensity $\delta\rho/\rho$ is specified by the ordinate. Large overdensities result in HSB galaxies, and low overdensities become LSB galaxies. For the specific choice of a CDM fluctuation spectrum, a $10^{10}M_{\odot}$ LSB galaxy corresponds to a $\sim$ 0.5σ perturbation, and an HSB galaxy a factor of five more dense results from a $\sim$ 2.5σ perturbation. Regardless of the adopted cosmological model or fluctuation spectrum, LSB galaxies will be more common at any given mass, and take longer to form than HSB galaxies. This is shown by t_m and t_c, the time for the overdensity to reach maximum expansion and the time to collapse, respectively. The actual formation time takes somewhat longer than t_c, but scales in the same fashion. Once formed, LSB galaxies will evolve more gradually because of their low surface densities. This means that LSB galaxies, as observed now, correspond to an earlier phase in the evolution HSB disks, as indicated by the dot-dashed line. They will continue to form stars from large reservoirs of gas well after HSB galaxies have exhausted their supply, so that they may become the prominent, "high" surface brightness galaxies of the future.

less evolved than HSB galaxies of the same mass, having lower metallicities and larger gas reservoirs. In this sense, the current conditions in LSB galaxies represent an early phase in the evolution of all disk galaxies. Though the details of disk evolution must become complicated as a galaxy nears gas depletion, the large gas mass fractions of LSB galaxies suggest that they will continue to form stars much longer than currently HSB galaxies. Thus, it seems that this epoch (Kennicutt 1983), and indeed every epoch, is characterized by proportionality rapid changes in the properties of star forming galaxies. It follows naturally from the nature of stellar evolution and the finite gas reservoirs of galaxies that stellar systems must evolve substantially over a Hubble time. Indeed, it may be that in another Hubble time, currently HSB galaxies will have exhausted their gas supplies and faded into obscurity, leaving the more slowly evolving LSB galaxies as the most prominent star forming objects amidst a field of invisible galaxies.

Conclusions

LSB galaxies are low density stellar systems with large gas mass fractions and high mass to light ratios. These indicate relatively young, unevolved objects imbedded in diffuse dark matter halos. Despite their large gas mass fractions, LSB galaxies are low in H I as well as stellar surface density, and the H I disks are more extended than the optical components relative to HSB galaxies.

The low degree of evolution of LSB galaxies is caused by their low surface densities. These are below the threshold for star formation discussed by Kennicutt (1989), causing LSB galaxies to form stars sporadically, and evolve slowly. Indeed, the existence of this threshold is more pertinent to the understanding of galaxy evolution than is the form of the Schmidt law.

There is no reason to believe that galaxies do not exist which are very low surface density, well below the threshold for star formation. These would never form stars, and remain invisible to both optical and H I surveys (e.g., Weinberg et al. 1991). These could be considered true protogalaxies, as they would take a long time to form and remain pristine indefinitely due to the suppression of star formation.

LSB galaxies are low density because they form from modest density fluctuations. Basic, model independent theoretical considerations demand that LSB galaxies be quite common. This suggests that the severe selection effects against discovering LSB galaxies have seriously limited our knowledge of the true galaxy population. Indeed, both the initial fluctuation spectrum and the probability distribution of fluctuations at a given mass must be rather flat in order to avoid the numerical dominance of LSB galaxies at *all* masses. The latter must be very nongaussian, while the former may be flat enough for hierarchical structure formation to interfere with the gradual formation of low density systems, especially on large mass scales.

That LSB galaxies exist, and arise from modest density fluctuations, means that the galaxy formation process is *not* strongly biased. However, LSB galaxies do appear to trace the same large scale structures seen in redshift surveys of HSB galaxies. This is a grave difficulty for the formation of large scale structure in the standard CDM scenario.

APPENDIX IV.A
H I SURFACE DENSITY MAPS

The surface density maps of atomic hydrogen constructed from the VLA data discussed in the text are displayed here, together with optical images. The resolution of the H I maps is $\approx 13''$, roughly 10 times less than that of the optical images. The pixel scale of the H I maps is 5 arcsec pixel^{-1}. The images are cropped to be the same size ($2.4'$ on a side). In all cases, North is up and East is to the left. The contrast varies from image to image so that the peak is always saturated; see Figure 4.3 for the actual surface densities.

In addition to the H I surface density maps, critical density maps are also displayed for objects which have some current star formation as indicated by Hα emission. The critical density maps are constructed using the simple criterion for a threshold to the star formation process in a rotating disk (Kennicutt 1989) to compute the radial dependence of Σ_c (see equation 4.9). For galaxies with flat rotation curves, this amounts to a convolution of the H I surface density maps with a linearly increasing function of radius:

$$\Sigma_c(r,\theta) \propto \Sigma_{HI}(r,\theta) * r. \tag{4.A.1}$$

The assumption of flat rotation curves will make the resulting maps meaningless in the central regions where this is not the case. Elsewhere, low values have been trimmed from the critical density maps so that only those regions which are close to or in excess of the star formation threshold remain. Note that very few pixels actually exceed the critical density in each map, and the majority of those displayed are subcritical.

While the resolution of the critical density maps is poor, and they have been constructed in a crude fashion, correspondence between peaks in the critical density maps and current sites of star formation as traced by Hα is reasonably good. Since the activity of star formation will disrupt the gas through the action of supernovae and stellar winds, the tracers of star formation may not appear to be correlated with the gas density if examined with sufficient resolution. However, the simple gravitational instability criterion for a density threshold to the star formation process seems able to adequately predict the locations of star forming sites on ~kiloparsec scales.

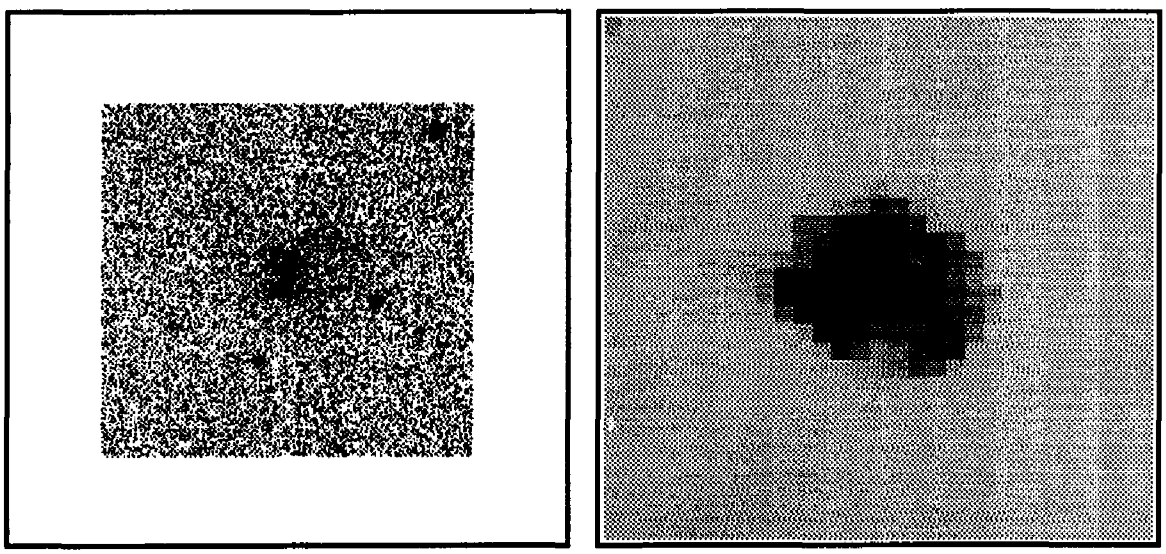

Figure 4.A.1— F571–V1 a) Left panel: *V* image. b) Right panel: H I surface density map. The displayed section of the *V* image is 1.6′ on a side. This galaxy has a central bar and some LSB plumes, but does not appear to be forming stars currently. The low surface density gas disk is below the threshold for star formation at all points. It also appears to be substantially larger than the optical portion of the galaxy (though this may be affected somewhat by the poor conditions under which the *V* image was obtained).

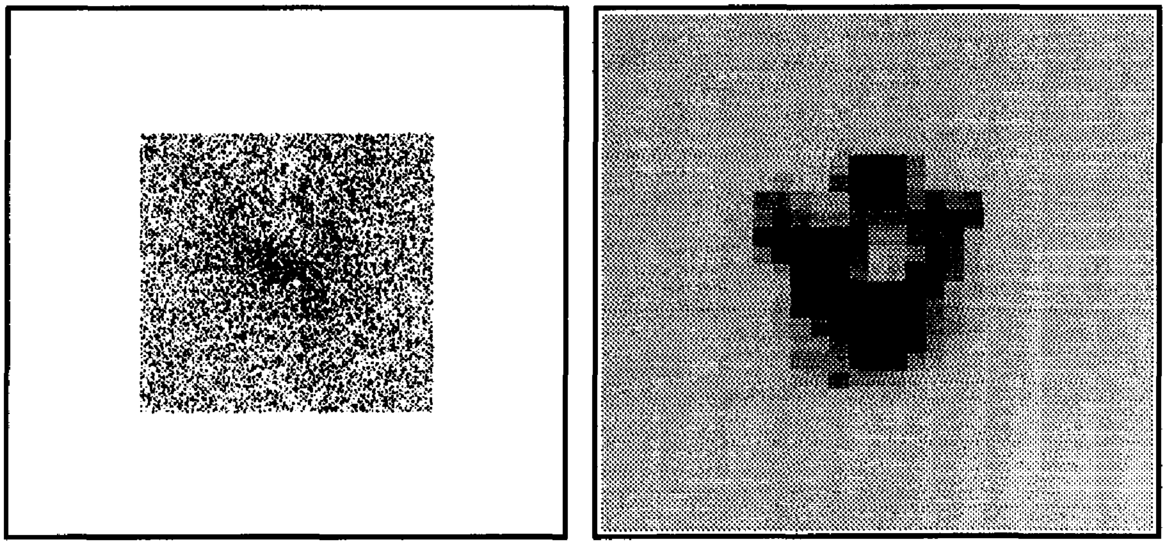

Figure 4.A.2— F574–2 a) Left panel: V image. b) Right panel: H I surface density map. The displayed section of the V image is 1.3′ on a side. This galaxy has a ring morphology in H I which may also occur in the optical. Again, the surface density of the gas is at or below the star formation threshold at all points, and no obvious star formation is currently occurring in this galaxy.

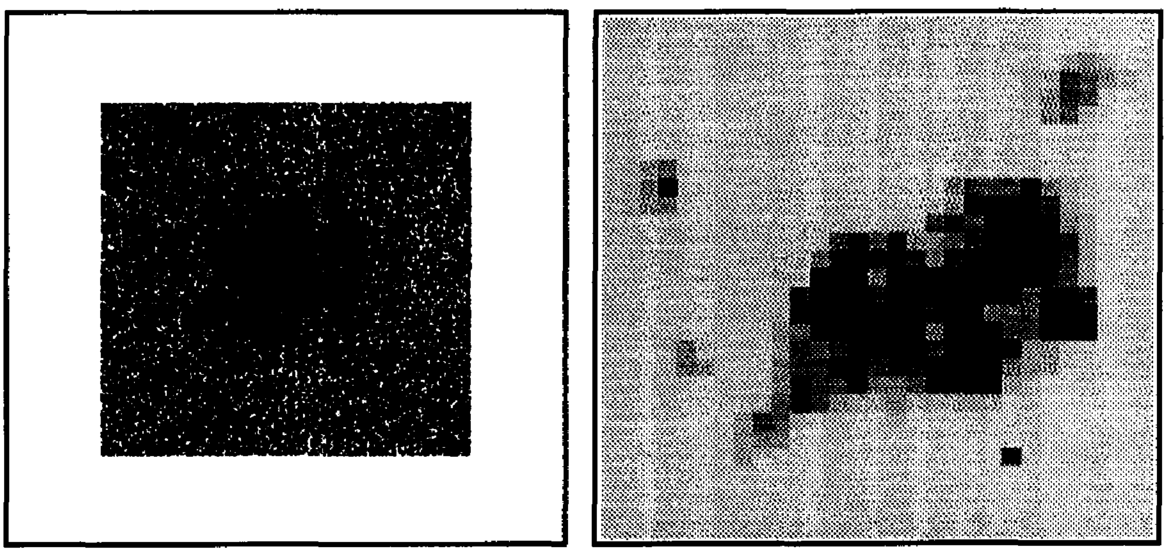

Figure 4.A.3— F579–V1 a) Left panel: V image. b) Right panel: H I surface density map. The displayed section of the V image is 1.6′ on a side. The amorphous, spheroidal optical component bears little resemblance to the clumpy, extended gas component. Indeed, it is not obvious which regions of these images overlap, and the positional accuracy of the optical image is inadequate to clarify this. Despite the clumpiness of the gas, it is all at very low surface density, consistent with the lack of star formation in this galaxy.

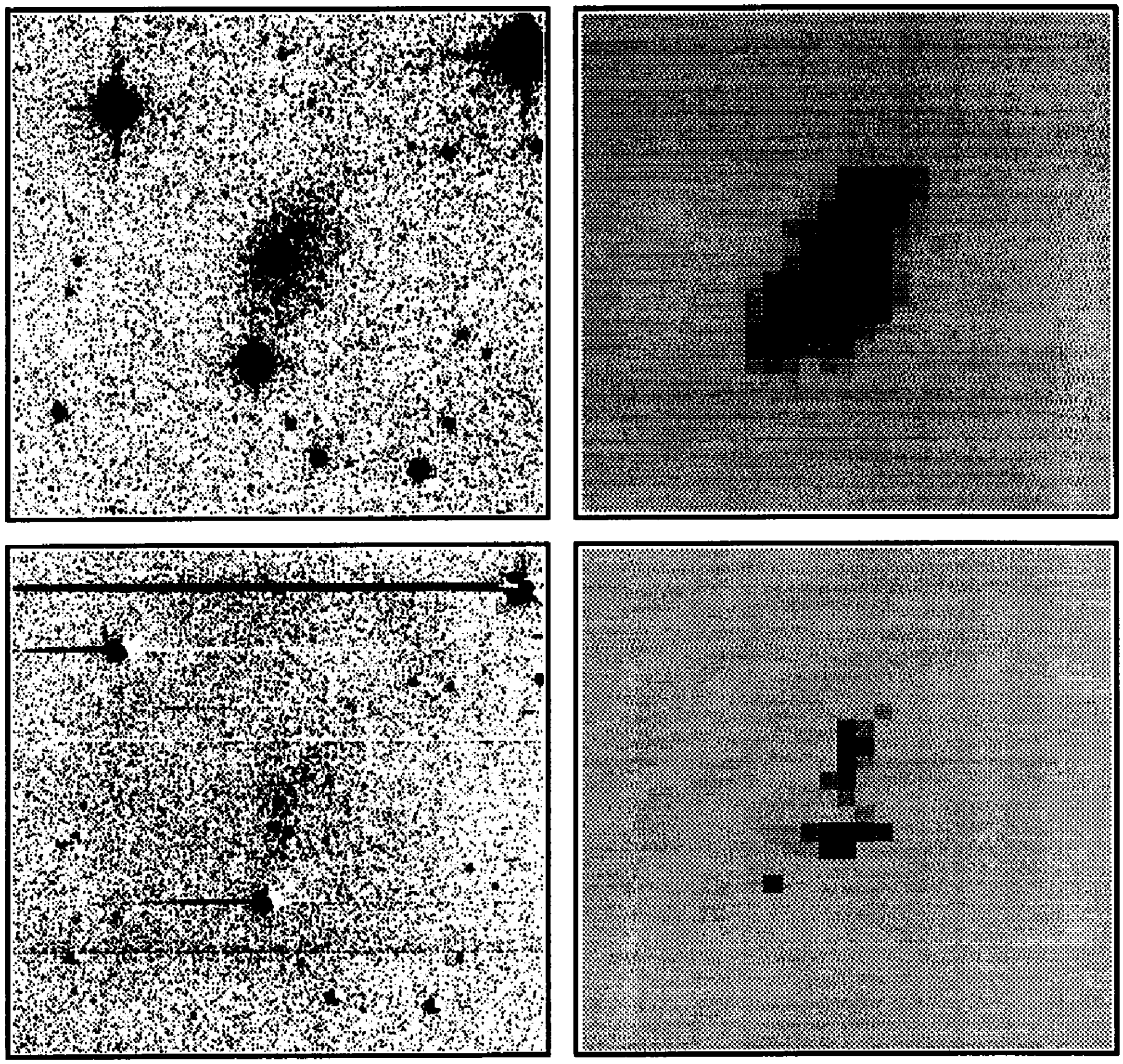

Figure 4.A.4— F563–V1. a) Upper left panel: *V* image. b) Upper right panel: H I surface density map. c) Lower left panel: continuum subtracted Hα image. d) Lower right panel: critical density map. The H I distribution (b) is similar to the stellar distribution (a); both are low surface density with the apparent size of the gas component being somewhat larger. Star formation is occurring in this galaxy, with the Hα image (c) showing three distinct sites of current star formation. One is near the center of the galaxy where the critical density map (d) is invalid. The other two are at the radius where Figure 4.4 indicates that the gas surface density exceeds the threshold for star formation. The gravitational instability criterion for this threshold predicts not only the radius of star formation correctly, but also its angular position — the star forming knots coincide with the peak in the critical density map.

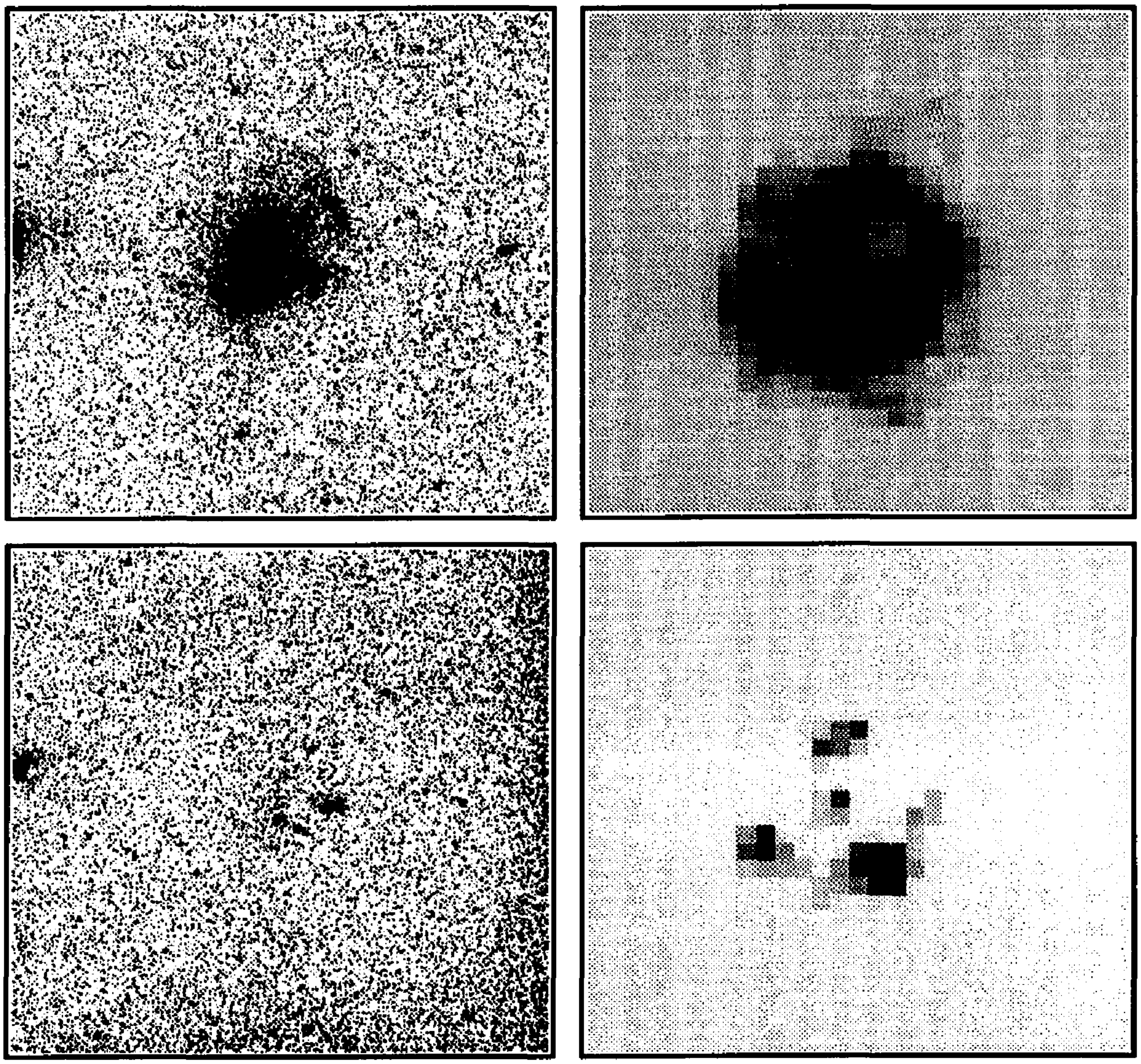

Figure 4.A.5— F563–V2. a) V image. b) H I surface density map. c) Continuum subtracted Hα image. d) Critical density map. This relatively HSB galaxy has an extended, clumpy gas disk with much structure apparent. Due to astrometric uncertainty, it is unclear which optical features correspond to which features in the gas disk (if any do). For example, the LSB plume to the northwest seems to be mimicked at larger a larger radius by the gas. The western star forming knots occur at the radius suggested by Figure 4.4, but are displaced northwards of the peak in the critical density map *if* the apparent geometric centers of the optical and gas disk coincide.

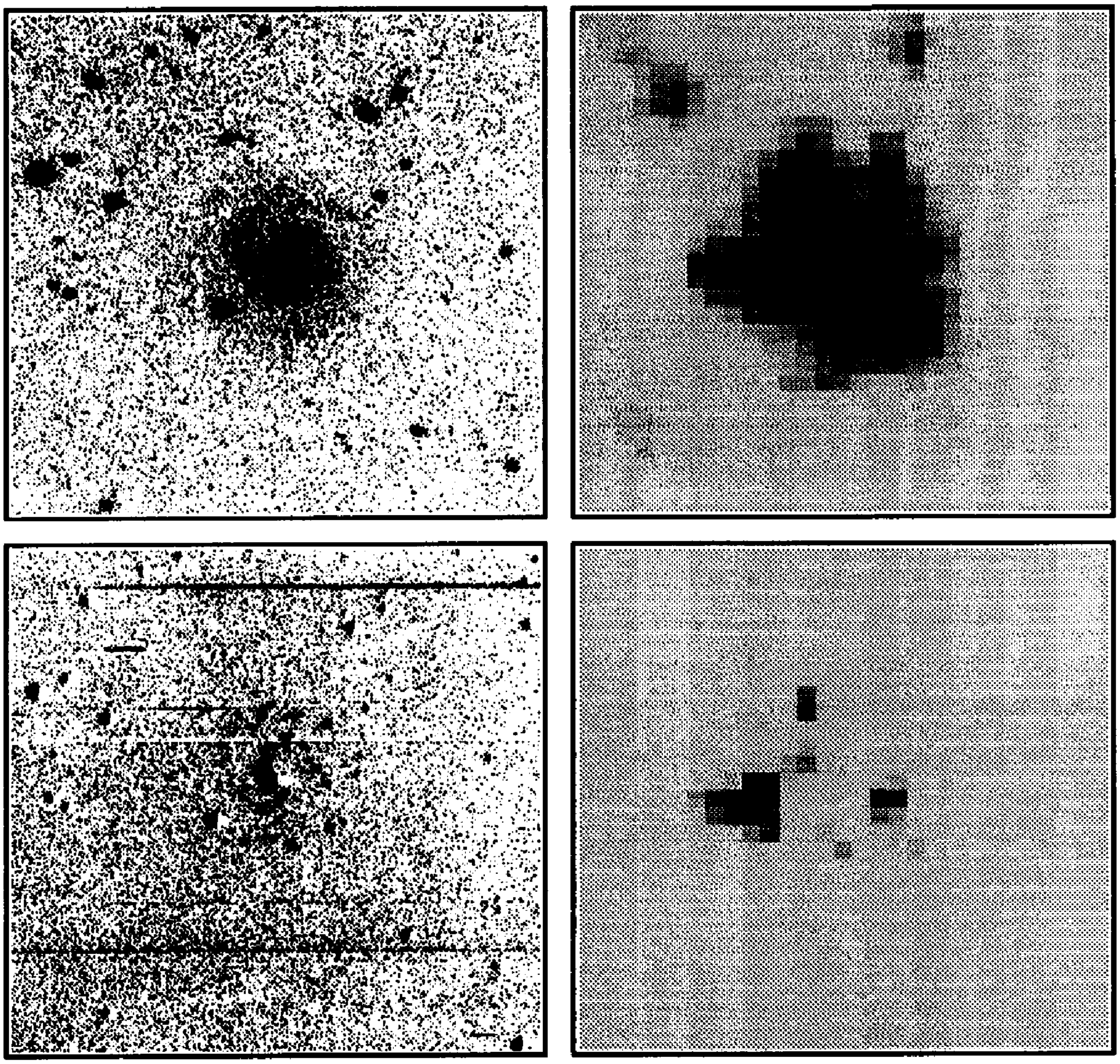

Figure 4.A.6— F568–1. a) I image. b) H I surface density map. c) Continuum subtracted Hα image. d) Critical density map. Though the continuum is poorly subtracted in the Hα frame, there are a few weak H II regions in the arms of this galaxy. That the threshold density exceeds the atomic gas density at all radii (cf. Figure 4.4) may be a result of the large inclination correction in this case, or it may be an indication that modest amounts of molecular gas are present in this galaxy. A ring of molecular material at $r \approx 9$ kpc with $\Sigma \geq 2\,M_{\odot}\mathrm{pc}^{-2}$ would bring the predictions of the gravitational instability threshold into accord with the observed sites of star formation. Alternatively, star formation may be occuring in the nonlinear regime (as it is not completely suppressed below the critical density), which may explain the feeble nature of this galaxy's H II regions.

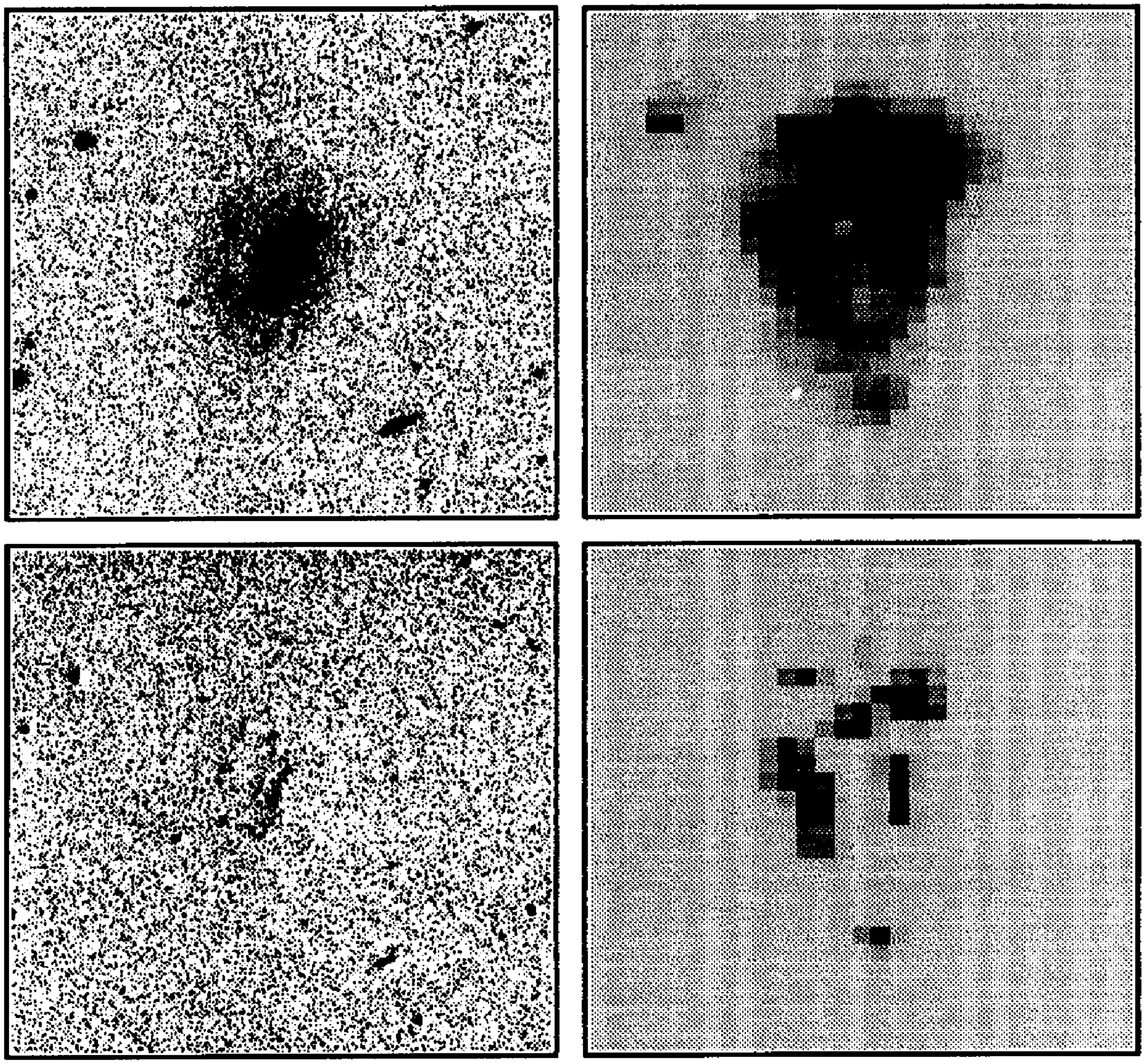

Figure 4.A.7— F568–3. a) V image. b) H I surface density map. c) Continuum subtracted Hα image. d) Critical density map. The H I maps have been displaced upwards somewhat in order to include the very low surface density gas plume to the south. The H II region at the southern end of the central bar appears to be associated with the southeastern peak in the critical density map.

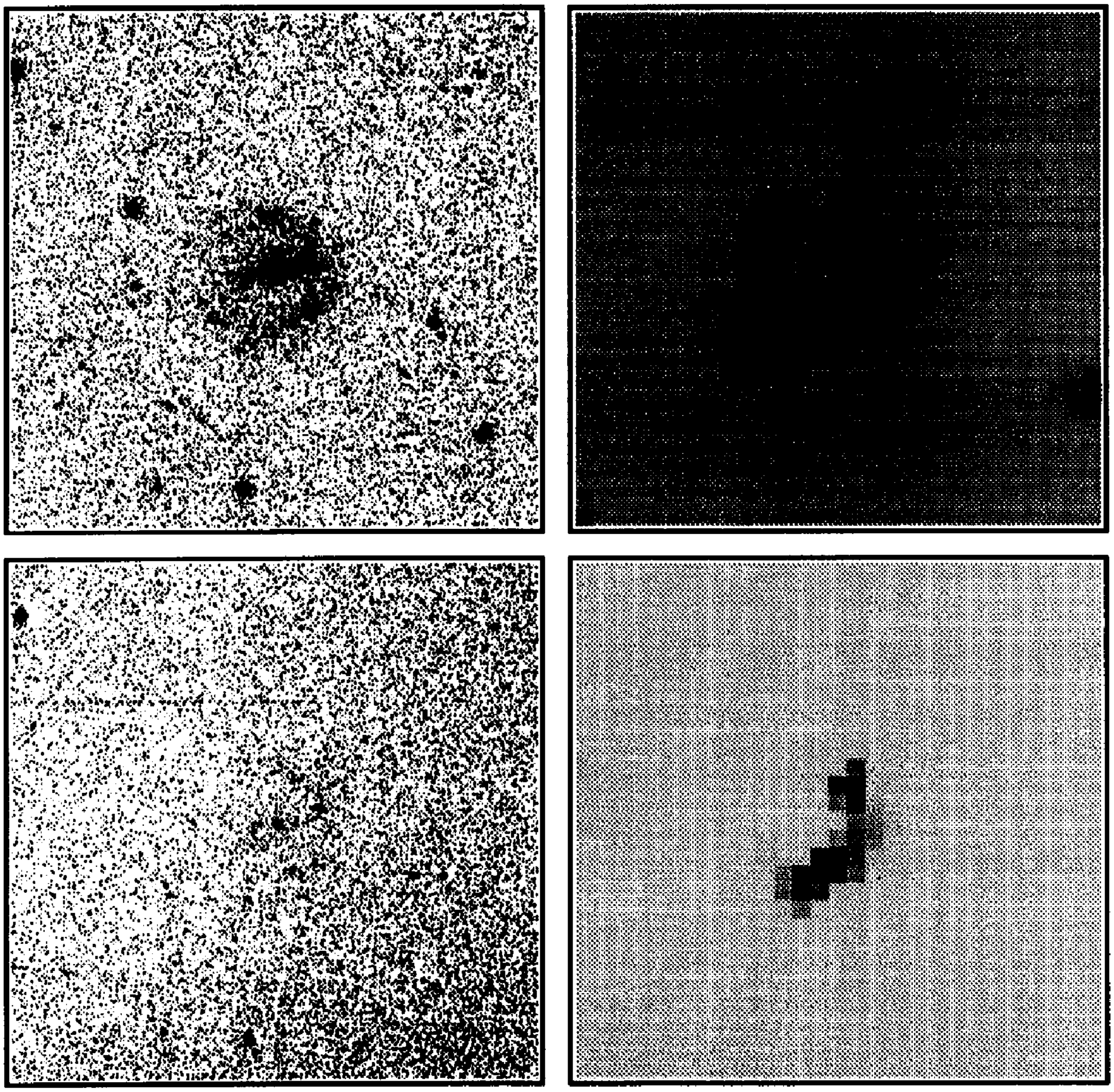

Figure 4.A.8— F577-V1. a) V image. b) H I surface density map. c) Continuum subtracted Hα image. d) Critical density map. In this case, the dynamical center of the gas is near the southern edge of the hole in the H I distribution, near the geometric center of (b), presumably coincident with the center of the bar in the optical image. The H I surface density profile in Figure 4.3 is centered on the peak in the H I distribution, which is $\sim$ 5 kpc from the dynamical center. For this reason, F577-V1 is not included in Figure 4.4, as the radial dependence of the star formation threshold is obviously associated with the dynamical center rather than the peak of the H I distribution. It is clear, however, that the two clumps in the critical density map do exceed the star formation threshold, and they are positionally coincident with the two H II regions to the west and southwest of the nucleus. (These star forming knots are perhaps more obvious in (a) than in the short Hα exposure).

REFERENCES

Bernardeau, F. 1992, ApJ, 392, 1

Blumenthal, G. R., Faber, S. M., Primack, J. R., & Rees, M. 1984, Nature, 311, 517

Bothun, G. D., Beers, T. C., Mould, J. R., & Huchra, J. P. 1986, ApJ, 308, 510

Bothun, G. D., Schombert, J. M., Impey, C. D., & Schneider, S. E. 1990, ApJ, 360, 427

Dekel, A., & Silk, J. 1986, ApJ, 303, 39

Dressler, A. 1980, ApJ, 236, 351

Impey, C. D., & Bothun, G. D. 1989, ApJ, 341, 89

Freeman, K. C. 1970, ApJ, 160, 811

Hoffman, Y., Silk, J., & Wyse, R. F. G. 1992, ApJ, 388, L13

Katz, N. 1992, ApJ, 391, 502

Katz, N., & Gunn, J. E. 1991, ApJ, 377, 365

Kennicutt, R. C. 1983, ApJ, 272, 54

Kennicutt, R. C. 1989, ApJ, 344, 685

Knezek, P. 1992, Ph.D. thesis, University of Massachusetts

Nilson, P. 1973, *Uppsala General Catalog of Galaxies* (Uppsala, Sweden: Societatis Scientiarum Upsaliensis) (UGC)

Oemler, A. 1974, ApJ, 194, 1

Puche, D., Westphal, D., Brinks, E., & Roy, J.-R. 1992, AJ, 103, 1841

Quirk, W. J. 1972, ApJ, 176, L9

Schmidt, M. 1959, ApJ, 129, 243

Schombert, J. M., & Bothun, G. D. 1988, AJ, 95, 1389

Schombert, J. M., Bothun, G. D., Impey, C. D., & Mundy, L. G. 1990, AJ, 100, 1523

Schombert, J. M., Bothun, G. D., Schneider, S. E., & McGaugh, S. S. 1992, AJ, 103, 1107

Silva, D. R. 1991, Ph.D. thesis, University of Michigan

Toomre, A. 1964, ApJ, 139, 1217

van der Hulst, J. M., McGaugh, S. S., & Bothun, G. D., 1993 in preparation

van der Hulst, J. M., Skillman, E. D., Kennicutt, R. C., & Bothun, G. D. 1987, A&A, 177, 63

Warmels, R. H. 1986, Ph.D. thesis, University of Groningen

Warmels, R. H. 1988, A&AS, 73, 453

Weinberg, D. H., Szomoru, A., Guhathakurta, P., & van Gorkom, J. H. 1991, ApJ, 372, L13

Weinberg, S. 1972, *Gravitation and Cosmology* (New York: John Wiley & Sons)

Wevers, B. M. H. R. 1984, Ph.D. thesis, University of Groningen

CHAPTER V

CONCLUSIONS

Summary

The essential results of this study of the physical properties of LSB galaxies are summarized by the following:

1) LSB galaxies are lower density than HSB spirals, but are comparable in size and mass.

2) No correlations exist between scale length, central surface brightness, disk color, and luminosity in this sample.

3) LSB galaxies tend to be quite blue, with complex stellar populations generally indicating a variety of star formation histories.

4) The blueness of LSB galaxies is most pronounced in $V - I$, suggesting that the giant branch is underpopulated as a result of sporadic star formation episodes.

5) *Some* LSB galaxies are *extremely* blue in all colors, and could be young objects.

6) LSB galaxies *do* contain massive ($M > 60 M_\odot$) stars.

7) LSB disks are chemically unevolved, having generally low ($Z \leq 30\%\ Z_\odot$) metallicities.

8) No correlation exists between metallicity and the nebular ionization parameter.

9) Empirically, the trends in the elemental abundance ratios indicate a source of enrichment extrinsic to these galaxies.

10) LSB galaxies are generally gas rich, possessing large reservoirs of atomic hydrogen despite being apparently devoid of molecular gas.

11) The gas disks of LSB galaxies are lower surface density and relatively larger than those of late type HSB spirals.

12) LSB galaxies evolve slowly because their gas surface densities are usually below the threshold for star formation.

13) LSB galaxies are low density because they form from modest initial fluctuations.

From these, a coherent (if schematic) picture for the formation and evolution of LSB galaxies has emerged. They result from the smooth, gradual collapse of relatively weak initial density perturbations, and evolve slowly because their low gas densities remain largely subcritical. While this picture holds in general, the development of individual objects can be quite complicated. A number of puzzling results remain, warranting further investigation.

Physical Relations

Having accumulated an extensive set of data on the luminosities, colors, metallicities, and gas content of a number of LSB galaxies, we can examine physical relations between these properties. Radius, luminosity, and metallicity appear to be correlated within broad morphological classes of the Hubble sequence. It is interesting to see what the situation is when a sample which is not confined to a narrow range of surface brightnesses is examined, and what implications this has for galaxies as physical objects.

It has already been established (Chapter 2) that no radius, color, or surface brightness-luminosity relations exist within this sample of LSB galaxies. Rather, galaxies occupy the entire volume defined by these parameters. This is the rule, not the exception, for all of the observed properties.

Specific Examples

While the comprehensive element data set resulting from the combination of the individual data sets described in the preceding chapters cannot be discussed in its entirety here, a number of specific examples serve to illustrate the general lack of correlations. Figure 5.1 gives one example of this, plotting the oxygen abundances from Chapter 3 against the structural parameters derived in Chapter 2. These are scatter diagrams, with metallicity following neither scale length nor surface brightness.

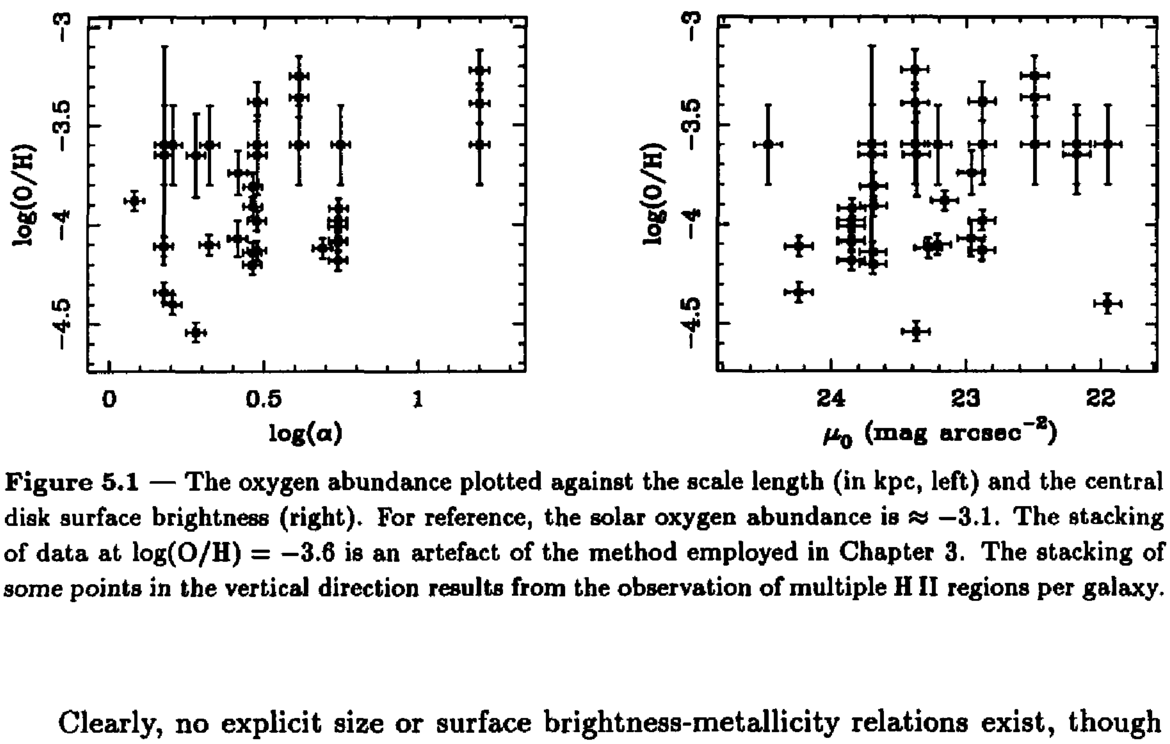

Figure 5.1 — The oxygen abundance plotted against the scale length (in kpc, left) and the central disk surface brightness (right). For reference, the solar oxygen abundance is ≈ -3.1. The stacking of data at $\log(O/H) = -3.6$ is an artefact of the method employed in Chapter 3. The stacking of some points in the vertical direction results from the observation of multiple H II regions per galaxy.

Clearly, no explicit size or surface brightness-metallicity relations exist, though surface brightness is a good general indicator of metallicity (i.e., LSB galaxies have subsolar abundances). This continues to hold when the structural parameters are combined to measure the disk luminosity (Figure 5.2). Hence, the size, surface brightness, and luminosity of a galaxy are *not* tightly correlated with its metallicity. Such relations must arise as the result of selection effects which restrict samples to a narrow range of high surface brightness objects.

Indeed, all measures of metallicity are inherently local (e.g., individual stars and H II regions) whereas the size, surface brightness, and luminosity are global properties

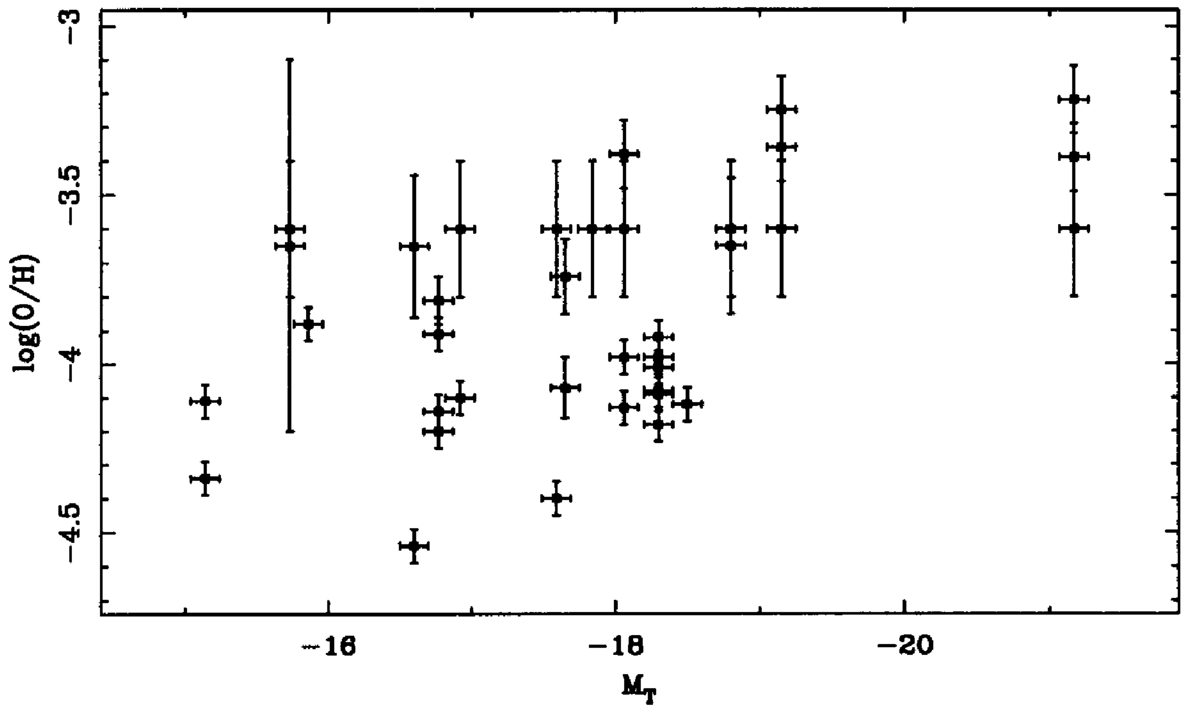

Figure 5.2 — The oxygen abundance plotted against the absolute magnitude. There is an apparent lack of objects with very low metallicity at bright absolute magnitude, but this probably stems from small number statistics. The three points with $M_T^B < -20$ are all due to F568–6, and only one of these approaches solar metallicity.

of a galaxy. The existence of metallicity gradients in galaxies makes it impossible to assign a global value for the metallicity (though the form of the stellar metallicity distribution would be a meaningful global property if adequately sampled), and it is hardly surprising that local and global properties are not tightly correlated. Whether there is a local surface brightness-metallicity relation in LSB galaxies which blends smoothly with that in HSB galaxies can be examined with these data, and will be done in the future.

Another property which is not correlated with the metallicity is the disk color. This is shown in Figure 5.3. While only $B-I$ is plotted, the same result holds for all colors. This reinforces the complexity of the stellar populations which compose these galaxies: they must in general be composed of a wide range of ages and metallicities. Indeed, the only hint of a systematic trend is in the spur at very low metallicity.

This is consistent with the evolution of a very young population, which enriches the gas as the massive stars evolve (this can be noticeable for log(O/H) < −4.3, Kunth & Sargent 1986). That the trend is for the galaxies to become more blue as the metallicity increases is an indication that the evolved states of the massive stars (the RSG and AGB) are dominating the optical colors as the population ages. Thus the most metal poor objects may be experiencing their first episode of star formation.

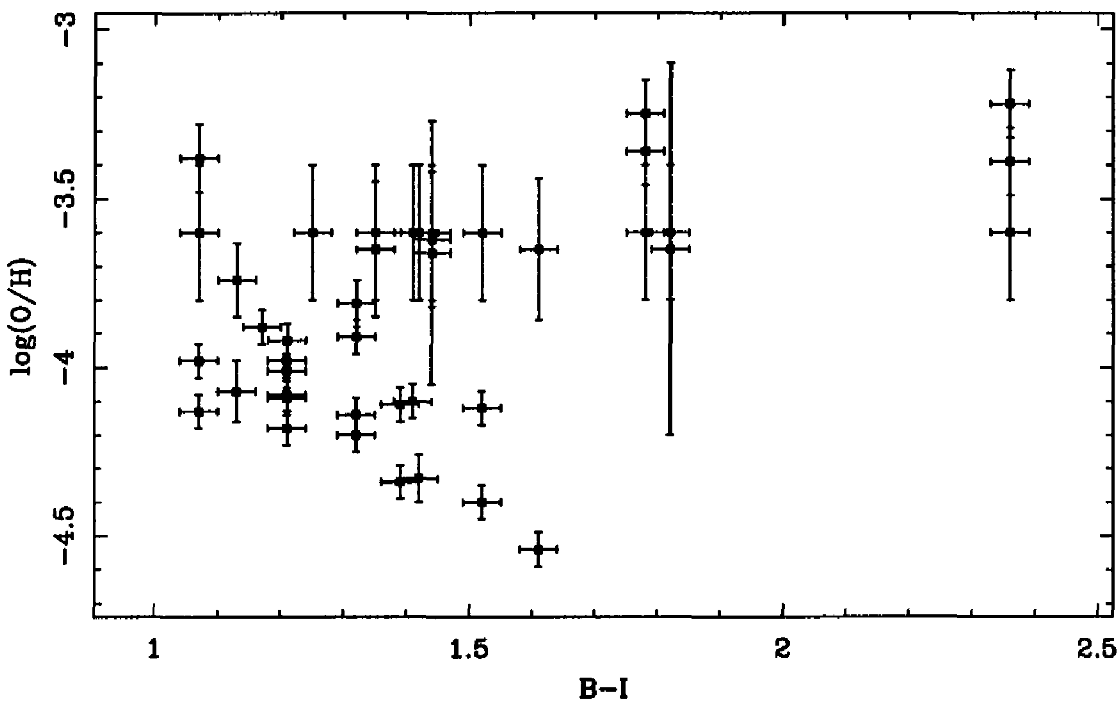

Figure 5.3 — The oxygen abundance plotted against the $B - I$ color. No correlation is apparent between metallicity and this or any other color. There is at very low oxygen abundance a trend with color which is consistent with the evolution of a very young stellar population.

A property which should be related to the metallicity is the gas mass fraction. The simple, closed box model of chemical evolution predicts the simple relation

$$Z = y\,ln\left(\frac{1}{\eta}\right), \tag{5.1}$$

where y is the yield of the stellar population (i.e., the fraction of initial mass converted into metals and returned to the gas). This predicts a line of slope y in Figure 5.4. That this is not the case may indicate variations in the IMF or failure of the assumption of a closed system due to gas loss or secondary infall (the latter perhaps being indicated as well by the elemental abundance ratios reported in Chapter 3). However, these gas mass fractions are again global values, and the comparison should properly be made with local values. These are difficult to derive because the activity of star formation enhances both the local surface brightness (from which the stellar mass is deduced), and the gas surface density (i.e., it must be above the critical density). This will be done in the future by using the profiles (Figures 2.1 and 4.3) to smooth over these enhancements to get an accurate idea of the local baryonic gas mass fractions. This would greatly facilitate the study of chemical evolution, as it would provide a direct comparison to equation (5.1) and more complicated theories. It is particularly useful to pursue this for those galaxies which have large gas mass fractions, as large η provide the most stringent constraints on theory, but are not available in HSB galaxies.

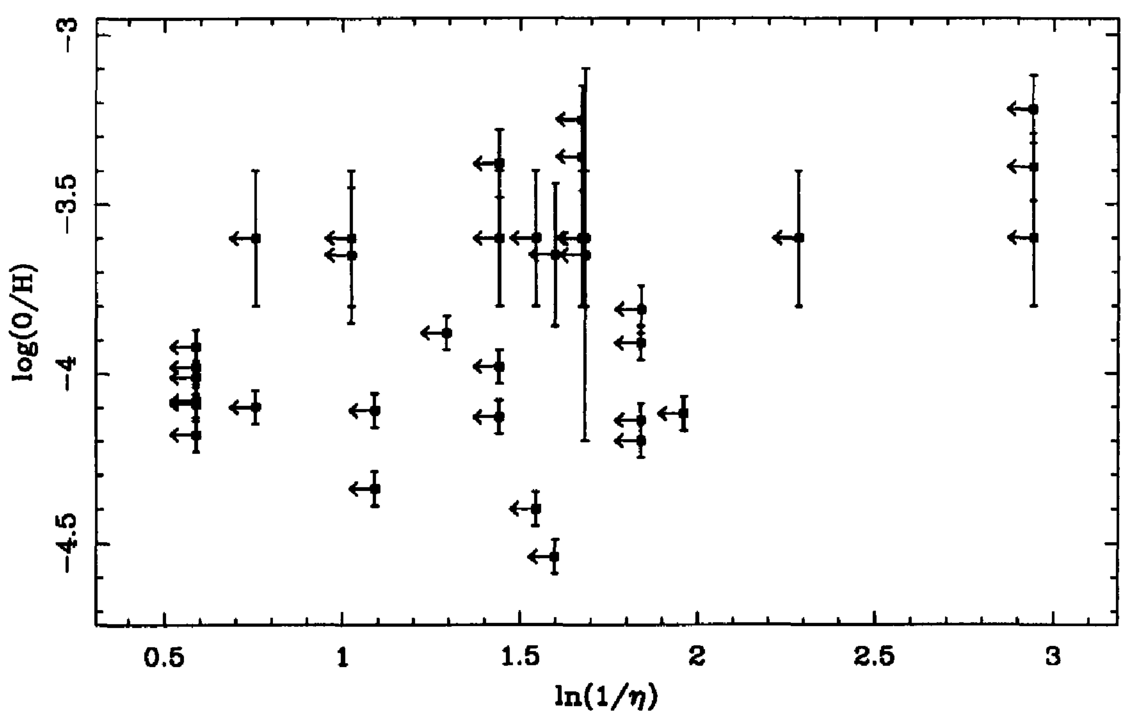

Figure 5.4 — The oxygen abundance plotted against the gas mass fraction. The values of η are global lower limits, hence arrows rather than error bars. That LSB galaxies do not follow the predictions of the closed box model of chemical evolution (a straight line in this diagram) again indicates the difficulty of comparing global and intrinsically local measures.

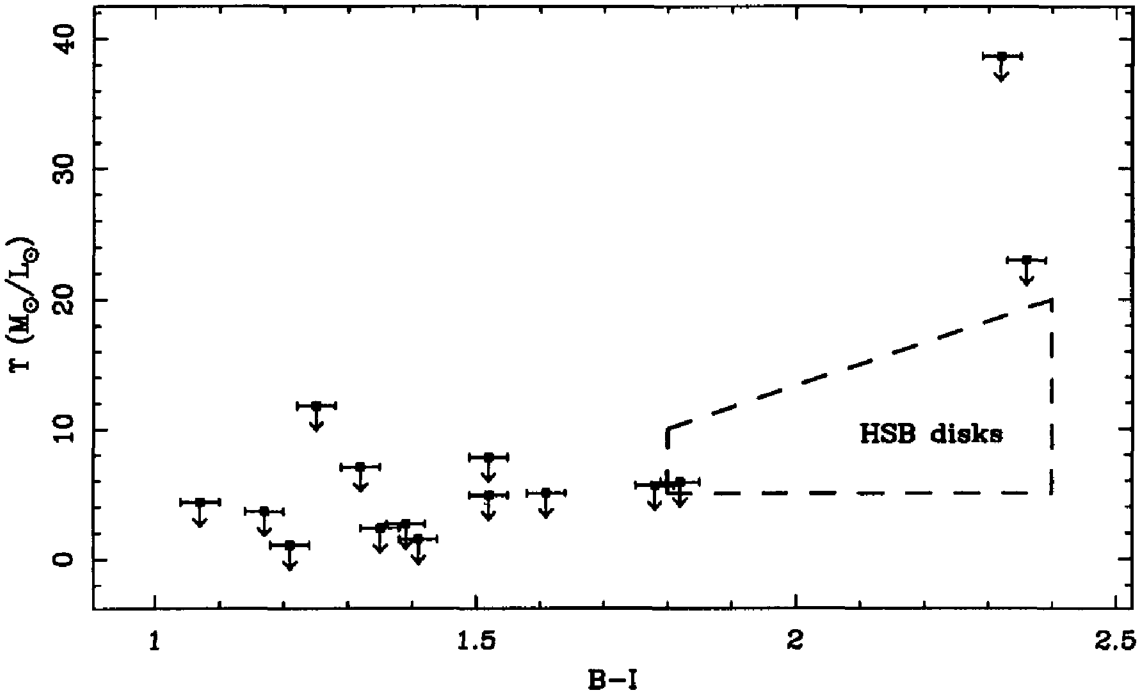

Figure 5.5 — The mass to light ratios (Υ) from Chapter 4 vs. the disk colors from Chapter 2. Even between these global properties, no correlation is evident. LSB galaxies occupy a considerably different and greater range than do HSB spirals, as approximately indicated by the region enclosed in dashed lines. Despite their nature, most LSB galaxies in this general field sample have low mass to light ratios (these are upper limits, as indicated by the arrows).

While some of the scatter in Figures 5.1–5.4 may be the result of comparing local and global properties, the latter are not correlated with one another either (Chapter 2, Chapter 4). Two global properties which have not previously been examined together are displayed in Figure 5.5. This plots the mass to light ratio of the stellar population against the disk color. If LSB galaxies had simple star formation histories, then a trend would be present in this figure. That one is not again indicates that individual galaxies can follow complicated and quite different evolutionary paths. Moreover, LSB galaxies occupy a distinctly different region of this diagram than do HSB galaxies. This, and the lack of other correlations, suggests that

1) Galaxies exist over a much broader range of properties than indicated by the Hubble sequence,

2) Selection effects have seriously limited our awareness of many galaxy types, and

3) Very little is actually known about the systematic properties of stellar systems.

Final Remarks

The cosmological view point of *homo sapiens* has evolved rapidly with the species' technological capacity to explore the world system in which it finds itself. Once the sacrosanct precinct of philosophers and theologians, the nature of the Universe has become grudgingly accessible to the application of testable hypotheses. Yet it remains the case that what you think about the Universe depends very much upon how you look at it.

Selection effects can seriously skew the physical interpretation of astronomical observations. Here, we have found that galaxies cover a much wider range of properties than previously suspected. In particular, examination of a sample of galaxies selected to be of low surface brightness has shown that the usual radius-luminosity-metallicity relations fail to hold, and result from selection effects which favor the narrow range of surface brightnesses exhibited by the Hubble sequence.

Even so, there is much cause for optimism. A rich field of exploration has opened as the result of the quantitative, empirical investigation of the unknown. Once again, the universe has proven itself to be a stranger and more interesting place than we had imagined.